Classifying Iron in Redox Reactions between Iron-Bearing Minerals and Environmental Contaminants

A DISSERTATION
SUBMITTED TO THE FACULTY OF THE
UNIVERSITY OF MINNESOTA
BY

Jeanette Leigh-Ann Voelz

IN PARTIAL FULFILLMENT OF THE REQUIREMENTS
FOR THE DEGREE OF DOCTOR OF PHILOSOPHY

Advised by
R. Lee Penn and William A. Arnold

August 2019

Acknowledgements

I was never alone during my journey to this achievement. Whether supported by teachers, family, friends, colleagues, supervisors, or other professionals, I always had a motivating voice to push me forward, an ear to listen to my troubles, a hand to help with projects, a shoulder to cry on, or a smile to lift my spirits.

I'm forever grateful for the guidance provided by my father and mother. They pushed me to study hard, they worked long hours to fund my education, and they were a bottomless well of encouragement, consolation, assistance, and love. My father taught me values of hard work, quality performance, responsibility, and duty. He told me to forge my own path instead of falling into societal expectations and perceived limitations. By teaching me woodworking and construction, he gave me the confidence to charge forward when something needed to be done. By teaching me the importance of plants and how to care for them, he taught me to value land, air, and especially water, which fostered a spiritual connection to nature and the desire to protect it through all aspects of my life. Whether intentional or inadvertent, his lessons over the years forged me into a strong, assertive, unapologetic woman that I lovingly refer to as 'a beast'. I'm proud to be the unstoppable force that I am today because of him.

My teachers have always been highly admired and respected mentors in my eyes, from elementary through graduate studies, but one person stands out among them all: my primary graduate advisor, Lee Penn. I would not have made it through graduate school without Lee's support. Lee's mentorship went far beyond the development of scientific expertise that is defined by graduate studies. They took the time to listen to my troubles, encouraged me to take time for self-care to keep my body and spirit strong, provided me with

resources to get the mental health care I needed, and went above and beyond to watch out for my health and safety. In addition, Lee's passion for diversity, inclusion, and equity has illuminated facets of personal integrity and ways to express compassion where I was previously naïve. In the past five years under Lee's mentorship, I've experienced fastest and most substantial intellectual growth and maturation in my life and I feel that I have become a better human being because of it.

My fellow Penn and Arnold group members have also helped me immensely. I especially want to thank Thomas Webber and Louis Corcoran for all the laughter that always helped to raise my spirits, Jennifer Strehlau for all the assistance and advice as I started my graduate studies, and Kenny Tritch who opened my eyes to the incalculable value of working on projects for/with communities in need. I also want to thank the undergraduates who worked with me on projects in this dissertation: Kaelynn Stahovich, Haleigh Ziebol, Nathan Harper, and Zachary Wiethorn. I appreciate their contributions, I'm thankful to have had the opportunity to work with each of them, and I'm grateful for their patience with my shortcomings and failures as I learned how to become a mentor.

My dog Cooper will never understand how much he means to me and how much I have relied on him for emotional support over these past five years. I adopted him in November 2014, in my first semester of graduate school. He is a fuzzy snuggle-buddy for days when I feel worthless. He's a joyous voice that always tells me (quite exuberantly) that he's happy I've come home. His simple requests to play and cuddle have been a valuable call for me to put aside the day's stresses and live in the moment. His presence in my life is the reason why I can roll out of bed on the worst days and put one foot in front of the other, so that I can always provide him the safe and loving home he deserves.

Dedication

This dissertation is dedicated to all past and future generations. I am one person among countless others who have lived and who will live, but my short existence will have an impact through a commitment to care for my fellow beings, to perpetuate the knowledge of my predecessors, and to expand the boundary of human knowledge to serve those yet to come.

I dedicate my life to serving our Mother Earth, on whom our existence depends and whose health is too often taken for granted or ignored. I commit to using every aspect of my life to foster sustainability in an environmentally-responsible lifestyle. I firmly believe that we all have a deep responsibility to protect and harmoniously tend the land that sustains us, and we must also whole-heartedly honor, respect, and serve our fellow human beings. Only then will we, as a collection of unique and diverse peoples, thrive on our precious planet.

These ideals were instilled in me by the Hawaiian community in which I was raised and are eloquently summarized in the official motto of Hawai'i, stated below. Please see Appendix F for detailed description of the cultural context and meaning behind these words.

ua mau ke ea o ka ʻāina i ka pono

"Our independence will forever be sustained by our precious

life-giving land if we do what is good and just."

Abstract

Iron-bearing minerals are ubiquitous in the environment and are important in many reactions with environmental contaminants. The ability to classify iron in various mineral phases and in aqueous media is important for assessing iron cycling in natural processes and in processes influenced by anthropogenic activities. Presented herein is a review of iron classification by chemical dissolution and aqueous quantification methods. This review considers a breadth of dissolution studies and outlines these methods in an effort to promote accessibility and provide standards for comparisons across data sets. Solid-state characterization methods are also important for classifying iron. In the reaction of a model nitrobenzene contaminant and Fe(II) adsorbed to hematite, goethite may form as the oxidative mineral growth phase, which affects the reactivity of the mineral surface. A quantitative analysis method using X-ray diffraction and calibrated standards of goethite and hematite was developed to assess the degree of goethite formation in post-reaction solids. This formation was dependent on the distribution of Fe(II)-activated surface sites, and more goethite formed in conditions having high density of these sites. In suspensions containing organic carbon, however, the oxidative growth on hematite takes on a rough morphology and/or shrinks the domain size of the acicular goethite structures. Consequently, the change in morphology render the XRD analysis method ineffective at quantifying goethite content in post-reaction solids where organic carbon was present. Solid-state analyses and chemical dissolution methods are complimentary techniques for classifying iron in iron-bearing mineral specimens, especially for specimens of complex mineral content. Using these techniques together can

help to identify promising materials as candidates for remediation reactions with environmental contaminants. A study presented herein assesses the use of iron-bearing minerals for reaction with sulfide from industrial aqueous waste streams and compares the reaction characteristics against material characteristics determined by chemical dissolution and XRD. The results of this study show that iron-bearing minerals with otherwise low economic value may have use in contaminant remediation applications.

Table of Contents

List of Tables

List of Figures

List of Abbreviations

4-ClAn	4-chloroaniline
4-ClNB	4-chloronitrobenzene
Ak	akaganeite
BET	Brunauer-Emmett-Teller
DLS	dynamic light scattering
EDX/EDS	energy dispersive X-ray spectroscopy
Fh/6L-Fh	ferrihydrite/6-line ferrihydrite
Gth/Gt	goethite
Hem/Ht	hematite
HPLC	high performance liquid chromatography
IC	ion chromatography
IHSS	International Humic Substances Society
Ilm	ilmenite
Kao	kaolinite
Lep	lepidocrocite
Mag	magnetite
MPMS	Magnetic Properties Measurements System
NOM	natural organic matter
OC	organic carbon
Ol	olivine
OM	organic matter
Qtz	quartz
Sd	siderite
SEM	scanning electron microscopy
SRB	Sulfide-Reducing Bacteria
TEM	transmission electron microscopy
XRD	X-ray diffraction
ZP	zeta potential

IHSS Organic Matter Abbreviations

ESFAI	Elliot Soil Fulvic Acid I
ESHA	Elliot Soil Humic Acid
LHA	Leonardite Humic Acid
PPFAI	Pahokee Peat Fulvic Acid I
PPHA	Pahokee Peat Humic Acid
SRFAI	Suwanee River Fulvic Acid I
SRFAII	Suwanee River Fulvic Acid II
SRHAI	Suwanee River Humic Acid I
SRHAII	Suwanee River Humic Acid II
SRNOM	Suwanee River Aquatic Natural Organic Matter
UMNOM	Upper Mississippi Aquatic Natural Organic Matter

Chapter 1. Quantitative Dissolution of Environmentally-Accessible Iron Residing in Iron-Rich Minerals: A Review

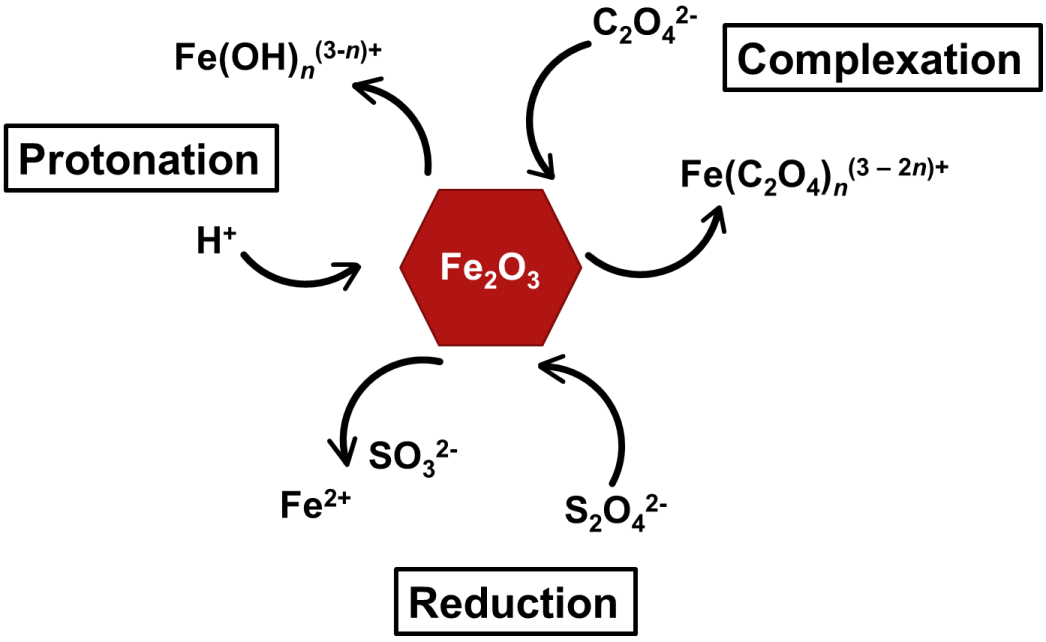

This chapter presents the results of a research project by Jeanette L. Voelz, advised by Nathan W. Johnson, Chan Lan Chun, William A. Arnold, and R. Lee Penn.

Voelz, J. L.; Johnson, N. W.; Chun, C. L.; Arnold, W. A.; Penn, R. L. Quantitative Dissolution of Environmentally-Accessible Iron Residing in Iron-Rich Minerals: A Review. *Submitted to ACS Earth Space Chem.*

Overview

Classifying iron residing in iron-bearing minerals is an important process across numerous disciplines. Iron exists in many forms and with varying degrees of accessibility for reactions. A wide range of procedures exist for identifying and quantifying iron in various forms, but they are scattered throughout numerous journals and typically have several variations. Methods for selective mineral dissolution and iron quantification are reviewed here to improve clarity and accessibility. The methods are described from least aggressive to most aggressive and include cation exchange with salt solutions and dissolutions by acetic acid to target carbonates, hydroxylamine-HCl to target ferrihydrite and lepidocrocite, sodium dithionite to target select iron (oxyhydr)oxides, oxidizing reagents to target organic matter, oxalic acid to target magnetite, concentrated HCl to target iron (oxyhydr)oxides, HF to target silicates, and acid-Cr to target iron sulfides. The dissolution methods using acetic acid, hydroxylamine-HCl, oxalic acid under darkness, and concentrated HCl were critically analyzed for quantifying iron residing in several natural and synthetic minerals. Iron quantification by UV-visible spectroscopy is reviewed, including the use of common colorimetric reagents such as potassium thiocyanate, substituted ortho-dihydroxybenzenes, and ferroin-bearing reagents. Iron detection using ferrozine in the presence of oxalate was also critically evaluated and results indicate that oxalate inhibits the formation of the Fe(II)-ferrozine complex but also efficiently photoreduces Fe(III). Natural samples, however, present several challenges and the presence of mineral salts and redox-active species must be considered. Finally, the importance of standard reporting protocols for fostering accessibility and facilitating comparisons between data sets is discussed.

Introduction

Classifying iron residing in iron-bearing minerals according to identity and accessibility to chemical reactions is an essential process across numerous disciplines. Iron and iron-bearing minerals are used in a wide range of applications including electronics,[1,2] environmental contaminant remediation,[3–5] and drug delivery and medical imaging.[6] Iron-bearing minerals provide valuable insight into Earth's geological record,[7,8] geochemical and biogeochemical iron cycling processes,[9] and mineral formation and transformation mechanisms.[10,11] The fundamental role of iron is often studied in structure-property relations of nanominerals and mineral nanoparticles,[12,13] and in biological processes of organisms.[14] Accurate and precise detection, quantification and classification of iron in its various forms is vital for understanding the role of iron in chemical processes and for making comparisons between the laboratory and field.

Methods of classifying iron have changed substantially over the last century. Procedures are scattered throughout numerous journals, often with limited accessibility and with several variations. The reasoning behind procedural differences may be unstated, unclear, or even unknown. To improve accessibility, clarity, and standardization across disciplines, we present a review of iron-bearing mineral dissolution methods (Section 2), and dissolved iron quantification using colorimetric reagents (Section 3). In considering natural specimens containing heterogeneous mixtures of minerals and other components, we include a discussion of common challenges and ways to mitigate their effects (Section 4). Finally, we propose standardized reporting parameters to foster accessibility and facilitate comparisons between data sets (Section 5).

Section 1: Material Characteristics Identified by Selective Mineral Dissolution

Iron exists in many forms: as dissolved, complexed, or adsorbed ions or incorporated into solids; it exists in several oxidation states, most commonly as Fe(0), Fe(II), or Fe(III); and it occurs in objects ranging in size from the molecular to the nano and to the bulk.[12] Iron materials range drastically in composition from pure iron metal to small fractions of a weight percent as substituents in minerals. Within iron-bearing minerals, the degree of crystallinity varies from the amorphous to the well-formed and highly-ordered. Laboratory syntheses may yield homogeneous iron-bearing structures, while natural soils are complex mixtures of both mineral and non-mineral materials.[15] The sheer magnitude of diversity in how iron occurs in natural and engineered environments necessitates the development of methods that can selectively quantify iron in its different forms. Additionally, these standardized quantification methods enable the comparison of data sets by accounting for differences in iron abundance.

The dissolution methods reviewed herein access iron in a wide range of forms and specimen types, such as soils and sediments, but this review primarily considers these methods as applied to crushed rock specimens. Crushed rock is valuable for applications that use materials with high iron content, such as in environmental contaminant remediation systems.[16,17] The most useful materials for such applications are locally-abundant, of low economic value, and contains few components that either interfere with the desired chemical reaction or exacerbate the contamination. Considering this context, three important material characteristics that are assessed by chemical dissolution are

mineral phase composition, Fe(II) and Fe(III) content, and 'reaction-accessible' iron content.

Mineral Phase Composition

Selective dissolution methods are used to identify the fractions from which iron is extracted. By these methods, the amount of iron residing in carbonates, (oxyhydr)oxides, and silicates are generally differentiable. Furthermore, some dissolution methods are effective at extracting iron from specific iron (oxyhydr)oxides, depending on factors such as pH, temperature, light exposure, and reagent identity.

Identifying mineral fractions present in heterogenous specimens is an important assessment because the various iron-bearing minerals may behave differently in reactions with environmental contaminants.[3] Quantifying the initial abundance of each mineral provides insight into the relative contributions of the minerals in the overall chemical reaction. Post-reaction mineral quantification enables an assessment of iron mass transfer, especially for the identification of transformation products, such as the formation of new mineral phases.

Fe(II) and Fe(III) Content

The identification of mineral phases by selective dissolution provides a qualitative assessment of the relative abundance of iron in each oxidation state. For example, a specimen containing primarily siderite would be high in Fe(II), while a specimen containing primarily magnetite would ideally contain a 1:2 ratio of Fe(II):Fe(III). Natural minerals, however, can vary substantially from ideal stoichiometries. It is therefore

important to directly quantify iron oxidation state. This assessment may be used to identify what reactions can occur and may provide insight into reaction mechanisms.[18] Iron abundance per oxidation state is also useful for normalizing reaction parameters such as reaction rate to compare differences in reactivity among a set of samples.[19,20]

In practice, the abundance of iron in each oxidation state can be quantified before and after reaction to determine iron mass transfer and assess reaction stoichiometry. When iron oxidation state is important for material characterization, both the dissolution method and the subsequent quantification steps for the iron digest must preserve the oxidation state until the analysis method requires a single oxidation state for total iron quantification. In other words, the reagents used in the analysis cannot be redox-active under the analysis conditions (e.g., consider light exposure and oxygen content) until such time as the analysis employs redox chemistry to access a particular oxidation state. For example, the dissolutions using acetic acid, oxalic acid under darkness, and hydrochloric acid can preserve the iron oxidation state, while the methods with hydroxylamine-HCl and dithionite dissolve minerals by redox chemistry and do not preserve oxidation state.

Reaction-Accessible Iron Content

Reaction-accessible iron content is an important characteristic that affects what reactions occur and their rate of reaction. Here, ‘reaction-accessible iron’ is defined as the iron available to participate in a given reaction. Attributes that impact iron accessibility include physical location (e.g., on the mineral surface) and reactive status (e.g., high solubility and/or redox potential), where the latter is a function of system conditions (e.g.,

temperature, light exposure), solution chemistry (e.g., pH, concentration of reactive species), and mineral properties (e.g., crystalline phase, stoichiometry, structural defects).[21,22] For the scope of this review, the chemical reactions in which accessible iron participates are limited to non-extreme environmentally-relevant reactions, such as reactions with environmental contaminants in water systems or microbial metabolic processes. Two major factors affecting the accessibility of iron are mineral surface characteristics and crystallinity.

Mineral surface characteristics such as the presence of structural access points or oxidized coatings affect the accessibility of iron. Structural access points include micro-fissures in larger particles[23] and regular openings in the mineral crystal structure (e.g., layers lepidocrocite or channels in akaganeite).[24] These access points present a greater surface area from which dissolution may occur. The effect that oxidized coatings have on iron accessibility depends on the nature of the reaction. Oxidized coatings can inhibit access to iron in the core material, such as in the dissolution of iron oxide-coated siderite by acetate[25] or in the reaction of siderite-coated metallic iron with nitroaromatics.[26] Thin coatings of oxidized material may not have large enough crystal domains to be detected by common mineral identification techniques, such as in X-ray diffraction (XRD), but dissolution methods may assist in detecting oxidized material on mineral surfaces.

The solubility of reaction-accessible iron is also a function of crystallinity. In general, highly-crystalline materials are more difficult to dissolve than materials of low crystallinity. For example, siderite having low crystallinity takes less time to dissolve in acetic acid than siderite of high crystallinity and also requires lower temperatures for the dissolution.[25] Another study described crushed hematite crystals as highly-crystalline and

less prone to dissolution by dithionite than powdered hematite, although the study did not present a detailed description of the differences in material characteristics.[27] The roles that particle size and crystallinity play in dissolution are difficult to differentiate. For example, ferrihydrite is often used in 2-line or 6-line form, as indicated by the number of diffraction peaks observed in X-ray diffraction patterns, but the composition of the mineral phase is closely linked to particle size.[12] Changes in particle size lead to change composition and in facet size and identity, which affects the ratio of participatory surface groups and therefore the rate and extent of reaction. Because of the complexities of crystallinity and the lack of intensive studies on the effects of crystallinity on dissolution rate, this review focuses mainly on differentiating mineral phase and only discusses crystallinity where dissolutions involving materials of different crystallinity are reported.

Identifying the portion of iron that is reaction-accessible is somewhat arbitrary, but it is an important assessment when comparing the relative reactivity of several samples under equivalent conditions. To quantify reaction-accessible iron in a set of samples, the extent of dissolution is limited by decreasing dissolution time, temperature, and/or reagent concentrations. The results are then used to normalize reaction characteristics such as reaction rates. The quantification of accessible iron is supported by an assessment of particle size and surface area, often determined using inert gas adsorption, particle measurements by transmission electron microscopy (TEM), or mechanical size separation using sieves.

Section 2: Iron-Bearing Mineral Dissolution Methods

This section provides a discussion of the most common selective dissolution methods for iron-bearing carbonates, (oxyhydr)oxides, silicates, and sulfides. The methods discussed herein are organized from least aggressive to most aggressive. Generally speaking, the least aggressive methods are most selective and the more aggressive dissolution methods yield much higher degrees of mineral dissolution to yield bulk iron or total iron measurements.

Planning a procedural outline of dissolution methods to determine iron content in a set of samples involves three main decisions. First, identify the material characteristics desired in the outcome (e.g., mineral identity, oxidation state, and/or reaction-accessible iron) to define the general experimental conditions (e.g., anoxic conditions for oxidation state information or shortened dissolution time for reaction-accessible iron). Then, choose the targeted fraction of the sample, whether it is a specific mineral (e.g., siderite, ferrihydrite, magnetite, etc.) or more general mineral fraction (e.g., carbonate-bound, oxide-bound, silicate-bound, etc.) to decide what dissolution method or set of methods should be used. Finally, if multiple dissolution methods are desired, consider whether the methods are best performed in sequence, in parallel, or as a combination of both.

Cation Exchange: Targeting Surface-Adsorbed Iron

Iron and other transition metals often adsorb to mineral surfaces in aqueous environments. Indeed, the degree of metal ion partitioning at the water-mineral interface plays a major role in metal transport through groundwater systems.[28] Some adsorbed

metals affect the fate and transport of organic contaminants in groundwater. Iron(II) adsorbed to iron oxides in anoxic environments, for example, often facilitates the redox transformation of environmental contaminants like halogenated amines,[29] chlorinated hydrocarbons,[3] and nitroaromatics.[30] Quantifying adsorbed iron is important for assessing natural reactivity and determining iron mass balances after redox experiments.

Adsorbed iron has long been extracted from hydrated environmental specimens like sediment using cation exchange with concentrated salt solutions (e.g., 1 M $CaCl_2$ or 1 M $MgCl_2$ at pH 7).[25,31,32] A known mass of the specimen is added to the salt solution and gently rinsed for five minutes. The resulting mixture is filtered, and the iron concentration in the filtrate is quantified. A potential complication is a cloudy suspension after allowing the sample to settle, caused by the dispersion of colloids, which can compromise adsorbed iron quantification. If a colloidal suspension forms, method parameters such as sample mass loading, pH, and salt identity need to be adjusted so that the colloid formation is prevented.

For treatment of large samples, dialysis bags (pore sizes <8 kD MWCO) are used.[33] Mineral slurries are loaded into dialysis bags, which are then placed into the salt solution and mixed gently, with care taken to prevent the formation of holes in the bags. Adsorbed metals are exchanged within 1 – 3 hours in dialysis.

Some studies report using acetate at basic pH to remove adsorbed iron.[34,35] Other studies, however, do not recommend the method because acetate etches some mineral surfaces, leading to an artificially high iron concentration.[32,33] Indeed, the ability of acetate to dissolve carbonates and its use for quantitative dissolution of iron-bearing carbonates is discussed below.

Acetic Acid: Targeting Iron Residing in Carbonates

In carbonate-rich systems, iron exists primarily in three types of mineral phases: iron (oxyhydr)oxides, iron carbonate, and iron substituted in other carbonates. Common iron (oxyhydr)oxides include goethite, hematite, and magnetite, and these minerals are valued for the geological information recorded at the time of deposition, such as local environmental conditions and planetary magnetic field characteristics.[36] Pure iron carbonate, siderite ($FeCO_3$), contains 48 mass% iron and is the end-member in solid-solutions with other carbonates, including calcite ($CaCO_3$), magnesite ($MgCO_3$), rhodochrosite ($MnCO_3$), and smithsonite ($ZnCO_3$).[37,38]

Carbonates are important for the acid-neutralizing capacity provided by the readily-solubilized carbonate anion. Limestone, for example, has been used in the treatment of acid mine drainage.[39] Carbonates have different acid-neutralizing capacities, however, as illustrated in the case of uranium tailings leachate migration in groundwater, where the migration velocity of the acidic waters and solubilized metals was calculated to be over 500× slower in the presence of calcite than in the presence of siderite.[37] In other cases, siderite is a valuable material for contaminant removal, such as in arsenic filtration, where siderite specimens generally removed 3× more As(V) and 50 % more As(III) at circumneutral pH than did most hematite specimens.[23]

Selective carbonate dissolution is used to release embedded iron (oxyhydr)oxides and/or liberate Fe(II), but the process is pH-dependent; a pH of 2 has been shown to dissolve (oxyhydr)oxides,[36] while pH >5 is ineffective at dissolving even highly-disordered siderite.[25] Acetic acid, with its pK_a of 4.7, has been recognized for decades as

an effective carbonate dissolution reagent, because the acid quickly reacts with basic carbonate via protonation to evolve carbon dioxide.[40] The most widely-reported dissolution method uses a 4:1 ratio of 2 M acetic acid and 1M sodium acetate to yield a pH 4 solution that readily dissolves $CaCO_3$ while leaving many iron (oxyhydr)oxide minerals intact.[36,41,42] A study in 2005, however, extensively tested mineral carbonate dissolution by acetic acid and found that the method dissolved other mineral phases at pH 4, where approximately 10 % of both ferrihydrite and lepidocrocite dissolved concurrently with siderite.[25]

The selectivity of the carbonate dissolution method is sensitive to solution pH and mineral crystallinity and degree of substitution.[25,32,43] Considering these variables, the solution recommended by Poulton and Canfield[25] for the selective dissolution of carbonates is 1 M sodium acetate adjusted to pH 4.5. Furthermore, they recommend that the dissolution of low-crystalline or highly-crystalline carbonate minerals should be performed at room temperature for 24 hours or at 50 °C for 48 hours, respectively.[25] Because ferrous iron may oxidize upon exposure to air to form a protective surface coating of iron (oxyhydr)oxides on carbonate particles that prevents dissolution, specimens should be ground or abraded immediately prior to use and the dissolution should be performed in anoxic conditions.[25]

Difficulties may arise for iron quantification in samples containing certain sulfides. Acetic acid is reported to dissolve 59 % of amorphous iron sulfide, up to 63 % of mackinawite, and up to 17 % of greigite.[44] In another study, 1 M sodium acetate adjusted to pH 5 with acetic acid was found to dissolve 28 % of amorphous iron sulfide.[31] Additionally, the conditions typically used to dissolve target sulfides are highly acidic

(see acid-chromium section below) and would also dissolve carbonates. Owing to these complications, specimens containing carbonates and sulfides may need solid-state characterization analyses and/or several parallel or sequential extractions to determine mineral phase composition.

Hydroxylamine-HCl: Targeting Iron Residing in Ferrihydrite and Lepidocrocite

Iron-bearing minerals with different crystal structures and variable degrees of crystallinity exhibit differing reactivity in environmental processes. For example, ferrihydrite and lepidocrocite react with sulfide within hours to produce iron sulfides, whereas iron-bearing silicates take several thousand years.[25] Sulfide is produced by sulfate-reducing bacteria in natural sediments but is often found in concentrations toxic to aquatic life when anthropogenic activities such as mining,[45] aquaculture,[46] and wastewater discharge[47] release sulfate into natural systems. Sulfide sequestration by iron-bearing minerals is a promising treatment for industrial waste streams, and quantifying ferrihydrite and lepidocrocite in iron-bearing feedstocks is an important step in selecting materials ideal for use in sulfide sequestration.[48]

Hydroxylamine-HCl as a dissolution reagent was first introduced in the 1970s to selectively dissolve manganese oxides in soils and sediments while leaving the co-occurring iron (oxyhydr)oxides largely intact as a way to assess the contribution of each fraction in various environmental processes.[49] For decades since its inception, hydroxylamine-HCl has been widely used to dissolve components of ferro-manganese nodules in sediments.[32,35,50] Method variations have included differences in hydroxylamine-HCl concentration, extraction temperature, and dissolution time. One

study that used the method for iron extraction from nodules found that 0.2 M hydroxylamine-HCl at 100 °C for 3 hours resulted in the greatest dissolution, and the second best dissolution used 1 M hydroxylamine-HCl at 20 °C for 4 hours.[50] Another study reported that 0.04 M hydroxylamine-HCl at 96 °C for 6 hours yielded the most complete iron extraction.[32] These studies, however, did not compare the dissolution of pure mineral phases to determine which specific minerals dissolved and to what degree.

In studies that assessed the dissolution of pure iron-bearing mineral phases, it is reported that hydroxylamine-HCl is effective for the selective dissolution of ferrihydrite and lepidocrocite.[25] Using 1 M hydroxylamine-HCl in 25 %(v/v) acetic acid (pH 1.5) at room temperature, nearly 100 % dissolution of synthetic ferrihydrite and lepidocrocite is reported after 48 hours, as well as 4 % dissolution of synthetic akaganeite, and <2 % dissolution of synthetic goethite, hematite, magnetite, and natural nontronite.[25] Similarly, a study using 0.25 M hydroxylamine-HCl and 0.25 M CH_3COOH or 0.25 M HCl and heated to 50 or 70 °C, showed that <1 % of goethite, hematite, and magnetite specimens dissolved, whereas natural and synthetic hydrous iron oxide dissolved up to 40 and 80 %, respectively.[51] Only 2-line ferrihydrite was used to compare dissolution among the synthetic iron (oxyhydr)oxides[25] and not 6-line ferrihydrite, which is the larger and/or more highly-ordered form. Because of this, our critical analysis of this dissolution method (see below) uses two 6-line ferrihydrite to assess dissolution rate.

There are several complications with using this dissolution method. One complication is that the native iron oxidation state is not preserved; two moles of Fe(III) are reduced for every mole of hydroxylamine-HCl oxidized to nitrous oxide.[52] As a result, only total iron is quantifiable.

Another complication is that iron bound by other minerals or organic matter may be solubilized by hydroxylamine-HCl. For example, exchangeable iron on mineral surfaces or weakly bound to organic matter are accessible by this method.[50,53] In addition, iron-bearing carbonates are soluble at acidic pH, as previously described, and it was shown that 99% of calcite and aragonite dissolved in this medium.[50] Dissolution of several sheet silicates was also tested at 100 °C for 3 hours and the results indicate that 10 % of montmorillonite, 8 % of illite, and 2 % of chlorite dissolved, while kaolinite was insoluble.[50] Because of the degree of dissolution for non-target fractions, this method should follow a sequential extraction procedure for exchangeable iron and then carbonate dissolution. Note, however, that carbonate dissolution with acetic acid dissolves <2 % of ferrihydrite and lepidocrocite.[25] Alternatively, dissolution methods could be performed in parallel to determine the iron residing in each fraction by difference.

Dithionite: Targeting Iron Residing in Select (Oxyhydr)oxides

Iron (oxyhydr)oxides are important components of soil and sediments linked to organic contaminant transformation,[3] phosphate fixation,[54] and podzolization.[55] Assessing both the composition and abundance of iron (oxyhydr)oxides assists in determining the magnitude of their role in such processes. In addition, the presence of iron (oxyhydr)oxides can interfere with the analysis of coexisting minerals like silicates. Iron (oxyhydr)oxides can act as cementing agents in layered materials, which may affect surface properties and interfere with spectroscopic studies, and should therefore be selectively removed prior to analysis of silicates.[56]

A dithionite-citrate-bicarbonate (DCB) solution is typically used for the selective removal of iron (oxyhydr)oxides from soils and clays.[56] Indeed, some reports of the DCB method show nearly 100 % dissolution of ferrihydrite, lepidocrocite, goethite, akageneite, and hematite nanoparticles, but also approximately 20 % dissolution of siderite and less than 5 % dissolution of magnetite and bulk hematite crystals.[25,27] There are, however, several reported variations of this dissolution method and the reasoning behind such variations is often not explained.

Dithionite as a reducing agent for iron (oxyhydr)oxides in the treatment of kaolin was originally proposed in 1934.[57] A later version in 1950 added 0.1 M sodium tartrate to complex with iron in an attempt to prevent metal sulfide precipitation.[55] Owing to difficulties with precipitation and slow dissolution times, another version proposed citrate as a more effective chelating agent and used Fe(III)-specific EDTA as an optional iron valence indicator.[58] Citrate has also been shown to induce the photoreduction of iron oxides in solutions of pH 4 – 8.2.[59] Because dithionite rapidly degrades when hydrated, it is more convenient to add powdered dithionite directly to iron digests rather than adding dithionite as an aqueous solution. The aqueous solution used NaOH, so the transition to powdered dithionite led to the introduction of sodium bicarbonate to maintain a basic pH.[56] Stoichiometrically, the oxidation of one mole of dithionite consumes four moles of OH^-. The dithionite reduction potential is higher at basic pH, and it was shown that pH 7.3 is optimal for preventing both the formation of elemental sulfur and the precipitation of metal sulfides.[58]

Other reagents are also useful in the DCB method. Acetone is used to flocculate fine particles and colloids, whereas methanol or ethanol are less effective.[58] Sodium

chloride assists the separation of clay minerals during centrifugation.[56,58] Both HCl and $CaCl_2$ are avoided in flocculation because HCl affects pH and because calcium forms a complex with citrate and affects the iron-citrate complex equilibrium.[60]

The DCB procedure reported here is a combination of reported methods.[25,56,58,61] For high-iron specimens (ca. >20 % extractable iron), serial extractions and shorter reduction times prevent sulfide precipitation by keeping the dissolved metal concentrations low. Reports of serial dithionite extractions have used between two and ten extractions.[56,58,61] Only total dissolved iron content is possible because of the reductive dissolution pathway and the oxidative treatment on the resulting iron digest.

For this method, the maximum target extractable iron is <0.2 g as iron (oxyhydr)oxides. The sample (0.1 – 4 g) is added to 40 mL of 0.3 M sodium citrate and 5 mL of 1 M sodium bicarbonate. The mixture is heated to 80 – 90 °C in a water bath and then solid sodium dithionite (0.5 – 1 g) is added. The resulting mixture is mixed well for 1 minute and then stirred occasionally for 5 min – 2 hours. Next, 10 mL of saturated NaCl is added to assist flocculation, the mixture is centrifuged, and the supernatant collected for iron quantification. The resulting color of the solid residue is indicative of the extent of mineral dissolution. If the solid appears blue-grey to white, it is likely that all the extractable iron has been dissolved. If, however, the residue is yellow, red, or brown, residual iron (oxyhydr)oxides are likely present and the protocol should be repeated until warm hues diminish.

Once the residue appears free of iron (oxyhydr)oxides, the solids are washed with 20 mL of 0.3 M sodium citrate to remove residual dissolved iron and NaCl and centrifuged to separate the solid and aqueous fractions. The filtrate is added to the iron

filtrate for quantification, and the process repeated as desired. If flocculation is inadequate during the washes, 10 mL of acetone is added and the mixture heated in a warm water bath, with care taken to avoid boiling the acetone.

Several pretreatment steps are used prepare the digest for iron quantification. The iron digest is first heated to 80 – 90 °C for 30 minutes and a color change to yellow/orange indicates iron oxidation. While maintaining the temperature, 30 % hydrogen peroxide is added dropwise until the solution turns fully yellow. Peroxide destroys the dithionite and citrate complexes, but elemental sulfur will form if peroxide is added too quickly. The solution is then cooled to room temperature and two to three drops from a 5 mL aliquot of 6 M HCl is added. If turbidity appears, the heated peroxide addition step is repeated. If no turbidity occurs, the remaining 6 M HCl is added and the solution is prepared as desired for spectroscopic quantification. UV-visible spectroscopy should not be used because residual dithionite, citrate, and organic matter complexes cause discrepancies, and H_2O_2 reacts with organic spectroscopic reagents.[25,62]

The solid fraction can be prepared for further analysis using washes of organic solvent. Trace sulfur is removed using four washes of 80 – 100 % methanol, followed by three washes of 75 % acetone, and one wash of 100 % acetone and these washes are discarded. For analyses requiring a higher degree of purity, one final wash is performed with perchloroethylene (PCE) heated to 30 – 50 °C.[58] It is important to note that PCE is a carcinogen and vapors are toxic; minimize hazard by using lower temperatures, smaller volumes, and a well-ventilated area, and only perform if acetone washes are inadequate.

When iron-bearing silicates are a target for further analysis, there are special considerations in performing the DCB method because dithionite is capable of reducing

silicate-bound Fe(III).[63,64] Iron reduction does not equate to iron dissolution, but varying degrees of dissolution does occur. For example, nontronite suspended in DCB solution in an anaerobic glove bag for 5 days resulted in 1 – 70 % Fe(III) reduction and up to 35 % iron dissolution, depending on reaction stoichiometries.[63] Similarly, 16 % of the iron residing in nontronite was dissolved when using the DCB reaction conditions recommended herein[25] but has also dissolved up to 30 % under other conditions.[27] Dithionite also causes Fe(III) reduction in smectite and illite, where up to 11 % of Fe(III) was reduced, but the extent of dissolution was negligible.[64] Interestingly, the reduction causes alterations in the layered crystal structure, which is restored by removing residual dithionite and washing the sample with 3 % H_2O_2.[64]

There is some reported uncertainty in the effectiveness of the DCB dissolution method in dissolving iron (oxyhydr)oxides. A method review published in 2006 showed incomplete extraction of iron from various soils and indicated that more iron was extracted using dithionite-citrate-oxalate, ascorbic acid-oxalate,[62] and titanium(III)-citrate-EDTA-bicarbonate.[62,65] There is, however, an important difference in these methods; the DCB method does not target magnetite, while oxalate is effective at magnetite dissolution, as discussed below. In addition, earlier work shows that DCB selectively dissolves ferrihydrite, lepidocrocite, goethite, and akageneite, while its effectiveness at dissolving hematite is a function of both particle size and crystallinity.[25,27,56,58] There are several methods for more complete extractions of iron, but DCB is an effective and selective technique for quantifying the iron present in select iron (oxyhydr)oxides.

Oxidizing Reagents: Targeting Iron Bound by Organic Matter

Organic matter is ubiquitous in natural samples and is formed by the microbial degradation of terrestrial organic materials. Organic matter varies greatly in both concentration and composition and contains many reactive groups that form complexes with dissolved metals like iron and aluminum. Organic matter also forms strong bonds with iron (oxyhydr)oxides, which serve as stabilizers to prevent the rapid disintegration of organic matter by microbial activity.[66] Quantifying the amount of dissolved metals complexed within organic matter is important for assessing the potential for metal leachate if organic matter is oxidized in the environment.[32]

Several methods are reported for breaking apart organic matter for iron quantification and three are presented here. These methods are applicable to either dissolved or solidified organic matter fractions. In one method, concentrated sulfuric acid is added to the specimen, followed by a molar equivalent of concentrated nitric acid.[67] This addition may cause the evolution of toxic NO_2 vapors. The resulting solution is subsequently diluted and the iron quantified.

Another method combines the specimen with 0.1 M sodium pyrophosphate at pH 10, and the resulting suspension is agitated for 16 hours, followed by centrifugation at 40,000 g. After centrifugation, the supernatant is vacuum-filtered using a 0.025 μm filter pre-washed with 0.1 M HCl, then the solution is prepared for iron quantification.[66,68]

A third method combines 3 mL of 0.02 M HNO_3 and 5 mL of 30 % H_2O_2 (adjusted to pH 2 with HNO_3) with the specimen, and the mixture is heated to 85 °C for 2 hours with occasional stirring. An additional 3 mL of the pH-adjusted peroxide solution is added to the mixture and further heated for 3 hours with occasional stirring. After the

solution is cooled to room temperature, 5 mL of 3.2 M ammonium acetate in 20 % (v/v) HNO_3 is added, and the mixture is diluted to 20 mL with ultra-pure water. Ammonium acetate prevents metal adsorption to solids. The mixture is agitated continuously for 30 min and then prepared for iron quantification.[32,35]

The reagents used in these methods are acidic and highly oxidizing, which introduces complications. One complication is that the reagents may dissolve coexisting iron-bearing minerals. Nitric acid, for example, is a component in the dissolution of some silicate and sulfide minerals, as will be discussed in the methods using hydrofluoric acid and acid-chromium reagents, respectively. With samples containing carbonates or (oxyhydr)oxides, less aggressive dissolution methods discussed above should be used to remove those minerals that would otherwise be affected by the more aggressive reagents used in this method.[32] Note that if this method is applied sequentially to the supernatant produced from a dithionite-based treatment, these steps are performed after the full addition of hydrogen peroxide described in the dithionite method.

Another complication is that the native iron oxidation state is not preserved. By nature, organic matter can itself reduce Fe(III) via electron-donating groups, and although Fe(II) does not typically bind with organic matter, it may form in solution after equilibration.[69] The use of oxidizing reagents in this dissolution method preclude oxidation state-specific quantification. For example, nitric acid often contains low levels of nitrous acid, which acts as an oxidizer in ambient conditions.[70] In addition, H_2O_2 has been shown to oxidize iron residing in phyllosilicates, which affects the oxidation state of minerals targeted by more aggressive dissolution methods.[64] Consequently, the sequential

quantification of silicate-bound iron would be limited to total iron, or the analysis could be performed in parallel instead of sequentially.

Oxalic Acid: Targeting Iron Residing in Select (Oxyhydr)oxides

Similar to the DCB method, solutions using oxalic acid also dissolve iron (oxyhydr)oxides. The most common dissolution method is referred to as acid-ammonium-oxalate (AAO) and is often used in conjunction with DCB, where the oxalate-extractable iron (Fe_O) defines the relative abundance of the short-range order (SRO) or amorphous Fe(III) fraction and dithionite-extractable iron (Fe_D) represents the crystalline fraction.[64,71] Considering iron abundance according to crystalline fraction is important for investigating its accessibility to microbial redox activity in sediment[64,72,73] and for determining the environmental conditions present during iron mineral deposition in ancient sediments.[71]

While advantageous in the simplicity of the comparison, the division of fractions according to accessibility may present ambiguity in the identification of mineral phase and does not represent all the iron (oxyhydr)oxides. Mineral phase can be further elucidated with solid-state analyses such as XRD or Mössbauer spectroscopy,[64,71] but other dissolution methods may also assist in both identifying the presence of (oxyhydr)oxide phases and quantifying iron in those phases. For example, using hydroxylamine-HCl and then DCB in sequence allows for the distinction between minerals of low crystallinity (e.g., amorphous Fe(III) and/or ferrihydrite) or with highly accessible structural features (e.g., lepidocrocite) and minerals having greater crystallinity (e.g., akaganeite, goethite, and in some cases hematite). Then in addition, the AAO

method can be used to quantify iron residing in magnetite, which is generally inaccessible by either of the aforementioned dissolution methods.[25]

Magnetite itself is an important mineral that warrants analysis by selective mineral dissolution. Magnetite is reactive towards environmental contaminants,[29,74] is involved in microbial metabolic processes,[75] has magnetic and electronic properties useful for technological applications,[76] and, at 72 mass% iron, is valuable for iron mining. AAO is the most selective method for dissolving magnetite, which rapidly occurs via photoreduction.[22]

Indeed, photochemistry is the driving mechanism for oxalate-assisted redox cycling of iron in atmospheric waters.[77,78] Ideally, the photoreduction of Fe(III)-oxalato complexes (equation 1) results in the generation of two moles of Fe(II) for every mole of oxalate oxidized.

$$2\ [Fe(C_2O_4)_n]^{(3-2n)+} \longrightarrow 2\ Fe^{2+} + (2n-1)\ C_2O_4^{2-} + 2\ CO_2 \qquad (1)$$

Additionally, the presence of oxygen generates H_2O_2 and introduces several new pathways for iron cycling by reactive oxygen species like hydroperoxyl ($HO_2^{\bullet}$), hydroxyl ($HO^{\bullet}$), and superoxide ($O_2^{\bullet -}$), as well as oxalate ($C_2O_4^{\bullet -}$) radicals. These species participate in both reduction and oxidation of dissolved iron, which prevents oxidation-specific iron quantification.[77,78] A selection of these reaction pathways are shown in Figure 1 to illustrate the complexity of the aerobic iron-oxalate redox system.[77]

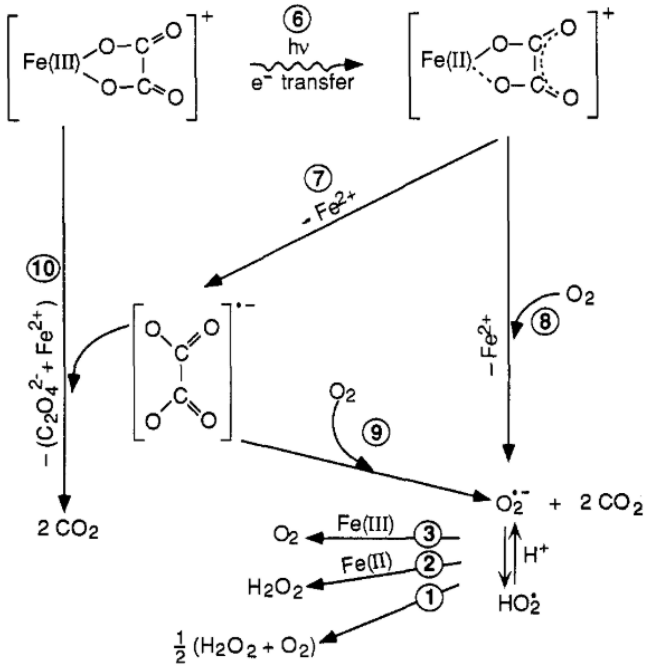

Figure 1.1. Aerobic iron-oxalate redox reaction pathways. Reproduced with permission from Ref. 77 , Copyright 1992 Environmental Science & Technology.

Although some procedures use oxalate to dissolve 'free iron oxides',[55,56,79] dissolution rates of the various iron (oxyhydr)oxides in oxalate solution differ greatly. Under light exposure, ferrihydrite, lepidocrocite, and magnetite reportedly dissolve completely after 6 hours in 0.27 M oxalate at pH 3.2.[25] By contrast, akaganeite released less than 4 % of its total iron, while goethite and hematite released less than 1 %.[25] Another study showed that lepidocrocite dissolved six times faster than goethite.[80] Furthermore, aluminum-substituted goethite (16 % Al), which is common in nature, dissolved 10 % more slowly in 0.025 M oxalate at pH 2.6 than did unsubstituted goethite.[80]

Important insight into the differences in dissolution rates among the various iron (oxyhydr)oxides was achieved by studying the rate of goethite dissolution in the presence

of oxalate and under irradiation.[80] The reaction initially generated only Fe(III) in solution, indicating dissolution via complexation. After a short time, however, Fe(II) and CO_2 were observed in stoichiometries consistent with the reductive dissolution pathway. The complexation step was circumvented by the addition of Fe(II) prior to irradiation, which suggested that Fe(II) acts as a catalyst in the reductive dissolution.[80] This effect of Fe(II) was also observed using sediment containing Fe(III) minerals where the microbial reduction of Fe(III) phases or the addition of dissolved Fe(II) promoted dissolution of iron from the phases otherwise less accessible to microbial reduction and/or oxalate dissolution.[73] Low crystallinity and/or high surface area loading enhance the catalytic effect in ferrihydrite,[81] and, similarly, breaking the hydrogen bonds in the layered structure of lepidocrocite quickly yields far greater surface area from which dissolution occurs.[80] Magnetite exhibits auto-catalytic behavior owing to the presence of structural Fe(II).[82]

An effective dissolution procedure uses 0.2 M ammonium oxalate with 0.17 M oxalic acid at pH 3.2 and room temperature for 6 hours under any light source.[25,67,83] Variations in this procedure have used 0.2 – 0.4 M oxalate at pH 2 – 3 and up to 6 hours of dissolution time.[55,67,83,84] Some studies found that using pH >4 resulted in insufficient buffering and incomplete iron dissolution, whereas the use of pH 2 – 3 resulted in stable pH to within 0.1 pH unit.[55,67] The precipitation of yellow solids indicates the formation of ferrous oxalate, and if such precipitates form, the procedure should be adjusted by intensifying the light source, decreasing the dissolution time, using less specimen mass, and/or increasing solution volume.[80] Because of the reductive dissolution process, oxidation state-specific quantification by UV-visible spectroscopy will not represent the

native oxidation state of iron in the sample. Also note that oxalate may cause interference in iron quantification by UV-visible spectroscopy, as will be discussed in Section 3.

While mineral dissolution with oxalate is often performed using photoreduction, oxalate also dissolves iron (oxyhydr)oxides via complexation when light and oxygen are excluded.[22] By preventing the photoreductive pathway, native Fe(II) and Fe(III) are quantifiable. This quantification is important for magnetite because although magnetite ideally contains a 1:2 ratio of Fe(II):Fe(III), it often occurs non-stoichiometrically with Fe(III) vacancies, with divalent transition metals substituted for Fe(II), or with low Fe(II) content as magnetite undergoes the thermodynamically-favored transition to hematite via maghemite.[22]

To obtain the most accurate Fe(II) to Fe(III) ratio, pretreatment to selectively remove coexisting minerals by physical separation[36] and/or chemical dissolution (e.g., removal of ferrihydrite and lepidocrocite via hydroxylamine) is essential. Then, the dissolution with oxalate is performed under strict anaerobic conditions and without exposure to light. After the desired dissolution time, the sample is filtered and prepared (still anaerobically and without light) with colorimetric reagents for iron detection via UV-visible spectroscopy. The samples are quickly analyzed with minimum light exposure and then returned to the anaerobic environment where they are exposed to light and periodically analyzed until the absorbance has reached a maximum, which indicates that the photoreduction is complete. Finally, the difference obtained by subtracting the initial Fe(II) value from the photoreduced Fe(II) gives the initial Fe(III) concentration, and then the Fe(II):Fe(III) ratio is calculated. Dissolution by complexation with oxalate is

slow and prolonged dissolution time to achieve more complete dissolution is not advised because ferrous oxalate precipitates over time.[80]

With samples containing phyllosilicates, there are some complications in using the AAO method that impact further analysis of those minerals. One complication is that oxalate can dissolve iron-bearing silicates. In a study of smectite-rich sediment, for example, samples treated with DCB to dissolve crystalline iron (oxyhydr)oxides and then with 0.2 M oxalate showed that as much as 70 % of the iron was released as compared to total Fe determined by HF.[71] The release of iron was attributed to the dissolution of trioctahedral smectites, which are reportedly more soluble in oxalate than dioctahedral smectites.[71] Comparatively, the dioctahedral smectite-group mineral nontronite was shown to release <1 % of its iron under the AAO conditions recommended herein.[25]

Another complication with phyllosilicate-bearing samples is that oxalate can permanently alter the coordination environment within the crystal structure of iron-bearing silicates. For example, XRD analyses showed that the crystal structures of smectite and illite were altered by the AAO dissolution method and treatment with H_2O_2 to restore the native iron oxidation state did not reverse the structural alterations.[64] The wide ranging degree of solubility for different silicate minerals and the substantial structural impacts effected by the various dissolution methods warrants further investigation.

Hydrochloric Acid: Targeting Iron Residing in (Oxyhydr)oxides

Iron (oxyhydr)oxides are ubiquitous soil constituents and their dissolution provides insight into iron cycling, specifically, nutrient availability, iron mobility, and mineral phase transformations.[24] Protonation dissolves iron (oxyhydr)oxides,[22] and HCl has been used as an effective dissolution reagent.[24,85–89] The chloride ion assists acidic dissolution through the formation of Fe – Cl surface complexes that weaken the Fe – O bond, as evidenced by increased dissolution rates with additional Cl^- as compared to added ClO_4^-, which does not form surface complexes with Fe(II) sites.[86,88]

Iron (oxyhydr)oxide dissolution rates vary with particle size and structural differences. One study reported dissolution rates that span three orders of magnitude ($0.03 – 6.4 \times 10^4$ g Fe dissolved/m^2/hr), with the dissolution rate of lepidocrocite > magnetite > akaganeite > maghemite > hematite > goethite in 0.5 M HCl at 25 °C.[86] In lepidocrocite, the mechanism proceeds by separation of the layered crystal structure connected by hydrogen bonds that exposes a high surface area to protonation.[24,80] Akaganeite is structurally-related to lepidocrocite, except that the hydrogen-bonded plane is replaced by double linkages of octahedra that form hollow channels along the c-axis.[22,24] The channels are stabilized by adsorbed Cl^- ions, but dislodging the Cl^- ions exposes higher surface area to protonation.[24] In magnetite, structural Fe(II) promotes dissolution, owing to the weaker Fe(II) – O bonds.[86] Comparatively, Fe(II) vacancies in maghemite are less susceptible to acid attack.[86] Hematite is more dense than maghemite, with iron occurring only in octahedral sites and without Fe(II) vacancies, further reducing the susceptibility to protonation.[86] In hematite, screw dislocations often occur at the (001) facet and are particularly susceptible to acid attack, yielding hollowed platelets during

dissolution, but all facets are otherwise equally etched by acid.[85] Goethite is related to lepidocrocite but lacks the hydrogen-bonded channels that grant access to the structural interior, thereby inhibiting dissolution.[86] Goethite dissolution occurs most quickly at acicular tips, forming channels that become holes bound by {210} (space group Pbma), and twin boundaries are especially susceptible to dissolution.[22,87]

Dissolution methods with HCl typically use concentrations ranging from 0.5 to 6 M at 25 – 60 °C,[86,90] and the use of concentrated HCl is less common.[27] In a method comparison, only ferrihydrite and siderite had near-complete dissolution after 24 hours in 1 M HCl at room temperature, whereas boiling in concentrated HCl for two minutes dissolved >90 % of each ferrihydrite, siderite, lepidocrocite, goethite, hematite nanoparticles, and magnetite.[27] In another comparison, FeS species were soluble in both room temperature 0.5 M HCl and hot 6 M HCl, but FeS_2 was not soluble under either condition.[31] Ilmenite dissolution has been studied under several conditions and 100 % dissolution was reported when using 6 M HCl at 75 °C for 250 minutes (acid-to-ilmenite mole ratio of 692:1), but procedures using HCl have more commonly reported 30 – 80 % dissolution.[91]

One complication with the HCl method is that iron forms several chloro complexes in the presence of high concentrations of chloride (>0.5 M).[92] These complexes may interfere with quantification of iron in its native oxidation state by preventing complexation with spectroscopic ligands and/or by shifting the equilibrium of Fe(II) and Fe(III) speciation. While sample acidification is often used to stabilize Fe(II) in solution and prevent the precipitation of Fe(III), preparations using HCl should

consider the effects of concentration and dissolution time on the iron oxidation state and use independent methods to support quantification results.

Samples containing silicates and sulfides present challenges for quantifying the iron (oxyhydr)oxide content because several iron sulfides are soluble under similar conditions. With silicates, for example, boiling 12 M HCl is reported to dissolved 31 % of nontronite, 41 % of chlorite, 20 % of biotite, and 12 % of glauconite.[27] With sulfides, 1 M HCl at room temperature dissolved 100 % of amorphous iron sulfide, 92 % of mackinawite, and 40 – 67 % of greigite, with similar results reported for 6 M HCl.[44] Analyzing such samples may require a combination of sequential and parallel extraction methods in addition to solid state characterization techniques to determine from what phase the measured iron is extracted.

Hydrofluoric and Other Acids: Targeting Iron Residing in Silicates

Silicates are an important fraction of minerals involved in both abiotic and microbially-assisted cycling of elements. Sediments often contain a large fraction of silicates, providing information about microbial communities and environmental conditions that is stored in geologic record through diagenesis.[93] The analysis of silicates has elucidated intricacies of natural weathering processes, such as the preferential transport of light iron isotopes from silicate to oxide phases, a process that is assisted by organic ligands in soil.[94] Several microbes that metabolize iron residing in phyllosilicates have been identified in sediment,[95] some of which are capable of reducing iron in both (oxyhydr)oxide and phyllosilicate phases.[96] Understanding the conditions under which

this bioreduction occurs assists investigations of other processes such as pollutant remediation[97] or nutrient exchange in plants.[95]

Several concentrated acids (or a combination thereof) are used in silicate dissolution methods, including hydrofluoric (HF), perchloric ($HClO_4$), sulfuric (H_2SO_4), nitric (HNO_3), and/or hydrochloric (HCl), and HF is the most common dissolution reagent. Note that many of these acids present substantial hazards and safe use may require the installation of special precautionary measures.

Perchloric acid and HF are used in several method variations for silicate dissolution. One method uses a 5:1 mixture of HF:$HClO_4$ that is added to the sample and evaporated to near dryness, followed by another 10:1 mixture that is again evaporated to dryness. Finally, an aliquot of concentrated $HClO_4$ is added and evaporated until white fumes appear, after which the residue is dissolved in concentrated HCl, diluted 25-fold, and analyzed by atomic absorption spectroscopy.[32] Another version uses a 2:2:3 mixture of HNO_3:HF:$HClO_4$ autoclaved at 180 °C for 6 hours, evaporated to dryness, re-dissolved in diluted HNO_3, again autoclaved overnight, then filtered for spectroscopic quantification.[93] Methods using $HClO_4$ are highly hazardous because the fumes precipitate as perchlorate salt on nearby surfaces and inside ventilation systems. This flammable and highly explosive residue is triggered by heat, shock, and exposure to other chemicals. Work with $HClO_4$ requires a chemical fume hood designed to handle perchlorate salts.

Methods using HF and H_2SO_4 are most commonly used to probe iron oxidation state in silicates. One version uses a 2:1 mixture of 9 M H_2SO_4 and concentrated HF boiled for 5 minutes, followed by the addition of an H_3PO_4 and H_3BO_3 solution (5 mL 7

M H_3PO_4 + 250 mL 0.5 M H_3BO_3) to remove excess HF, and then stored in the dark to preserve samples while awaiting voltammetric measurement of the Fe(II) and Fe(III) oxidation states.[93,98,99] Another version uses a mixture of 1 mL concentrated HF, 12 mL of 1.8 M H_2SO_4, and 2 mL of 10% 1,10-phenanthroline under red light or darkness to preserve the iron oxidation state.[100] Iron oxidation is observed in dissolutions using only HF because the Fe(III)-fluoride complex is strongly favored, causing a shift in equilibrium.[101] This phenomenon is prevented by the addition of 1,10-phenanthroline and H_2SO_4.

More recently, a method was developed to quantify iron residing refractory minerals that are otherwise difficult to dissolve and quantify by established silicate dissolution methods, such as spinels.[101] The digest solution contains HF and silver fluoride (AgF), where AgF is an important component that enables Fe(II) quantification by oxidimetry. In this method, 40 mg of the spinel (containing < 32 mg Fe) is massed into a 7 mL perfluoroalkoxy (PFA) vial and transferred to a N_2 chamber. Under reduced lighting, 6 mL of a solution containing 0.030 M AgF in 48 % HF is added to the sample, which is then capped, placed in a 98 °C sand bath, and incubated under darkness for 48 hours. Once the sample is dissolved, Fe(II) is determined by oxidimetry with $HONH_2$, H_3BO_3, and KBr and total Fe is determined by colorimetry with phenanthroline and sodium citrate. Given the completeness of this dissolution and the high degree of accuracy and precision in quantifying both Fe(II) and total iron, this is a valuable method for accessing iron in silicates.[101]

Complications with HF include the interference of fluoride in UV-visible spectroscopic analyses.[100,102] Using HF also requires special preparation to minimize

hazards. HF readily penetrates skin, which may not present symptoms for hours and can damage tissues for days if left untreated. Severe exposure of HF can result in death. Calcium gluconate gel should be nearby for immediate application to any skin that comes into contact with any HF solution.

For those wishing to avoid HF, a different silicate dissolution method is available that reports >96 % iron extraction.[25,43] In the procedure, specimens are heated to 450 °C for 8 hours to produce an ash residue, which is then boiled in 6 M HCl for 24 hours.[43] The filtered iron extracts are quantified by either UV-visible or atomic absorption spectroscopy (AAS).[43,48]

Acid – Chromium: Targeting Iron Residing in Sulfides

Iron and sulfur cycling in the environment are closely related. Sulfate enters surface waters through oxidation of sulfur-bearing minerals like pyrite (FeS_2) or wastewater effluents and diffuses into sediments.[45,47] In the absence of oxygen, sulfate-reducing bacteria produce hydrogen sulfide (H_2S) that reacts with Fe(II) and iron (oxyhydr)oxides to produce iron sulfide minerals along with elemental sulfur and other species.[48,103–105] Iron sulfides are important for investigating sulfide toxicity to aquatic life,[105] the impact of acid mine drainage,[106] and the information retained in geological record,[107] and have applications in electronics[108] and in engineered systems designed to prevent contaminant transport.[45] Because S(II) reduces Fe(III), most natural environments with large quantities of S(II) have little Fe(III), except near redox transition zones. As such, most methods for quantifying iron in sulfidic environments do not differentiate between Fe(II) and Fe(III).

Acid-volatile sulfide (AVS) is a widely-used technique for quantifying sulfur species and is sometimes used to quantify Fe(II) from FeS. The AVS method has several variations that generally involve combining the solid specimen with HCl (1 M – 12 M), pushing inert gas (e.g., N_2) through the vessel and into a solution that captures $H_2S_{(g)}$ (e.g., zinc acetate buffer solution[109]), then equilibrating the specimen for 15 min – 4 hrs at a selected temperature (e.g. room temp to boiling).[31,103,110] The dissolved iron in the acid solution is then quantified. This method, however, also etches iron-bearing carbonates, iron (oxyhydr)oxides, and pyrite, and may not fully dissolve mackinawite or greigite, therefore precluding AVS for the selective quantification of iron residing in sulfides.[110]

Instead, iron residing in iron sulfides is quantified using a two-part sequential extraction technique using acid and Cr that selectively liberates the more soluble sulfur species before dissolving highly-insoluble pyrite.[31,111] The acid-Cr method is highly effective at sulfide dissolution, extracting 100 % of amorphous FeS, 100 % of mackinawite, 100 % of greigite, up to 100 % of synthetic pyrite, and >87 % of natural pyrite.[31,44] Iron sulfide extraction should follow other dissolution methods that selectively remove iron-bearing carbonates and iron (oxyhydr)oxides.

In the first part of the acid-Cr method, FeS, S^0, SO_4^{2-}, and ester SO_4^{2-} are removed. An acidic mixture containing 150 mL of 57 % hydroiodic acid (HI), 32.5 mL of 50 % phosphinic acid, and 75 mL of 97 % formic acid is heated to 115 °C for 30 minutes in low light and under anaerobic conditions (HI reacts with oxygen).[31] Then 1 – 3 g of the finely-ground specimen and 8 mL of the acid mixture are combined under N_2 and boiled for 1 hour and evolved H_2S is captured with zinc acetate solution. The solids are separated from solution using vacuum filtration then washed with a known volume of

ultra-pure water, which is then added to the filtrate. Dissolved iron in the filtrate is best quantified using AAS or inductively coupled plasma – mass spectrometry (ICP-MS) or – atomic emission spectroscopy (ICP-AES).

In the second part, the chromium reagent is freshly prepared to avoid oxidation that would otherwise limit its use as a reducing agent. First, zinc granules are amalgamated with 2 % $Hg(NO_3)_2$ and packed into a column, and then the chromium reagent is prepared by dissolving $CrCl_3$ in 0.5 M HCl to yield a 1 M Cr(III) solution. The solution is passed through the Zn column under vacuum and should turn from green to blue, indicating the reduction to Cr(II). The solids from the first extraction are then combined with 2 mL of ethanol, 12 mL of the chromium reagent, and 3 mL of 12 M HCl under N_2 and boiled for 1 – 2 hours and evolved H_2S is again captured using a zinc acetate solution. The residue and solution are separated using vacuum filtration, the solids washed with a known volume of ultra-filtered water, and the solution prepared for iron quantification.[112]

Several other methods are also available for dissolution of iron sulfides. Some have reported using concentrated HNO_3 or aqua regia (3:1 mixture of HCl:HNO_3) for pyrite dissolution.[103,111] Nitric acid is a strong oxidizing agent, which produces Fe(III) from pyrite dissolution.[113] Using this method involves adding nitric acid to the mineral sample and agitating for up to 2 hours while capturing the evolved H_2S using zinc acetate solution, then diluting with ultra-filtered water and filtering the solution for iron quantification via AAS or ICP-AES[111] Note, however, that toxic NO_2 gas may evolve. Some sulfides are dissolved to varying degrees by other methods including acetate and HCl, as previously discussed.[27,31,44,110]

Guide for Selecting Extraction Procedures to Target Specific Mineral Fractions

The most important consideration in choosing an extraction technique or series of extractions is mineral selectivity; in other words, the extraction should target only the mineral or fraction of interest while leaving the other mineral components relatively intact. Unfortunately, no iron extraction method provides perfect selectivity, as seen in Table 1. This table summarizes the degrees of mineral dissolution for each method presented in Section 2, generally organized from least aggressive to most aggressive method. Table 1 shows that even the less-aggressive dissolution methods, such as the acetic acid method that is typically used to dissolve carbonates, will facilitate substantial dissolution in other mineral fractions, such as iron sulfides. Because no dissolution method is perfectly selective, it has been suggested that extracted iron is labeled as a product of the dissolution method rather than as originating from a targeted phase (e.g., 'acetate-extractable Fe' rather than 'Fe residing in siderite').[114] The fraction of extracted iron is therefore 'operationally defined'.[114,115] Such a labeling scheme avoids placing an unwarranted degree of certainty on the identification of the iron source. Using several dissolution methods in conjunction with solid-state characterization methods improves phase identification but cannot eliminate ambiguity in phase origin.

Table 1.1. A summary of the mineral targets for each major dissolution technique, coded according to extent of dissolution: target dissolution is 100 – 90 % (black), moderate is 80 – 50 % (grey), low is 50 – 15 % (diagonal lines), marginal is 15 – 2 % (horizontal lines), and minor is < 2% (dots), as determined by studies described in the dissolution methods of Section 2. Unmarked boxes indicate the absence of data for the degree of dissolution.

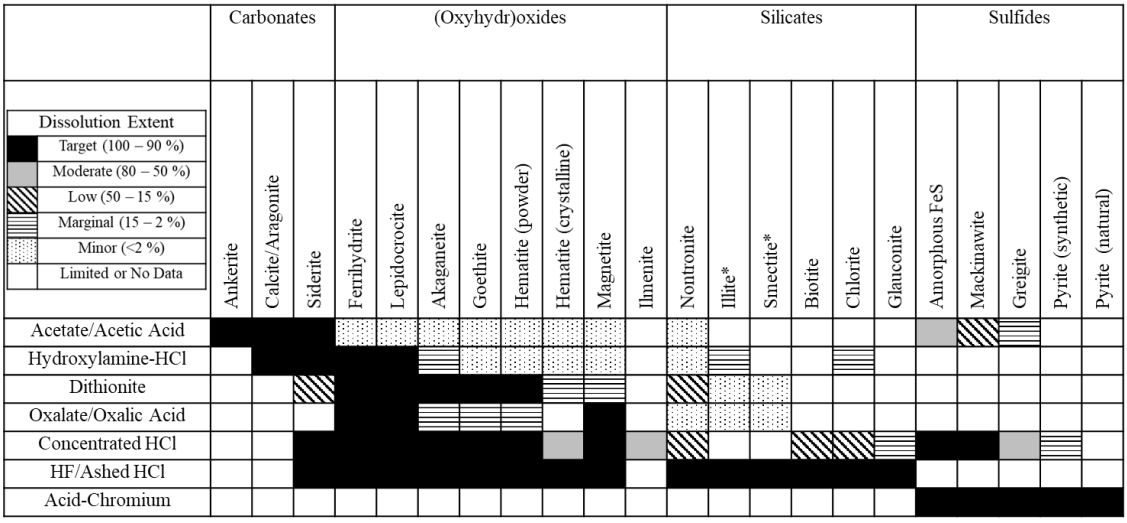

*These minerals exhibit Fe(III) reduction and structural deformation when exposed to dithionite and oxalate, which is reversed by washing with H_2O_2 in the dithionite system but is irreversible in the oxalate system.[64]

Several publications have outlined procedures using various dissolution methods and solid-state characterization techniques for the classification of iron-bearing components in sediment and soil.[25,31,32,66,111,114,116,117] Many of these procedures include sequential extractions, where the dissolution methods progressively become more aggressive to remove iron-bearing minerals. Other procedures use parallel extractions and use the calculated difference to quantify iron extracted from a specific fraction.

Most recently, Poulton and Canfield (2005) proposed an extraction sequence for iron classification in sediments.[25] They emphasized this method sequence in terms of dissolution reagent and suggested the targeted iron-bearing phase: magnesium chloride for exchangeable iron; acetate for carbonate-bound; hydroxylamine-HCl for ferrihydrite

and lepidocrocite; dithionite for akaganeite, goethite, and hematite; oxalate for magnetite; concentrated HCl for poorly reactive sheet silicates; acid-chromium for pyrite; and ashing followed by HCl for total iron. Tessier et. al. (1979) applied a similar iron extraction sequence to fluvial sediments but instead described the sequence in terms of the iron-bound fraction: exchangeable (by $MgCl_2$), bound to Fe-Mn oxides (by dithionite), bound to organic matter (by H_2O_2), and residual iron (by HF).[32] Note that although this list is appears to classify iron according to the targeted phase, the researchers still discuss complications with mineral selectivity and suggest complementary measures such as elemental analysis to determine the extent of untargeted mineral dissolution.

Miller et. al. (1986) proposed an eight-step procedure for Fe, Cu, and Mn extraction from soils.[115] While the article states the importance of using extractions by the operational definition, their recommended procedure may lead to misidentification of the iron source because of the emphasis on target descriptions. For example, they suggest first targeting Mn oxides with hydroxylamine-HCl, followed by 'amorphous Fe oxides' with oxalate under darkness, and finally 'crystalline Fe oxides' with hot oxalate under irradiation. As previously discussed, however, hydroxylamine-HCl used in the first step dissolves SRO Fe oxides, which are the intended target in the second step in this suggested sequence. The proposed extraction for Mn oxides is relatively quick (30 minutes) and is reported elsewhere as an efficient dissolution method for the target phase,[49,118] but these same studies report the co-dissolution of SRO Fe oxides without independently testing the dissolution extent with pure materials. The proposed sequence likely results in partial dissolution of SRO Fe oxide in step 1, which is completed in step 2 (potentially alongside partial magnetite dissolution), and then followed by the more

intensive iron (oxyhydr)oxide dissolution in step 3. This provides a good example of the importance of using pure minerals to evaluate the selectivity and extent of dissolution methods.

La Force and Fendorf (2000) propose an eight-step extraction sequence for soil that uses a combination of extraction techniques proposed by Tessier (1979) and Shumer (1985).[32,117,119] The procedure suggests the sequence: magnesium chloride for exchangeable iron, sodium hypochlorite for iron bound by organic matter, acetate for carbonates, hydroxylamine-HCl with HNO_3 for Mn oxides, oxalate under darkness for SRO oxides, hydroxylamine-HCl with acetic acid for crystalline Fe oxides, potassium perchlorate with HCl and HNO3 for sulfides, and finally HF with HCl and HNO_3 for residual iron.[117] Note that this procedure has the same issue regarding SRO Fe oxide dissolution as the procedure proposed by Miller et. al. (1986). Additionally, they report that the use of hydroxylamine-HCl with acetate in this manner likely underrepresents the iron associated by crystalline iron oxides.

Sequential dissolutions like those discussed above are not required. Indeed, parallel dissolutions are also used to determine iron bound in various fractions, as calculated by difference. For example, Heron et. al. (1994) reported on iron extraction from natural and synthetic minerals using both sequential and parallel dissolution treatments.[31] In their reported procedure, the sequential extractions with HI/H_3PO_2/formic acid solution followed by acid-Cr solution were used to quantify iron residing in FeS and FeS_2, respectively. In parallel, they also performed separate dissolutions using $CaCl_2$, sodium acetate, 0.5 M HCl, 5 M HCl, 6 M boiling HCl, ammonium oxalate under darkness, DCB, and Ti-EDTA solution. Owing to the concurrent dissolution of various

carbonates and (oxyhydr)oxides for most methods, they report difficulties in phase identification. They also encountered difficulties dissolving siderite and magnetite, both of which are explained by their chosen conditions; sodium acetate at pH 5 and room temperature is insufficient to dissolve highly crystalline siderite originating from natural rock, and complete magnetite dissolution using oxalate requires light exposure.[25] Because of the varying levels of mineral selectivity, sample composition should influence decisions of parallel versus sequential extraction procedures.

Critical Analysis of Select Dissolution Methods

Four dissolution methods described herein were tested in parallel to determine their efficacy, including the dissolution by acetate buffer, hydroxylamine-HCl, oxalate buffer under darkness, and concentrated HCl. Eleven natural or synthetic reference minerals were used in these experiments and are listed in Table 2, along with their abbreviations, ideal formula, and stoichiometric iron content (mg Fe/g sample). X-ray diffraction patterns for each are provided in supplemental information as Figures S1 – S9.

Table 1.2. Reference mineral specimens used in several parallel dissolution procedures to compare method selectivity and degree of dissolution.

Mineral	Distinguishing Features	Abbreviation[a]	Formula	Stoichiometric Fe (mg/g sample)
Quartz		Qz	SiO_2	0
Kaolinite		Kln	$Al_2Si_2O_5(OH)_4$	0
Olivine	approx. Fo_{90}:Fa_{10}	Ol	$(Mg,Fe)_2SiO_4$	approx. 75
Siderite	brown	B-Sd	$FeCO_3$	483
Siderite	white	W-Sd	$FeCO_3$	483
Ilmenite		Ilm	$FeTiO_3$	369
Magnetite		Mag	$Fe^{II}Fe^{III}_2O_4$	725
Ferrihydrite	4 nm, 6-line	4 nm 6L-Fh	$Fe_2O_3 \bullet 0.5H_2O$	661
Ferrihydrite	6 nm, 6-line	6 nm 6L-Fh	$Fe_2O_3 \bullet 0.5H_2O$	661
Goethite	synthetic, nano, acicular	S-Gth	α-FeOOH	630
Hematite	synthetic, nano, rhombohedral	S-Hem	α-Fe_2O_3	701

[a]Mineral abbreviations are based on standardized nomenclature. Ref 120.
See SI for specific mineral origins.

Experimental details of the extractions are provided in supplemental information and the results are summarized in Table 3. For our purposes, the dissolution with concentrated HCl represents total extractable iron, and the results are compared to the ideal mineral stoichiometries to yield a theoretical dissolution extent (% of stoic.). Dissolution extent (% dissolved) from less aggressive dissolution methods is calculated by dividing the total iron (Fe(tot)) extracted in that method by the Fe(tot) extracted by the HCl method then multiplying by 100.

Table 1.3. Results showing the quantity of iron extracted from various reference mineral specimens (in mg of Fe/g of specimen) from parallel dissolution experiments using acetic acid buffer, hydroxylamine-HCl, oxalic acid buffer in darkness, and concentrated HCl. Dissolved % for each method is calculated as Fe(tot)/HCl Fe(tot). The HCl method represents total extractable iron and the HCl Fe(tot) is compared with the stoichiometric iron content in each mineral to yield '% of Stoic.' Refer to Table 1 for mineral abbreviations.

		Qtz	Kao	Ol	B-Sd	W-Sd	Ilm	Mag	4nm 6L-Fh	6nm 6L-Fh	S-Gth	S-Hem
Acetate	Fe(II)	0	0	7 ± 1	207 ± 9	150 ± 12	0	0	0	0	0	0
	Fe(III)	0	0	1.9 ± 0.4	0.3 ± 0.1	6 ± 5	0	0	2.6 ± 0.7	0	0	0
	Fe(tot)	0	0	9.2 ± 0.7	205 ± 7	153 ± 7	0	0	2.6 ± 0.7	0	0	0
	% Dissolved	N/A	N/A	24	50	40	0	0	0.4	0	0	0
Hydroxylamine-HCl	Fe(tot)	0	0	19.1 ± 0.3	327 ± 7	211 ± 2	1.5 ± 0.2	8 ± 2	653 ± 22	690 ± 11	22.8 ± 0.1	6.4 ± 1.2
	% Dissolved	N/A	N/A	50	78	54	2	1	114	112	4	1
Oxalate (dark)	Fe(II)	0	0	6.3 ± 0.1	86 ± 11	77 ± 5	0	60 ± 6	0	0	0	0
	Fe(III)	0	0	0.14 ± 0.01	0	2 ± 3	1.8 ± 0.2	172 ± 11	350 ± 10	360 ± 23	103 ± 8	92 ± 15
	Fe(tot)	0	0	6.4 ± 0.1	86 ± 11	78 ± 4	1.8 ± 0.2	232 ± 9	350 ± 10	360 ± 23	103 ± 8	92 ± 15
	% Dissolved	N/A	N/A	17	21	20	2	40	61	58	18	13
HCl(conc)	Fe(II)	0	0	27 ± 2	317 ± 17	254 ± 18	17 ± 3	135 ± 17	0	0	0	0
	Fe(III)	0	0	11.5 ± 0.9	104 ± 4	137 ± 18	70 ± 4	450 ± 19	575 ± 1	618 ± 17	587 ± 9	695 ± 10
	Fe(tot)	0	0	38 ± 1	418 ± 16	391 ± 8	87 ± 1	585 ± 10	575 ± 1	618 ± 17	587 ± 9	695 ± 10
	% of Stoic.	N/A	N/A	N/A	87	81	24	81	87	94	93	99

In general, the dissolution results agree with ideal mineral compositions and show comparable extents of dissolution to those stated in Table 1. The concentrated HCl method completely dissolved siderite, ferrihydrite, goethite, and hematite, as determined by visual inspection using a laser pointer, which showed no indication of light scattering in those vials. Quartz, kaolinite, olivine, and ilmenite had substantial particle residues at

the time of sampling, which is unsurprising based on their anticipated solubilities. The natural magnetite specimen had a few grains of particle residue at the time of sampling, which may be a result of impurities in the sample or fractions of higher crystallinity. The iron extracted from synthetic hematite nanoparticles was 99 % that of the calculated ideal stoichiometry. Both siderite specimens, both ferrihydrite specimens, and the goethite specimen were all found to have released >80 % of the stoichiometric iron. The reduced mass percent of iron observed in natural siderite specimens may be a consequence of metal substitution or the presence of other mineral phases. In synthetic ferrihydrite and goethite, however, this deviation is indicative of chloro complexes preventing ferrozine complexation necessary for quantification by UV-visible spectroscopy. Indeed, this explanation is supported by results from the hydroxylamine-HCl method, where approximately 15 % more iron was detected in both ferrihydrite samples, as compared to the concentrated HCl method.

The method using hydroxylamine-HCl effectively dissolved ferrihydrite as hypothesized, and there was no observable laser light scattering at the time of sampling. This method also dissolved a substantial fraction of brown and white siderite, at 78 and 54 % of iron, respectively, as compared to the total liberated by concentrated HCl. Hydroxylamine-HCl is reported to dissolve iron (oxyhydr)oxides other than ferrihydrite to only a minor extent, which is supported by our results where 2 % of the iron in ilmenite, 1 % in magnetite, 4 % in goethite, and 1 % in hematite was liberated, as compared to dissolution by HCl. Considering that ilmenite and magnetite are natural samples, it is reasonable to hypothesize that the iron liberated in this method originates from SRO coatings on the mineral surfaces that result from natural oxidation. This

hypothesis is supported by the results from the method using oxalate buffer under darkness, where an equivalent amount iron was liberated and it was only found as Fe(III).

The oxalate method performed under darkness is important for assessing the Fe(II) and Fe(III) oxidation states in each of these minerals. In magnetite, the ideal ratio of Fe(II):Fe(III) is 0.5, but the results here indicate a ratio of 0.35 as determined by dissolution in oxalate and 0.3 by dissolution in concentrated HCl. This difference is not likely from SRO oxide coatings because hydroxylamine-HCl dissolved only 1 % of the Fe(tot) as compared to HCl. Instead, the Fe(II) deficiency in this material (originally beach sand) likely stems from the thermodynamically-favored maghematization process.[22] Dissolution by oxalate is slow under darkness and no reference mineral achieved 100 % dissolution. Both 2-line and 6-line ferrihydrite dissolved to the greatest extent, at circa 60 % iron dissolution, as compared to that by HCl. The next greatest was magnetite at 40 %, then siderites at circa 20 %, and goethite and hematite at 18 % and 13 %, respectively. Goethite and hematite contained only Fe(III), as predicted by the ideal structure formula, and brown siderite contained only Fe(II), but 4 % of the iron extracted from white siderite was in the oxidized form. As natural specimens, minor oxidation in these siderite samples may be expected.

Comparing the oxidation state-specific results from siderite samples, dissolution by concentrated HCl showed that 25 % and 35 % of the iron residing in brown siderite and white siderite, respectively, was in the oxidized form. By contrast, 4 % and <1 % of the iron liberated from white siderite and brown siderite, respectively, was in the oxidized form in the dissolution using acetate buffer. There was, however, substantial particle residue at the time of sampling in the vials containing siderite and acetate buffer.

Although acetate is expected to target carbonates, only 50 % and 40 % of the iron residing in brown and white siderite were released, respectively, as compared to dissolution by HCl. The procedure previously recommended by Poulton and Canfield (2005) indicated that two days were sufficient for complete siderite dissolution, but our results, collected after four days of heating at 55 °C, show that this procedure is insufficient. The degree of crystallinity is known to strongly influence the results of this dissolution method, and that may explain the results here, especially considering both of these samples originated from bulk mineral samples > 1 cm in diameter before being ground to powder. Besides siderite, less than 1 % of 4 nm ferrihydrite dissolved in acetate, but no iron was detected from the 6 nm ferrihydrite specimen or from other (oxyhydr)oxides.

Interestingly, acetate buffer liberated Fe(II) and Fe(III) from the olivine specimen, where Fe(III) may originate from SRO (oxyhydr)oxides caused by natural weathering. Of the iron liberated from olivine, which ideally bears only Fe(II), 76 % was Fe(II) in the acetate method, 98 % was Fe(II) in oxalate, and 71 % was Fe(II) in concentrated HCl. Because the dissolution using oxalate preferentially dissolves Fe(II), the higher amount of Fe(II) found in oxalate buffer is not surprising. Because of the variation in iron content of natural olivine samples, more studies of olivine dissolution are warranted.

While quartz is expected to be insoluble in all these solutions, the sheet silicate kaolinite may dissolve somewhat in concentrated HCl, similar to other sheet silicates listed in Table 1. Still, no iron was liberated from either quartz or kaolinite, which served as negative controls in these experiments.

Section 3: Dissolved Iron Quantification

The most common techniques for dissolved iron quantification include UV-visible spectroscopy, atomic absorption spectroscopy (AAS), and inductively coupled plasma mass spectrometry (ICP – MS) or atomic emission spectroscopy (ICP – AES). Voltammetry,[121] oxidimetry,[101] ion chromatography,[122] chemiluminescence,[123] and fluorimetry[124] are also used and a review of several of these techniques for iron quantification is available.[92] Instrument combinations, such as coupling spectrophotometry and AAS, are a valuable way to simultaneously detect two quantities (e.g., Fe(II) and total Fe) using the same sample injection.[125–127] UV-visible spectroscopy is a leading method for iron quantification because it is relatively inexpensive, simple, and can access Fe(II) and/or Fe(III) via colored complexes. This review will therefore focus on common colorimetric reagents for UV-visible spectroscopy and methods for quantifying both Fe(II) and Fe(III).

The formation of colored complexes for iron quantification by UV-visible spectroscopy, also known as colorimetry, is most often reported using thiocyanate,[58,128–130] dihydroxybenzene derivatives,[131] or ferroin-bearing organics.[132–134] The need to quantify low levels of iron in natural waters as well as in numerous concurrent samples has driven development of better colorimetric reagents.[134] Preferred colorimetric ligands selectively form strong iron complexes that are not inhibited by other species in solution and that have high molar absorptivity, are stable in a wide pH range, are soluble in water, and can participate in redox reactions (e.g., photoreduction or chemical reduction) to

facilitate the quantification of total iron. Short sample preparation times are also desirable.

Colorimetric methods are generally performed three ways: (A) quantifying total iron from completely oxidized or reduced samples, (B) simultaneously quantifying Fe(II) and Fe(III) complexes using different wavelengths, or (C) sequentially quantifying each oxidation state. The sequential quantification requires four steps: (1) quantifying $Fe(II)_{initial}$, (2) reducing Fe(III) to Fe(II), (3) quantifying $Fe(II)_{total}$, and (4) subtracting $Fe(II)_{initial}$ from $Fe(II)_{total}$ to yield $Fe(III)_{initial}$.

Potassium Thiocyanate

Potassium thiocyanate (KSCN) has been used for over a century to quantify total iron.[70,76,129] Fe(III)-thiocyanate is a red complex with a maximum absorbance at 480 nm[76] and is stable at pH 0 – 2.5.[128] The most recent reports using the thiocyanate method first digest iron with 6 – 12 M HCl and then oxidize Fe(II) with 1 % H_2O_2. The colored complex is formed with the addition of 1 – 5 % NH_4-SCN or KSCN, and the absorbance is subsequently measured.[76,135]

There are several complications using the thiocyanate method. Some procedures recommend digestion using HNO_3 because HCl preserves Fe(II) and H_2SO_4 does not completely oxidize Fe(II).[70] Nitric acid, however, contains NO_2^- that produces an interfering red complex upon addition of NH_4SCN, but the addition of H_2O_2 both removes NO_2^- and promotes Fe(II) oxidation.[70] Sometimes $KMnO_4$ is used as a supplementary oxidizing agent, but the reagent reportedly introduces interfering species and may be contaminated with iron, and should therefore be avoided.[70,129] Other

interfering species include Sn(II), Mo(VI), Co(II), V(IV), Mn(II), Ni(II), Cu(II), and Ag(I), but most common anions including citrate, oxalate, sulfite, fluoride, and phosphate do not reportedly interfere.[128]

While the thiocyanate method is simple, the detection limit for the iron-thiocyanate complex is higher than for other iron complexing reagents. A recent study, for example, developed two flow injection spectrophotometric methods for iron quantification and compared colorimetric reagents thiocyanate and ferrozine. Ferrozine had a lower detection limit in both methods, and the most sensitive method achieved LODs of 0.05 μg/L for ferrozine and 0.52 μg/L for thiocyanate.[136]

Substituted Ortho-Dihydroxybenzenes

Iron-complexing reagents are often large organic molecules containing functional groups that bind strongly to iron and are highly conjugated, which means they absorb light in the visible region. Substituted ortho-dihydroxybenzenes are one type of these reagents. For example, disodium-1,2-dihydroxybenzene-3,5-disulfonate (DHBD) has been used for Fe(III) quantification. The Fe(III)-DHBD complex is red at pH >7, violet at pH 5.7 – 6.5, and blue at pH <5.[131] The red complex has a 1:3 ratio of Fe(III):DHBD and has the highest molar absorptivity in the series, while the blue complex does not display a stable complexation ratio and has the lowest molar absorptivity.[131] Samples prepared with this reagent are slow to reach full complexation, exhibiting a 5 % increase in absorption 18 hours after preparation.[131] Such variations preclude the use of DHBD as a reliable and efficient colorimetric reagent.

Ferroin-Bearing Reagents

The ferroin group, R–N=C–C=N–R', has long been recognized as an effective Fe(II) complexing agent. Several molecules containing this functional group form stable and highly-colored Fe(II) complexes that are suitable for colorimetric Fe(II) quantification (Table 4).[102,132,133]

Table 1.4. Properties of common chelators used for iron quantification by UV-visible spectroscopy that contain the ferroin group. Properties include the logarithm of the bis or tris formation constant (β_2 or β_3) and forward rate constant (k_f), the negative log of the acid dissociation constants (pK_1 and pK_2), the molar absorptivity (ε_{max}), and the wavelength of maximum absorption (λ_{max}).[102,133,134,137–142]

Colorimetric Ligand	log β_2	log β_3	log k_f ($M^{-1}s^{-1}$)	pK_1	pK_2	ε_{max} ($M^{-1}cm^{-1}$)	λ_{max} (nm)
2,2'-Bipyridine		17.2[f]	13.1[f]	4.33	-	8700	522
1,10-Phenanthroline		21.4[f]	17.4[f]	4.96	-	11,100	512
Bathophenanthroline[a]		21.8[f]		4.84	-	22,100	533
TPTZ[b]	11.0[g]			2.19	3.40	22,600	593
Ferrozine[c]		15.7[f]	11.5[f]	3.2	-	27,900	562
PPDT[d]						28,700	561
Terosite[e]						30,200	583

[a]Common name for 4,7-diphenyl-1,10-phenanthroline
[b]Common name for 2,4,6-Tris(2-pyridyl)-1,3,5-triazine
[c]Trade name for 3-(2-pyridyl)-5,6-diphenyl-1,2,4-triazine-4′,4″-disulfonic acid
[d]Common name for 3-(4-phenyl-2-pyridyl)-5,6-diphenyl-1,2,4-triazine
[e]Common name for 2,6-bis(4-phenyl-2-pyridyl)-4-phenyl-pyridine
[f]Determined at 25 °C and 0.1 M ionic strength.[142]
[g]Determined at 23 °C and 0.5 M ionic strength.[140]

One commonly used compound containing the ferroin group is 1,10-phenanthroline (phen), which complexes both Fe(III) and Fe(II) and can be used to simultaneously determine the concentration of each using wavelengths 360 nm and 512 nm, respectively.[134,143] Phen is valuable because the forward rate constant and the formation constant for the tris complex are relatively high as compared to other ferroin-type compounds, which minimizes competition by other ions in solution.[142] Stepwise

quantification of Fe(II) and Fe(III) is also possible with phen via photochemical reduction because the Fe(III)-phen complex is reduced when exposed to wavelengths <500 nm.[134,144–146] An early procedure proposing the photoreduction method for iron quantification using phen observed that the addition of reducing agents like hydroxylamine-HCl caused instability in the reduced complex.[100] A later study showed that photoreduction was an unreliable method for iron quantification in solutions containing Mn(II), where absorbance values for photoreduced Fe(II) were lower than values obtained by chemical reduction using hydroxylamine-HCl.[147]

There are several complications regarding the stability of iron-phen complexes. Procedures often instruct phen addition directly to HF or HCl digest solutions because substantial Fe(II) oxidation occurs if it is added later.[144–146] A shift in oxidation state is also observed if the Fe(II) concentration is <1 mg/L, or if the samples sit longer than 15 minutes, because the ferrous complex is more thermodynamically stable.[134] For stable color development, the phen concentration must be >30×$Fe_{(total)}$.[134] Interfering cations include Cu(II), Zn(II), Ni(II), and others, which form competing complexes that result in either lower absorbance of the iron complex because of competing complexation, or increased absorbance because of overlapping peaks in the absorption spectrum.[134] Interfering anions (e.g., oxalate, fluoride) should also be considered because of the impact on pH and/or the formation of competing complexes.[134] The presence of fluoride, a common component of dissolution methods that target silicate, at a concentration exceeding 10 mM also result in lower absorbance values of the Fe(II)-phen complex, which is attributed to ligand exchange.[100] Reagent quality can also affect results; good quality phen crystals should have a melting point of 90 – 100 °C and hydration content of

7 – 10 %.[145] Finally, the detection parameters are less than ideal because detection of the Fe(III) complex requires quartz cuvettes, which are costly, and the molar absorptivity of the Fe(II) complex is lower as compared to other colorimetric reagents, which negatively impacts the detection limit.

The limit of detection of iron improved with the introduction of bathophenanthroline (4,7-diphenyl-1,10-phenanthroline) because the ferrous complex is easily extracted into immiscible organic solvent, which concentrates the complex and separates it from some interfering species.[134,139] The molar absorptivity is also double that of the Fe(II)-phen complex. Several other ferroin-bearing compounds with similar properties are widely-used reagents for colorimetric iron analysis, including 2,2'-pyridine,[137] TPTZ (2,4,6-tris(2-pyridyl)-1,3,5-triazine),[140] and ferrozine (3-(2-pyridyl)-5,6-diphenyl-1,2,4-triazine-4′,4″-disulfonic acid).[133]

Ferrozine is the most common colorimetric reagent for iron quantification and was developed while balancing low production costs and high molar absorptivity.[133] Ferrozine is also highly water-soluble and stable over a wide pH range (pH 4 – 9).[138,148] The most-commonly cited ferrozine assay method uses three reagents: (A) 10 mM ferrozine prepared in 0.1 M NH_4-acetate, (B) 1.4 M hydroxylamine-HCl prepared in 2 M HCl, and (C) 10 M NH_4-acetate buffered to pH 9.5 with NH_4OH.[148] Some studies dissolve reagent A in ultra-filtered water[149] or 50 mM HEPES buffer,[83] but potential differences caused by the buffer medium have not been explored.

The selectivity of ferrozine for Fe(II) and interferences from other ions still fall short of the ideal. The most commonly-interfering species is Fe(III). The 'revised ferrozine method' was developed using the additive property of the Beer-Lambert law to

account for Fe(III) co-absorption.[148] A calibration curve of 5 – 30 μM Fe(III) was used to show that the Fe(III)-ferrozine complex has an absorbance 1 – 3 % that of the chemically-reduced Fe(II) complex.[148] Additionally, thermodynamic reduction was shown to occur in as little as 5 minutes when both Fe(II) and Fe(III) were present, as compared to solutions containing only Fe(II). This shift occurred with and without light exposure, but the effects of the reduction are avoided by immediately taking absorption measurements after preparation.[144,148,150]

Several other ions also interfere with the ferrozine method, including 2 – 50 ppm Hg(II), Co(II), Cr(III), Cu(I), Cu(II), Ni(II), CN^-, and NO_2^-; 100 ppm $C_2O_4^{2-}$; and 500 ppm Mn(II) and F^-.[102,133] Concentrations of 1000 ppm Li^+, Na^+, K^+, NH_4^+, Mg^{2+}, Ca^{2+}, Sr^{2+}, Ba^{2+}, Zn^{2+}, Cd^{2+}, Ag^+, Al^{3+}, Sn^{2+}, Pb^{2+}, Th^{4+}, Cl^-, Br^-, I^-, ClO_3^-, SO_3^{2-}, SO_4^{2-}, $S_2O_3^{2-}$, $S_2O_8^{2-}$, SCN^-, NO_3^-, $C_2H_3O_2^-$, and PO_4^{3-} did not substantially affect iron quantification.[102] Dissolved organic carbon at relatively high concentration of 35 ppm also did not affect absorbance measurements.[148] Still, matrix effects in any buffer system can be investigated by preparing standards with equivalent concentrations of co-occurring species.

Oxalate Interference in Ferrozine Assay

Iron quantification using the ferrozine assay is affected by the presence of oxalate in several ways. It is important to determine the extent of the effects, and ways to mitigate them, especially when using UV-vis for iron quantification after mineral dissolution with oxalate. To test the effects of oxalate on the ferrozine assay, we prepared

standards in four groups: under darkness without oxalate, exposed to light without oxalate, under darkness with oxalate, and exposed to light with oxalate (see supplemental for experimental details). The oxalate buffer used in this preparation was identical to that used for mineral dissolution by oxalate, and the final concentration of oxalate in the cuvettes was always 11 mM. Absorbance values of the ferrozine complex were measured after each of three steps: (1) preparation and 3-day equilibration (Figure S10), (2) addition of 0.3 mL of the 1.4 M hydroxylamine-HCl reagent, 2-hour equilibration, addition of 0.1 mL of 10 M NH_4-acetate, 15-minute equilibration, and (3) 5-hour equilibration. Results are shown in Figure 2.

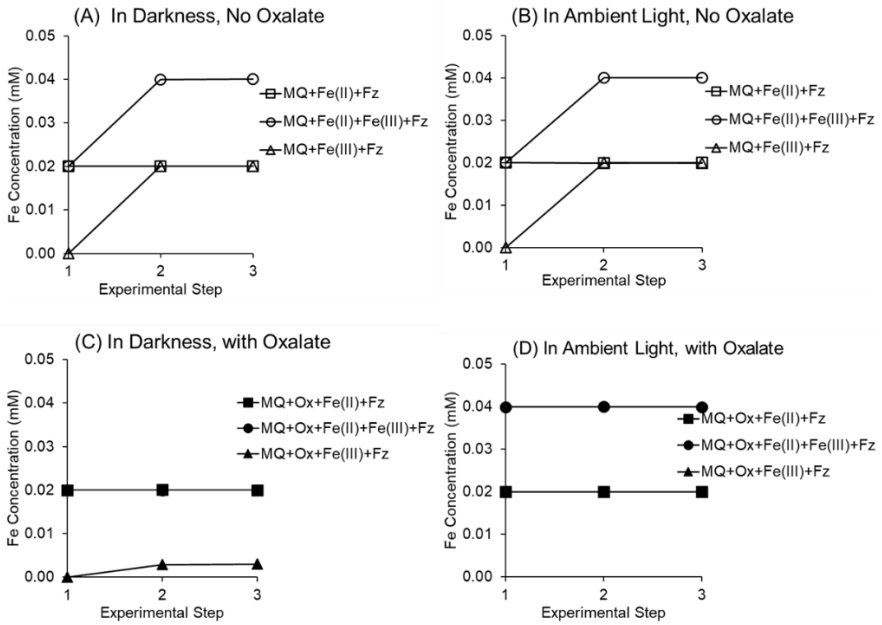

Figure 1.2. Concentration of Fe(II) in polystyrene cuvettes as determined by ferrozine assay without the addition of oxalate and (A) in darkness or (B) in ambient light, and with the addition of oxalate and (C) in darkness or (D) in ambient light. The cuvettes were taken through the following experimental steps in an anaerobic glove bag: (1) cuvette preparation using ultra-filtered water, oxalate buffer (if present), Fe(II) and/or equal parts Fe(III), and ferrozine, then equilibrated for 3 days; (2) chemical reduction by hydroxylamine-HCl, two-hour equilibration, pH adjustment with NH_4-acetate, and then 15-minute equilibration; and (3) five hours later. See Table S1 for cuvette preparation volumes and concentrations. Raw absorption data is provided in Figure S11.

First, the results show that hydroxylamine-HCl is an ineffective reducing agent in the presence of oxalate. Chemical reduction occurred as expected in the absence of oxalate, with and without light exposure (Step 2, Figure 2A, 2B), where absorption measurements showed the appropriate mass balance of 0.02 mM Fe(II) before reduction and 0.04 mM Fe(II) after reduction. When the samples contained oxalate and were equilibrated in darkness (Figure 2C), the addition of hydroxylamine-HCl did not cause chemical reduction in samples containing Fe(II) and Fe(III). The absorbance increased slightly, however, for samples containing only Fe(III), to yield 0.003 mM Fe(II), calculated using a calibration curve containing oxalate and Fe(II). Chemical reduction did not progress further after 5 hours (step 3).

Second, the results show that oxalate effectively photoreduces Fe(III). Samples prepared with only 0.02 mM Fe(II) or Fe(III) and oxalate then exposed to ambient light (Figure 2D) contained only Fe(II) after the initial 3-day equilibration. The samples containing both Fe(II) and Fe(III) showed an appropriate mass balance of 0.04 M Fe(II) after the 3-day equilibration, indicating complete photoreduction of iron.

A comparison of all samples prepared under darkness and containing only Fe(II) or both Fe(II) and Fe(III) (Table 5) show that oxalate competes with ferrozine for Fe(II). In each case, standards containing oxalate yielded absorbance values 3 – 10 % lower than equivalent standards without the addition of oxalate. To counteract this effect, any prepared standards should be representative of samples containing oxalate and contain an equivalent concentration of oxalate.

Table 1.5. Absorbance values of calibration curve standards prepared in triplicate with ferrozine assay and equilibrated in anaerobic environment under darkness overnight (16 hours). Components were added to the cuvette in the order listed: ultra-filtered water (MQ), oxalate buffer (Ox), Fe(II), 1:1 Fe(III), and ferrozine (Fz). Percent difference values are given to show the effects of Fe(III) and of oxalate on the Fe(II)-ferrozine complex formation. Oxalate concentration was constant at 11 mM.

	0.005 mM Fe(II)			0.010 mM Fe(II)			0.020 mM Fe(II)		
	Avg	Stdev	% Stdev	Avg	Stdev	% Stdev	Avg	Stdev	% Stdev
MQ+Fe(II)+Fz	0.1307	0.0003	0.2	0.2618	0.0005	0.2	0.5179	0.0009	0.2
MQ+Fe(II)+Fe(III)+Fz	0.1356	0.0002	0.1	0.2649	0.0006	0.2	0.5239	0.0003	0.06
% difference	4			1			1		
MQ+Ox+Fe(II)+Fz	0.1221	0.0008	0.6	0.2506	0.0005	0.2	0.5017	0.0003	0.06
MQ+Ox+Fe(II)+Fe(III)+Fz	0.1223	0.0002	0.2	0.2486	0.0009	0.4	0.5027	0.0002	0.05
% difference	0.1			-0.8			0.2		
Oxalate Comparison:									
% diff. with Fe(II)	-7			-4			-3		
% diff. with Fe(II)+Fe(III)	-10			-6			-4		

The results in Table 5 also illustrate the effect of Fe(III) in the detection of Fe(II) by ferrozine, both in the absence and presence of oxalate. In each case, percent difference was calculated using the formula $((A_{Fe(II)+Fe(III)} - A_{Fe(II)})/A_{Fe(II)})\times 100$. Absorbance values from samples containing only Fe(III) were not used because absorbance was below the limit of quantification. Samples without oxalate mirror the observation by Voillier et. al. (2000), that the absorption of the Fe(III) complex is 1 – 4 % that of the Fe(II) complex at equivalent concentration.[148] Similar results were obtained when comparing samples prepared under darkness and in ambient light (Table S2). In the presence of oxalate, however, the difference between samples with Fe(II) and those with Fe(II) and Fe(III) is less than ± 1 % and is approximately equivalent to the standard deviation as calculated from triplicate samples.

Section 4: Challenges of Using Natural Samples

Crushed rock specimens that contain iron are often heterogeneous mixtures that include iron-bearing minerals, other minerals, inorganic carbon (CO_3^{2-}), and sometimes organic carbon (e.g., natural organic matter). For accurate and precise analysis of iron in such heterogeneous samples, it is necessary to prevent interference from these species and prevent reactions that may change the form of iron. Several species, for example, form strong complexes with dissolved iron, block reactive surface sites on iron-bearing surfaces, or interact (e.g., precipitate) with iron in unintended reactions. This section briefly describes potential complications from mineral salts and redox-active components and suggests steps to overcome some associated challenges.

Mineral Salts

Natural samples often contain highly soluble mineral salts. When suspended in water, these salts dissolve to produce ions that impact the surface chemistry of the remaining minerals. Volcanic ash, for example, contains many soluble salts that produce dissolved Ca^{2+}, Na^{+}, Mg^{2+}, SO_4^{2-}, PO_4^{3-}, and Cl^{-} when exposed to water.[151] Even slight changes in ionic strength may affect sensitive experiments, such as in the formulation of rate laws or identification of rate-determining steps.[152] The impact of salt ions on reactions occurring at the solution-mineral interface is often pH-dependent, linked to ion speciation and mineral surface charge as determined by the degree of surface hydroxyl protonation.[153,154]

Salt dissolution itself can affect pH by releasing acidic or basic ions, such as SO_4^{2-} and PO_4^{3-}, and change in pH may affect the solubility of other solids.[151,155] For example, calcite dissolution releases CO_3^{2-} and increases pH, and CO_3^{2-} may precipitate in the form of metal carbonates, such as siderite.[156] Higher pH as a result of CO_3^{2-} release leads to precipitation of metal hydroxides such as $Fe(OH)_3$ and $Al(OH)_3$.[39,155] Solubility of mineral phases is also affected by the common ion effect, where the dissolution of a reactive mineral is inhibited by the presence of constituent ions.[157] Suspending the sample in ultra-filtered water and checking pH and solution conductivity provides a quick and potentially quantitative assessment of salt dissolution. Another method to quantify the total dissolved solids involves suspending a sample of known mass in water and then filtering after the desired dissolution time. The solution is collected into a vessel of known mass, boiled to evaporate the water, and then weighed again to determine the mass of the salts.[155]

Dialysis is often used to remove salts while minimizing loss of solids, as controlled by the molecular weight cutoff (MWCO). Dialysis typically involves mixing solids with a well-characterized medium (e.g., ultra-filtered water) to produce a slurry, which is then added to cellulose dialysis bags (e.g., Spectra/Por 7; MWCO 2 kD), and plastic clips are used to secure the ends. The bags are suspended in an exchange medium, and the medium is agitated to maximize diffusion rate. Published procedures recommend that the exchange medium is changed at 3-hour intervals on the first day, and at 6- to 12-hour intervals on succeeding days, until nine medium changes occur and the solution conductivity is equivalent to that of pure exchange medium.[158,159] The slurry is then removed from the dialysis bags, concentrated by centrifugation, and sometimes freeze-

dried. Note that dialysis may also result in loss of small organic molecules and mineral colloids.

Redox-Active Specimens

Redox-active materials are affected by cycles of wetting and drying and transitions between anoxic and oxic environments. These changes may lead to dissolution, oxidation, or precipitation, and may have unanticipated effects on iron speciation and subsequent reactions. An example of this behavior is observable with pyrite and pyrrhotite ($Fe_{1-x}S$), where exposure to water and oxygen generates leachate bearing dissolved iron and sulfate. The impact of this process is seen in acid mine drainage, where the redox-active leachate is further acidified as Fe(II) oxidizes and subsequently precipitates as iron (oxyhydr)oxides downstream.[152,155,160]

Some minerals exposed to oxidizing conditions may generate (oxyhydr)oxide coatings, as can be seen with siderite. This coating may inhibit accessibility of the mineral interior, which impacts its use in reactions such as dissolution analyses or contaminant remediation.[25] For natural specimens already coated in an (oxyhydr)oxide layer, crushing or abrasion exposes new surfaces for access to the ferrous mineral.[25] Synthetic samples are also subject to oxidation and should be stored and used under anoxic conditions to prevent oxidation.

Materials collected from naturally anoxic environments, such as in sediment, present challenges in preserving the natural oxidation state of iron in the material and in the pore water. Ineffective preservation may lead to oxidation and precipitation of new mineral phases that would impact the characterization of the natural minerals. Several

variables including pH, oxygen content, redox potential, temperature, and conductivity of pore water should be characterized and monitored during the handling of samples from these anoxic zones in order to assess the quality of sample preservation.[161] Such samples are best stored under redox-inactive gas, analyzed immediately, or preserved with acid or salt prior to quantification of redox-active species.[161,162]

Section 5: Standardized Reporting Protocols

Development of the dissolution methods described herein arose from the need to thoroughly classify and quantify iron in iron-bearing materials and to make comparisons that elucidate fundamental chemical processes occurring at the solution-mineral interface. Comparisons are regularly made to literature values, but results may not be truly comparable because of the wide range of experimental conditions that researchers use. Especially considering that literature data can be useful for applications outside of the original study, detailed descriptions of iron-bearing materials and all experimental conditions are essential to enable meaningful comparisons between data sets. While several parameters are well-reported (e.g., mineral mass loading and buffer identity), other parameters are often not well-reported (e.g., surface area loading and degree of light exposure), some of which could substantially affect results.

Material Properties

Material composition is often reported according to mineral identity as determined by XRD, Mössbauer spectroscopy, or other method, but there are several other important parameters to consider, some of which are determined by dissolution experiments. The most common parameter is iron content (mg Fe/g sample) as accessed by the various dissolution reagents. This is an important parameter because it provides an assessment of the accessibility of different minerals for participation in chemical reactions. It can also determine the presence of phases not readily detected by other methods like XRD, such as the presence of SRO iron (oxyhydr)oxides coated on mineral surfaces or minerals present in mass fractions below the limit of detection. Furthermore, it can provide an assessment of crystallinity, as discussed for siderite and hematite in Section 2, where more aggressive methods are needed to dissolve highly crystalline forms. Other important information provided by dissolution experiments include the Fe(II):Fe(III) ratio, identity and concentrations of other species (e.g., salts , and degree of elemental substitution.

Beyond the information provided by chemical dissolution methods, several parameters relating to the variation within natural and synthetic samples are also important to report to facilitate better comparisons. Natural samples always have a degree of heterogeneity, whether in the form of other species or in varying size of the crystalline domain. Besides providing a detailed report of the sample composition, there are steps to mitigate the effects of this variability on experimental results. These steps can include, for example, abrasion or sieving in sample preparation to homogenize the material, using

larger sample masses in experiments to minimize the effects of any single grain, and performing replicate experiments to capture the range of sample variation.

Mineral characteristics such as particle morphology, size, and degree of aggregation are important for assessing which crystal facets are accessible to reaction. Particles of different morphologies are bounded by different facets, each having a unique arrangement of atoms.[163,164] The arrangement of reactive groups on the mineral surface influences the interactions with aqueous species,[165,166] as well as mass transfer to the surface.[167,168] An example of how these characteristics affect mineral dissolution is seen in hematite, where the (001) facet was shown to preferentially dissolve in oxalate because of the presence of screw dislocations.[85] Using well-defined synthetic minerals from standardized procedures can minimize differences in mineral characteristics and precise synthetic methods are reported for hematite,[164] goethite,[169] magnetite,[170,171] and maghemite nanoparticles,[172] among others.

Using well-defined morphologies also enables statistical analyses of particle size and size distribution. One method involves collecting at least 20 images by transmission electron microscopy from at least 4 grid locations and measuring the dimensions of at least 400 particles.[173] Standardized methods to quantify size and shape have been successfully used to identify the relative reactivity of different crystal facets. For example, particle size and size distribution data of acicular goethite particles was used in pairwise Kolmogorov−Smirnov (K−S) tests to identify statistical differences in oxidative mineral growth occurring at two major facets as reaction conditions were varied.[167]

Material Loading

The form of material loaded to reaction vessels (e.g., as suspensions or powders) is also sometimes an underreported parameter for both natural and synthetic samples. The manner of loading, such as dry powders (e.g., via benchtop drying, freeze-drying, solvent replacement, etc.) or freshly prepared suspensions of materials that have never been dried, is important, and the implications of this are well illustrated by ferrihydrite. Synthetic ferrihydrite is often dried to prevent the thermodynamically-favored transformation to goethite while in suspension, but ferrihydrite particles are difficult to fully resuspend after drying, which can lead to a decrease in accessible reactive surface area.[158,169] Thus, ferrihydrite should be loaded into reactors as freshly prepared suspensions.

For materials that are stable in suspension, concentrated stock suspensions provide precise mass loading (mg/mL), particularly for the addition of milligram levels of material. The mass loading of the stock suspension must be determined periodically to account for solvent evaporation. Pairing particle mass loading with surface area measurements (m^2/g) provides information about surface area loading (m^2/mL), and incorporating morphological data allows for an estimation of facet-specific loading via geometric calculations.[158] Such parameters are especially important for comparing reaction rates across different mineral phases as well as particle sizes and morphologies.[3]

Reaction Conditions

Reaction conditions substantially impact reaction pathways and unintended factors may contribute to results. Commonly reported parameters include buffer identity, pH, and reagent concentrations, source, and purity, but several other factors are also important. The presence of oxygen can promote oxidation and light exposure can result in the production of reactive oxygen species or promote photochemistry. Both of these factors have an impact on redox chemistry, as described in the oxalate method in Section 2, but these parameters are infrequently reported. In anaerobic chambers, consider reporting oxygen content as determined by an oxygen probe. Besides excluding light using an opaque layer on reaction vessels (e.g., aluminum foil wrapping), consider reporting degree of light exposure determined by light sensor.

Reaction rates can vary with agitation intensity and temperature. Indeed, mass transport can be tied to agitation intensity in diffusion-limited reactions. It is therefore important to report agitation intensity in accessible units, such as revolutions per minute (rpm) for magnetically-stirred solutions, and also include rotor radius (cm) for rotational platforms. Additionally, because temperature affects solubility and reaction rate, consider validating temperature settings with a secondary thermometer or thermocouple.

Labware Material Composition

Special considerations should also be made when selecting vessels to contain iron-bearing solutions such as digests, controls, and stock solutions because partitioning of iron may occur with the vessel material. Metal containers can release metal ions when in contact with acidic solutions,[174] and glass vessels may release components from tinting

agents or impurities in the glass, such as iron and manganese.[175,176] Iron adsorbs to many plastics and to borosilicate glass,[177] but polyethylene and polycarbonate show the lowest levels of iron adsorption.[178] Containers will continue to adsorb ions over time, and it is best practice to minimize analysis time, consistently employ standard operating procedures, and compare samples to appropriate controls. Reporting the material composition of all labware used in preparations, reactions, and analyses is important because different plastics adsorb different dissolved species. Especially for trace metal analysis, consider the ion exchange capacity of filters and other materials. Surfactant-free cellulose-acetate membrane filters (0.15 – 0.45 μm) were previously recommended for working with solutions with low iron content to minimize loss to adsorption.[151,161]

Acknowledgements

Funding for this work was provided by the State of Minnesota for the Minnesota Mining Innovation Initiative and the National Science Foundation (grant CHE-1507496).

Chapter 2. Redox-Induced Nucleation and Growth of Goethite on Synthetic Hematite Nanoparticles

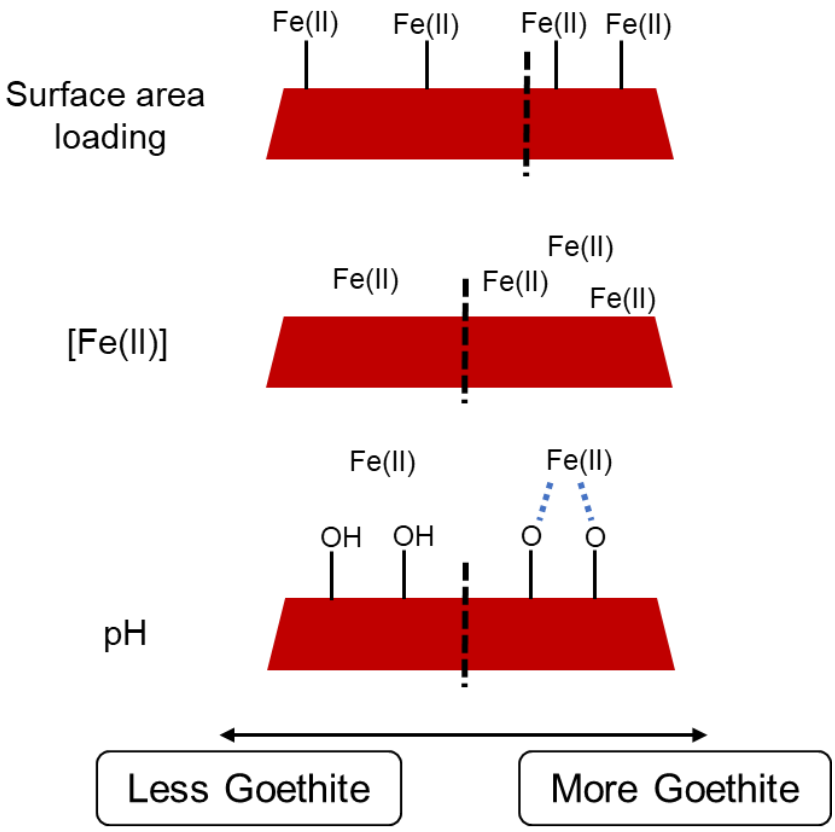

This chapter presents the results of a research project by Jeanette L. Voelz,

advised by William A. Arnold, and R. Lee Penn.

Voelz, J. L.; Arnold, W. A.; Penn, R. L. Redox-Induced Nucleation and Growth of Goethite on Synthetic Hematite Nanoparticles *Am. Mineral.* **2018**, *103*, 1021-1029.

Overview

The iron (oxyhydr)oxides hematite (α-Fe_2O_3) and goethite (α-FeOOH) are natural and reactive minerals common in soils and sediments, and their adsorption of Fe(II) produces reactive surface sites that facilitate reduction of oxidized environmental pollutants. Single-exposure experiments with 4-chloronitrobenzene showed that hematite is more reactive than goethite, when normalized by surface area loading. Interestingly, the product of Fe(II) oxidation is a mixture of goethite and hematite, and the goethite to hematite ratio depends on the distribution of Fe(II) activated surface sites, which is a function of aqueous Fe(II) concentration, surface area loading, and pH. More goethite is produced under conditions of higher Fe(II), lower surface area loading, and higher pH. Recurrent-exposure experiments showed a substantial decrease in reaction rate after one to three exposures, a trend suggestive of reaction contributions from the increasing goethite surface area over time. Using known atomic surface geometry for goethite and hematite, the hematite {012} facet is proposed as the site of primary mineral growth with goethite {021} at the interface between the two minerals. These results have implications in contaminant fate modeling, where the mineral phases present in the environment, the minerals likely to form, and the surrounding aqueous conditions all have an impact on contaminant reaction rate.

Introduction

Iron is one of the most abundant elements on Earth, and its oxides, oxyhydroxides, and hydroxides (collectively termed 'iron oxides') are currently tabulated at seventeen recognized crystal structures.[1] Iron oxide minerals form in a range of mild to extreme environmental conditions, with phases produced dependent on temperature, pressure, pH, aqueous ion concentrations, hydration state, and oxygen fugacity.[2–4]

Anthropogenic influences, however, rapidly alter minerals, and the geological impacts of industrial activities like mining[5,6] and agriculture[7] are still under investigation. The release of highly oxidized chemicals into reduced groundwaters facilitates redox reactions that not only transform the contaminants[8,9] but alter mineral surfaces as well.[10,11] Minerals are recognized as important tools for environmental remediation via natural attenuation,[12,13] permeable reactive barriers,[14] or *in-situ* redox manipulation,[15] but alterations from inadvertent anthropogenic influences must also be considered so that they are recognized, rather than mistaken for natural processes.

The specific adsorption of Fe(II) to iron oxide surfaces is known to occur through bidentate complexes with contiguous singly-coordinated hydroxyl group pairs.[16,17] The subsequent electron transfer to the bulk oxide results in the formation of new Fe(III) surface structures[18,19] and activates these minerals for participation in redox reactions. This electron transfer process has been demonstrated for goethite and hematite using Mössbauer spectroscopy[20–22] and calculated in detail for hematite using molecular orbital calculations.[23] Many highly oxidized environmental contaminants, such as nitroaromatic compounds, are readily reduced when they encounter these Fe(II)-activated surfaces.[24–27]

Measuring the concurrent oxidative mineral growth provides important information about which surfaces were readily accessible to and most reactive with aqueous Fe(II).[10,11,28]

It has been proposed that Fe(II) adsorption on hematite leads to magnetite precipitation,[29,30] but this proposal has not been supported in other works.[19,31] Rather, observations of Fe(II) adsorption on hematite {012} by crystal truncation rod diffraction indicate that the oxidized surficial Fe(III) have Fe-O bond lengths of 1.93 – 2.18 Å, which is in agreement with Fe-O bond lengths in the bulk lattice of both goethite and hematite but not magnetite.[19,32] These reports of Fe(III) surface structures resulting from the adsorption of Fe(II) on hematite are limited by the adsorption capacity of the mineral surface.[19]

To further investigate evolving mineralogy requires the addition of another electron-accepting species to oxidize Fe(II) beyond the adsorption capacity of the underlying hematite. For example, the model contaminant 4-chloronitrobenzene (4-ClNB) efficiently participates in redox reactions in systems containing iron oxides and Fe(II).[13,28,33] Oxidation of Fe(II) in suspensions of hematite may result in (1) hematite growth on existing hematite faces, (2) homogeneous nucleation of new particles, or (3) heterogeneous nucleation of new phases on existing hematite surfaces. Oxidative growth on goethite and hematite surfaces after the addition of Fe(II) and reaction with nitrobenzenes has been characterized using Mössbauer spectroscopy.[34] On hematite, the deposition of 4-6 monolayers of hematite was observed, followed by the formation of a new phase identifiable as goethite, which comprised 25 % and 95 % of the growth on hematite needles and hexagonal platelets, respectively. Changes to solution conditions (pH, buffer identity, ionic strength, and Fe(II) concentration) were not shown to have a

profound effect on the monolayer onset of goethite formation on hematite, suggesting that goethite formation is instead a function of thermodynamic factors.

Evolving surface features resulting from oxidative growth (i.e. particle size, morphology, surface roughness, or phase composition) affect the availability and accessibility of Fe(II)-reactive sites. The comparison of particle dimensions via electron microscopy before and after reaction reveal the locations of oxidative mineral growth, which may indicate the relative Fe(II) reactivities of various facets.[10,11,28] For example, where goethite particle tips became roughened in appearance after redox, the surfaces could no longer be well-described as terminated by {021} facets that were prominent prior to reaction, rather they compose a mixture of crystal surfaces, which changes the ratio of surface sites and, therefore, affects the reaction rate.[11]

Recurrent-exposure reactions are a valuable tool for evaluating the evolving reactivity of mineral surfaces. As an example, two studies investigating the evolving reactivity of goethite in 1 mM Fe(II) after five exposures of 100 μM 4-ClNB report decreasing reaction rates with each exposure.[11,28] Both these studies, however, did not include pH readjustment after each sequential spike, which is expected to affect reaction kinetics as surface hydroxyl groups are more densely protonated at lower pH, therefore inhibiting the adsorption of Fe(II) and limiting the available reaction sites. A recent study of goethite reactivity under related conditions showed no significant change in rate across five to ten additions of 4-ClNB when the pH was readjusted after each sequential spike, suggesting the resulting oxidative mineral growth formed a balance between inhibitory surface roughening and increasing reactive surface area.[10]

Results from the evolving reactivity of iron oxide surfaces enable a deeper understanding of how redox reactions at the water-mineral interface may proceed in the environment, particularly in cases where minerals have undergone substantial reactions with anthropogenic species. Here, we investigate oxidative mineral growth as a function of the availability of Fe(II)-activated surface sites at the hematite surface. The reaction variables tested include pH, Fe(II) concentration, reactive surface area, and particle morphology. Both single-exposure and recurrent-exposure reactions are performed to assess the effects of solution conditions on reactivity and to evaluate structural changes due to oxidative growth. Finally, a detailed description of the observed epitaxial growth is proposed based on lattice measurements and known geometric atomic configurations of goethite and hematite facets.

Experimental

Ultrapure water from a MilliPore Milli-Q Advantage A10 system was used for all synthesis, dialysis, and experimental processes. All solutions of HCl and NaOH for pH adjustments were prepared from concentrated solutions of HCl (BDH Aristar, 12.1 M, 36.5 – 38.0 %) and NaOH (Fisher Scientific, 19 M, 50 % w/w). All experiments were performed in a Coy Laboratory Products vinyl anaerobic glovebag with 5 % H_2, 95 % N_2 (Matheson) atmosphere.

Hematite Syntheses

Rhombohedral and equidimensional hematite particles were synthesized using modified procedures.[2] Rhombohedral particles (hereafter denoted as 'R' in tables and figures) were synthesized in a 1 L Pyrex glass bottle, where 1 L of 0.002 M HNO_3 (ACS Reagent Grade) was heated to 98 °C in an oven and 8.08 g (0.02 M Fe) of $Fe(NO_3)_3 \cdot 9H_2O$ (Sigma-Aldrich, 98 %) was added with vigorous stirring until the salt dissolved. The bottle was capped with aluminum foil (to minimize evaporation but also prevent pressurizing) then promptly returned to the 98 °C oven and heated for seven days. The foil never had contact with the solution. The suspension was cooled to room temperature, the supernatant decanted, and the concentrated suspension was dialyzed using cellulose dialysis membranes (Spectra/Por® 7, 2 kD, 38 mm × 24 mm). Dialysis water was changed nine times, with at least four hours between water changes. The suspension was transferred to a Nalgene bottle, sparged with nitrogen (Matheson 99.99 %) for two hours, and stored in the anaerobic glove bag. Equidimensional particles (hereafter denoted as 'E' in tables and figures) were synthesized in a 2 L Nalgene bottle, where 2 L of 0.002 M HCl (BDH Aristar 36.5-38.0 %) were heated to 98 °C in an oven and 10.81 g (0.02 M Fe) of $FeCl_3 \cdot 6H_2O$ (Fisher 97.3 %) was added with vigorous stirring until dissolved. Paralleling the rhombohedral synthesis, the bottle was capped with aluminum foil, promptly returned to the 98 °C oven, and heated for ten days. After cooling to room temperature, the suspension was concentrated, dialyzed, sparged, and stored in the anaerobic glove bag.

Initial Particle Characterization

Following dialysis, the mass loading of each hematite stock suspension was determined as described in the Supplemental Information Section I (Figure B1). The dried particles from the mass loading analysis were gently ground into a powder for XRD analysis. The mineral content of the powder was analyzed using a PANalytical X'Pert PRO X-ray diffractometer equipped with a cobalt source (1.7909 Å) and an X'Celerator detector. Both synthetic materials were analyzed from 10-90 °2θ with an effective dwell time of 100 s per step and a step size of 0.0167 °2θ.

Particle dimensions were determined using calibrated images collected with an FEI Tecnai T12 transmission electron microscope operating at 120 kV. TEM samples were prepared by diluting one drop of stock suspension with methanol until the suspension appeared lightly red (ca. 1000x), one drop of which was placed onto a Cu 200 mesh holey carbon grid and air-dried. Particle dimensions are reported as the average ± standard deviation of 500 measurements with approximately ten particles measured per image.

Surface area measurements were performed using N_2 adsorption by Brunauer-Emmett-Teller (BET) analysis on a Quantachrome Autosorb iQ2-MP at 77 K with outgassing at 90 °C for 12 h. Specific surface areas were determined using the adsorption branch from P/P_o = 0.1 to 0.28.

Batch Reactor Preparation

Batch reactors were prepared in 120 mL serum bottles capped with PTFE-lined rubber septa and magnetically stirred with PTFE-coated stirbars at a rate of 500 rpm. All reactors contained a buffer of 10 mM $NaHCO_3$ (Sigma-Aldrich 99.7 %) adjusted to pH 7.0 ± 0.1 with 1 M HCl. Particle surface area loading varied from 0.007 m^2/mL – 0.043 m^2/mL, which corresponds to mass loading of 0.100 to 0.600 mg/mL for rhombohedral particles and 0.383 to 1.149 mg/mL for equidimensional particles. The 175 mM Fe(II) stock solution was prepared from oxygen-free solid $FeCl_2 \bullet 9H_2O$ (Fisher 101.5 %) and 0.3 M HCl. Reactors contained Fe(II) concentrations of 0.25, 0.50, or 1.00 mM. Reactors were loaded with hematite, pH buffer, and Fe(II), and then pH adjusted, as needed, to 7.0 or 6.5 ± 0.1 using 1 M HCl or 0.5 M NaOH.

Single-Exposure and Recurrent-Exposure Reaction Sets

Reactors receiving one spike of 4-ClNB (Acros Organics 99 %) are termed single-exposure reactions and were prepared in duplicate along with an additional control reactor to which no 4-ClNB was added. All prepared reactors equilibrated for 21 hours prior to 4-ClNB addition. A 10 mM 4-ClNB stock solution prepared in methanol (Fisher Chemical 99.9 %), was added to the reactors to achieve an initial concentration of one-tenth the reactor Fe(II) concentration. Reactors receiving multiple additions of 4-ClNB were labeled recurrent-exposure reactions. For these, three to five serum bottles were identically prepared under the desired reaction conditions. One reactor functioned as a control, with no injection of 4-ClNB nor additional Fe(II). The remaining reactors received additions of 4-ClNB and sacrificed for post-reaction characterization after one,

two, three, or six exposures. To perform the reaction sequence, the prepared reactors equilibrated for 21 hours, and then the appropriate amount of 4-ClNB stock solution was added (10 % of the initial Fe(II) concentration). The first reactor in each sequence was monitored by HPLC to determine the 4-ClNB transformation rate. After 24 hours, the first reactor was tested for the presence of 4-ClNB again by HPLC. If 4-ClNB was no longer detected, the Fe(II) concentration was measured by UV-visible spectroscopy and the amount of Fe(II) needed to return the reactors to the initial Fe(II) concentration was added to all remaining reactors. Finally, the pH was adjusted to 7.0 ± 0.1 with 0.5 M NaOH. The remaining reactors equilibrated for 21 hours before the next addition of 4-ClNB, and the process was repeated. After determining the 4-ClNB reaction rate in a reactor, it was sacrificed for post-reaction characterization. The control was sacrificed along with the last reactor in the set. For a schematic describing the recurrent-exposure process, see Figure B2.

Reaction Kinetics

Reaction kinetics were monitored by quantifying 4-ClNB concentration using high-performance liquid chromatography on an Agilent 1220 Infinity equipped with Zorbax SB-C18 4.6 × 150 mm, 5-μm column. The eluent was composed of a 30 : 70 mixture of 12 mM ammonium acetate (Sigma-Aldrich 97 %) in 90 vol% water and 10 vol% acetonitrile adjusted to pH 7.0 with ammonium hydroxide (Sigma-Aldrich 28 %) : pure acetonitrile. The flow rate was 0.7 mL/min, and the detection wavelength was set to 254 nm. Standards with a concentration range of 5 – 100 μM 4-ClNB were made in methanol. For sampling, 0.5 mL of the reaction mixture was filtered into autosampler

vials using PALL Life Sciences Acrodisc® 13 mm syringe filters with 0.2 μm nylon membrane starting 1 min after the 4-ClNB injection and continued until approximately 80 % of the 4-ClNB had been reduced (1 – 3 hours).

Fe(II) Adsorption

The concentration of Fe(II) in the reactors was determined via the ferrozine assay and UV-visible spectroscopy on an Agilent 8453 equipped with tungsten and deuterium lamps. A 10 mM ferrozine (3-(2-pyridyl)-5,6-diphenyl-1,2,4-triazine-p,p'-disulfonic acid monosodium salt hydrate, Sigma-Aldrich 97 %) was prepared in water. To remove suspended particles, 0.8 mL of the reaction mixture was filtered through PALL Life Sciences Acrodisc® 13 mm syringe filters with 0.2 μm nylon membrane. Polypropylene cuvettes measuring 1 cm wide were prepared in triplicate with 0.4 mL of 10 mM ferrozine, 3.4 mL water, and 0.2 mL of filtered reaction mixture. Standards prepared with ferrozine, water, and 0.15 mM $FeCl_2$ (diluted from 175 mM stock $FeCl_2$ solution) ranged 0.005-0.050 mM Fe(II). Absorption at 562 nm was recorded in triplicate for each cuvette. The Fe(II) concentration in the reaction mixture was analyzed prior to 4-ClNB addition and after the reaction was complete.

Post-Reaction Characterization

Particles were collected from sacrificed reactors by centrifugation using an Eppendorf 5804 centrifuge programmed to run at 4427 rcf for four minutes. The reactor contents were first concentrated in a 50 mL centrifuge tube using up to three rounds of

centrifugation, where the tube was only opened under anaerobic atmosphere to decant the supernatant. Once concentrated, the particles were washed four times with 35 mL aliquots of deoxygenated water, again only decanted under anaerobic atmosphere. After the final wash, the tubes were opened to ambient atmosphere, the supernatant decanted, and the concentrated slurry transferred to weigh boats to dry at room temperature in a fume hood. A portion of the dried particles was gently ground to produce a uniform powder for XRD analysis. For TEM analysis, a minute quantity of unabraded powder was added to 0.5 mL of methanol and sonicated for 30 seconds or until the suspension appeared light red. For electron diffraction, the same suspension was sonicated for 15 minutes to assist in separating the rods from the larger particles. To prepare the samples for TEM analysis, one drop of the suspension was placed onto a Cu 200 mesh holey carbon grid, allowed to dry overnight, and analyzed on an FEI Technai T12 transmission electron microscope operated at 120 kV.

XRD Calibration Curve

An X-ray diffraction calibration curve was used to quantify hematite and goethite present after reaction. Calibration standards containing 1 – 50 mass% goethite were prepared from aqueous suspensions using mixtures of goethite (10.00 mg/mL) and rhombohedral hematite (3.93 mg/mL). Goethite (space group Pnma) was obtained from the starting material used for experiments described in Penn et al. (2006), and the particles had average dimensions of 90 nm by 10 nm. Two standards were prepared with equidimensional hematite (8.29 mg/mL) to test comparability. All standards and reaction

samples were analyzed from 18-32° 2θ with an effective dwell time of 950 s per step and a step size of 0.0167° 2θ. The (110) reflection of goethite (at 24° 2θ with the Co source) and (012) reflection of hematite (at 28° 2θ with the Co source) were chosen because of the strong scattering intensity and baseline separation from other goethite and hematite reflections. Origin (OriginLab Corporation 2016, version 93E) was used to zero the spectral background, and the peaks were individually fitted using the PsdVoigt1 function to obtain integrated peak areas. Peak areas were multiplied by the goethite (110) and hematite (012) structure factors squared to correct for relative peak intensities, which were calculated to be 31.9 and 102.9, respectively. See Supplemental Section II for a detailed description of these calculations.

Results

Initial Hematite Particle Characterization

Hematite particles with two different morphologies were successfully synthesized. Collected XRD patterns for the as-synthesized materials are both consistent with the hematite PDF 33-0664 (Figure B3). No additional phases were detected. The rhombohedral hematite particle dimensions were 43 ± 8 nm by 29 ± 6 nm, and the nominally equidimensional hematite particles had a diameter measuring 88 ± 13 nm. See Figure B4 for graphics describing measurement geometry and particle size distribution. Specific surface areas were determined using N_2 adsorption and were 72.3 m^2/g and 18.9 m^2/g for rhombohedral and equidimensional hematite, respectively.

Based on TEM images and electron diffraction patterns, the rhombohedral hematite particles are well described as rhombohedra with a slightly truncated pseudocubic morphology, which is a hybrid of two morphologies described by Guo and Barnard (2011). Purely rhombohedral hematite is bound only by {101} facets, while fully truncated pseudocubic morphologies have sizeable {012} facets at the far tips of the rhombohedra. TEM images of the particles used here (Figure B5) show only minor {012} facets, giving the particles a mostly rhombohedral morphology. The crystallographic structure of hematite dictates that the {101} and {012} planes are orthogonal, which is consistent with the lattice fringe spacings observed in TEM images (Figure B5) as well as the observation that the {012} lattice fringes are perpendicular to the adjacent {101} facets of the rhombohedron. For the equidimensional particles, tilt series confirm the equidimensional morphology, rather than a plate-like structure (not shown).

Oxidative Mineral Growth on Hematite Nanoparticles

The products of the oxidative mineral growth are a mixture of goethite and hematite, and the relative amount of each mineral was tracked as a function of Fe(II) concentration, surface area loading, pH, and the morphology (rhombohedral vs equidimensional) of the hematite particle. The reference condition, which was selected because it is consistent with the aqueous conditions used in previous work with goethite,[10,28] used the rhombohedral particles with surface area loading of 0.0072 m^2/mL (0.100 mg/mL mass loading) and 1 mM Fe(II) at pH 7.0 with one exposure of 100 μM 4-ClNB, and is hereafter denoted R-r. The post-reaction solid contained 15(2) % goethite by mass as determined by XRD.

To quantitively compare the products of oxidative growth as a function of reaction conditions, the stoichiometric maximum of goethite that could be produced by oxidative mineral growth, expressed as a mass percent in the final solid after the reaction has gone to completion, was calculated. For each reaction condition, the stoichiometric mass percent of goethite was calculated using the following restrictions: (1) all six electrons needed for the reduction of 4-ClNB are provided through Fe(II) oxidizing to Fe(III) and (2) all Fe(III) is incorporated into the crystal structure as α-FeOOH. For example, the stoichiometric maximum for R-r is 35 mass% goethite after the reaction has gone to completion. The stoichiometric maximum of goethite for each reaction condition is reported in Table 2.1 as goethite max (mass%). The difference in aqueous Fe(II) measured before and after reaction is stoichiometrically consistent with the Fe(II) mass balance (Figure B6).

Table 2.1. Summary of reaction conditions in suspensions of rhombohedral (R) and equidimensional (E) hematite. Abbreviations are surface area loading (S.A. Loading), stoichiometric maximum of goethite (Gth Max.), observed goethite (Gth Obs.), and standard deviation of the observed goethite mass% across replicate reactors (St Dev). Dash symbol (-) indicates not detected.

Set	ID	Mass Loading (mg/mL)	S.A. Loading (m^2/mL)	# Exposures, ([4-ClNB] μM)	pH	Fe(II) (mM)	Gth Max (mass%)	Gth Obs (mass%)	St. Dev. (mass%)
Ref.	R-r	0.100	0.0072	1, (100)	7.0	1.00	35	15.4	2.2
a	R-a1	0.200	0.0145	1, (100)	7.0	1.00	21	trace	
	R-a2	0.275	0.0199	1, (100)	7.0	1.00	16	-	
	R-a3	0.300	0.0217	1, (100)	7.0	1.00	15	-	
	R-a4	0.325	0.0235	1, (100)	7.0	1.00	14	-	
b	R-b1	0.300	0.0217	3, (100)	7.0	1.00	35	9.3	0.8
	R-b2	0.600	0.0434	6, (100)	7.0	1.00	35	1.9	0.6
c	R-c1	0.100	0.0072	1, (100)	6.5	1.00	35	trace	
d	R-d1	0.100	0.0072	2, (50)	7.0	0.50	35	9.5	1.2
	R-d2	0.100	0.0072	4, (25)	7.0	0.25	35	6.2	0.8
e	E-e1	0.383	0.0072	1, (100)	7.0	1.00	12	5.2	0.7
	E-e2	1.149	0.0217	3, (100)	7.0	1.00	12	1.9	0.4

Set a (Table 2.1) tested the effect of increased surface area loading for a single-exposure reaction of 100 μM 4-ClNB with 1 mM Fe(II) at pH 7.0. When the surface area loading was doubled (R-a1) as compared to the reference condition, the formation of goethite decreased substantially, with only trace goethite (< 1 mass%) detected by XRD. In reactors prepared with even higher surface area loading (i.e. R-a2, R-a3, and R-a4), no goethite was detected. TEM micrographs of the post-reaction material support this result, with few rods observed in R-a1 and no rods observed in post-reaction material from R-a2, R-a3, and R-a4 (Figure B7). With high surface area loading, it is possible that Fe(III) is incorporated as goethite layers too thin to be detected either in TEM images or through XRD. Indeed, a quick calculation assuming 37 nm spherical particles yields approximately a 1 nm shell distributed over the entire particle surface. As such, recurrent-exposure reactions were used to further probe high surface area loading conditions, where the ratio of total oxidized Fe(II) to initial hematite mass is held constant.

Set b (Table 2.1) tested the effect of increased surface area loading in recurrent-exposure reactions, with the cumulative stoichiometric maximum of goethite equal to R-r, at 35 mass%. Sequence R-b1 contained three times the surface area loading as R-r and received three additions of 100 μM 4-ClNB, and sequence R-b2 contained six times the surface area loading as R-r and received six additions of 4-ClNB. In comparison to R-r, there was a decrease in the observed goethite content: from 15(2) mass% for one exposure in R-r, to 9.3(8) mass% for three exposures in R-b1, and 1.9(4) mass% for six exposures in R-b2 (Figure 2.1).

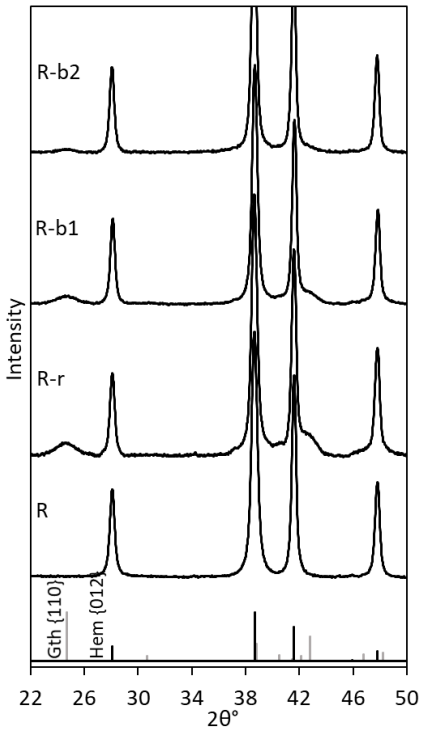

Figure 2.1. X-ray diffraction patterns for a recurrent-exposure set using rhombohedral hematite. Refer to Table 2.1 for sample identifiers. The diffraction pattern of the pure rhombohedral stock suspension is denoted R. Origin (OriginLab Corporation 2016, version 93E) was used to subtract the baseline, smooth the data using 3 average-adjacent data points, and normalize each pattern to the hematite {012} peak intensity. See Figure B9 for the raw pattern of sample R-r.

Set c (Table 2.1) tested the effect of decreased pH by using an initial pH of 6.5 while matching all other variables of the reference reaction. After reaction, only trace goethite was detected (< 1 mass%) by XRD. TEM micrographs of the R-c1 post-reaction material supports this result, with few rods observed (Figure B7).

Set d (Table 2.1) tested the effect of decreased aqueous Fe(II) concentration. Two recurrent-exposure experiments were prepared; as compared to the reference, the Fe(II) and 4-ClNB concentrations were halved and two exposures were performed in R-d1, and the concentrations were quartered with four exposures performed in R-d2. For both

sequences, the stoichiometric maximum of goethite was 35 mass%. All reactors in R-d1 and R-d2 were analyzed by XRD for mineral content, and the trends are presented in Figure 2.2. At halved concentrations, only trace goethite (<1 mass%) was observed after the first exposure while the vast majority of the observed goethite formed during the second exposure, giving a total observed goethite in R-d1 of 9(1) mass%. At quartered concentrations, there was no detectable goethite formed after either the first or second exposure, but 2.3(5) mass% was observed after the third exposure, and the remaining goethite formed in the fourth exposure to total 6.2(8) mass% in R-d2. The data presented in Figure 2.2 show two main points: (1) as Fe(II) concentration decreases, less goethite is formed, and (2) under recurrent-exposure conditions, goethite forms later in the exposure sequence.

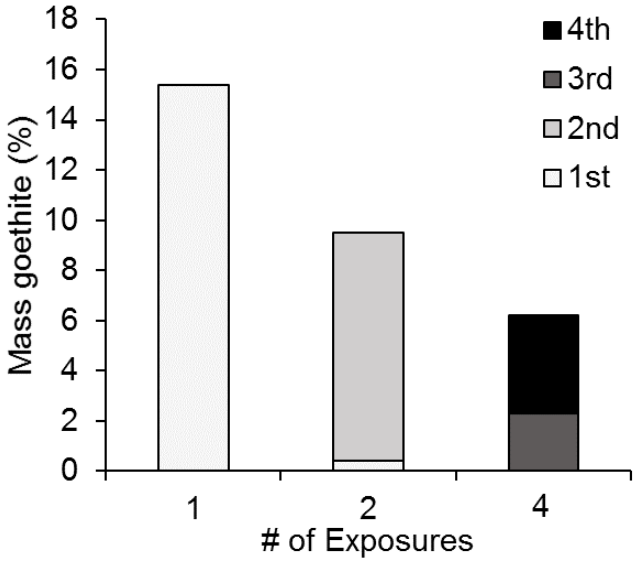

Figure 2.2. Mass% of goethite present after each exposure of 4-ClNB in the single-exposure reference and in the recurrent-exposure reactors of Set d, where the Fe(II) and 4-ClNB concentrations were halved and quartered as compared to the reference condition and given two and four exposures, respectively.

Set e (Table 2.1) tested how the aforementioned surface area loading results compare with hematite of a different morphology, given that the exposed surfaces are quite different. The single-exposure condition (E-e1) and recurrent-exposure condition (E-e2) were matched in surface area loading to the rhombohedral reference R-r (0.0072 m^2/mL) and recurrent-exposure R-b1 (0.0217 m^2/mL) as calculated from the BET measurements. Due to the larger particle size of equidimensional hematite, and thus higher mass loading, the stoichiometric maximum of goethite for each condition was 12 mass%. Condition E-e1 produced 5.2(7) mass% goethite and condition E-e2 produced 1.9(4) mass% goethite.

Comparing reactors that have equivalent ratio of oxidized Fe(II) to surface area loading demonstrates that the goethite mass percent formed on rhombohedral and equidimensional hematite are both negatively correlated with an increase in surface area loading (Figure 2.3). The stoichiometric maxima of goethite for all reactors in Set b and Set e are 35 mass% and 12 mass%, respectively. The observed mass percent of goethite in each sample was lower than the stoichiometric maximum, and some samples showed a trend: in the single-exposure experiments with rhombohedral and equidimensional hematite (0.0072 m^2/mL surface area loading), approximately 45 % of the stoichiometric maximum goethite formation was observed. In recurrent-exposure experiments (0.0217 m^2/mL surface area loading), approximately 27 % of the stoichiometric maximum goethite formed on the rhombohedral particles and 16 % formed on the equidimensional particles.

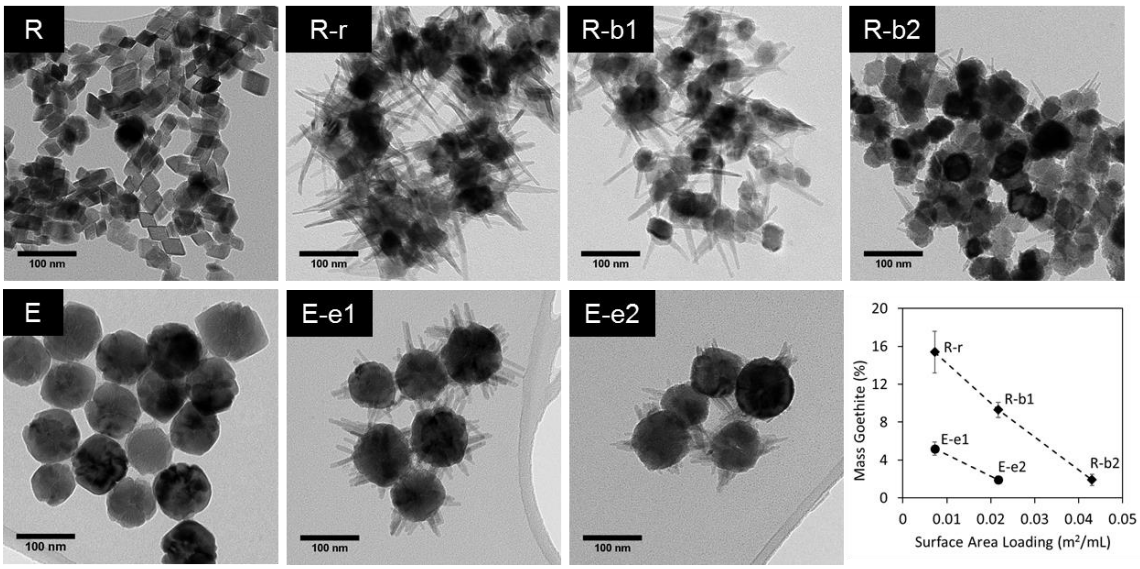

Figure 2.3. TEM images of solid materials collected from batch reactors prepared with the synthetic rhombohedral (R) and equidimensional (E) hematite particles. See Table 2.1 for corresponding sample identifiers, reactor conditions, and mineral phase quantification. The plot shows observed goethite mass percent vs reactor surface area loading for each post-reaction material shown in the given TEM images. Dashed lines are used to guide the eye for each reaction set. Error bars represent the standard deviation of replicate reactors and/or XRD scans.

Supporting the trends in oxidative mineral growth observed by XRD, TEM micrographs show that the length and number of rod-like particles in the post-reaction material for both Set b and Set e decreases as the surface area loading increases (Figure 2.3). Images of samples containing pure hematite (R, E of Figure 2.3) exhibited no particles with the rod morphology characteristic of goethite. There was no detectable goethite by XRD or TEM in any of the control reactors.

Reaction Kinetics

The effects of solution conditions on hematite reactivity were studied in both single-exposure and recurrent-exposure experiments. For comparison, literature values

for goethite reactivity (Table B1) were selected with the restrictions that mineral size and solution conditions were similar to the conditions used in this study.[11,28,35] All rates are normalized to reactor surface area loading (m^2/mL).

The single-exposure reduction rate of 4-ClNB by Fe(II) in suspensions containing rhombohedral and equidimensional hematite increases as the surface area loading increases, as seen in Figure 2.4a, which correlates with an increase in the number of available reactive sites. When compared to reactions using goethite and 4-ClNB, rhombohedral and equidimensional hematite react faster than goethite (Figure 2.4a).

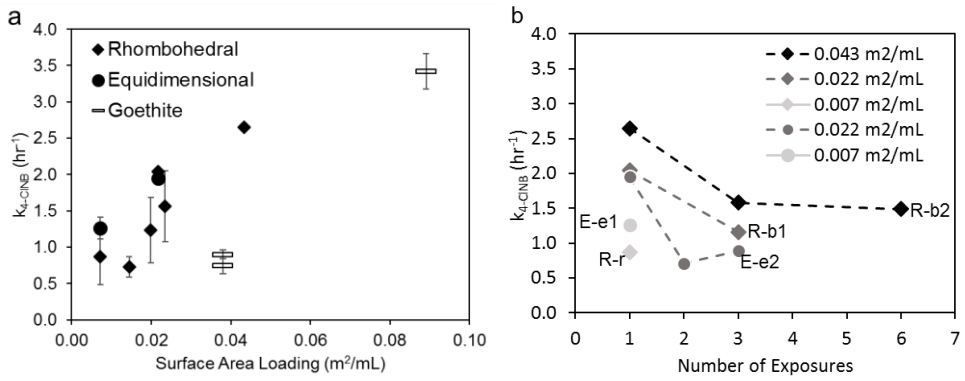

Figure 2.4. Reaction rate data for (a) single- and (b) recurrent-exposures of 4-ClNB on hematite nanoparticles of rhombohedral and equidimensional morphologies. Error bars represent the 95 % confidence interval. Dashed lines in (b) are intended to guide the eye among exposure sequences. Goethite rate data points are literature values with their reported 95 % confidence intervals.[11,28,35]

In the recurrent-exposure experiments of 4-ClNB on both rhombohedral and equidimensional hematite (Figure 2.4b), reaction rates drop substantially over the course of the exposure sequence. For the first exposure, Figure 2.4b shows again that as surface area loading increases, reaction rate increases. For further 4-ClNB exposures, reaction rates progressively decrease with each exposure. In the recurrent-exposure experiment containing R-b2, reactors were sacrificed for determining the 4-ClNB reduction rate after

one, three, and six exposures. The rate dropped from 2.7(4) h^{-1} for the first exposure to 1.6(2) h^{-1} and 1.5(2) h^{-1} in the third and sixth exposure, respectively. Further, in the recurrent-exposure experiment containing R-b1, the reaction rate decreased from 2.0(3) h^{-1} in the first exposure to 1.2(2) h^{-1} after the third exposure. In both R-b1 and R-b2, the observed rates decrease to approximately 60 % of the initial rate. In the recurrent-exposure experiment with equidimensional hematite, the rate decreased from 2.0(3) h^{-1} in the first exposure to 0.7(1) h^{-1} then 0.9(1) h^{-1} after the second and third exposures, respectively. These rates were both approximately 40-50 % of the initial rate.

Post-Reaction Mineral Identification by TEM

TEM imaging shows that many of the rhombohedral particles have a 'kite-and-tail' morphology after reaction with 4-ClNB, as seen in Figure 2.5a. The tails, composed of newly-formed material on hematite {012}, are referred to as rods within this work. Selected area diffraction of extensively sonicated samples enabled facile collection of diffraction patterns of the rods (Figure 2.5b, left inset), which were consistent with the goethite crystal structure in all tested samples (more examples given in Figure B8). Lattice fringe measurements indicated the presence of goethite in both rhombohedral and equidimensional post-reaction specimens, with the (110) (Figure 2.5b, right inset) and the (040) lattice planes (Figure B8) aligned with the growth direction, which is consistent with the known elongation direction of goethite.

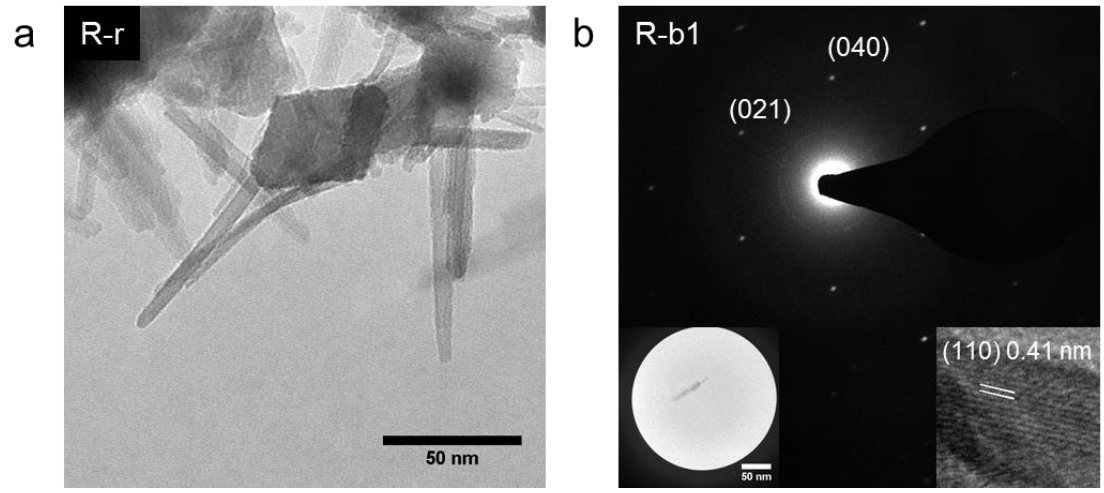

Figure 2.5. TEM images showing (a) the kite-shaped particle morphology post-reaction and (b) electron diffraction pattern and crystal lattice measurements (right inset), which indicate the presence of goethite. The left inset shows a selected rod aggregate that produced the diffraction pattern viewed down the [100] zone axis. Additional electron diffraction patterns and crystal lattice measurements for other reactors are shown in Figure B8.

Discussion

Contrary to what has been previously reported,[34] the mass fraction of goethite in the post-reaction solids depended strongly on the reaction conditions: the observed goethite mass percent in the post-reaction material decreased when surface area loading increased, when initial pH decreased, and when the aqueous Fe(II) concentration decreased. The difference between these results may be attributed to the conditions employed, which differed in buffer identity (3-(*N*-morpholino)propanesulfonic acid), mass loading (>3×), Fe(II) concentration (3×), and pH (>7.0). These results indicate that the heterogeneous nucleation of new phases on the hematite surface is dependent on the distribution of Fe(II)-activated surface sites in aqueous suspensions containing carbonate.

Fe(II)-Activated Surface Site Geometry

Structural considerations support the notion that the atomic surface geometry of hematite {012} serves as an epitaxial template for goethite formation. The specific adsorption of Fe(II) is known to occur at the contiguous singly-coordinated hydroxyl group pair sites;[16,17] both goethite {021} and hematite {012} have approximately four contiguous singly-coordinated hydroxyl group pairs per nm^2 (Table 2.2). The Fe atoms directly below these contiguous singly-coordinated hydroxyl groups are positioned at equivalent distances below the outermost oxygen atoms, at 0.178 and 0.177 nm in hematite and goethite, respectively (Figure 2.6). Additionally, these contiguous singly-coordinated hydroxyl group pairs have the same spatial positioning above their coordinated Fe(III). Hematite {012} has equivalent surface densities of triply- and singly-coordinated hydroxyl groups, at 7.3 hydroxyl groups per nm^2, and no doubly-coordinated groups.[17] The addition of new Fe(III) at only one-half the hydroxyl groups on hematite {012} produces a layer of material that has structural similarity to goethite, which has approximately one-half the Fe density of hematite. Indeed, equilibrium experiments have shown a plateau in the maximum adsorption of Fe(II) on hematite {012} where roughly half of the available binding sites were occupied.[19] These structural similarities are crystallographically consistent with the observed transition in phase composition from hematite to goethite.

Table 2.2. Areal density of contiguous singly-coordinated hydroxyl group pairs across four Miller indices of hematite and goethite with corresponding lattice spacing.[17]

Miller Index	d-Spacing (Å)	Areal Density of Contiguous Singly-Coordinated Hydroxyl Groups (pairs per nm^2)
Hem {113}	2.21	2.1
Hem {110}	2.52	2.5
Hem {100}	4.36	2.9
Hem {012}	3.68	3.7
Gth {110}	4.18	1.5
Gth {100}	4.61	1.7
Gth {010}	9.96	3.6
Gth {021}	2.58	4.1

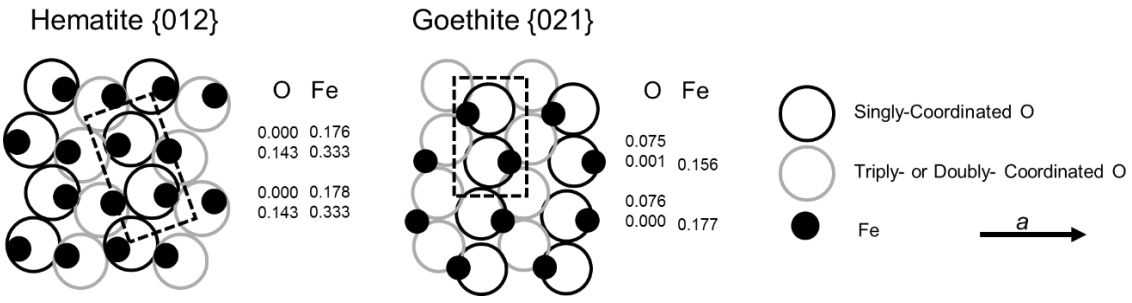

Figure 2.6. Schematic of the hematite {012} and goethite {021} surface Fe and O positions. Gray open circles indicate singly-coordinated hydroxyl groups. Black open circles indicate triply-coordinated hydroxyl groups on hematite and doubly-coordinated hydroxyl groups on goethite. Dotted-line boxes contain a pair of contiguous singly-coordinated hydroxyl groups. Columns of numbers to the right of each schematic are the distances (in nm) of the respective atoms (O or Fe) below the surface as defined by the positions of the oxygen anions labeled with 0.000. Both surfaces are positioned according to the *a* unit cell axis. Adapted from Barron and Torrent, 1996.

Rhombohedral hematite is one of the least thermodynamically favored hematite morphologies.[36] Because of the high free energy of formation and high surface energies relative to goethite,[36,37] substantial growth of the existing hematite crystal is unlikely in aqueous conditions at room temperature. Additionally, goethite formation is favorable in aqueous systems containing carbonate.[2] There are, however, substantial gaps in understanding this phase transformation. Detailed thermodynamic calculations and modeling are needed, because reactive surface structures are a function of Fe(II) concentration, equilibration time, peripheral ion concentrations, pH, and extent of reaction with oxidized molecules, and the nature of evolving reactivity calls for an iterative approach to such calculations.

Reaction Kinetics

Faster reaction rates observed with higher surface area loading is expected because a greater number of reaction sites allows more Fe(II) adsorption to occur and, thus, more electron transfer to the bulk and more rapid 4-ClNB reduction. Differences in 4-ClNB reduction rates between these results with hematite and literature rates for goethite (normalized for surface area loading) arises from the differences in reactivity across accessible facets. For goethite, the majority of oxidative mineral growth occurs on {021} rather than {110} in circumneutral pH conditions in the absence of species that inhibit Fe(II) adsorption and/or the approach of the contaminant (e.g. dissolved organic matter[10]). The {021} of the goethite crystals comprise a minor fraction of the accessible surface area. The faster rate observed for the reaction on rhombohedral hematite could

mean that either a greater fraction of the total accessible surface area adsorbs Fe(II) or the secondary facets adsorb more Fe(II) than those on goethite, or both.

In recurrent-exposure experiments with hematite, the dramatic decrease in reaction rate between the first and third exposures of 4-ClNB is a consequence of the changing distribution and identity of accessible reactive sites. Initially, the surface is solely comprised of hematite. Once goethite sites form, the reaction rate slows as hematite surface sites are blocked by the goethite, and the more slowly reacting goethite surface sites comprise an increasing fraction of the total accessible surface sites. This is shown in Figure 2.4, where recurrent-exposure reaction rates (Figure 2.4b) decrease to a level fitting the trend of goethite rates (Figure 2.4a). Growth formed through further reactions would not be expected to have a substantial impact on rate, even as the goethite surface area increases slightly. Indeed, previous studies have shown that goethite rate remains relatively constant over pH-controlled recurrent-exposure reactions.[10]

Implications

The evolving reactivity of hematite and goethite nanoparticles in anoxic aqueous environments is important for applications in pollutant fate modeling. Projecting the fate and transport of oxidized contaminants and their products in groundwater systems containing iron oxides requires a detailed understanding not only of the chemical transformation of the contaminant but also the characteristics of reactive sites on mineral surfaces and how those characteristics change as reactions progress.

Specifically addressing the water-mineral interface, the reactivity of iron oxide surfaces is sensitive to aqueous conditions such as Fe(II) concentration, pH, and availability of accessible surface sites. The reactivity of the minerals, however, is determined by what surfaces are present at a particular time. As the exposed surfaces grow or dissolve, the reactivity of the system evolves and disordered or roughened surfaces lead to substantial changes in the kinetics of contaminant reduction and concurrent oxidative mineral growth. Under conditions that favor hematite production on hematite nanoparticles, reactivity is expected to be relatively unchanging. Conditions that favor goethite production on hematite surfaces, however, could lead to vastly different reaction rates; a hematite particle coated in a goethite shell would behave as goethite, regardless of which mineral is present in larger mass.

With two mineral phases present, the most important parameter is accessible surface area of the respective minerals. As reactions progress, however, this parameter is a moving target. Ultimately, the aqueous conditions determine which mineral phase forms on the hematite particles, and those conditions can be used to predict reactivity based on evolving mineralogy. Illustrated by the results presented here for hematite particles, fate models for contaminated ground water systems should consider not only initial mineral composition and surface area at the time of contaminant exposure but also the minerals that may form as a result of surface reactions to predict changes in pollutant transformation rates.

Acknowledgements

This work was funded by the NSF grant ECS-1012193 and CHE-1507496. Parts of this work were carried out in the Characterization Facility, University of Minnesota, which receives partial support from NSF through the MRSEC program. Thanks to Thomas E. Webber, who performed the BET measurements.

Chapter 3. The Effects of Organic Matter and a Phenolic Surrogate on the Reactivity and Oxidative Growth of Hematite Nanoparticles

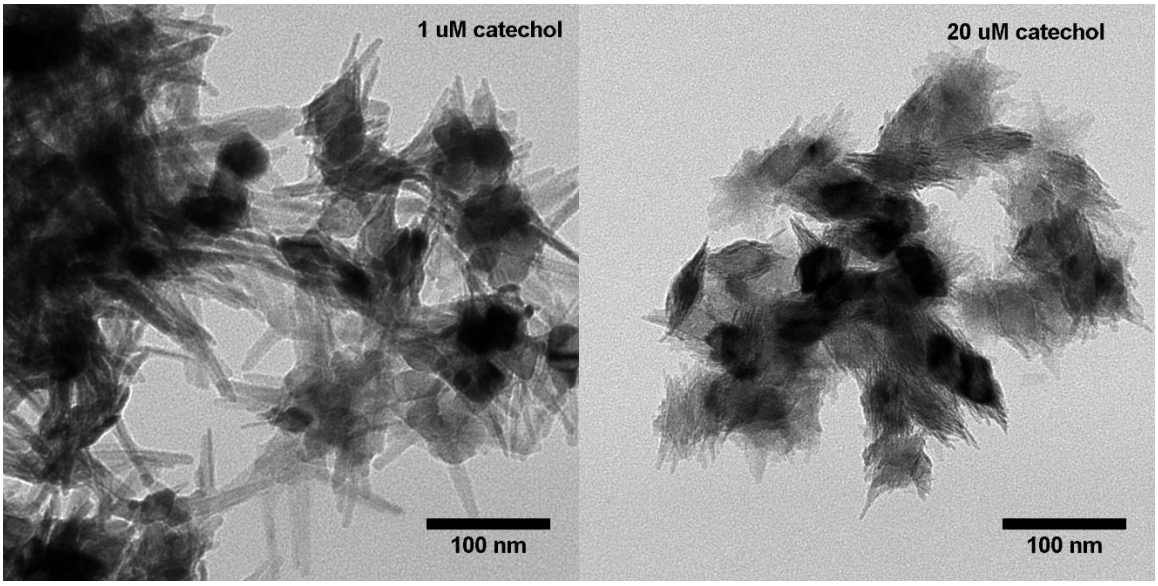

This chapter presents the results of a research project by Jeanette L. Voelz in collaboration with Kaelyn A. Stahovich, Haleigh E. Ziebol, and Nathan A. Harper, and advised by William A. Arnold and R. Lee Penn.

Voelz, J. L.; Stahovich, K. A.; Ziebol, H. E.; Harper, N. A.; Arnold, W. A.; Penn, R. L. The Effects of Organic Matter and a Phenolic Surrogate on the Reactivity and Oxidative Growth of Hematite Nanoparticles. *In Preparation.*

Overview

Hematite is common and reactive mineral found in the environment. Previous studies of the reaction between Fe(II) adsorbed to nano hematite and a model nitrobenzene contaminant found that heterogeneous nucleation of goethite occurred. The extent goethite formation depended on reaction conditions (pH, concentration of Fe(II), mineral surface area). Here, the addition of natural and surrogate organic matter molecules is used to further probe how solution conditions impact the reactivity of Fe(II) adsorbed to hematite and the resulting oxidative mineral growth. Organic matter is ubiquitous in the environment and it interacts with mineral surfaces, potentially facilitating or inhibiting reactions with contaminants, but the molecular characteristics that lead to the observed effects are not well understood. A common moiety found in organic matter is catechol (1,2-dihydroxybenzene), which is known to form complexes with iron at the mineral surface. Catechol is used here as a surrogate to selectively study its effect on reactivity of Fe(II) adsorbed to hematite. Results indicate that higher loading of both organic matter and catechol cause a decrease in reaction rate and drastic changes in both the morphology and amount of goethite nucleated on hematite surfaces. This demonstrates that the evolution of accessible surface area of goethite and hematite are sensitive to the nature and amount of organic matter present. As reactions progress, reactive surface area is a moving target. Ultimately, the solution composition and conditions and the mineralogy of the contaminated site, can be used to predict evolving mineralogy and therefore the reactivity of Fe(II)-adsorbed iron oxide nanoparticles.

Introduction

Understanding reactions of environmental contaminants that occur at water-mineral interfaces is important for assessing contaminant fate and transport. These reactions are typically sensitive to solution conditions, such as pH, ionic strength, and concentrations of other reactive species.[1,2] Determining rate constants and assessing physical changes that occur to mineral surfaces after reactions with contaminants under environmentally-relevant conditions leads to better predictions of contaminant fate and transport in the environment.[3,4]

Hematite is a common mineral, and Fe(II) adsorbed to hematite participates in redox reactions in anoxic groundwaters with some oxidized environmental contaminants.[4–6] Previous studies showed that the reaction between Fe(II) adsorbed to hematite and the model contaminant 4-chloronitrobenzene (4-ClNB) can lead to heterogeneous nucleation of goethite.[4] The degree of goethite formation was shown to depend on the density of Fe(II)-activated surface sites as a function of suspension conditions including surface area loading, pH, and Fe(II) concentration.[4] Another solution condition not yet probed is the addition of organic matter (OM).

Natural organic matter (NOM) is ubiquitous, commonly found in natural waters, sediments, and soils, and generally refers to a complex mixture of large molecules containing a diversity of moieties.[1] NOM varies from site to site in terms of the concentrations and identities of the molecular constituents. It is known that NOM adsorbs to iron oxide surfaces, which affects the rate of reactions facilitated by those surfaces.[1,3,6–11] Many studies have investigated the effects of the presence of added OM on the

reactivity of Fe(II) adsorbed to goethite,[3,6,7,9] and some studies have used hematite and magnetite.[6]

In general, the addition of OM inhibits the reaction between nitrobenzene-type contaminants and Fe(II) adsorbed to iron oxides.[3,6,7,9] This effect was observed most drastically in suspensions containing magnetite and goethite and least in suspensions of hematite, which were compared using surface area-normalized rate constants from reactors prepared with and without added OM.[6] Furthermore, the degree to which the reaction rates decreases depends on the type of OM added; it was observed that the smaller fulvic acid-type OM materials affect the reaction rate more strongly than the larger humic acid-type OM materials.[7] Statistical analyses showed that the presence of OM caused the mineral growth that occurs as a product of Fe(II) oxidation to deposit more on the goethite (110) facets as compared to reactions without OM, and it was inferred that OM inhibits the goethite (021) facets, where oxidative growth primarily occurs in reactions without OM.[3]

Simple surrogate organic matter molecules provide the opportunity to probe structure-reactivity relationships, and judicious selection of surrogates help to elucidate the impacts of OM-bound moieties. The surrogate OM catechol (1,2-dihydroxybenzene) is used here to represent phenolic moieties in OM, which is a commonly-reported property of OM that is determinable by titration.[12] Catechol is of interest because it adsorbs to iron oxide surfaces.[13–17] At neutral pH, catechol primarily exists in solution as the fully protonated species (pK_{a1} = 9.45).[17] Still, a small fraction of the catecholate monoanion exists at pH 7.0, and this charged species forms an inner-sphere complex with iron residing at the iron oxide surface (ca. 1.3 μmol/m^2 on goethite).[17] The complexation

initiates as a mononuclear-monodentate species and later converts to a binuclear-bidentate ligand that bridges two surface-bound iron sites.[17] Adsorption isotherms for hematite have been reported and show that ca. 2.5 μmol/m^2 of catechol adsorbs to hematite at pH 7.0.[15]

The complexation of Fe(II) at the mineral surface by catechol or other phenolic moieties may affect the accessibility of those Fe(II)-activated surface sites to reactions occurring at the hematite surface. As such, the effects of sorbed organic ligands in the form of standardized organic matter and catechol are studied here as they impact oxidative mineral growth and evolving reactivity of synthetic hematite nanoparticles in the redox reaction between Fe(II) and a model contaminant with hematite.

Experimental

Ultrapure water (MilliPore Milli-Q Advantage A10, 18.2 Ω•cm) was used in all solutions and experimental processes. All experiments were performed in an anaerobic glovebag (Coy Laboratory Products) equipped with an O_2 monitor (Coy Laboratory Products) and Pd-catalyzed O_2 scrubber under an atmosphere composed of 5:95 v/v H_2:N_2. All reaction vessels were wrapped in aluminum foil to exclude light. All solutions that required pH adjusting used 1 M HCl or 0.5 M NaOH solutions that were prepared from concentrated stocks of HCl (Aristar, 12.1 M, 36.5 – 38.0 %) or NaOH (Fisher Scientific, 19 M, 50 %w/w). Rhombohedral hematite particles were synthesized and described in a previous study.[4]

Batch reactors were prepared in 120 mL serum bottles containing 10 mM sodium bicarbonate (Sigma-Aldrich, 99.7 %), 0.007 or 0.023 m^2/mL hematite, and 1 mM Fe(II) ($FeCl_2 \cdot 9H_2O$, Fisher, 101.5 %), with or without the presence of added organic carbon (OC) in the form of catechol or standardized OM, and were equilibrated for 21 hours. Catechol (Fisher, >99 %) was added to reaction vessels as an aqueous 1 mM solution diluted from an aqueous 10 mM stock solution. Suwanee River aquatic natural organic matter standard (SRNOM, catalog number 1R101N) was purchased from the International Humic Substances Society for use as standardized OM and was added to reaction vessels from an aqueous stock solution (2000 ppm OC). Reactions that did not contain OC were used as reference conditions. Following equilibration, the model contaminant 4-chloronitrobenzene (4-ClNB, Acros Organics, 99 %) was dissolved in methanol (Fisher Chemical 99.9 %) and added to the reactors to yield a concentration of 100 μM 4-ClNB and 1 % methanol. The reduction was monitored by high performance liquid chromatography (HPLC, Agilent Infinity 1220) to obtain the rate constant using a method described elsewhere.[4] After the reaction was complete, the reaction solids were concentrated and washed with four 30-mL aliquots of Milli-Q water by centrifugation and then dried in a fume hood.

A recurrent-exposure experiment involved preparing three identical reactors without OM as described above, where two reactors received additions of 4-ClNB and one reactor served as a control. Only one of the reactors was sampled during the first reaction for determination of the observed rate constant. After the reaction was complete, the particles were concentrated, washed, and dried as described above. In the second reactor, the pH was raised back to pH 7.0 and Fe(II) was added to adjust the

concentration back to 1 mM. After equilibration for another 21 hrs, 4-ClNB was again added and the reactor was sampled for determination of the observed rate constant. When the reaction was complete, the particles were concentrated, washed, and dried.

The concentration of Fe(II) was determined by ferrozine (Sigma-Aldrich 97 %) assay (λ_{max} = 652 nm) using UV-visible spectroscopy (Agilent 8453), as described by a previously-reported method.[4] The mineral composition of the dried powders was analyzed using an X-ray diffractometer (PANalytical X'Pert Pro) equipped with cobalt source (1.7909 Å) and X'Celerator detector. The materials were analyzed from 18–32 °2θ with an effective dwell time of 950 s per step and a step size of 0.0167 °2θ, and the hematite (012) and goethite (110) reflections were used to determine the mass fraction of each mineral, as previously described.[4] The particles were imaged by transmission electron microscopy (FEI Technai T12, 120 kV accelerating voltage) to assess particle morphology.

Quantifying Goethite Content

All solids were analyzed by XRD to assess mineral identity after reaction. Calculations that determine the mass% of goethite and hematite present in the solids are based on XRD patterns collected from samples comprised of known masses of synthetic goethite and hematite.[4] This type of calculation requires a strong, fully resolved peak from each component. For these specimens, calculations use peak areas of goethite (110) (I = 100 %) and hematite (012) (I = 30 %), adjusted for their respective scattering intensities.[4]

Following the redox reaction with Fe(II) and 4-ClNB, the total possible goethite formation is calculated from reaction stoichiometry. The reaction requires the transfer of six electrons, each provided by the oxidation of Fe(II) to Fe(III). The precipitation of Fe(III) as only FeOOH is defined as the stoichiometric maximum of goethite formation. For one addition of 100 μM 4-ClNB in the presence of 1 mM Fe(II), the stoichiometric maximum of goethite in the post-reaction solids is 35 mass%.[4]

Results

Quantitative Relation between Organic Matter and a Surrogate

The organic matter standards considered for testing herein are available through the International Humic Substances Society (IHSS) and are listed in Table 3.1. Each material is given an abbreviation (Table C1) based on the collection location, organic matter (OM) fraction (e.g., humic acid, fulvic acid, or aquatic natural OM), and batch number, and the associated ID is the catalog number assigned by the IHSS. These organic matter samples have been characterized extensively, and the results are reported in the product descriptions on the IHSS website.

Table 3.1. Phenolic content of organic matter standard materials offered by the International Humic Substances Society (IHSS). The IHSS assigns each material a catalog number and reports parameters such as the phenolic content (meq/g C). Phenolic content was converted to catechol equivalents (μM catechol) at different concentrations of OC (Table C2). Plotting catechol equivalents versus OC concentration yields a curve with a slope of catechol equivalents loading (μM/ppm OC) (Figure C1).

IHSS Organic Matter Standards	IHSS Catalog Number	Phenolic Content (meq/g C)	Catechol Equiv. Loading (μM /ppm OC)
SRHAI	1S101H	4.24	2.1
SRNOM	1R101N	3.94	2.0
SRHAII	2S101H	3.72	1.9
SRFAI	1S101F	2.91	1.5
SRFAII	2S101F	2.84	1.4
PPFAI	1S103F	2.32	1.2
LHA	1S104H	2.31	1.2
ESFAII	2S102F	2.27	1.1
PPHA	1S103H	1.91	1.0
ESHA	4S102H	1.87	0.9
UMNOM	1S110N	0.83	0.4

Elemental composition of OM standards is provided by the IHSS. This report includes the content of ash, water, and carbon for each material, among other elemental and isotope data. These three parameters are used to calculate the organic carbon content (ppm OC) in the organic matter material. First, the fraction of ash and water are subtracted out and the remaining mass fraction is multiplied by the carbon content to yield the mass fraction of OC. The mass fraction of OC is then multiplied by the measured sample mass to yield a mass of OC present in the sample. The massed sample is then dissolved in the desired volume of water to yield solutions of OC (ppm).

The acidic functional group content (i.e., the carboxyl and the phenolic content, expressed in meq/g OC) for OM standards is also provided by the IHSS, as determined by titration.[12] The OC content and the phenolic content are two parameters used in a

calculation performed herein to establish a conversion factor that relates the widely-used OM standards to a phenolic-type surrogate OM. This conversion factor is important for comparing results of reactions using different OM materials. The conversion factor developed here equates a concentration of OC (ppm) to a concentration of catechol (μM), which contains two phenolic alcohols.

The conversion was defined and calculated as follows. The phenolic components were identified in the titration analyses as two times the change in charge density between pH 8.0 and 10.0.[12] The units for phenolic content were based on calculations of molar charge concentrations and were given units of meq/g OC.[12] If each charge equivalent represents one phenolic hydroxyl group, then the units are presented as mmol phenol/g OC. The simplest calculation assumes that 100 % of the phenolic hydroxyl groups are in the form of a catechol moiety. It is unlikely, however, that all the phenolic hydroxyl groups exist as catechol moieties, and using this assumption greatly over estimates the catechol loading. Using the conversion that two phenolic hydroxyl groups are present in one catechol molecule, the units are converted to mmol catechol/g OC. By multiplying this value by a concentration of organic carbon, the concentration of catechol equivalents (μM) at the specified concentration of OC is determined.

These calculations were performed for a range of OC concentrations (Table C2). Plotting the results yields a visual representation of how the catechol equivalents concentration varies for each of the OM standards (Figure C1). The slope of this curve gives a conversion factor of catechol equivalents loading (μM/ppm OC).

Suwanee River Aquatic Natural Organic Matter (SRNOM) was selected for comparisons with catechol because it has high catechol equivalents loading (2.0 μM/ppm

OC). Several trends were observed in the catechol equivalents loading across the different organic matter standards (Table 3.1). Suwanee River samples have the highest catechol equivalents, at 1.9 – 2.1 μM/ppm OC for humic acids and NOM and 1.4 – 1.5 μM/ppm OC for fulvic acids. Fulvic acids are generally grouped together, at 1.1 – 1.5 μM/ppm OC. Humic acids are also grouped and have lower catechol equivalents loading than fulvic acids, at 0.9 – 1.2 μM/ppm OC. UMNOM contains by far the lowest catechol equivalents, at 0.4 μM/ppm OC.

Reaction Kinetics

Results presenting the rate constants for reference reactions and reactions using various concentrations of SRNOM and catechol are provided in Figure 3.1.

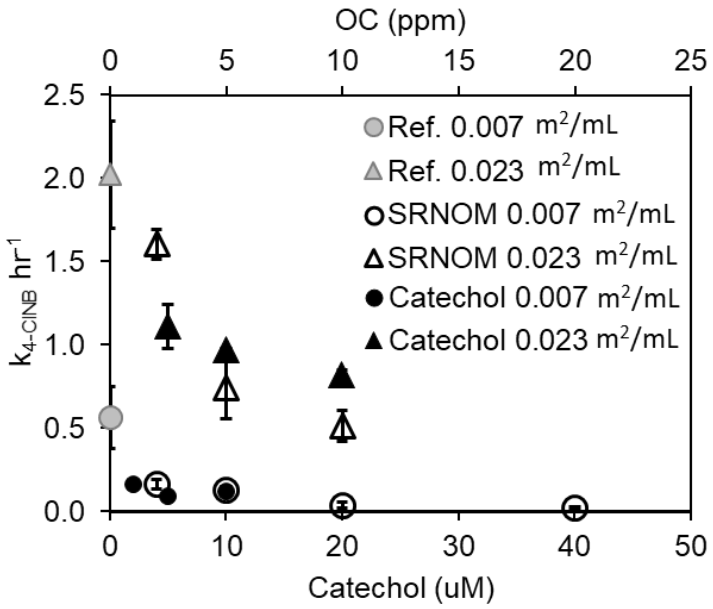

Figure 3.1. Rate constant of 4-ClNB reduction (hr^{-1}) in suspensions containing hematite nanoparticles, Fe(II), and organic carbon in the form of SRNOM (open black markers) or catechol (closed black marker). Reference reactions (grey filled markers) did not contain organic carbon. SA loading was 0.007 (circles) or 0.023 (triangles) m^2/mL. Error bars represent standard deviation of triplicate reactors. Some error bars are contained completely within the marker.

Reference reactions that contained only hematite, Fe(II), and 4-ClNB yielded rate constants that scaled equivalently with surface area (SA) loading. The lower SA loading of 0.007 m^2/mL (i.e. 1×) yielded a rate constant of 0.6 ± 0.2 hr^{-1}, and the higher SA loading of 0.023 m^2/mL (i.e. 3.25×) yielded a rate constant of 2.0 ± 0.3 hr^{-1}.

In reactions containing SRNOM, increasing the concentration of added OC resulted in lower observed rate constants and the rate constants did not scale with SA loading. At 1× hematite SA loading, the rate constants for 2, 5, 10, and 20 ppm added OC were 0.17 ± 0.03 hr^{-1}, 0.14 ± 0.02 hr^{-1}, 0.04 ± 0.02 hr^{-1}, and 0.03 ± 0.01 hr^{-1}, respectively. At 3.25× hematite SA loading, the rate constants for 2, 5, and 10 ppm added OC were 1.61 ± 0.09 hr^{-1}, 0.8 ± 0.2 hr^{-1}, and 0.52 ± 0.09 hr^{-1}, respectively.

The presence of SRNOM more greatly affected the observed rate constant in reactions having lower hematite SA loading. This effect is seen by representing the rate constant at different concentrations of added OC as a percentage of the rate constant from the reference reaction. In the reactions having 3.25× hematite SA loading, the observed rate constants for reactions containing 2 ppm and 10 ppm added OC were 80 % and 26 % that of the reference rate. Comparatively, reactions having 1× hematite surface area loading had observed rate constants at 28 % and 7 % of the reference value.

In reactions containing catechol, increasing the catechol concentration also resulted in lower observed rate constants. For reactions at 3.25× hematite SA loading, the rate constants for the reactors containing 5, 10, and 20 μM catechol were 1.1 ± 0.1 hr^{-1}, 0.97 ± 0.01 hr^{-1}, 0.82 ± 0.03 hr^{-1}, respectively. For reactions at 1× hematite SA loading,

the rate constants for reactors containing 2, 5, and 10 μM catechol were 0.16 ± 0.03 hr^{-1}, 0.091 ± 0.002 hr^{-1}, 0.12 ± 0.02 hr^{-1}, respectively.

Oxidative Mineral Growth by XRD

Goethite mass% in solids from reactors containing 1× hematite SA loading and SRNOM or catechol were compared to each other and against a reference reactor that contained no OC. The results are presented in Figure 3.2, and includes a conversion factor of 2.0 μM catechol/ppm OC, which enables comparison between the two data sets. Representative XRD patterns are provided in Figure C2. No goethite was detected in solids from reactions at 3.25× hematite SA loading.

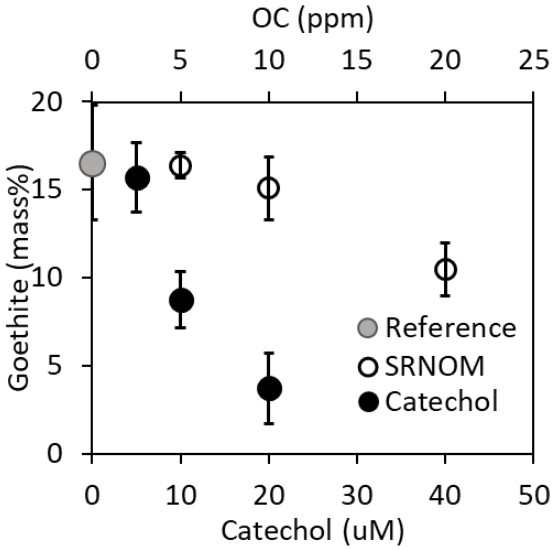

Figure 3.2. The mass percent of goethite present in dried post-reaction solids versus the concentration of catechol (black filled markers) or added OC from SRNOM (black open markers). Reference reactors (grey filled marker) did not contain added OC or catechol. Hematite SA loading was 0.007 m^2/mL. Error bars represent standard deviation of triplicate reactors.

The post-reaction solids from the reference reaction, performed without OC present, contained 17 ± 3 mass% goethite. Calculations using the amount of iron oxidized by the reaction and the mass% of goethite formed in the reaction show that 38 % of the oxidized iron was deposited in the form of goethite. By difference then, 62 % of the iron oxidized in the reaction is deposited as hematite, as another material, or as goethite in domain sizes too small to be detected by XRD.

In the post-reaction solids from reactors containing SRNOM, the goethite mass% decreases with increasing OC concentration. For concentrations of 5, 10, and 20 ppm OC, the analysis yielded 16 ± 1 mass%, 15 ± 2 mass%, and 10 ± 2 mass%. Similarly, in the post-reaction solids from reactors containing catechol, the goethite mass% decreases with increasing catechol concentration. For concentrations of 5, 10, and 20 μM catechol, the analysis yields 16 ± 2 mass%, 9 ± 2 mass%, and 4 ± 2 mass%.

Oxidative Mineral Growth by TEM

Post-reaction solids were characterized using transmission electron microscopy (TEM), and representative images for the material collected from the reactor containing 1× hematite SA loading and varying concentrations of SRNOM are shown in Figure 3.3. In the reference reactor (Figure 3.3A), which contained no added OC, single crystals of goethite formed on the far opposite tips of the hematite rhombohedra. These rods are approximately 20 – 80 nm long and 10 nm wide. Shorter rods are generally associated with smaller hematite crystallites.

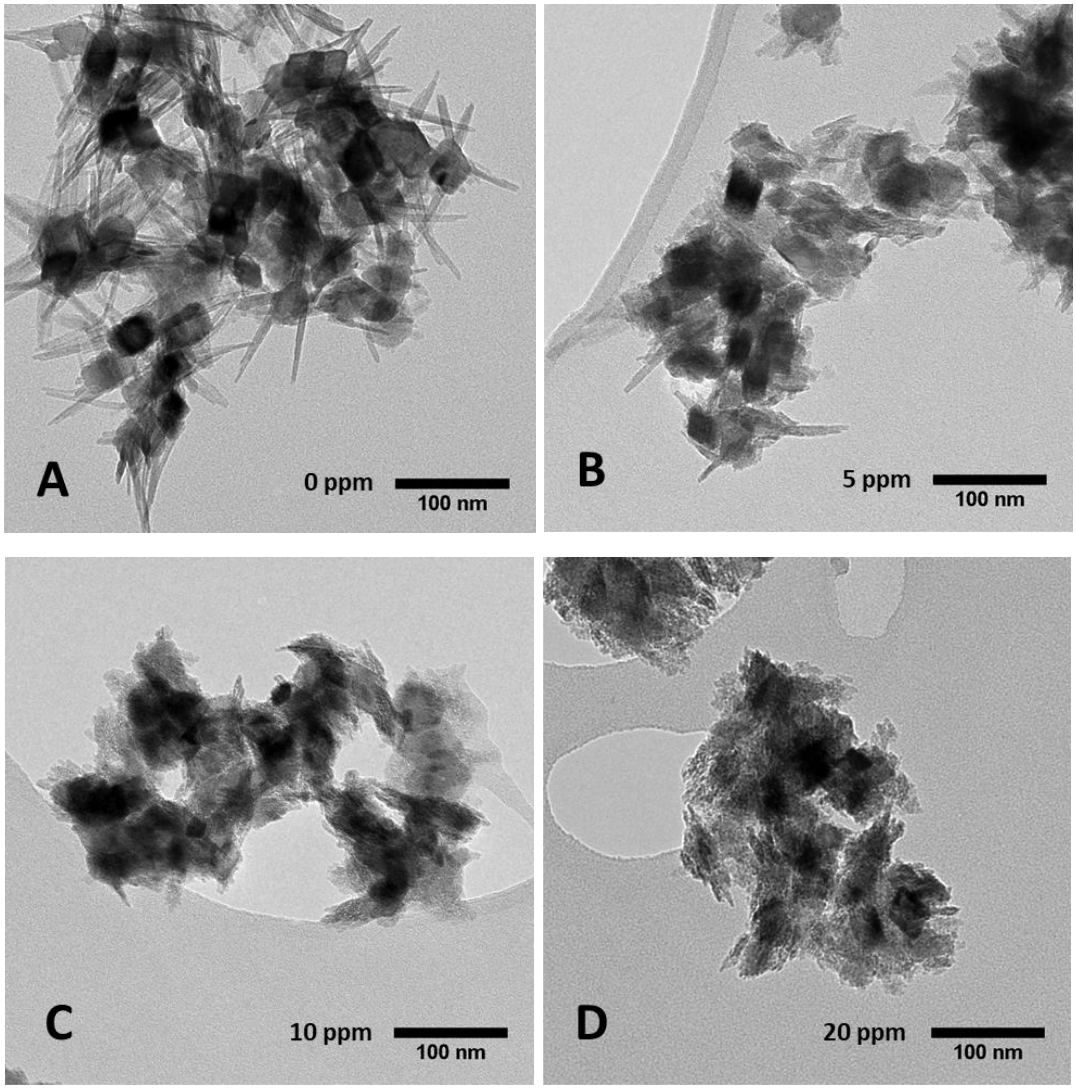

Figure 3.3 TEM images showing the formation of goethite on the surface of hematite nanoparticles after reaction with 4-ClNB and Fe(II). Hematite surface area loading was 0.007 m^2/mL. The reference reactor (A) did not contain organic carbon. Other reactors contained SRNOM in concentrations of 5 ppm (B), 10 ppm (C), and 20 ppm (D).

In reactors containing SRNOM, the average goethite crystallite size decreased as the concentration of SRNOM increased. In reactors containing 5 ppm SRNOM (Figure 3.3B), subtle differences in morphology are observed; some rods have similar structure as the reference condition, but many rods have a rougher surface and/or are no longer

uniformly distributed along the axis of growth (i.e., the c-axis of goethite). The rhombohedral hematite seed and the acicular rods are more difficult to define and differentiate among the roughly formed oxidative growth.

More dramatic differences in morphology are observed in the particles from the reactions containing 10 ppm and 20 ppm SRNOM (Figures 3.3C and 3.3D, respectively). In these solids, the hematite seed is often indistinguishable from the oxidative growth, which is mostly roughly-formed. Sporadically, there is semblance of acicular structures residing on the far tips of the hematite rhombohedron, but these structures are not well-formed and appear to be multiple parallel structures.

In reactors containing catechol at 1× hematite SA loading, the morphology of the oxidative growth progressively roughened as catechol concentration increased in a manner similar to the reactors containing SRNOM (Figure C3). Close inspection of post-reaction solids from the reactor containing 10 μM catechol and 1× hematite SA loading at higher magnification (Figure 3.4) reveals more intricate differences in morphology, as compared to the reference reaction. The oxidative growth primarily occurs at the far opposite tips of the hematite rhombohedra, which is consistent with all other observations, but this growth is instead composed of multiple parallel acicular structures (ca. 5 – 8 rods). These structures are thinner and shorter than the rods in the reference condition, measuring 10 – 50 nm long and ca. 5 nm wide.

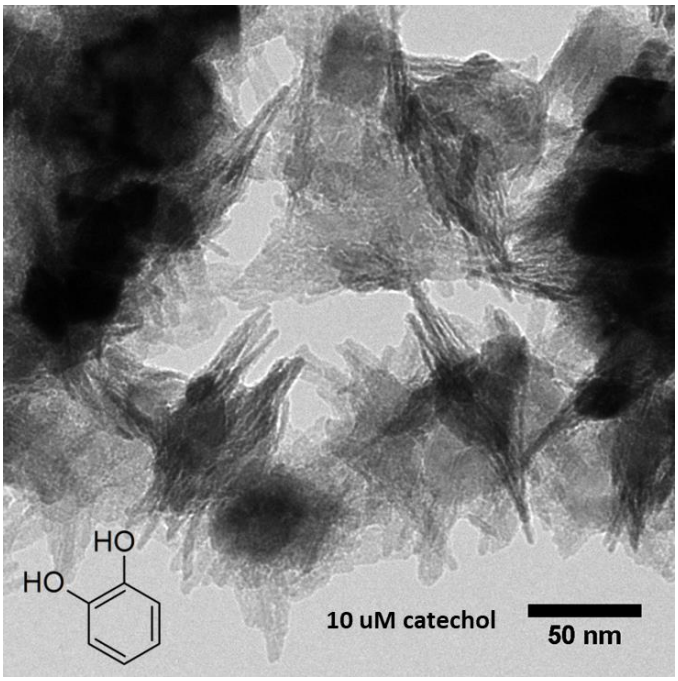

Figure 3.4. TEM image of post-reaction solids dried from a reactor containing 10 μM catechol with 0.007 m^2/g hematite surface area loading. Oxidative mineral growth occurring in the presence of catechol forms multiple parallel rod structures (ca. 5 – 8) at far opposite tips of the hematite rhombohedra. These rods are shorter and thinner than those in the reference.

No rod-like structures were observed in post-reaction solids from reactors containing 3.25× hematite SA loading, with or without added OC as SRNOM (Figure C3). It was observed, however, that the particle surfaces become rougher with increasing OC content.

Evolving Mineralogy

A sequential spike experiment at reference conditions (i.e. without the presence of added OC) was used to probe the evolving mineralogy of the solid material present after the first round of reaction. Figure 3.5 plots the mass% of goethite in the post-reaction

solids, as compared to the stoichiometric maxima, after the first and second spikes and shows a representative TEM image of the post-reaction material after the second spike.

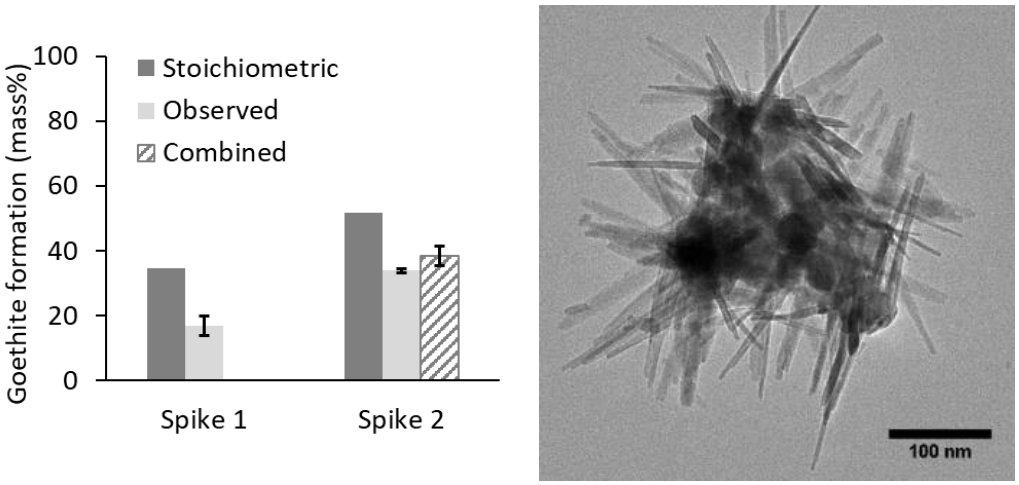

Figure 3.5. The plot (right) shows the mass% of goethite for each of two reactions (spikes) at reference conditions without added OC as calculated from reaction stoichiometry (dark grey bar), as observed in reactors sacrificed after each spike (light grey bar), and as calculated by adding the stoichiometric mass% of spike 2 to the observed mass% from spike 1 (diagonal stripe bar). The TEM image (left) shows the morphology after spike 2.

In both reactors, the observed mass% of goethite is lower than the stoichiometric maxima. Assuming 100 % conversion of Fe(II) to goethite, the stoichiometric maxima for spike 1 and 2 are 35 mass% and 52 mass%, respectively. The observed values are 17 ± 3 mass% and 34 ± 1 mass%, respectively. A calculation was also performed that combined the observed value from spike 1 and the stoichiometric maximum of spike 2. This combined value represents a scenario where iron oxidized forms goethite and hematite in spike 1 and forms only goethite in spike 2. The result of this calculation is 39 ± 3 mass%, represented by the diagonally-stripped bar in the plot provided in Figure 3.5. The combined value is similar to the observed value.

Discussion

Selection of Standardized Organic Matter for Catechol Comparison

Based on the established quantitative relation between the various organic matter standards and catechol, SRNOM was selected as the OM standard for this study. An OM with high phenolic content was most desirable because a higher density of phenolic content increases the probability that the catechol moiety is present. Of the IHSS reference materials with highest catechol equivalents loading, only SRNOM was on-hand and well characterized. In addition, previous studies had been conducted using SRNOM to elucidate the effects of OM on the reaction between Fe(II) and 4-ClNB with goethite. These studies were performed at identical pH, buffer concentration, and reagent concentrations used herein, thereby allowing for comparisons between goethite and hematite.[3,7]

Reaction Kinetics

The negative correlation observed between the concentration of added OC from SRNOM and the rate constant in this system is similar to results from another study that used goethite under identical solution conditions.[7] The SA loading of hematite used here and of goethite used in the related study differed, but comparisons can be made by normalizing results to known and reported surface area parameters. For this comparison, the ratio of added OC concentration to surface area loading was computed. Then, the observed rate constants for the conditions with similar ratios were represented as a fraction of the rate constant from the reference condition (i.e. without added OC).

One of the ratios from the goethite reactions matches that of a reaction performed in the hematite system, and two ratios are compared to estimates based on a linear relationship of the collected data herin. For goethite, the reactions with 5, 10, and 20 ppm added OC contained 4.6 m^2 total surface area to yield 1.0, 2.2, and 4.4 ppm added OC/m^2, respectively.[7] These ratios resemble conditions in the hematite system of ca. 3 ppm added OC with 3.25× SA loading (2.8 m^2), 2 ppm added OC with 1× SA loading (0.9 m^2), and ca. 4 ppm added OC 1× SA loading, respectively.

A comparison of the rate constants at these ratios suggests that the reaction in the hematite system is more strongly impacted by the presence of added OM than the goethite system. At these ratios, the rate constants were 100, 70, and 23 % of their initial value in the goethite system,[7] and ca. 67, 36, and ca. 24 % in this hematite system. This comparison suggests OM adsorbs to goethite and hematite differently, perhaps blocking reactive sites on hematite more than on goethite. At the ratio of highest OC:surface area (4.4 ppm added OC/m^2), the rate constant in both cases was ca. 20 % that of the reference rate constant. This occurs in both systems at ca. 0.5 mg OC/m^2 and may indicate a level at which added OC inhibits both surfaces equally. This level corresponds to 4 ppm added OC in the hematite system.

Oxidative Mineral Growth

High concentrations of added OC appear to inhibit reactive sites on hematite such that the formation of distinctly acicular goethite does not occur. At 5 ppm added OC, some of the oxidative growth occurs as acicular rods but most of the oxidized material is

poorly-defined. At greater concentrations of added OC, the oxidized growth occurs only as only poorly-defined material.

Similarly, increasing the catechol concentration causes more of the oxidative growth to occur as poorly-defined structures, and the growth morphology is comparable between the data sets according to the catechol equivalents loading conversion. For example, the conversion factor relates the 10 μM catechol condition to the 5 ppm OC condition. Approximately the same degree of oxidative growth occurs in both of these conditions as acicular rods but overall the growth is more poorly-defined than the reference condition.

Under close inspection, the oxidative growth in the reactors containing high concentrations of catechol (e.g. 20 μM) occurs as finger-like structures emerging from the far tips of hematite rhombohedra (Figure C4). The tips have previously been identified as hematite (012) surfaces.[4] The formation of binuclear-bidentate complexes between catechol-like species and adsorbed Fe(II) would inhibit two reactive sites on hematite (012) and then inhibit further Fe(II) adsorption at those sites. This would decrease the density of accessible Fe(II)-activated surface sites and may prevent further iron oxidation at those sites. We hypothesize that this interaction causes multiple islands of goethite nucleation sites, rather than a continuous film, leading to epitaxial growth of several goethite rods from the surface.

Simple calculations suggest that the mass residing in the finger-like structures (Figure 3.4) occurring in the 10 μM catechol condition is approximately equivalent to the mass residing in the single acicular structure observed in the reference condition. These finger-like rod structures are approximated by cuboids measuring 35 nm long, 5 nm wide,

and 5 nm thick. Using an average of 6 rods per hematite vertex, the approximate volume of newly-formed material is 5300 nm^3 per vertex. By comparison, one rod measuring 60 nm long, 10 nm wide, and 10 nm thick yields a volume of 6000 nm^3 per vertex. These volumes are approximately equivalent, suggesting that the same amount of material is deposited near the hematite vertices, but questions remain regarding its mineral identity.

The results from XRD suggest that less of the oxidized material occurs as goethite, but the mass% detected by XRD may be influenced by differences in crystal domain rather than caused by actual differences in mass%.[18] The XRD calibration curve uses the peak area of the goethite (110), which is parallel to the axis of growth in goethite. The diffraction pattern is impacted by the size of this domain, or the depth of the material perpendicular to the plane. In these samples, the size of that domain decreases and/or becomes less defined as the concentrations of OC or catechol increase. These traits lead to peak broadening and may inhibit the detection of goethite. Development of another XRD method based on a different goethite peak is challenging because goethite (110) is already the most intense reflection and other goethite peaks must be deconvoluted from hematite peaks.

Owing to these complications, the previously developed XRD calibration curve method may not be reliable for quantifying goethite formation on hematite when high concentrations of OC are present during the redox reaction. Either a new XRD method must be developed, or magnetic measurements should be used, such as Mössbauer magnetometer, which have a far lower limits of quantification than XRD.[19,20]

Evolving Mineralogy

The results from sequential spike reactions performed without added OC show that the mineral identity of the material oxidized during a reaction depends on the identity of the minerals present at the start of the reaction. Initially, when only hematite was present, the oxidized Fe(II) formed both goethite and hematite in approximately equivalent mass%. Then in the second spike, goethite continued to form on the goethite surface and almost no hematite formed. This may suggest that all reactive sites on hematite transition to goethite after a certain amount of epitaxial oxidative growth. Another possible explanation is that Fe(II)-activated sites on goethite are preferred for this reaction, and the results of TEM imaging show that most of the oxidative growth from the second spike occurred on the goethite (021) surfaces such that the rods formed after the first spike nearly doubled in length.

Implications

The results described herein show that the presence of OC inhibits the redox reaction between a model nitrobenzene contaminant and Fe(II) adsorbed to hematite. This has implications in contaminant transformation, where the reaction would occur more slowly in environments high in OM. This effect may be a positive characteristic in situations where the product is more hazardous (e.g., more toxic or more water-soluble), or a negative characteristic in cases where contaminant reduction is the desired outcome.

When this reaction occurs, heterogeneous nucleation of a new phase can drastically change the reactivity of the system. The results here demonstrate that once

goethite forms it becomes the surface on which further reactions occur, leading to systems that are dominated by the reactivity of goethite. Furthermore, the reactivity is a moving target because surface area increases as oxidative growth occurs, an effect that may be magnified in conditions where the multiple finger-like structures form. Ultimately, the solution composition and conditions and the mineralogy of the contaminated site are important for predicting the evolving mineralogy and reactivity of Fe(II)-adsorbed iron oxide nanoparticles.

Finally, the morphological changes that occur as a result of the presence of OM (e.g., the decreasing domain size of goethite or the poorly-formed domains) presents a challenge in identification and quantification of the growth phase. The XRD method used herein may not provide accurate results for specimens reacted in the presence of OM and therefore may not apply to specimens from natural settings where OM is ubiquitous. More investigation of solid-state characterization methods is needed to accurately evaluate oxidative growth of particles from suspensions containing OM.

Acknowledgements

This work was funded by the NSF (CHE-1507496). Parts of this work were carried out in the Characterization Facility, University of Minnesota, which receives partial support from NSF through the MRSEC program.

Chapter 4. Iron-Bearing Minerals for Sulfide Removal from Industrial Aqueous Waste: Characterizing Low-Value Solid Wastes for Use as Feedstocks

Iron mine tailings waste located in Grand Rapids, MN.

This chapter presents the results of a research project by Jeanette L. Voelz,

in collaboration with Jacob Daire, Nathan W. Johnson, and Chan Lan Chun,

and advised by William A. Arnold and R. Lee Penn.

Voelz, J. L.; Daire, J.; Johnson, N. W.; Arnold, W. A.; Chun, C. L.; Penn, R. L. Iron-Bearing Minerals for Sulfide Removal from Industrial Aqueous Waste: Characterizing Low-Value Solid Wastes for Use as Feedstocks. *In Preparation.*

Overview

Sulfate contamination of freshwater resources is a major concern for mines in regions where sulfur-bearing minerals are abundant. Sulfate-reducing bacteria produce sulfide, which is toxic to aquatic organisms. One known sink for sulfide is iron. Iron ore processing generates solid waste materials that are not economically viable for iron extraction but contain iron-bearing minerals such as goethite, hematite, magnetite, siderite, ilmenite, and olivine. Some of these minerals react with sulfide to form iron sulfides. Depending on the mineral makeup of iron-rich waste solids, these materials may have use in sulfur-capture systems treating aqueous discharge streams. The composition of iron-rich waste solids from mines in Minnesota were characterized by XRD and chemical dissolution methods. The quantity of iron liberated from mine materials by dissolution was compared to relatively pure reference minerals to assist in identifying the mineral phase from which the iron originated. The values of Fe(II), Fe(III), and Fe(tot) as accessed by different dissolution reagents were considered material parameters. The mine specimens and reference minerals were exposed to sulfide in three different buffer systems: 10 mM acetate at pH 4.7, and 10 mM carbonate at pH 8.0 and 9.0. Reaction rate and extent of reaction were two main reaction parameters collected. Reaction parameters were mapped versus material parameters to identify possible correlations that would enable quicker screening of mine materials as candidates for sulfide removal. The reference minerals best suited for sulfide removal were goethite, hematite, and siderite. Mine materials containing larger quantities of these minerals generally performed better than those lacking these minerals, and the material RW-IO reacted faster and reacted with more sulfide than any other mixed mineral specimen at pH 4.7.

Introduction

Mining activities have occurred around the world for millennia and are necessary for providing raw materials to many industries. The energy industry, for example, relies on mining coal for coal-fired power plants,[1] uranium for nuclear reactors,[2] and quartz sand for silicon solar panels.[3] Consumer electronics are often the destination of mined heavy metals (e.g., Cu, Pb, Zn, Co, Cd, and Cr),[4,5] platinum group metals (e.g., Ru, Rh, Pd, Ox, Ir, and Pt), and rare earth elements.[6] Mined diamonds and gold have been used as adornments but now also find use in other consumer goods.[7,8] Technological advancements and population growth have caused demand for these raw materials to grow exponentially, and the expansion of mines, the close proximity of people to mining areas and processing facilities, and the more aggressive processes used for gaining to access lower grade ores have led to severe detrimental impacts to environmental and human health.[1–8]

While sulfur is itself a mined commodity, it is also a contaminant generated by mining activities in the form of sulfate. Sulfate contamination of freshwater resources is a major concern for mines in regions where sulfur-bearing minerals are abundant. Sulfur often co-occurs with iron and one of the most common iron sulfide minerals is pyrite (FeS_2).[9] Other iron sulfides include troilite (FeS), marcasite (FeS_2), pyrrhotite ($Fe_{1-x}S$ (x = 0 – 0.2)) and greigite ($Fe^{II}Fe^{III}_2S_4$), and mixed metal sulfides include mackinawite ($(Fe,Ni)_{1+x}S$ (x = 0 – 0.11)), chalcopyrite ($CuFeS_2$),and arsenopyrite (FeAsS).[9,10] These minerals oxidize when exposed to water and oxygen, producing an acidic solution of sulfate and dissolved iron known as acid mine drainage.[5,9,11]

When sulfate enters natural waters, sulfate-reducing bacteria (SRB) generate hydrogen sulfide as part of their metabolic function.[4,12] While sulfate is relatively non-toxic in surface waters, the elevated levels of sulfide generated by SRB in anoxic sediments has been shown to inhibit lifecycle processes in plants.[13,14] To protect aquatic species, the waste streams causing sulfate contamination must be treated before waters are discharged to the environment. One possible treatment method may utilize SRB to intentionally transform sulfate into sulfide and then capture sulfide before the waste is discharged.

Iron is known to react with sulfide. In fact, it is the generation of iron sulfide plaques on wild rice roots, modeled in a study using *Zizania palustris*,[14] that motivates the investigation herein. Previous studies have shown that ferrihydrite-coated zeolite is effective at removing sulfide from artificial seawater at pH 8.5.[15] In a related study, sulfide removal from saline solutions at pH 7.5 found that the rate varied across several iron (oxyhydr)oxide minerals, increasing in the order goethite < hematite < magnetite << lepidocrocite ≈ hydrous ferric oxides.[16] These results vary slightly from those reported in an earlier study, where rate constants at pH 7.5 were ordered magnetite < hematite < goethite < lepidocrocite << ferrihydrite, but it was noted that differences surface area loading influence rate results.[17] Sheet silicates also react with sulfide but only slowly, with half-life of approximately 100,000 years.[17]

In an engineered remediation system, waste material from iron mining may be useful for sulfide capture from nearby aqueous waste streams. Iron mines generate several crushed materials that contain iron (oxyhydr)oxides of identities and/or concentrations that are not economically viable for use as ore. Provided that the crushed

materials do not themselves release hazardous substances like heavy metals or sulfate, using a local benign solid waste as a feedstock for treating local hazardous waste aligns well with green chemistry principles and sustainable engineering practices.[18,19] In this study, several solids produced from iron mine processing streams in northern Minnesota were tested for potential use as sulfide remediation feedstocks. The results were compared to the results of sulfide removal using relatively pure reference minerals in three different buffer systems, spanning pH 4.7 – 9.0 and using either acetate or bicarbonate buffer to represent environmentally-relevant conditions.

Materials and Methods

All experiments were performed in an anaerobic glove bag (Coy Laboratory Products) under atmosphere containing 5 % H_2 (Matheson, 10 % H_2, 90 % N_2) and 95 % N_2 (Matheson, 99.999%) with oxygen monitor (Coy Laboratory Products). Ultra-filtered water (MilliPore Advantage A10, 18.2 MΩ•cm) was used in all solutions and reaction vessels.

Mine Materials

Industry professionals collected mixed mineral specimens at various points the iron ore processing stream from facilities in Northern Minnesota. Specimens include waste rock (RW), tailings (T), ore (O), ore concentrate (OC), and fired ore (OF) and were crushed in a ball mill then sieved (200 – 100 mesh, 75 – 150 μm). Quikrete all-purpose

sand was purchased and used as a control. Each specimen was dialyzed to remove mineral salts and oxidize surfaces newly exposed by crushing. The dry solids were mixed with ultra-filtered water to produce a slurry, which was then added to cellulose dialysis bags (Spectra/Por 7, MWCO 2kD) and the ends were secured with plastic clips. The bags were suspended in ultra-filtered water in Nalgene bottles without solution agitation. The water was changed at 3-hour intervals on the first day, and at 6- to 12-hour intervals on succeeding days, for a total of nine water changes over 10 days. The specimens were then removed from the bags, concentrated by centrifugation, freeze-dried, and analyzed by X-ray diffraction.

Reference Minerals

Natural reference mineral specimens that were collected or purchased included quartz (Rue des Lys, France), kaolinite (Washington County, Georgia), olivine (Kohlstedt Research Group, UMN; nominally Fo_{90}; Peridot, Arizona), brown siderite (Feinberg Research Group, Institute for Rock Magnetism, University of Minnesota), white siderite (Ward's Science; Mt. St. Hilaire, Quebec), ilmenite (Laguna Clay Company), magnetite (Gold Beach, Oregon). Both siderite specimens were ground to a fine powder by mortar and pestle upon receipt. The ilmenite and magnetite specimens were further concentrated using neodymium magnets and then ground to a fine powder by mortar and pestle. Synthetic minerals were prepared according to established procedures and included 4 nm and 6 nm 6-line ferrihydrite,[20] acicular goethite,[20] and nominally-equidimensional hematite.[21] Ferrihydrite specimens were dialyzed then dried within two days in a fume hood.

Materials Characterization

Mineral composition was identified prior to reaction for all specimens by X-ray diffraction (PANalytical X'Pert PRO, Co K_α 1.7909 Å, X'Celerator detector). Specimens were analyzed from 10 – 90 °2θ with a step size of 0.0167 °2θ and an effective dwell time of 100 s per step. Select post-reaction solids were also analyzed by XRD. These materials were transferred to 50 mL centrifuge tubes inside the glove bag, centrifuged at 5500 rcf for 3 minutes, then returned to the glove bag to decant the supernatant. Milli-Q water was the added to the tubes and the centrifugation process repeated with a total of four washes. The concentrated slurries were transferred to weigh boats and dried in a fume hood before being analyzed by XRD.

Chemical Dissolution

The dissolutions by acetate, hydroxylamine-HCl, oxalate, and concentrated hydrochloric acid are previously described.[22] The dissolution by aqua regia is modified from EPA Method 3050B, section 7.5. Approximately 0.1 g of material was added to a 250 mL Florence flask, combined with 10 mL of concentrated hydrochloric acid (HCl) and 2.5 mL of concentrated nitric acid (HNO_3). The mixture was refluxed at 95 °C for 30 minutes. The digest was filtered through a 0.45 um PTFE filter into a 100 mL volumetric flask and brought to volume with 0.5% HNO_3. The solutions were analyzed by atomic absorption spectroscopy (Varian AA240FS, air/acetylene mixture) for total iron and by inductively coupled plasma mass spectrometry for elemental analysis. Aqua regia extractions were performed in duplicate.

Batch Experiments

Reactions with sulfide were performed in 60 mL borosilicate serum bottles. Solid specimens were massed directly into serum bottles, a magnetic stir bar added, and the vessels transferred to the anaerobic chamber for overnight equilibration.

All buffer solutions were prepared inside the anaerobic chamber in Nalgene bottles. Water used for the buffer solutions was deoxygenated by bubbling N_2 (Matheson, 99.999 %) for 1.5 hrs and then transferred to the anaerobic chamber for overnight equilibration. A 20 mL solution of 4 M acetic acid was prepared from glacial acetic acid (Aristar) outside of the glove bag, deoxygenated for 30 minutes, and transferred to the glove bag for use as a stock solution to prepare 10 mM acetate buffer. Solid sodium bicarbonate (Sigma-Aldrich, 99.7 %) was massed outside the glove bag into a scintillation vial, transferred to the glove bag, and equilibrated overnight before use. Bicarbonate buffer was always prepared fresh and used immediately. All buffer solutions were pH adjusted using 1 M HCl (made from concentrated, Aristar) or 0.5 M NaOH (made from 50 % w/w, Fisher Chemical).

Sodium sulfide nonahydrate (Sigma Aldrich, >98 %) was stored in the glove bag. Crystals were washed with water, patted dry, and then massed for a 500 mg/L S stock solution. The well-mixed 500 mg/L S stock solution was aliquoted into 2 mL amber vials immediately to prevent outgassing of hydrogen sulfide (H_2S) and these vials were used for multi-spike experiments within 4 days. This solution was diluted to 10 mg/L S for calibration curve standards.

Batch reactions were performed by loading the equilibrated serum bottles with the appropriate buffer to the point of no headspace, then crip-capped and wrapped in

aluminum foil to prevent light exposure. The 500 mg/L S solution (0.600 mL) was loaded into a syringe (Norm-Ject, 1 mL) with needle tip (Covidien Monoject, 21 GA, 1.5 inch) and constant-volume sampling was performed by quickly injecting this solution into the reactor and allowing the extra volume to be received by an equivalent syringe and needle. This sampled solution was filtered (Agilent, 13 mm, 0.2 μm, nylon) into acrylic cuvettes, then 0.3 mL of the filtrate was transferred to another acrylic cuvette containing 2.600 mL Milli-Q water. Methylene blue reagent was made in-situ by adding 50 μL of Sulfide Reagent 1 (Hach, cat. 181632) and 50 μL of Sulfide Reagent 2 (Hach, 131732). The solution was capped, inverted 3×, and then the absorbance at 665 nm measured by UV-visible spectroscopy (Agilent 8453) after 5 minutes. Water served as the blank for these measurements and the absorbance at 500 nm was used as a baseline. The reactions were sampled until the reaction was complete, or 1.5 hours had passed, whichever occurred first.

Post-Reaction Analytical Methods

Dissolved Fe(II) was quantified by ferrozine assay (3-(2-pyridyl)-5,6-diphenyl-1,2,4-triazine-p,p'-disulfonic acid monosodium salt hydrate, Sigma-Aldrich 97 %).[21] Chemical reduction was then performed with each cuvette by adding 0.300 mL of 1.4 M hydroxylamine-HCl (Sigma-Aldrich, >99 %) in 2 M HCl, allowing overnight equilibration, then adding 0.100 mL of 10 M ammonium acetate (Sigma-Aldrich, >97 %) buffered to pH 9.5 with NaOH and allowing 5 hrs for equilibration before measuring total absorbance again. The difference between the two Fe(II) concentration values represents the Fe(III) concentration.

Elemental sulfur content was determined by a published method for high performance liquid chromatography (Agilent Infinity 1220).[23] Samples of post-reaction solids were prepared by combining 4 mL of well-mixed reactor suspension and 2 mL of tetrachloroethylene (PCE, Sigma-Aldrich, >99 %) in a borosilicate scintillation vial. The suspension was shaken gently and left to equilibrate overnight on the benchtop. The PCE layer was then filtered (Agilent, 13 mm, 0.2 μm, nylon) into an amber vial.

Sulfate and thiosulfate concentrations were determined by ion chromatography (Metrohm 930 Compact IC Flex). For each reactor, 10 mL of suspension was filtered (Agilent, 13 mm, 0.2 μm, nylon) into borosilicate scintillation vials. For those that contained aqueous Fe(II), the vials were removed from the glove bag and solid sodium bicarbonate (ca. 100 mg) was immediately added to precipitate iron out of solution. The solutions were filtered after 30 minutes then more sodium bicarbonate was added. This process repeated until there was no further precipitation. The solutions were run in duplicate using a buffer of 3.2 mM sodium carbonate (anhydrous, Fisher Chemical, HPLC grade) and 1 mM sodium bicarbonate (Sigma-Aldrich, 99.7 %).

Samples were submitted for further elemental analyses by inductively-coupled plasma mass spectrometry (ICP-MS) to the Research Analytical Laboratory at the University of Minnesota. These digests were prepared by combining 0.250 mL of well-mixed reactor suspension and 4.000 mL of concentrated HCl. The mixture digested overnight in a fume hood, then a portion of the solution was diluted 100× in a volumetric flask. An aliquot of the diluted solution was filtered, 1 mL of the filtrate was combined with 10 mL of 1 % nitric acid solution (prepared from concentrated, Sigma-Aldrich, 70 %) in a 15 mL polypropylene centrifuge tube, and then the solution was submitted for testing.

Results and Discussion

This study was conducted in three phases. In the first phase, the iron residing in all mine materials and reference minerals was classified by phase and oxidation state using solid-state and chemical dissolution techniques. Phase two used batch reactions to study the rate and extent of reaction of sulfide with each of the mineral specimens when sulfide was added to the reactors in three different buffer systems. The third phase mapped the material parameters determined in the classification phase versus reaction parameters determined in the reaction phase to identify what metrics are best used to select optimal materials for sulfide removal from wastewater.

Material Source and Phase Classification

Mine materials were sourced from several points within the iron mine processing stream from several facilities in northern Minnesota. These collection points are highlighted in Figure 4.1. In the field, the material covering the valuable ore is called the overburden. This material may contain some of the mined commodity (e.g., iron) but often the concentration is too low to be considered economically viable. Overburden is therefore removed and piled offsite and is labeled here as ‘rock waste’. Iron ore is then transported to a processing facility where it is crushed and magnetically separated to yield ore concentrate. These processes produce a fine dust in the facility, which is captured by air filters. Material collected from those filters is labeled here as ‘tailings dust’. Tailings is composed of the material remaining after the magnetic extraction. These materials are commonly seen in large piles in mining areas. Ore concentrate undergoes

further processing to form pellets for easy transporting to steel-making facilities. The pellets are heat-treated in a furnace and the waste (e.g., broken pellets) from the fired pellets are considered 'fired ore waste'. The highlighted boxes in Figure 4.1 indicate the points at which specimens used in this study were collected. The asterisks indicate the products of low economic value. Specimens obtained from these collection points are assigned source abbreviations of RW for rock waste, TD for tailings dust, T for tailings, O for ore, OC for concentrated ore, and OF for fired ore. As a negative control, a non-iron-bearing sand was sourced from standard bags of all-purpose construction sand and is abbreviated as STD.

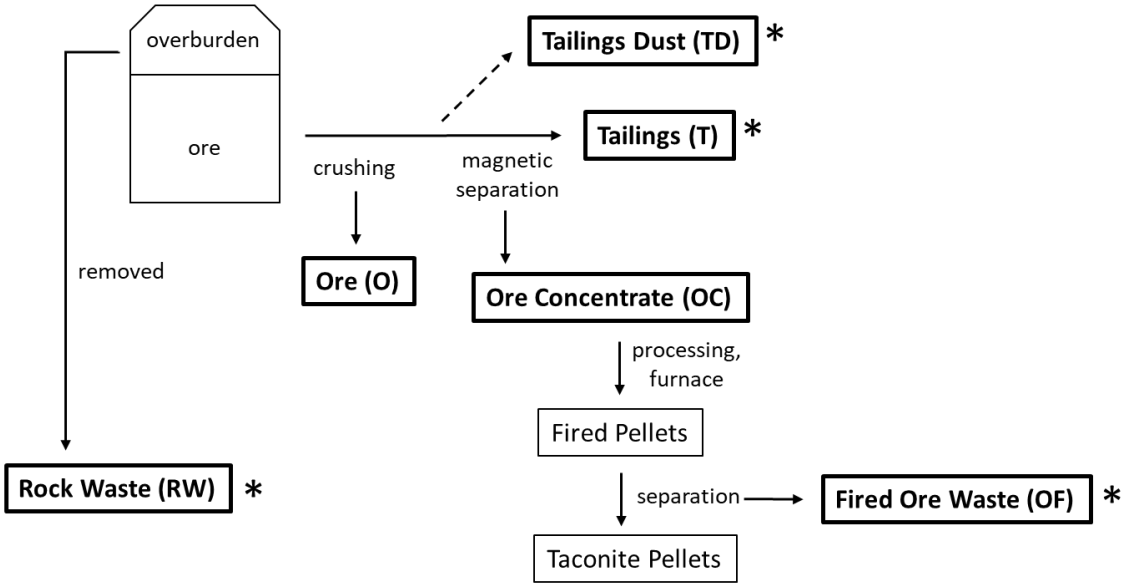

Figure 4.1. Generalized diagram depicting the iron mining process. Bolded boxes indicate specimen collection points. Asterisks (*) indicate products of low economic value.

Specimens collected from iron mining facilities are heterogeneous mineral mixtures and the mineral composition of each was determined by XRD. The results of this analysis are presented in Table 4.1, where the minerals detected are nominally listed

in order of decreasing relative abundance. The diffraction patterns for each are provided in the supplemental (Figures D1 – D10). Based on the XRD results, the mixed specimens were grouped into one of five classes: iron oxides (IO), siderite (S), magnetite (M), mixed iron (MI), and non-iron (NI) specimens. The classes IO, S, and M were selected because they represent the hypothesized major reactive component. The MI class grouped the specimens that were otherwise difficult to classify because of their complex mineral composition, and the NI class solely comprised of the material used as a negative control. Each of the specimens in Table 4.1 are also identified by the material's source within the iron processing stream as outlined in Figure 4.1. By combining the abbreviations for mineral class and source identity, each mixed mineral specimen was assigned an ID for use in figures and tables herein and is provided in Table 4.1.

Table 4.1 Mixed mineral specimens collected from iron processing facilities in Northern Minnesota with corresponding source identity, ID used in figures and tables, and major mineral detected by XRD. The non-iron specimen used as a control was all-purpose construction sand.

Class	Source Identity	ID	Major Minerals Detected by XRD*
Iron Oxide	Rock Waste	RW-IO	Quartz, Magnetite, Hematite, Goethite
Iron Oxide	Tailings, Dust	TD-IO	Quartz, Hematite, Dolomite, Magnetite
Siderite	Rock Waste	RW-S	Quartz, Siderite, Chlorite
Siderite	Tailings	T-S	Quartz, Siderite, Hematite, Dolomite
Siderite	Ore	O-S	Quartz, Siderite, Hematite, Magnetite, Dolomite
Magnetite	Ore, Concentrate	OC-M	Magnetite, Hematite, Quartz, Calcite, Dolomite
Magnetite	Ore, Fired	OF-M	Magnetite, Hematite, Quartz, Calcite, Dolomite
Mixed Iron	Tailings	T-MI	Lizardite, Chlorite, Magnetite, Quartz, Ilmenite, Hematite, Kaolinite
Mixed Iron	Ore, Concentrate	OC-MI	Ilmenite, Magnetite, Chlorite
Non-Iron	Std. Material	STD-NI	Quartz, Aragonite, Dolomite

*Mineral detected are nominally listed in order of decreasing relative abundance.

The mixed mineral specimens varied greatly in mineral composition. To illustrate the degree of heterogeneity, a rough Rietfeld refinement was performed on the diffraction

patterns of the T-S and OF-M specimens. The T-S specimen was found to contain approximately 75 % quartz, 15 % hematite, and 10 % siderite by mass. The OF-M specimen contained approximately 55 % magnetite, 35 % hematite, and 10 % quartz by mass. The results for the T-S specimen show that the assigned mineral class does not necessarily indicate which mineral is most abundant; rather, it only identifies the mineral hypothesized to have the greatest impact on the reaction with sulfide. Noting that a large fraction of hematite is present in both cases, these results illustrate the point that minerals coexisting with the hypothesized reactive component may also have a substantial impact on the reaction with sulfide. As such, parallel reactions with relatively pure reference minerals are important for identifying the primary reactive component of these mineral mixtures and assessing the contributions of secondary reactive components.

Eleven relatively pure reference minerals were collected, purchased, or synthesized to evaluate their reactivity with sulfide. These minerals are listed in Table 4.2 and their diffraction patterns are given in the supplemental (Figures D11 – D21). Two non-iron-bearing minerals, quartz and kaolinite, were used as negative controls. The Fe(II)-bearing minerals included olivine, siderite, and ilmenite, Fe(III)-bearing minerals included ferrihydrite, goethite and hematite, and the sole mixed valence mineral was magnetite. Two different siderite specimens were included because although their diffraction patterns indicated pure siderite (Figures D14 and D15), the color difference suggested the presence of elemental substitutions or other components present in masses below the limit of detection for XRD that could impact reactivity. Two 6-line ferrihydrite specimens were included because their synthesis methods differed, which may result in

differences in reactivity. Pure natural goethite was unavailable, so synthetic material was used instead, and synthetic hematite was used as a comparison for goethite.

Table 4.2. Collected, purchased, and synthesized reference minerals with chemical formula, sample ID, remarks on the incidence of iron in the sample, and the ideal iron oxidation state.

Mineral	Ideal Formula	ID*	Remarks	Fe Oxidation State
Quartz	SiO_2	Qz		NA
Kaolinite	$Al_2Si_2O_5(OH)_4$	Kln		NA
Olivine	$(Mg,Fe)_2SiO_4$	Ol	Nominally Fo_{90}:Fa_{10}	Fe(II)
Siderite	$FeCO_3$	W-Sd		Fe(II)
Siderite	$FeCO_3$	B-Sd		Fe(II)
Ilmenite	$FeTiO_3$	Ilm	Magnetically concentrated	Fe(II)
Magnetite	Fe_3O_4	Mag	Magnetically concentrated	Fe(II) & Fe(III)
Ferrihydrite	$5Fe_2O_3•9H_2O$	4nm 6LF	Size identified by procedure	Fe(III)
Ferrihydrite	$5Fe_2O_3•9H_2O$	6nm 6LF	Size identified by procedure	Fe(III)
Goethite	α-FeOOH	Gth	Synthetic source	Fe(III)
Hematite	$α\text{-}Fe_2O_3$	Hem	Synthetic source	Fe(III)

*Mineral ID is the standard abbreviation,[24] and prefixes white (W) and brown (B) are used to differentiate minerals from multiple sources.

Determining mineral identity and approximate mass composition is common by XRD, but there are challenges with using this method. One challenge occurs with identifying minerals of low mass percent because the limit of detection for XRD is typically lies at 1 – 4 mass%.[25] If oxidized coatings reside on mineral surfaces, for example, these layers may not be detectable by XRD. Another challenge presents itself in specimens of highly complex mineral composition, where deconvoluting patterns may be impossible. In some cases, therefore, other methods to supplement XRD analysis are important for assisting with the determination of mineral identity and mass composition.

Iron Classification by Chemical Dissolution

Chemical dissolution methods may provide valuable information about sample composition that is not necessarily accessible by XRD. Many dissolution methods are available and are often described as targeting specific mineral phases.[22] For methods with high mineral selectivity, chemical dissolution may enable iron classification for mineral fractions present in low mass percent that are not detectable by XRD. Some dissolution procedures also preserve the native iron oxidation state, which allows for the specific quantification of Fe(II) and Fe(III). Dissolution methods also vary in aggressiveness, thereby allowing access to some minerals and not others, which is especially valuable when estimating Fe(II) and Fe(III) content for specific mineral targets. Dissolution methods are not 100 % selective for specific minerals, however; in most cases, iron dissolves from multiple mineral phases including non-targeted minerals, if only to a minor degree. It is therefore important to emphasize that quantifying iron liberated by a dissolution method cannot be identified as residing only in a specific mineral. Instead, chemical dissolutions should only suggest mineral phases as a primary or likely source of iron.[22,26]

Four chemical extraction methods were performed in parallel on all mineral specimens to compliment XRD analyses. These methods included concentrated HCl or aqua regia to quantify total iron residing in (oxyhydr)oxides, acetate buffer to target carbonates, $HONH_2$-HCl to target SRO iron (oxyhydr)oxides, and oxalate buffer under darkness to target SRO iron (oxyhydr)oxides and magnetite. Those methods that preserved the iron oxidation state include the dissolutions using acetate buffer, oxalate buffer under darkness, and concentrated HCl. The amount of Fe(II), Fe(III), and Fe(total)

are valuable for normalizing reaction rates to determine characteristics by which promising reactive materials can be identified. Data obtained from reference mineral dissolution assisted the compositional analysis of the mixed mineral specimens according to what mineral fractions were accessed by each dissolution method. The results of these dissolution experiments are presented graphically in Figure 4.2, in tabular form in the supplemental (Table D1 – D4), and critically analyzed in a previous study.[22]

The results from the reference mineral digestion using concentrated HCl and from the mixed mineral digestion using aqua regia are used to represent 'total Fe' in the samples and are presented in plots A and B within Figure 4.2, respectively. These methods do not achieve complete sample digestion (silicate dissolution requires HF or autoclave temperatures),[27] but the results are appropriate representations for 'total accessible Fe' in reactions with sulfide under mild conditions presented here. The value of 'total accessible Fe' is used to compare extent of dissolution for several methods and represents one parameter by which kinetic data can be normalized.

For the reference minerals (Figure 4.2A), concentrated HCl completely dissolved all siderite, 6-line ferrihydrite, goethite, and hematite specimens, as determined by visual inspection. The vial containing magnetite had few crystals remaining. The vials containing ilmenite, olivine, quartz, and kaolinite had a large fraction of the material remained at the time of sampling. The solution phase for ilmenite and olivine became yellow, indicating iron dissolution, and olivine grains turned white. The solution phase for quartz and kaolinite remained clear and colorless.

The results for total accessible iron in mixed mineral samples as determined by dissolution using aqua regia (Figure 4.2B) show correlations to the material source.

Specimens OC-M and OC-F originate from the same ore material but are collected at different points in the process stream. These materials contain primarily magnetite and hematite and were found to have approximately the same total iron content, at 610 ± 10 and 602 ± 26 mg Fe/g, respectively. The other ore concentrate, OC-MI, is sourced from a different mine and appears to contain substantially less iron. The primary component of OC-MI is ilmenite, as identified by XRD (Table 4.1), but the results in Figure 4.2A show that ilmenite is not readily dissolved by strong acid. The quantity of iron residing in OC-MI, therefore, is likely underrepresented by this dissolution method. The specimen originating from ore high in siderite (O-S) also contained a substantial fraction of iron, at 425 ± 70 mg Fe/g. This specimen originated from the same material as OC-M and OF-M but was again collected at a different point in the process stream. Tailings and rock waste specimens generally contained less iron than the ore and ore concentrates, as expected. The exception to this trend is RW-IO, which contained nearly as much iron as O-S, at 405 ± 11 mg Fe/g. This material contained mostly quartz, but also small amount of magnetite, hematite, and goethite (Table 4.1), and it is unrelated to any of the other specimens. No mixed mineral specimen achieved complete dissolution at the time of sampling, attributable mainly to the presence of silicates.

The reference mineral dissolution results using acetate buffer (Figure 4.2C) show that primarily siderite dissolved, as was targeted by the method. Approximately 50 % of the brown siderite and 40 % of the white siderite dissolved, as compared to the method using concentrated HCl. The inability to achieve complete dissolution even after extending the recommended dissolution time[27] from two days to four days, indicates that these siderite samples were highly crystalline and may require longer dissolution times,

hotter temperatures, and/or more concentrated reagents to achieve full dissolution.[22,27] Some of the iron residing in olivine and 4 nm 6-line ferrihydrite was also extracted using acetate buffer, which illustrates the point that iron liberated by a dissolution method cannot be identified as solely residing in the targeted mineral. These results from this experiment also show that this method is effective at preserving the iron oxidation state, because the brown siderite contained only Fe(II) and the 4 nm 6-line ferrihydrite contained only Fe(III), as expected based on ideal mineral composition. Four percent of the iron released from white siderite was Fe(III), which may have originated from weathering of this natural specimen.

The results from the reference mineral dissolution by acetate buffer can be used to assess the composition of the mixed mineral specimens in conjunction with XRD analyses (Figure 4.2D). The specimens grouped into the siderite class (RW-S, T-S, and O-S) are expected to have the greatest amounts of Fe(II) liberated by acetate buffer. As hypothesized, those specimens released more Fe(II) than Fe(III) and also released more Fe(II) than most of the other specimens. The TD-IO specimen contained a surprising amount of Fe(II), even though siderite was not detected in this specimen. All the mixed mineral specimens, however, originated in geologic formations containing iron silicates, iron sulfides, and iron carbonates, which are potential sources of Fe(II) even if not identified by XRD because of low masses or convoluted diffraction patterns. Indeed, the diffraction pattern for TD-IO (Figure D2) contained several small unidentifiable peaks that may originate in another Fe(II)-bearing mineral solubilized by acetate, such as carbonates or sulfides.[10,22,28] The amount of iron released by TD-IO may also relate to particle size. While all mixed mineral specimens were sieved to particle size 75 – 150

microns after crushing, nanoparticles adhering to larger grains were likely not removed. Fine particles present a larger surface area from which iron could dissolve. Because TD-IO originated as a dust, this sample may have contained more fine particles than the other specimens, leading to an artificially high dissolved iron value.

Simple calculations were performed to estimate the quantity of siderite in TD-IO. Considering that acetate dissolved approximately 50 % of reference siderite samples and approximately 15 mg Fe/g was liberated in TD-IO, then it is expected that 30 mg Fe/g resides siderite in TD-IO. This mass equates to approximately 60 mg of siderite per gram of material, or 0.6 % of the sample. By comparison, the sample with most Fe(II) liberated by acetate (T-S) is estimated to contain 1 % siderite by the same calculation. Both values are at or below the limit of detection for XRD. The fact that it was detected in the T-S specimen, however, indicates that siderite is present in higher mass% than calculated according to the dissolution results, again suggesting that the siderite is highly crystalline and resists dissolution by this method.

The dissolution using $HONH_2$-HCl is used to target iron residing in short-range order (SRO) iron(oxyhydr)oxides (Figure 4.2E). It is usually performed sequentially after acetate dissolution because the acidic hydroxylamine solution also dissolves carbonates. The dissolution was performed here in parallel instead to assess the extent of dissolution from each mineral phase. After four days, the dissolution of the 4 nm and 6 nm 6-line ferrihydrite specimens was complete, as determined by visual inspection using laser pointer light. Siderite dissolution by hydroxylamine was incomplete, as noted by visual inspection, but approximately 50 % more iron was liberated by hydroxylamine than by acetate. This method was most selective for siderite and ferrihydrite, and only liberated 8

± 1 mg Fe/g from magnetite, 22.8 ± 0.1 mg Fe/g from goethite, and 6 ± 1 mg Fe/g from hematite, which are 1, 4, and 1 % of the total extracted by HCl, respectively.

In the mixed mineral specimens, hydroxylamine released more iron by far from RW-S than any other sample, at 129 ± 3 mg Fe/g specimen (Figure 4.2F), which accounts for 60 % of the iron extracted by aqua regia. The remaining specimens can be separated into two groups: those where 20 – 35 % of the iron liberated by aqua regia is extracted by hydroxylamine, which includes TD-IO, T-S, and T-MI; and those where <10 % is extracted by hydroxylamine, which includes (in descending order) OC-MI, O-S, OF-M, OC-M, and RW-IO. The results for the RW-IO specimen, where hydroxylamine extracted 2 % of the iron extracted by aqua regia, is interesting because as a rock waste it is likely to be subject to weathering, of which ferrihydrite is a common product. This specimen, however, appears to contain little ferrihydrite. Assuming a formula mass for ferrihydrite of 168.7 g/mole, RW-IO is calculated to contain approximately 13 mg of ferrihydrite/g of material, as compared to 195 mg/g for RW-S. A possible reason for the difference in SRO iron oxide content may relate to the results of the acetate method presented in Figure 4.2D. The rock waste RW-S contains more Fe(II)-bearing minerals accessible to acetate than the RW-IO specimen, and it is possible that natural oxidation of these minerals led to the formation of SRO iron oxides.

The dissolution using oxalate buffer was performed under darkness specifically to preserve the oxidation state because exposure to light induces photoreduction.[29] Dissolution by oxalate under darkness is slower than with irradiation and by limiting the dissolution time to two days, the results are used to represent ‘surface-accessible’ iron. The method using oxalate under darkness favors the dissolution of SRO iron

(oxyhydr)oxides, but also dissolves Fe(II)-bearing (oxyhydr)oxides like magnetite through an autocatalytic dissolution mechanism.[30] This acidic solution also causes the dissolution of siderite, but to a lesser degree than the target minerals.[22] For this reason, 'surface-accessible' iron includes iron residing at or near the surface of minerals with lower solubility as well as iron residing more deeply within highly soluble phases.

The results from dissolution of the reference minerals by oxalate align well expectations (Figure 4.2G). Approximately half of the iron residing in magnetite and both 6-line ferrihydrite specimens were liberated, as compared to the HCl dissolution, and 25 % and 20 % were liberated from siderites and other iron oxides (goethite and hematite), respectively. This method preserved the oxidation state, as seen by the release of primarily Fe(II) in siderites and only Fe(III) in ferrihydrite, goethite, and hematite. Similar Fe(II):Fe(III) ratios in magnetite is observed in both the HCl and the oxalate extractions, at 0.30 and 0.34, respectively. This is lower than the ideal ratio of 0.5, but this specimen originated as beach sand grains and may have undergone partial oxidation to maghemite.

Analyzing the Fe(II);Fe(III) ratio as accessed by the oxalate method can assist in sample composition analysis in the mixed mineral specimens (Figure 4.2H). Only the specimens containing siderite (RW-S, T-S, and O-S) had an Fe(II):Fe(III) ratio >1, at 2.0, 2.9, and 1.2, respectively. This would suggest that siderite primarily comprises the most accessible iron-bearing mineral in these specimens. The Fe(II):Fe(III) ratio for OC-M and OF-M are higher than expected, at 0.74 and 0.71, respectively. These samples, however, are known to contain siderite because they come from the same initial material as T-S and O-S. If approximately 2 – 3× the value of Fe(II) extracted by the acetate method (ca.

10 mg Fe(II)/g) is subtracted from the oxalate results (2 – 3× because of the 50 % dissolution of reference siderite in this method), then the new Fe(II):Fe(III) ratio for these samples is close to 0.5. The specimen RW-IO had the lowest Fe(II):Fe(III) ratio, at 0.17, which corresponds well with other results. There was little Fe(II) liberated from RW-IO by acetate and XRD results indicate the presence of primarily goethite, hematite, and magnetite, the latter of which is the likely source of oxalate-soluble Fe(II).

The results of mixed mineral dissolution by oxalate (Figure 4.2H) correspond well to the results by aqua regia (Figure 4.2B), where the relative amounts of iron among the mixed mineral specimens remains approximately the same. This suggests that the 'surface-accessible iron' method is representative of bulk sample composition and not greatly impacted by variations in particle size or mineral identity. In both dissolution methods, the specimens can be grouped by highest, moderate, and lowest iron content: those with highest iron include OC-M and OF-M; moderate iron include O-S and OC-MI; and lowest iron include TD-IO, RW-S, T-S, and T-MI. While the values of iron content change between the two methods, the three groups hold together. trends hold. Only the RW-IO sample differs from this trend, where it falls into the moderate iron category in aqua regia but the high iron category in oxalate. The presence of an Fe(II)-bearing mineral that is specifically targeted by this method (magnetite) does not account for this difference because many of these samples contain magnetite and OC-M and OF-M are especially concentrated in magnetite. Rather, this difference could arise from the presence of fine goethite and hematite particles. Indeed, the quantity of Fe(III) extracted by oxalate in this specimen is higher than in either OC-M or OF-M, and the liberated Fe(III) is not indicative of ferrihydrite, as was previously discussed.

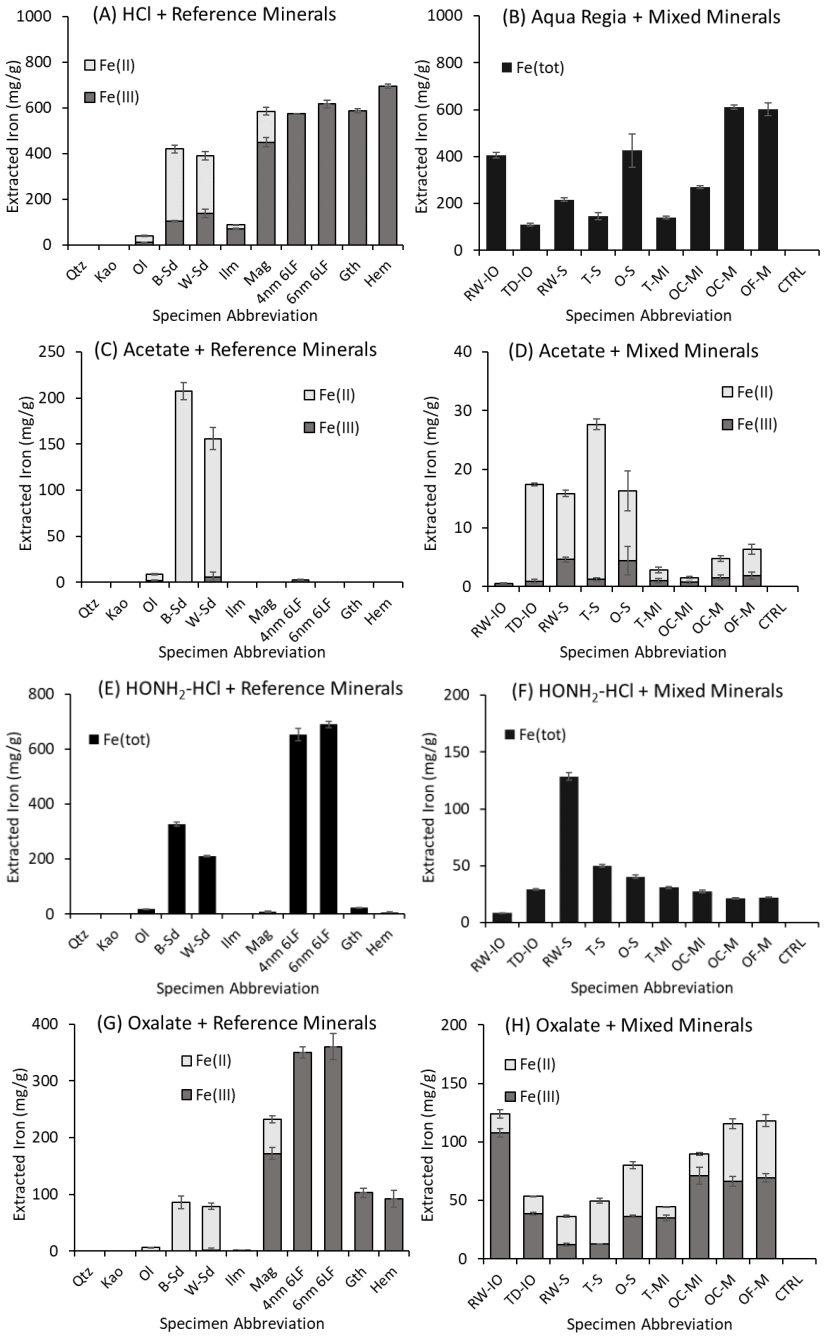

Figure 4.2. Iron content (mg Fe/g sample) of reference minerals (left column) mixed mineral specimens and a control (right column) and as determined by parallel mineral dissolution using concentrated HCl (A), aqua regia (B), acetate (C and D), $HONH_2$-HCl (E and F), and oxalate under darkness (G and H). Black bars represent Fe(tot) where methods do not differentiate iron by oxidation state. Segmented bars represent Fe(II) (light grey upper segment) and Fe(III) (dark grey lower segment) as determined by ferrozine assay. Refer to Table 4.1 and Table 4.2 for specimen abbreviations.

The values of Fe(II), Fe(III), and total Fe extracted by each dissolution method, as well as mass loading, were used as material parameters by which to normalize reaction parameters. Natural mineral specimens can vary greatly in mineralogy, reactive surface area, and potentially contain competing species that interfere with the desired chemical reaction.[16] Comparing reaction parameters to various material parameters is therefore an important step in determining the effects of various characteristics on the reaction with sulfide. Those characteristics that contribute most to the reaction with sulfide should be targeted when choosing a material for sulfur remediation.

Rate and Extent of Reaction

The two main reaction parameters monitored here are reaction rate and amount of sulfide reacted. The reaction of sulfide with these materials was approximated using zero-order kinetics model and a sample plot is given in the supplemental (Figure D23). Rate constants are derived from the slope of sulfur concentration (mg/L) versus time (hr). Reaction capacity is defined here generally as the point at which the material can no longer remove sulfide within a reasonable timeframe. The reasonable timeframe will vary by application. The specific limit imposed here is the point at which approximately 60 % of the injected sulfide remains in the reactor after one hour, which translates to a minimum rate constant of k = 2 ppm/hr.

The reference minerals and mixed mineral specimens were exposed to sulfide in three different buffer systems to map the reaction rates and reaction capacity. These buffer systems included 10 mM acetate at pH 4.7 and 10 mM sodium bicarbonate at pH 8.0 and 9.0. Acetate buffer was chosen because of its use in metabolic processes by

micro-organisms that also serve functions in iron and sulfur cycling, such as *Geobacter* and *Desulfuromonas* species.[31] Bicarbonate buffer was chosen because it is one of the most common buffers in natural systems.[32] The pH values were chosen based on the regions of optimal buffering. The pKa of acetic acid is 4.75 and the major carbonate species at pH 8.0 and 9.0 is HCO_3^-. The speciation of sulfur (Figure D24) is expected to be 99.5 % H_2S at pH 4.7, 91.3 % HS^- at pH 8.0, and 99.1 % HS^- at pH 9.0. Because reactions were performed in closed vessels without headspace and occurred on short time scales (<1 hr), loss of sulfide through the evolution of $H_2S(g)$ was not expected. Indeed, this was shown to be a reasonable assumption because the reactors containing quartz and kaolinite in acetate buffer at pH 4.7, as well as the blank reactor that contained only buffer, showed loss of sulfide occurred only at the rate predicted by dilution through sampling (Figure D25).

In general, the mass-normalized initial rate constant for all mixed minerals was not drastically different between either buffer system or across any pH (Figure D26). In most cases, the rate constant was ca. <10 ppm/g•hr. The exception to this is specimen RW-IO, which had an initial rate constant of 78 ± 10, 33 ± 7, and 17 ± 5 ppm/g•hr at pH 4.7, 8.0, and 9.0, respectively (Figure D27). In all cases, the reaction rate decreased for each subsequent spike in all systems.

The fast reaction rate of the RW-IO specimen may be due to the presence of goethite, a hypothesis that is supported by the rate results from the reference mineral specimens. Goethite reacted faster than any reference mineral at pH 4.7, having an initial mass-normalized rate constant of 398 ± 14 ppm/g•hr (Figure D28A). Like the mining minerals, the reaction rate slowed for each subsequent spike of sulfide until the rate

slowed to below the defined limit. The hypothesis that mass loss during sampling may account for the decrease in reaction rate is shown to be invalid by calculations performed using the goethite reactor at pH 4.7. Using 0.5 mL volume exchange during sampling, each sampling event removes 0.8 % of the total mineral mass. Sixty sampling events had occurred by the end of nine spikes, leaving approximately 60.5 % of the initial mass was remaining, not considering the negligible mass added by FeS or FeS_2 formation. Using the instantaneous mass to instead normalize the rate constant does not substantially alter the trend (Figure D28B), which indicates that the decrease in rate constant is not attributable to mass lost during sampling. Of the remaining reference minerals used in this study, only brown siderite and hematite were also reactive at pH 4.7, with initial mass-normalized rate constants of 92 ± 9 and 34 ± 6 ppm/g•hr, respectively (Figure D28A). Hematite was also present in RW-IO and although the reference hematite exhibits reactivity far slower than goethite, hematite may also contribute to the reaction in RW-IO.

At pH 9.0, the rate constant for goethite was lower than the threshold defined by the reaction capacity (Figure D29) and only the first spike for B-Sd was above the this threshold. This decrease matches the trend observed in the mixed mineral specimens, where the rate for RW-IO also decreased with increasing pH. The reaction with goethite used equivalent mass (i.e., equivalent surface area loading) in both the pH 4.7 and 9.0 systems, but note that reaction rate is surface area-dependent because with greater surface area there comes more reaction sites.[16,33] This relationship is seen with in the reaction of goethite at two different mass loading at pH 9.0 (Figure D29) where reaction rate increased as mass loading increased. This would suggest that reactors with higher surface

area loading, such as column reactors packed with solids, would react with sulfide faster than low mass loading batch reactors.

Interestingly, the reaction with siderite was independent of pH (Figure D30). The mass-normalized rate constant for the first spike was 76 – 92 ppm/g•hr for pH 4.7, 8.3, and 9.0. This rate constant decreased equivalently with each subsequent spike to ca. 18 ppm/g•hr after three spikes for both the pH 4.7 and pH 8.3 systems.

Optimal Material Selection

The rate constant and extent of reaction were normalized to sample mass for each of the mining minerals studied over all three pH regions and the results are presented in Table 4.3. Normalizing the rate constants to initial sample mass is trivial here because all mixed mineral specimens had a mass ca. 0.5 g. In industry, however, factoring in mass is an essential component of system design. The most cost-effective system is one that minimizes mass while maximizing reactivity.

Table 4.3. Tabulation of mass (g), reacted sulfide (umol), and initial rate constant (ppm/hr) for each mixed mineral specimen at three different pH along with the calculated parameters of reacted sulfur per mass (umol/g) and initial rate constant per mass (ppm/g•hr). These parameters are later mapped versus iron dissolution results in Figures D31 – D42.

	ID	Mass (g)	Captured S (umol)	Initial Rate (ppm/hr)	Reacted S per Mass (umol/g)	Initial Rate per Mass (ppm/g•hr)
pH 4.7	RW-IO	0.5028	46.4	39.3	92.3	78.2
	TD-IO	0.5139	0	1.7	0.0	3.3
	RW-S	0.5025	14.0	2.4	27.9	4.8
	T-S	0.5087	33.6	3.7	66.1	7.2
	T-MI	0.5120	0	1.8	0.0	3.5
	OC-M	0.5045	49.1	3.2	97.3	6.3
pH 8.0	RW-IO	0.4967	50.5	16.6	101.6	33.4
	TD-IO	0.5041	9.8	3.2	19.4	6.2
	RW-S	0.4988	45.5	4.8	91.2	9.6
	T-S	0.5056	19.3	4.7	38.2	9.4
	T-MI	0.4984	0	2.1	0	4.1
pH 9.0	RW-IO	0.5016	19.4	8.5	38.7	17.0
	TD-IO	0.5002	0	1.1	0	2.1
	RW-S	0.6019	16.6	3.6	27.6	6.0
	T-S	0.5997	17.9	3.2	29.8	5.3
	O-S	0.5928	17.3	5.2	29.2	8.8
	T-MI	0.5019	0	1.0	0	2.0
	OC-MI	0.5019	0	1.8	0	3.5
	OC-M	0.5025	9.5	2.0	18.9	4.0
	OF-M	0.5012	8.8	2.1	17.6	4.1

An example of a mass-reactivity analysis is presented in Figure 4.3, where the mass-normalized rate (ppm/g•hr) is mapped versus mass-normalized value of reacted sulfide (μmol/g) for each mixed mineral specimen studied at pH 4.7 (Figure 4.3A), pH 8.0 (Figure 4.3B), and pH 9.0 (Figure 4.3C). The most desirable material would rank highly in both attributes and lie in the upper right quadrant of these plots. In all cases, RW-IO ranks higher than any other mixed mineral specimen in both reaction rate and sulfide removal, although at pH 9.0 both attributes for RW-IO decrease to 22 % and 40 %

of their value at pH 4.7, respectively. Generally for all other specimens, the mass-normalized rate constant is no larger than 10 ppm/g•hr at any pH. In the pH 4.7 and 8.0 systems, the amount of reacted sulfide is up to ca. 100 μmol/g, but no more than 30 μmol/g at pH 9.0. These results indicate that the material RW-IO is a promising candidate for sulfide removal processes. Additionally, these results suggest that remediation systems would function more efficiently if using the pH 4.7 or 8.0 conditions rather than the pH 9.0 conditions.

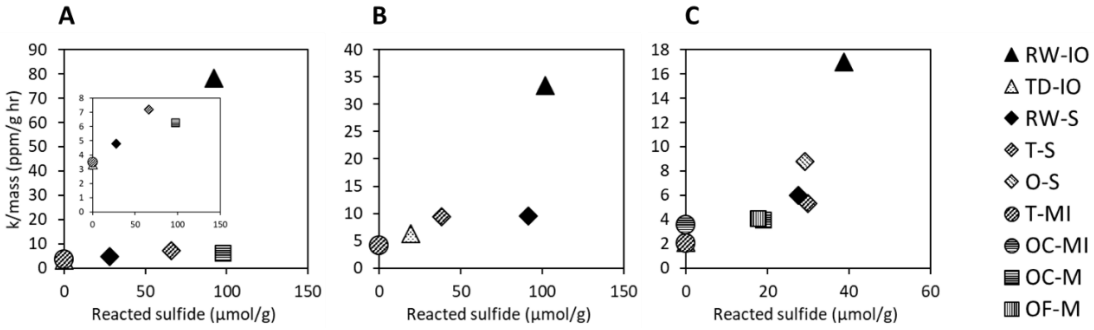

Figure 4.3. Comparison of reaction rate and reacted sulfide for nine mixed mineral specimens and three reference minerals in 10 mM acetate at pH 4.7 (A), 10 mM carbonate at pH 8.0 (B), and 10 mM carbonate at pH 9.0 (C) after multiple additions of 150 μM (5 mg/L S) HS^-. The most desirable material for engineered contaminant removal systems has fast reaction rate and high value of reacted sulfide.

The mass-normalized reaction parameters were then mapped versus the material parameters determined in the chemical dissolution procedures, and the results are presented in Figures D31 – D42 for mixed mineral specimens and Figures D43 – D46 for reference minerals. Most dissolution parameters showed no correlation with the reaction parameters but some correlations may be elucidated with testing more mixed mineral specimens to increase sample size. For reaction rate, there may be a positive correlation with oxalate-extractable Fe(II) at pH 4.7, acetate-extractable Fe(III) at pH 9.0, and

oxalate-extractable Fe(II) at pH 9.0. For the amount of reacted sulfide, there may be a positive correlation with oxalate-extractable Fe(II) at pH 4.7, and acetate-extractable Fe(II) at pH 9.0. There are too few materials studied at pH 8.0 to suggest correlations. In addition to increasing sample size, several changes to the chemical dissolution procedures could be made to more precisely define the material parameters.

Analytical Changes for Improved Material Selection

There are several improvements that can be made to the material characterization process to better quantify iron residing in the most reactive mineral fractions (e.g., goethite, hematite, and siderite). The first improvement is to perform dissolution methods sequentially rather than in parallel. In parallel dissolutions, the more aggressive methods dissolve more than the targeted mineral phase. For example, the oxalate method dissolved siderite, magnetite, ferrihydrite, goethite, and hematite, all of which exhibited different reactivities towards sulfide. This lack of selectivity means that the iron quantified by that method may not represent the iron participating in the reaction with sulfide, which likely contributes to the lack of correlation between material parameters and reaction parameters.

Outlined here is a potential sequential extraction procedure that may assist in selectively dissolving siderite, goethite, and hematite at different stages.[22] Following crushing and sieving to achieve the desired particle size, the materials would first undergo dialysis. Dialysis serves two purposes, first two dissolve salts and second to allow the surfaces previously residing within bulk material to undergo oxidation. The second point is important because these materials would generally be exposed to

weathering in an industrial setting where materials are commonly stored outdoors in piles. After dialysis and between each subsequent selective dissolution procedure, the materials should be washed to prevent carryover of dissolved iron and dried to obtain accurate masses. The first dissolution could use acetate to dissolve carbonates. The procedure used in this study, however, was shown to be ineffective at complete dissolving siderites and a different procedure should be investigated to maximize siderite dissolution but also minimize dissolution of other phases. Second, hydroxylamine-HCl could be used to target ferrihydrite and other SRO-iron (oxyhydr)oxides. Third, dithionite-citrate-bicarbonate (DCB) could be used to target goethite. There are some cases where hematite also dissolved using this method, and the degree of dissolution could be assessed using additional natural and synthetic hematite specimens as reference. Fourth, oxalate with irradiation could be used to target magnetite. The illuminated method facilitates quicker dissolution of magnetite within 6 hrs while leaving the remaining mineral phases relatively intact.[27] With illumination, however, photoreduction occurs and prevents Fe(II) and Fe(III) quantification. A subset of the material undergoing these sequential procedures could be used in a parallel dissolution with oxalate under darkness to obtain Fe(II) and Fe(III) data. Finally, if hematite did not dissolve in the DCB method, concentrated HCl could be used for the complete dissolution of iron (oxyhydr)oxides.

More pure reference minerals should also be studied to further assess the degree to which each dissolves in various reagents. Most importantly, the degree of dissolution for various iron sulfides such as mackinawite, greigite, and pyrite needs to be determined for each of the suggested dissolution methods listed above. Assessing the degree of

dissolution for 2-line ferrihydrite is also appropriate because the materials likely contain newly-oxidized (and likely SRO) mineral phases after dialysis. Several different natural and synthetic hematite specimens should also be tested to determine what kinds of hematite more effectively dissolve in the DCB versus the HCl methods.

Reaction-Limiting Parameters in Evolving Systems

Several solution and material parameters have the potential to substantially impact the rate and extent of the reaction between sulfide and iron-bearing minerals. The rate and extent of reaction with sulfide and initial Fe(II), Fe(III), and Fe(tot) in the mineral specimens as accessed by various chemical dissolution methods were already discussed. Mineral surface characteristics and solution chemistry are both evolving as the reactions progress, however, and both have an impact on reactions occurring at the water-mineral interface.

One possible change occurring at the mineral surface is the formation of an unreactive shell of iron sulfide material covering the reactive mineral surface. If iron sulfide nucleation occurs at the reactive sites, then the newly-formed material presents a barrier between aqueous sulfide and the reactive mineral surface. As a result, the reaction rate will decrease with subsequent spikes until all the reactive sites are inhibited by the shell of iron sulfide material. The formation of an unreactive shell has the implication that the bulk mass of reactive minerals does not participate in the reaction; instead, the reaction is limited by surface area and smaller particles that maximize the surface area to volume ratio would be preferred. As an illustrative example, the synthetic goethite particles used in these experiments measure 79 ± 22 nm long by 12 ± 4 nm wide. Simple

calculations using a rectangle of sides length 80 × 12 × 12 nm to represent the acicular morphology reveal that 7 % of the surface area is present on the tips, or the (021) facet, while 93 % resides on along the length of the particle, or the (110) facet. If the tips are the primary reactive surface, then the formation of even a partial shell the tips would substantially impact the reaction.

TEM images were used to compare the morphology of unreacted goethite and the post-reaction material after the reaction of 968 μmol/g in the pH 4.7 system (Figure D47). No obvious change in roughness of the (021) or (110) facets is observed. This result is unsurprising given the calculated maximum deposition of iron sulfide material. Using the goethite surface area measurement obtained using nitrogen absorption (106.4 m^2/g) and the goethite mass loading and captured sulfur amounts from Table D5, a maximum mass of 6.6 mg FeS is produced. If that mass were concentrated only on the goethite tips, and assuming the tips represent 7 % of the total surface area, then that would result in a layer of FeS (density 4.8 g/cm^3) only 2.4 nm thick. Comparatively, if the same mass were distributed over the entire goethite surface area, the layer of FeS would only be 0.2 nm thick. These domain sizes are too small to be detected visually.

Solution composition also changes as the reaction progresses, which may then impact future reactions. In the system with acetate buffer at pH 4.7 for example, the aqueous Fe(II) concentration increased with each subsequent spike of sulfide to reactors containing mixed mineral specimens (Figure 4.4A) and reference minerals (Figure 4.4B). Faster reaction rates do not correlate with greater concentrations of aqueous Fe(II). In the mixed mineral specimens, RW-IO reacted far faster than any other mineral but yields the least aqueous Fe(II). In the reference minerals, siderite and hematite reacted more slowly

than goethite but aqueous Fe(II) concentrations were ordered siderite >> hematite ≈ goethite. For goethite, the moles of Fe(II) in solution after the final reaction with sulfide is approximately 45 % higher than the total moles of S added. This approximate 1:2 ratio of added sulfide to aqueous Fe(II) generated from iron (oxyhydr)oxide surfaces has been observed elsewhere.[16] The additional Fe(II) generated in the siderite reactor may be due to dissolution by acetate. No aqueous Fe(II) was detected at pH 8.0 or 9.0, and no aqueous Fe(III) was detected at any pH.

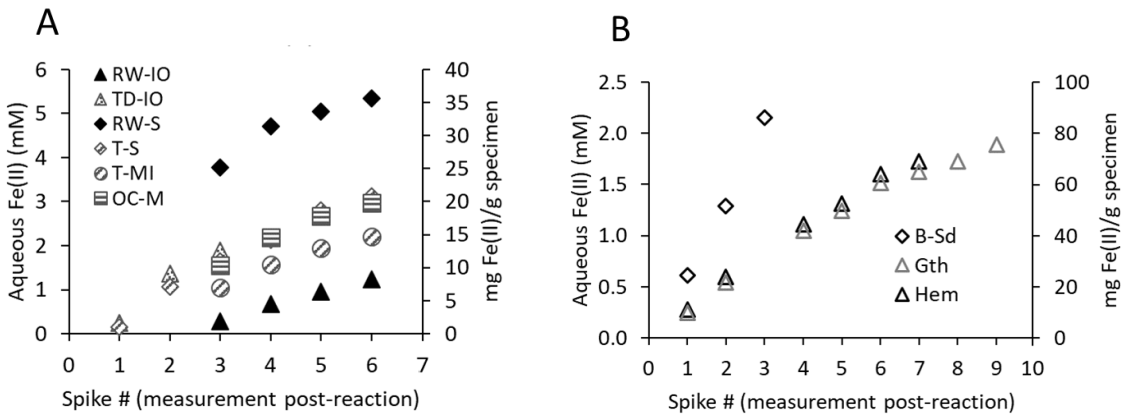

Figure 4.4. Liberated Fe(II) from mixed mineral specimens (A) and from reference minerals (B) after reaction with sulfide in 10 mM acetate at pH 4.7, as determined by ferrozine assay. Sampling for Fe(II) measurements occurred after the reaction for each spike was complete. Fe(II) was not detected at pH 8.0 or 9.0, and Fe(III) was not detected at any pH.

The generation of Fe(II) is consistent with the known reaction of HS^- and iron (oxyhydr)oxide surfaces. In this reaction, one mole of Fe(II) is liberated for every mole of sulfur radical produce, then sulfur radicals reduce surface-bound Fe(III) to liberate eight moles of Fe(II) for every mole of S_8^0 produced.[15,16] A system dominated by elemental sulfur production would exhibit a 1:2 ratio of added sulfide to aqueous Fe(II). Aqueous

Fe(II), however, also reacts with dissolved HS^- to form metastable iron monosulfide solids.[15,16,33] The ratio of added sulfide to aqueous Fe(II) and the trend of decreasing rate constant for subsequent spikes suggest that the reaction of sulfide and aqueous Fe(II) is not dominant in this system. These observations instead support the hypothesis that the primary reaction is occurring at reactive sites on the mineral surface, which become inhibited as new phases nucleate.

Sulfur Mass Balance

The formation of elemental sulfur as a major product of the reaction between sulfide and iron (oxyhydr)oxides is supported by XRD results obtained from the analysis of solids collected after the final reaction was completed (i.e., the specimen had reached reaction capacity and no $HS^-_{(aq)}$ remained). Because of the low mass loading of the reference materials, the detection new phases having low mass% is possible by XRD. For the reaction containing goethite at pH 4.7, the diffraction pattern shows that elemental sulfur is a major reaction product (Figure 4.5). Neither iron sulfide nor pyrite are observed in the diffraction pattern, but an iron sulfide phase having low crystallinity and small domain size would have a broad peak that is difficult to distinguish from the baseline. For the mixed mineral specimens, XRD results were inconclusive for the detection of new solid phases. This challenge stems from the large sample mass (ca. 0.5 g) used in the reactors as compared to the calculated mass of newly-formed material (ca. <5 mg as FeS), which is below the detection limit.[25]

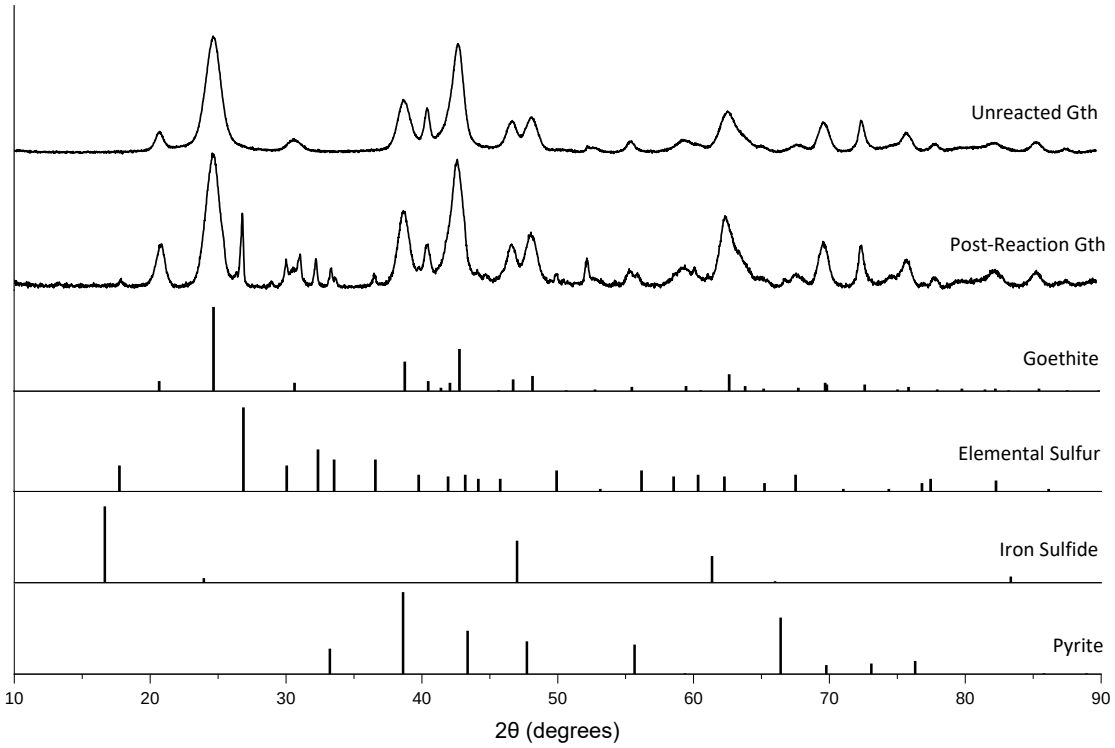

Figure 4.5. Results from XRD analysis of goethite before reaction and after receiving nine additions of sulfide at pH 4.7 in 10 mM acetate buffer indicating the formation of elemental sulfur.

The sulfur mass balance was investigated for the mixed mineral specimens at pH 4.7 and 8.0 using a variety of analytical methods. The targeted species were sulfate, thiosulfate, and elemental sulfur, and the results are presented in Table 4.4. At pH 4.7, sulfate and thiosulfate were present at amounts no greater than 4 % of the total sulfur added to RW-IO, RW-S, and OC-M. Elemental sulfur accounted for 21 % and 24 % of the total sulfur added to RW-IO and OC-M, respectively. None of these species were detected at pH 8.0 for RW-IO, RW-S, or T-S. Sulfite levels were not measured, but a method for detection is available[34] and the species has not been detected as a major product in reactions elsewhere.[16] Total $FeS_{(s)}$ generated has previously been determined by difference between the total sulfur added and the sum of sulfide, sulfate, sulfite,

thiosulfate, and elemental sulfur.[16] These specimens contained no dissolved sulfide at the time of measurement. Assuming that sulfite concentrations are negligible and no sulfur was lost to outgassing, $FeS_{(s)}$ formation accounts for approximately 72 %, 99 %, and 70 % of the sulfur mass balance in RW-IO, RW-S, and OC-M, respectively, at pH 4.7 in acetate. At pH 8.0, the same assumptions yield complete transformation of sulfide to $FeS_{(s)}$.

Table 4.4. Sulfur speciation in acetate pH 4.7 (top set) and carbonate pH 8.0 (bottom set).

	Sample ID	Sulfur Added (μmol)	Sulfur as SO_4 (μmol)	Sulfur as S_2O_3 (μmol)	Sulfur as S_8^0 (μmol)
pH 4.7	RW-IO	46.4	1.6	1.7	9.7
	RW-S	47.6	0.6	0	0
	OC-M	49.4	1.2	1.5	12.1
pH 8.0	RW-IO	63.2	0	0	0
	RW-S	55.9	0	0	0
	T-S	39.0	0	0	0

True mass balance of sulfur in the mixed mineral specimens is challenging and needs further development. Additional testing for sulfite and polysulfides[33] is warranted. It is possible to digest the reaction mixture using concentrated acids and then capture and quantify total evolved sulfur.[22,28] These specimens, however, naturally contain sulfur, the distribution of sulfur within the mixtures varies because of the wide range in grain size, sample masses used in the reactors are small enough to be affected by sample heterogeneity, and the quantity of total sulfur added to the reactors is similar in magnitude to the initial sulfur content as determined by ICP-MS (Table D6). Further refinement of the sampling methods used for sulfur mass balance quantification is warranted and should be compared to results of reference mineral reactions.

Conclusion

Iron mines generate several products that contain iron (oxyhydr)oxides but are not economically-viable as ore materials. Such materials may have use in engineered systems designed to capture sulfur from aqueous waste streams before discharge to the environment. The use of local waste products to treat local hazardous waste demonstrates a more sustainable and environmentally-conscious engineering design.

Because of the wide variety of solids generated from iron mining facilities, there is a need to quickly assess materials for their value as a feedstock for sulfide removal. The assessment could involve chemical dissolution or solid-state material analyses. The various iron-bearing minerals are expected to react differently with sulfide, in both rate and extent of reaction. Identification of the mineral components is therefore essential for determining which materials are promising candidates.

The chemical dissolution procedures performed here using acetate buffer, hydroxylamine-HCl, oxalate buffer under darkness, and aqua regia or concentrated HCl do not enable a clear identification of material composition because the dissolutions were run in parallel. An improved procedure is proposed in which the dissolutions are run in sequence, the oxalate extraction is performed under irradiation, and an extraction using dithionite-citrate-bicarbonate is added to the sequence after hydroxylamine-HCl but before oxalate. The proposed dissolution method would enable better quantification of the siderite, ferrihydrite, goethite, magnetite, and hematite content of the mixed mineral specimens, which is otherwise difficult to determine because of the complexity of the mixtures.

The results from monitoring the reaction of sulfide with the mixed mineral specimens in acetate buffer at pH 4.7 and in carbonate buffer at pH 8.0 show that specimen RW-IO is a promising candidate for sulfide removal. Compared to the reference minerals, goethite is likely the major participant in reactions with sulfide, but hematite likely also contributes to the reaction. Reactions occurred faster and to a greater extent in the acetate buffer at pH 4.7. Reactivity generally decreases for systems at higher pH, but the reactivity of siderite remains approximately equivalent in each buffer system.

Although Fe(II) is liberated over the course of the reaction in acetate buffer at pH 4.7, the rate constants decrease with subsequent reactions. Rather than reacting with aqueous Fe(II), sulfide likely reacts predominantly with iron (oxyhydr)oxide surfaces, deposits solid material at the reactive sites, and thereby inhibits further reaction. A major product of this reaction is elemental sulfur, as detected by XRD and chemical extraction, but the sulfur mass balance as determined by difference suggests that FeS(s) is the most abundant product.

Acknowledgements

Iron-bearing mining materials were generously provided by Arcelor Mittal and U.S. Steel. This research was funded by the State of Minnesota and supported by the Natural Resource Research Institute – University of Minnesota.

Chapter 5. Conclusion

Classification of iron in solid materials and in aqueous media is important for assessing iron-cycling processes in the environment. Chemical dissolution is one avenue for classification of iron and various methods of iron-bearing mineral dissolution and dissolved iron quantification were reviewed herein. Presenting an up-to-date guide of chemical dissolution methods and a critical evaluation of those methods promotes accessibility for researchers across disciplines and using standardized methods allows for comparisons between data sets.

Accurately quantifying the form of iron in different fractions before and after chemical reactions helps to elucidate iron transport mechanisms. Understanding the reactions of environmental contaminants in the presence of iron-bearing minerals is important for assessing contaminant fate and transport. Several solid-state characterization methods provide quantitative analyses of iron residing in different mineral phases. An analysis method by XRD was presented here to quantify iron occurring as goethite in the oxidative growth on hematite surfaces after reaction with a model nitrobenzene contaminant and adsorbed Fe(II). This solid-state method, however, is insufficient when this reaction occurs in the presence of organic matter and other solid-state methods, such as magnetic measurements, will be required for further assessment of phase identity and quantification.

Quantifying iron residing in different mineral phases is essential when selecting iron-bearing mineral specimens for various applications. In the study presented herein that used natural specimens having heterogeneous iron-bearing mineral content to react

with aqueous sulfide as a contaminant, each mineral reacted at different rates and to differing extents. Heterogeneous iron-bearing mineral specimens can be highly complex mixtures that are difficult to classify by solid-state characterization methods. Instead, chemical dissolution methods may be used to assess the mineral content so that these complex mineral mixtures may be screened to determine whether or not their mineral makeup has the necessary characteristics for the desired application. Using complex mineral mixtures that are of otherwise low economic value for applications in contaminant sequestration may bring value to waste materials and is in-line with sustainable engineering practices.

References

References for Chapter 1

(1) Yamashita, I.; Iwahori, K.; Kumagai, S. Ferritin in the Field of Nanodevices. *Biochim. Biophys. Acta* **2010**, *1800*, 846–857.

(2) Wheeler, D. A.; Wang, G.; Ling, Y.; Li, Y.; Zhang, J. Z. Nanostructured Hematite: Synthesis, Characterization, Charge Carrier Dynamics, and Photoelectrochemical Properties. *Energy Environ. Sci.* **2012**, *5* (5), 6682–6702.

(3) Elsner, M.; Schwarzenbach, R. P.; Haderlein, S. B. Reactivity of Fe(II)-Bearing Minerals toward Reductive Transformation of Organic Contaminants. *Environ. Sci. Technol.* **2004**, *38* (3), 799–807.

(4) Hofstetter, T. B.; Heijman, C. G.; Haderlein, S. B.; Holliger, C.; Schwarzenbach, R. P. Complete Reduction of TNT and Other (Poly)Nitroaromatic Compounds under Iron-Reducing Subsurface Conditions. *Environ. Sci. Technol.* **1999**, *33* (9), 1479–1487.

(5) Zhang, W. X. Nanoscale Iron Particles for Environmental Remediation: An Overview. *J. Nanoparticle Res.* **2003**, *5* (3–4), 323–332.

(6) Andrivola Silva, A. K.; Espinosa, A.; Kolosnjaj-Tabi, J.; Wilhem, C.; Gazeau, F. Medical Applications of Iron Oxide Nanoparticles. In *Iron Oxides: From Nature to Applications*; Faivre, D., Ed.; Wiley - VCH: Weinheim, Germany, 2016.

(7) Maxbauer, D. P.; Feinberg, J. M.; Fox, D. L. Magnetic Mineral Assemblages in Soils and Paleosols as the Basis for Paleoprecipitation Proxies: A Review of Magnetic Methods and Challenges. *Earth-Science Rev.* **2016**, *155*, 28–48.

(8) Lagroix, F.; Banerjee, S. K.; Jackson, M. J. Geological Occurrences and Relevance of Iron Oxides. In *Iron Oxides: From Nature to Applications*; Faivre, D., Ed.; Wiley - VCH: Weinheim, Germany, 2016.

(9) Miot, J.; Etique, M. Formation and Transformation of Iron-Bearing Minerals by Iron(II)-Oxidizing and Iron(III)-Reducing Bacteria. In *Iron Oxides: From Nature to Applications*; Faivre, D., Ed.; Wiley - VCH: Weinheim, Germany, 2016.

(10) Yuwono, V. M.; Burrows, N. D.; Soltis, J. A.; Penn, R. L. Oriented Aggregation: Formation and Transformation of Mesocrystal Intermediates Revealed. *J. Amercian Chem. Soc.* **2010**, *132*, 2163–2165.

(11) Barron, V.; Torrent, J. Evidence for a Simple Pathway to Maghemite in Earth and Mars Soils. *Geochim. Cosmochim. Acta* **2002**, *66* (15), 2801–2806.

(12) Hochella Jr., M. F.; Lower, S. K.; Maurice, P. A.; Penn, R. L.; Sahai, N.; Sparks, D. L.; Twining, B. S. Nanominerals, Mineral Nanoparticles, and Earth Systems. *Science* **2008**, *319* (March), 1631–1636.

(13) Waychunas, G. a.; Kim, C. S.; Banfield, J. F. Nanoparticulate Iron Oxide Minerals in Soils and Sediments: Unique Properties and Contaminant Scavenging Mechanisms. *J. Nanoparticle Res.* **2005**, *7*, 409–433.

(14) Collingwood, J. F.; Telling, N. D. Iron Oxides in the Human Brain. In *Iron Oxides: From Nature to Applications*; Faivre, D., Ed.; Wiley - VCH: Weinheim, Germany, 2016.
(15) Torrent, J.; Barrón, V. Iron Oxides in Relation to the Colour of Mediterranean Soils. *Applied Study of Cultural Heritage and Clays*. **2003**, 377–386.
(16) Yu, R.; Andrachek, R. G.; Lehmicke, L. G.; Freedman, D. L. Remediation of Chlorinated Ethenes in Fractured Sandstone by Natural and Enhanced Biotic and Abiotic Processes: A Crushed Rock Microcosm Study. *Sci. Total Environ.* **2018**, *626*, 497–506.
(17) Smyth, D. J. A.; Blowes, D. W.; Ptacek, C. J.; Baker, M. J.; Ford, G.; Foss, S.; Bernstene, E. Removal of Phosphate and Waterborne Pathogens from Wastewater Effluent Using Permeable Reactive Materials. In *Proceedings of the 55th Canadian Geotechnical and 3rd Joint IAH-CNC and CGS Groundwater Specialty Conferences*; Stolle, D., Piggott, A. R., Crowder, J. J., Eds.; Southern Ontario Section of the Canadian Geotechnical Society: Niagra Falls, Ontario, 2002.
(18) Wehrli, B.; Sulzberger, B.; Stumm, W. Redox Processes Catalyzed by Hydrous Oxide Surfaces. *Chem. Geol.* **1989**, *78* (3–4), 167–179.
(19) Middlemost, E. A. K. Iron Oxidation Ratios, Norms, and the Classification of Volcanic Rocks. *Chem. Geol.* **1989**, *77*, 19–26.
(20) Rusevova, K.; Kopinke, F.-D.; Georgi, A. Nano-Sized Magnetic Iron Oxides as Catalysts for Heterogeneous Fenton-like Reactions — Influence of Fe (II)/Fe (III) Ratio on Catalytic Performance. *J. Hazard. Mater.* **2012**, *241*, 433–440.
(21) Strehlau, J. H.; Toner, B. M.; Arnold, W. A.; Penn, R. L. Accessible Reactive Surface Area and Abiotic Redox Reactivity of Iron Oxyhydroxides in Acidic Brines. *Geochim. Cosmochim. Acta* **2017**, *197*, 345–355.
(22) Cornell, R. M.; Schwertmann, U. *The Iron Oxides: Structure, Properties, Reactions, Occurences and Uses*, 2nd ed.; Wiley - VCH: Weinheim, Germany, 2003.
(23) Guo, H.; Stüben, D.; Berner, Z. Removal of Arsenic from Aqueous Solution by Natural Siderite and Hematite. *Appl. Geochemistry* **2007**, *22* (5), 1039–1051.
(24) Cornell, R. M.; Giovanoli, R. Acid Dissolution of Akaganeite and Lepidocrocite: The Effect on Crystal Morphology. *Clays Clay Miner.* **1988**, *36* (5), 385–390.
(25) Poulton, S. W.; Canfield, D. E. Development of a Sequential Extraction Procedure for Iron: Implications for Iron Partitioning in Continentally Derived Particulates. *Chem. Geol.* **2005**, *214*, 209–221.
(26) Agrawal, A.; Tratnyek, P. G. Reduction of Nitro Aromatic Compounds by Zero-Valent Iron Metal. *Environ. Sci. Technol.* **1996**, *30* (1), 153–160.
(27) Raiswell, R.; Canfield, D. E.; Berner, R. A. A Comparison of Iron Extraction Methods for the Determination of Degree of Pyritisation and the Recognition of Iron-Limited Pyrite Formation. *Chem. Geol.* **1994**, *111*, 101–110.
(28) Smith, K. S. Metal Sorption on Mineral Surfaces; an Overview with Examples Relating to Mineral Deposits. *Rev. Econ. Geol.* **1999**, *6A*, 161–182.
(29) Vikesland, P. J.; Valentine, R. L. Iron Oxide Surface-Catalyzed Oxidation of Ferrous Iron by Monochloramine: Implications of Oxide Type and Carbonate on Reactivity. *Environ. Sci. Technol.* **2002**, *36* (3), 512–519.

(30) Stemig, A. M.; Do, T. A.; Yuwono, V. M.; Arnold, W. A.; Penn, R. L. Goethite Nanoparticle Aggregation: Effects of Buffers, Metal Ions, and 4-Chloronitrobenzene Reduction. *Environ. Sci. Nano* **2014**, *1*, 478–487.
(31) Heron, G.; Crouzet, C.; Bourg, A. C. M.; Christensen, T. H. Speciation of Fe(II) and Fe(III) in Contaminated Aquifer Sediments Using Chemical Extraction Techniques. *Environ. Sci. Technol.* **1994**, *28* (9), 1698–1705.
(32) Tessier, A.; Campbell, P. G. C.; Bisson, M. Sequential Extraction Procedure for the Speciation of Particulate Trace Metals. *Anal. Chem.* **1979**, *51* (7), 844–851.
(33) Gibbs, R. J. Transport Phases of Transition Metals in the Amazon and Yukon Rivers. *Geol. Soc. Am. Bull.* **1977**, *88* (6), 829–843.
(34) Wagemann, R.; Brunskill, G. J.; Graham, B. W. Composition and Reactivity of Some River Sediments from the Mackenzie Valley, N.W.T., Canada. *Environ. Geol.* **1977**, *1* (6), 349–358.
(35) Gupta, S. K.; Chen, K. Y. Partitioning of Trace Metals in Selective Chemical Fractions of Nearshore Sediments. *Environ. Lett.* **1975**, *10* (2), 129–158.
(36) Strehlau, J. H.; Hegner, L. A.; Strauss, B. E.; Feinberg, J. M.; Penn, R. L. Simple and Efficient Separation of Magnetic Minerals from Speleothems and Other Carbonates. *J. Sediment. Res.* **2014**, *84*, 1096–1106.
(37) Morin, K. A.; Cherry, J. A. Trace Amounts of Siderite near a Uranium-Tailings Impoundment, Elliot Lake, Ontario, Canada, and Its Implication in Controlling Contaminant Migration in a Sand Aquifer. *Chem. Geol.* **1986**, *56*, 117–134.
(38) Jensen, D. L.; Boddum, J. K.; Tjell, J. C.; Christensen, T. H. The Solubility of Rhodochrosite (MnCO3) and Siderite (FeCO3) in Anaerobic Aquatic Environments. *Appl. Geochemistry* **2002**, *17*, 503–511.
(39) Cravotta III, C. A.; Trahan, M. K. Limestone Drains to Increase pH and Remove Dissolved Metals from Acidic Mine Drainage. *Appl. Geochemistry* **1999**, *14*, 581–606.
(40) Anderson, T. F.; Lawrence, J. R. *Stable Isotope Investigation of Sediments, Basalts, and Authigenic Phases from LEG 35 Cores*; 1979.
(41) Perkins, A. M. Observations under Electron Microscopy of Magnetic Minerals Extracted from Speleothems. *Earth Planet. Sci. Lett.* **1996**, *139*, 281–289.
(42) Freeman, R. Magnetic Mineralogy of Pelagic Limestones. *Geophys. J. R. Astron. Soc.* **1986**, *85*, 433–452.
(43) Aller, R. C.; Mackin, J. E.; Cox, R. T. Diagenesis of Fe and S in Amazon Inner Shelf Muds: Apparent Dominance of Fe Reduction and Implications for the Genesis of Ironstones. *Cont. Shelf Res.* **1986**, *6* (1–2), 263–289.
(44) Cornwell, J. C.; Morse, J. W. The Characterization of Iron Sulfide Minerals in Anoxic Marine Sediments. *Mar. Chem.* **1987**, *22* (2–4), 193–206.
(45) Utgikar, V. P.; Harmon, S. M.; Chaudhary, N.; Tabak, H. H.; Govind, R.; Haines, J. R. Inhibition of Sulfate-Reducing Bacteria by Metal Sulfide Formation in Bioremediation of Acid Mine Drainage. *Environ. Toxicol.* **2002**, *17* (1), 40–48.
(46) Kawahara, N.; Shigematsu, K.; Miura, S.; Miyadai, T.; Kondo, R. Distribution of Sulfate-Reducing Bacteria in Fish Farm Sediments on the Coast of Southern Fukui Prefecture, Japan. *Plankt. Benthos Res.* **2008**, *3* (1), 42–45.

(47) Khanal, S. K.; Huang, J.-C. Anaerobic Treatment of High Sulfate Wastewater with Oxygenation to Control Sulfide Toxicity. *J. Environ. Eng.* **2003**, *129* (12), 1104–1111.
(48) Poulton, S. W.; Krom, M. D.; Raiswell, R. A Revised Scheme for the Reactivity of Iron (Oxyhydr)Oxide Minerals towards Dissolved Sulfide. *Geochim. Cosmochim. Acta* **2004**, *68* (18), 3703–3715.
(49) Chao, T. T. Selective Dissolution of Manganese Oxides from Soils and Sediments with Acidified Hydroxylamine Hydrochloride. *Soil Sci. Soc. Am. J.* **1972**, *36* (5), 764–768.
(50) Chester, R.; Hughes, M. J. A Chemical Technique for the Separation of Ferro-Manganese Minerals, Carbonate Minerals, and Adsorbed Trace Elements from Pelagic Sediments. *Chem. Geol.* **1967**, *2*, 249–262.
(51) Chao, T. T.; Zhou, L. Extraction Techniques for Selective Dissolution of Amorphous Iron Oxides Form Soils and Sediments. *Soil Sci. Soc. Am. J.* **1983**, *47*, 225–232.
(52) Bengtsson, G. A Kinetic Study of the Reaction between Fe(III) and Hydroxylamine in Strongly Acid Perchlorate Solutions. *Acta Chem. Scand.* **1973**, *27*, 1717–1724.
(53) Varsányi, I.; Kovács, L. Ó. Arsenic, Iron and Organic Matter in Sediments and Groundwater in the Pannonian Basin, Hungary. *Appl. Geochemistry* **2006**, *21* (6), 949–963.
(54) Borggaard, O. K.; Jorgensen, S. S.; Moberg, J. P.; Raben-Lange, B. Influence of Organic Matter on Phosphate Adsorption By Aluminum and Iron Oxides in Sandy Soils. *J. Soil Sci.* **1990**, *41*, 443–449.
(55) Deb, B. C. The Estimation of Free Iron Oxides in Soils and Clays and Their Removal. *J. Soil Sci.* **1950**, *1* (2), 212–220.
(56) Mehra, O. P.; Jackson, M. L. Iron Oxide Removal from Soils and Clays by a Dithionite-Citrate System Buffered with Sodium Bicarbonate. *Clays Clay Miner.* **1960**, *7*, 317–327.
(57) Galabutskaya, E.; Govorova, R. Bleaching of Kaolin. *Miner. syr'e* **1934**, *9*, 27–30.
(58) Aguilera, N. H.; Jackson, M. L. Iron Oxide Removal from Soils and Clays. *Soil Sci. Soc. Am. J.* **1953**, *17* (4), 359–365.
(59) Waite, T. D.; Morel, F. M. M. Photoreductive Dissolution of Colloidal Iron-Oxide - Effect of Citrate. *J. Colloid Interface Sci.* **1984**, *102* (1), 121–137.
(60) Francis, A. J.; Dodge, C. J.; Gillow, J. B. Biodegradation of Metal Citrate Complexes and Implications for Toxic-Metal Mobility. *Nature* **1992**, *356*, 140–142.
(61) Anderson, B. J.; Jenne, E. A. Free-Iron and -Manganese Oxide Content of Reference Clays. *Soil Sci.* **1970**, *109* (3), 163–169.
(62) Varadachari, C.; Goswami, G.; Ghosh, K. Dissolution of Iron Oxides. *Clay Res.* **2006**, *25*, 1–18.
(63) Jaisi, D. P.; Dong, H.; Morton, J. P. Partitioning of Fe(II) in Reduced Nontronite (NAu-2) to Reactive Sites: Reactivity in Terms of Tc(VII) Reduction. *Clays Clay Miner.* **2008**, *56* (2), 175–189.

(64) Wu, T.; Shelobolina, E.; Xu, H.; Konishi, H.; Kukkadapu, R.; Roden, E. E. Isolation and Microbial Reduction of Fe(III) Phyllosilicates from Subsurface Sediments. *Environ. Sci. Technol.* **2012**, *46* (21), 11618–11626.
(65) Ryan, J. N.; Gschwend, P. M. Extraction of Iron Oxides from Sediments Using Reductive Dissolution by Titanium(III). *Clays Clay Miner.* **1991**, *39* (5), 509–518.
(66) Wagai, R.; Mayer, L. M.; Kitayama, K.; Shirato, Y. Association of Organic Matter with Iron and Aluminum across a Range of Soils Determined via Selective Dissolution Techniques Coupled with Dissolved Nitrogen Analysis. *Biogeochemistry* **2013**, *112*, 95–109.
(67) McKeague, J. A.; Day, J. H. Dithionite- and Oxalate-Extractable Fe and Al as Aids in Differentiating Various Classes of Soilds. *Can. J. Soil Sci.* **1966**, *46* (1), 13–22.
(68) Jeanroy, E.; Guillet, B. The Occurrence of Suspended Ferruginous Particles in Pyrophosphate Extracts of Some Soil Horizons. *Geoderma* **1981**, *26* (1–2), 95–105.
(69) Poulin, B. A.; Ryan, J. N.; Aiken, G. R. Effects of Iron on Optical Properties of Dissolved Organic Matter. *Environ. Sci. Technol.* **2014**, *48* (17), 10098–10106.
(70) Walker, W. B. The Determination of Small Amounts of Iron by Colorimetric Methods. *Analyst* **1925**, *50* (591), 279–283.
(71) Schwertmann, U.; Friedl, J.; Stanjek, H.; Murad, E.; Bender Koch, C. Iron Oxides and Smectites in Sediments from the Atlantis II Deep, Red Sea. *Eur. J. Mineral.* **1998**, *10*, 953–968.
(72) Lovley, D. R.; Phillips, E. J. Availability of Ferric Iron for Microbial Reduction in Bottom Sediments of the Freshwater Tidal Potomac River. *Appl. Environ. Microbiol.* **1986**, *52* (4), 751–757.
(73) Phillips, E. J. P.; Lovley, D. R.; Roden, E. E. Composition of Non-Microbially Reducible Fe(III) in Aquatic Sediments. *Appl. Environ. Microbiol.* **1993**, *59* (8), 2727–2729.
(74) Strehlau, J. H.; Berens, M. J.; Arnold, W. A. Mineralogy and Buffer Identity Effects on RDX Kinetics and Intermediates during Reaction with Natural and Synthetic Magnetite. *Chemosphere* **2018**, *213*, 602–609.
(75) Lovley, D. R.; Stolz, J. F.; Nord, G. L.; Phillips, E. J. P. Anaerobic Production of Magnetite by a Dissimilatory Iron-Reducing Microorganism. *Nature* **1987**, *330*, 252–254.
(76) Zaitsev, V. S.; Filimonov, D. S.; Presnyakov, I. A.; Gambino, R. J.; Chu, B. Physical and Chemical Properties of Magnetite and Magnetite-Polymer Nanoparticles and Their Colloidal Dispersions. *J. Colloid Interface Sci.* **1999**, *212* (1), 49–57.
(77) Zuo, Y.; Holgné, J. Formation of Hydrogen Peroxide and Depletion of Oxalic Acid in Atmospheric Water by Photolysis of Iron(III)-Oxalato Complexes. *Environ. Sci. Technol.* **1992**, *26*, 1014–1022.
(78) Sedlak, D. L.; Hoigné, J. The Role of Copper and Oxalate in the Redox Cycling of Iron in Atmospheric Waters. *Atmos. Environ.* **1993**, *27A* (14), 2173–2185.
(79) DeEndredy, A. S. Estimation of Free Iron Oxides in Soils and Clays by a Photocatalytic Method. *Clay Miner. Bull.* **1963**, *9*, 209–217.

(80) Cornell, R.; Schindler, P. Photochemical Dissolution of Goethite in Acid/Oxalate Solution. *Clays Clay Miner.* **1987**, *35* (5), 347–352.
(81) Childs, C. W. Ferrihydrite: A Review of Structure, Properties, and Occurence in Relation to Soils. *J. Plant Nutr. Soil Sci.* **1992**, *155*, 441–448.
(82) Blesa, M. A.; Marinovich, H. A.; Baumgartner, E. C.; Maroto, A. J. G. Mechanism of Dissolution of Magnetite by Oxalic Acid-Ferrous Ion Solutions. *Inorg. Chem.* **1987**, *26*, 3713–3717.
(83) Phillips, E. J. P.; Lovley, D. R. Determination of Iron(III) and Iron(II) in Oxalate Extracts of Sediment. *Soil Sci. Soc. Am. J.* **1987**, *51*, 938–941.
(84) Tamm, O. *Om Bestämning Av de Oorganiska Komponenterna i Markens Gelkomplex*; Stockholm, Sweden, 1922.
(85) Cornell, R. M.; Giovanoli, R. Acid Dissolution of Hematites of Different Morphologies. *Clay Miner.* **1993**, *28*, 223–232.
(86) Sidhu, P. S.; Gilkes, R. J.; Cornell, R. M.; Posner, A. M.; Quirk, J. P. Dissolution of Iron Oxides and Oxyhydroxides in Hydrochloric and Perchloric Acids. *Clays Clay Miner.* **1981**, *29* (4), 269–276.
(87) Cornell, R. M.; Posner, A. M.; Quirk, J. P. Crystal Morphology and the Dissolution of Goethite. *J. Inorg. Nucl. Chem.* **1974**, *36*, 1937–1946.
(88) Cornell, R. M.; Posner, A. M.; Quirk, J. P. Kinetics and Mechanisms of the Acid Dissolution of Goethite (α-FeOOH). *J. Inorg. Nucl. Chem.* **1976**, *38*, 563–567.
(89) Schwertmann, U. The Influence of Aluminium on Iron Oxides: IX. Dissolution of Al- Goethites in 6 M HCl. *Clay Miner.* **1984**, *19* (1), 9–19.
(90) Skei, J. M. Formation of Framboidal Iron Sulfide in the Water of a Permanently Anoxic Fjord - Framvaren, South Norway. *Mar. Chem.* **1988**, *23*, 345–352.
(91) Van Dyk, J. P.; Vegter, N. M.; Pistorius, P. C. Kinetics of Ilmenite Dissolution in Hydrochloric Acid. *Hydrometallurgy* **2002**, *65* (1), 31–36.
(92) Pehkonen, S. Determination of the Oxidation States of Iron in Natural Waters: A Review. *Analyst* **1995**, *120* (11), 2655–2663.
(93) Haese, R. R.; Wallmann, K.; Dahmke, A.; Kretzmann, U.; Müller, P. J.; Schulz, H. D. Iron Species Determination to Investigate Early Diagenetic Reactivity in Marine Sediments. *Geochim. Cosmochim. Acta* **1997**, *61* (1), 63–72.
(94) Wiederhold, J. G.; Teutsch, N.; Kraemer, S. M.; Halliday, A. N.; Kretzschmar, R. Iron Isotope Fractionation in Oxic Soils by Mineral Weathering and Podzolization. *Geochim. Cosmochim. Acta* **2007**, *71* (23), 5821–5833.
(95) Shelobolina, E.; Konishi, H.; Xu, H.; Benzine, J.; Xiong, M. Y.; Wu, T.; Blöthe, M.; Roden, E. Isolation of Phyllosilicate-Iron Redox Cycling Microorganisms from an Illite-Smectite Rich Hydromorphic Soil. *Front. Microbiol.* **2012**, *3*, 1–10.
(96) Kukkadapu, R. K.; Zachara, J. M.; Fredrickson, J. K.; McKinley, J. P.; Kennedy, D. W.; Smith, S. C.; Dong, H. Reductive Biotransformation of Fe in Shale-Limestone Saprolite Containing Fe(III) Oxides and Fe(II)/Fe(III) Phyllosilicates. *Geochim. Cosmochim. Acta* **2006**, *70* (14), 3662–3676.
(97) Kostka, J. E.; Stucki, J. W.; Nealson, K. H.; Jun, W. U. Reduction of Structural Fe(III) in Smectite by a Pure Culture of Shewanella Putrefaciens Strain MR-1. *Clays Clay Miner.* **1996**, *44* (4), 522–529.

(98) Beyer, M. E.; Bond, A. M.; McLaughlin, R. J. W. Simultaneous Polarographic Determination of Ferrous, Ferric, and Total Iron in Standard Rocks. *Anal. Chem.* **1975**, *47* (3), 479–482.
(99) Shapiro, B. L.; Brannock, W. W. *Rapid Analysis of Silicate Rocks*; Washington, D.C., 1962.
(100) Stucki, J. W. The Quantitative Assay of Minerals for Fe(2+) and Fe(3+) Using 1,10-Phenanthroline: II. A Photochemical Method. *Soil Sci. Soc. Am. J.* **1981**, *45*, 638–641.
(101) Amonette, J. E.; Matyáš, J. Determination of Ferrous and Total Iron in Refractory Spinels. *Anal. Chim. Acta* **2016**, *910*, 25–35.
(102) Schilt, A. A.; Hoyle, W. C. Improved Sensitivity and Selectivity in the Spectrophotometric Determination of Iron by Use of a New Ferroin-Type Reagent. *Anal. Chem.* **1967**, *39* (1), 114–117.
(103) Morse, J. W.; Millero, F. J.; Cornwell, J. C.; Rickard, D. The Chemistry of the Hydrogen Sulfide and Iron Sulfide Systems in Natural Waters. *Earth-Science Rev.* **1987**, *24* (1), 1–42.
(104) Wan, M.; Shchukarev, A.; Lohmayer, R.; Planer-Friedrich, B.; Peiffer, S. Occurrence of Surface Polysulfides during the Interaction between Ferric (Hydr)Oxides and Aqueous Sulfide. *Environ. Sci. Technol.* **2014**, *48* (9), 5076–5084.
(105) LaFond-Hudson, S.; Johnson, N. W.; Pastor, J.; Dewey, B. Iron Sulfide Formation on Root Surfaces Controlled by the Life Cycle of Wild Rice (Zizania Palustris). *Biogeochemistry* **2018**, *141* (1), 95–106.
(106) McGuire, M. M.; Hamers, R. J. Extraction and Quantitative Analysis of Elemental Sulfur from Sulfide Mineral Surfaces by High-Performance Liquid Chromatography. *Environ. Sci. Technol.* **2000**, *34* (21), 4651–4655.
(107) Berner, R. A. Sedimentary Pyrite Formation: An Update. *Geochim. Cosmochim. Acta* **1984**, *48*, 605–615.
(108) Nath, M.; Choudhury, A.; Kundu, A.; Rao, C. N. R. Synthesis and Characterization of Magnetic Iron Sulfide Nanowires. *Adv. Mater.* **2003**, *15* (24), 2098–2101.
(109) Landers, D. H.; David, M. B.; Mitchell, M. J. Analysis of Organic and Inorganic Sulfur Constituents in Sediments, Soils and Water. *Int. J. Environ. Anal. Chem.* **1983**, *14* (4), 245–256.
(110) Rickard, D.; Morse, J. W. Acid Volatile Sulfide (AVS). *Mar. Chem.* **2005**, *97* (3–4), 141–197.
(111) Lord, C. J. A Selective and Precise Method for Pyrite Determination in Sedimentary Materials. *J. Sediment. Res.* **1982**, *52* (2), 664–666.
(112) Canfield, D. E.; Raiswell, R.; Westrich, J. T.; Reaves, C. M.; Berner, R. A. The Use of Chromium Reduction in the Analysis of Reduced Inorganic Sulfur in Sediments and Shales. *Chem. Geol.* **1986**, *54*, 149–155.
(113) Epstein, I. R.; Kustin, K.; Warshaw, L. J. A Kinetics Study of the Oxidation of Iron(II) by Nitric Acid. *J. Am. Chem. Soc.* **1980**, *102* (11), 3751–3758.
(114) Rennert, T. Wet-Chemical Extractions to Characterise Pedogenic Al and Fe Species-A Critical Review. *Soil Res.* **2019**, *57* (1), 1–16.

(115) Miller, W. P.; Martens, D. C.; Zelazny, L. W. Effect of Sequence in Extraction of Trace Metals from Soils. *Soil Sci. Soc. Am. J.* **1986**, *50* (3), 598–601.
(116) Parfitt, R. L.; Childs, C. W. Estimation of Forms of Fe and Al: A Review, and Analysis of Contrasting Soils by Dissolution and Moessbauer Methods. *Aust. J. Soil Res.* **1988**, *26*, 121–144.
(117) La Force, M. J.; Fendorf, S. Solid-Phase Iron Characterization During Common Selective Sequential Extractions. *Soil Sci. Soc. Am. J.* **2000**, *64* (5), 1608–1615.
(118) Chao, T, T. Use of Partial Dissolution Techniques in Geochemical Exploration. *J. Geochemical Explor.* **1984**, *20*, 101–135.
(119) Shuman, L. M. Fractionation Method for Soil Microelements. *Soil Sci.* **1985**, *140* (1), 11–22.
(120) Whitney, D. L.; Evans, B. W. Abbreviations for Names of Rock-Forming Minerals. *Am. Mineral.* **2010**, *95* (1), 185–187.
(121) Aldrich, A. P.; van den Berg, C. M. G. Determination of Iron and Its Redox Speciation in Seawater Using Catalytic Cathodic Stripping Voltammetry. *Electroanalysis* **1998**, *10* (6), 369–373.
(122) Schnell, S.; Ratering, S.; Jansen, K.-H. Simultaneous Determination of Iron(III), Iron(II), and Manganese(II) in Environmental Samples by Ion Chromatography. *Environ. Sci. Technol.* **1998**, *32* (10), 1530–1537.
(123) Elrod, V. A.; Johnson, K. S.; Coale, K. H. Determination of Subnanomolar Levels of Iron(II) and Total Dissolved Iron in Sea Water by Flow Injection Analysis with Chemiluminescence Detection. *Anal. Chem.* **1991**, *63* (9), 893–898.
(124) Pulido-Tofiño, P.; Moreno, J. M. B. M.; Pérez-Conde, M. C. A Flow-through Fluorescent Sensor to Determine Fe(III) and Total Inorganic Iron. *Talanta* **2000**, *51*, 537–545.
(125) Giokas, D. L.; Paleologos, E. K.; Karayannis, M. I. Speciation of Fe(II) and Fe(III) by the Modified Ferrozine Method, FIA-Spectrophotometry, and Flame AAS after Cloud-Point Extraction. *Anal. Bioanal. Chem.* **2002**, *373* (4–5), 237–243.
(126) Kozak, L.; Niedzielski, P.; Wachowiak, W. The Tandem Analytical Method of Flow Injection Diode Array Spectrophotometry and Flame Atomic Absorption Spectrometry (FI-DAD(Vis)-FAAS) in Iron Speciation Studies Using 1,10-Phenanthroline Complexes. *Microchem. J.* **2013**, *110*, 54–60.
(127) Costa, R. C. de C.; Araújo, A. N. Determination of Fe(III) and Total Fe in Wines by Sequential Injection Analysis and Flame Atomic Absorption Spectrometry. *Anal. Chim. Acta* **2001**, *438* (1–2), 227–233.
(128) Qureshi, M.; Varshney, K. G. Selective Determination of Iron by Potassium Cyanide-Potassium Ferrocyanide Reagent. *Anal. Chem.* **1967**, *39* (8), 1034–1035.
(129) Stugart, R. Determination of Iron in Milk and Other Biological Materials. *Ind. Eng. Chem. - Anal. Ed.* **1931**, *3* (4), 390–393.
(130) Mihaljević, B.; Katušin-Ražem, B.; Ražem, D. The Reevaluation of the Ferric Thiocyanate Assay for Lipid Hydroperoxides with Special Considerations of the Mechanistic Aspects of the Response. *Free Radic. Biol. Med.* **1996**, *21* (1), 53–63.
(131) Yoe, J. H.; Jones, A. L. Colorimetric Determination of Iron with Disodium-1,2-Dihydroxybenzene-3,5-Disulfonate. *Ind. Eng. Chem. - Anal. Ed.* **1944**, *16* (2), 111–115.

(132) Saywell, L. G.; Cunningham, B. B. Determination of Iron: Colorimetric o-Phenanthroline Method. *Ind. Eng. Chem. - Anal. Ed.* **1937**, *9* (2), 67–69.
(133) Stookey, L. L. Ferrozine-A New Spectrophotometric Reagent for Iron. *Anal. Chem.* **1970**, *42* (7), 779–781.
(134) Lee, G. F.; Stumm, W. Determination of Ferrous Iron in the Presence of Ferric Iron With Bathophenanthroline. *J. Am. Water Works Assoc.* **1960**, *52* (12), 1567–1574.
(135) Shamsipour, F.; Zarnani, A. H.; Ghods, R.; Chamankhah, M.; Forouzesh, F.; Vafaei, S.; Bayat, A. A.; Akhondi, M. M.; Ali Oghabian, M.; Jeddi-Tehrani, M. Conjugation of Monoclonal Antibodies to Super Paramagnetic Iron Oxide Nanoparticles for Detection of Her2/Neu Antigen on Breast Cancer Cell Lines. *Avicenna J. Med. Biotechnol.* **2009**, *1* (1), 27–31.
(136) Páscoa, R. N. M. J.; Tóth, I. V.; Rangel, A. O. S. S. A Multi-Syringe Flow Injection System for the Spectrophotometric Determination of Trace Levels of Iron in Waters Using a Liquid Waveguide Capillary Cell and Different Chelating Resins and Reaction Chemistries. *Microchem. J.* **2009**, *93* (2), 153–158.
(137) Jankiewicz, B.; Ptaszyński, B.; Turek, A. Spectrophotometric Determination of Iron (II) in the Soil of Selected Allotment Gardens in Łódź. *Polish J. Environ. Stud.* **2002**, *11* (6), 745–749.
(138) Thompsen, J. C.; Mottola, H. A. Kinetics of the Complexation of Iron(II) with Ferrozine. *Anal. Chem.* **1984**, *56* (4), 755–757.
(139) Smith, F.; McCurdy, W. H.; Diehl, H. The Colorimetric Determination of Iron in Raw and Treated Municipal Water Supplies by Use of 4,7-Diphenyl-1,10-Phenanthroline. *Analyst* **1952**, *77*, 418–422.
(140) Fraser, F. H.; Epstein, P.; Macero, D. J. The Formation Constant of Bis[2,4,6-Tri(2-Pyrrdyl)-l,3,5-Triazine]Iron(II). Evidence for Formation of a Protonated Bis Complex. *Inorg. Chem.* **1972**, *11* (9), 2031–2034.
(141) Zak, B.; Epstein, E.; Baginski, E. S. 2,6-Bis(4-Phenyl-2-Pyridyl)-4-Phenyl-Pyridine as an Aqueous Micro Iron Reagent. *Microchem. J.* **1969**, *14*, 155–160.
(142) Amonette, J. E.; Khan, F. A.; Scott, A. D.; Ghan, H.; Stucki, J. W. Quantitative Oxidation-State Analysis of Soils. In *Quantative Methods in Soil Mineralogy*; Luxmoore, R. J., Bartels, J. M., Eds.; Soil Science Society of America: Madison, Wisconsin, 1994.
(143) Harvey, A. E.; Smart, J. A.; Amis, E. S. Simultaneous Spectrophotometric Determination of Iron(II) and Total Iron with 1,10-Phenanthroline. *Anal. Chem.* **1955**, *27* (1), 26–29.
(144) Anastácio, A. S.; Harris, B.; Yoo, H. I.; Fabris, J. D.; Stucki, J. W. Limitations of the Ferrozine Method for Quantitative Assay of Mineral Systems for Ferrous and Total Iron. *Geochim. Cosmochim. Acta* **2008**, *72* (20), 5001–5008.
(145) Komadel, P.; Stucki, J. W. Quantitative Assay of Minerals for Fe(2+) and Fe(3+) Using 1,10-Phenanthroline: III. A Rapid Photochemical Method. *Clays Clay Miner.* **1988**, *36* (4), 379–381.
(146) Stucki, J. W.; Anderson, W. L. The Quantitative Assay of Minerals for Fe(2+) and Fe(3+) Using 1,10-Phenanthroline: I. Sources of Variability. *Soil Sci. Soc. Am. J.* **1981**, *45*, 633–637.

(147) Amonette, J. E.; Charles Templeton, J. Improvements to the Quantitative Assay of Nonrefractory Minerals for Fe(II) and Total Fe Using 1,10-Phenanthroline. *Clays Clay Miner.* **1998**, *46* (1), 51–62.
(148) Viollier, E.; Inglett, P. W.; Hunter, K.; Roychoudhury, a N.; Van Cappellen, P. The Ferrozine Method Revisited: Fe (II)/Fe (III) Determination in Natural Waters. *Appl. Geochemistry* **2000**, *15* (6), 785–790.
(149) Vindedahl, A. M.; Stemig, M. S.; Arnold, W. A.; Penn, R. L. Character of Humic Substances as a Predictor for Goethite Nanoparticle Reactivity and Aggregation. *Environ. Sci. Technol.* **2016**, *50* (3), 1200–1208.
(150) Im, J.; Lee, J.; Löffler, F. E. Interference of Ferric Ions with Ferrous Iron Quantification Using the Ferrozine Assay. *J. Microbiol. Methods* **2013**, *95*, 366–367.
(151) Witham, C. S.; Oppenheimer, C.; Horwell, C. J. Volcanic Ash-Leachates: A Review and Recommendations for Sampling Methods. *J. Volcanol. Geotherm. Res.* **2005**, *141* (3–4), 299–326.
(152) Williamson, M. A.; Rimstidt, J. D. The Kinetics and Electrochemical Rate-Determining Step of Aqueous Pyrite Oxidation. *Geochim. Cosmochim. Acta* **1994**, *58* (24), 5443–5454.
(153) Davis, J. A.; James, R. O.; Leckie, J. O. Surface Ionization and Complexation at the Oxide/Water Interface. *J. Colloid Interface Sci.* **1978**, *63* (3), 480–499.
(154) Davis, J. A.; Leckie, J. O. Surface Ionization and Complexation at the Oxide/Water Interface 3. Adsorption of Anions. *J. Colloid Interface Sci.* **1980**, *74* (1), 32–43.
(155) Brezonik, P. L.; Arnold, W. A. *Water Chemistry: An Introduction to the Chemistry of Natural and Engineered Aquatic Systems*; Oxford University Press: New York, New York, 2011.
(156) Köber, R.; Schlicker, O.; Ebert, M.; Dahmke, A. Degradation of Chlorinated Ethylenes by Fe0: Inhibition Processes and Mineral Precipitation. *Environ. Geol.* **2002**, *41*, 644–652.
(157) Runnells, D. D. Diagenesis, Chemical Sediments, and the Mixing of Natural Waters. *J. Sediment. Petrol.* **1969**, *39* (3), 1188–1201.
(158) Anschutz, A. J.; Penn, R. L. Reduction of Crystalline Iron(III) Oxyhydroxides Using Hydroquinone: Influence of Phase and Particle Size. *Geochem. Trans.* **2005**, *6* (3), 60–66.
(159) Soltis, J. A.; Feinberg, J. M.; Gilbert, B.; Penn, R. L. Phase Transformation and Particle-Mediated Growth in the Formation of Hematite from 2-Line Ferrihydrite. *Cryst. Growth Des.* **2016**, *16* (2), 922–932.
(160) Chopard, A.; Benzaazoua, M.; Bouzahzah, H.; Plante, B.; Marion, P. A Contribution to Improve the Calculation of the Acid Generating Potential of Mining Wastes. *Chemosphere* **2017**, *175*, 97–107.
(161) Lyngkilde, J.; Christensen, T. H. Redox Zones of a Landfill Leachate Pollution Plume (Vejen, Denmark). *J. Contam. Hydrol.* **1992**, *10* (4), 273–289.
(162) Bjerg, P. L.; Rugge, K.; Pedersen, J. K.; Christensen, T. H. Distribution of Redox-Sensitive Groundwater Quality Parameters Downgradient of a Landfill (Grindsted, Denmark). *Environ. Sci. Technol.* **1995**, *29* (5), 1387–1394.

(163) Barron, V.; Torrent, J. Surface Hydroxyl Configuration of Various Crystal Faces of Hematite and Goethite. *J. Colloid Interface Sci.* **1996**, *177* (2), 407–410.
(164) Huang, X.; Hou, X.; Zhang, X.; Rosso, K. M.; Zhang, L. Facet-Dependent Contaminant Removal Properties of Hematite Nanocrystals and Their Environmental Implications. *Environ. Sci. Nano* **2018**, *5* (8), 1790–1806.
(165) Huang, X.; Hou, X.; Song, F.; Zhao, J.; Zhang, L. Facet-Dependent Cr(VI) Adsorption of Hematite Nanocrystals. *Environ. Sci. Technol.* **2016**, *50* (4), 1964–1972.
(166) Noerpel, M. R.; Lee, S. S.; Lenhart, J. J. X-Ray Analyses of Lead Adsorption on the (001), (110), and (012) Hematite Surfaces. *Environ. Sci. Technol.* **2016**, *50* (22), 12283–12291.
(167) Strehlau, J. H.; Stemig, M. S.; Penn, R. L.; Arnold, W. A. Facet-Dependent Oxidative Goethite Growth As a Function of Aqueous Solution Conditions. *Environ. Sci. Technol.* **2016**, *50* (19), 10406–10412.
(168) Catalano, J. G.; Fenter, P.; Park, C.; Zhang, Z.; Rosso, K. M. Structure and Oxidation State of Hematite Surfaces Reacted with Aqueous Fe(II) at Acidic and Neutral pH. *Geochim. Cosmochim. Acta* **2010**, *74* (5), 1498–1512.
(169) Burleson, D. J.; Penn, R. L. Two-Step Growth of Goethite from Ferrihydrite. *Langmuir* **2006**, *22* (1), 402–409.
(170) Sun, S.; Zeng, H. Size-Controlled Synthesis of Magnetite Nanoparticles. *J. Am. Chem. Soc. Commun.* **2002**, *124* (28), 8204–8205.
(171) Wang, W. W.; Zhu, Y. J.; Ruan, M. L. Microwave-Assisted Synthesis and Magnetic Property of Magnetite and Hematite Nanoparticles. *J. Nanoparticle Res.* **2007**, *9* (3), 419–426.
(172) Vidal-Vidal, J.; Rivas, J.; López-Quintela, M. A. Synthesis of Monodisperse Maghemite Nanoparticles by the Microemulsion Method. *Colloids Surfaces A Physicochem. Eng. Asp.* **2006**, *288* (1–3), 44–51.
(173) Strehlau, J. H.; Schultz, J. D.; Vindedahl, A. M.; Arnold, W. A.; Penn, R. L. Effect of Nonreactive Kaolinite on 4-Chloronitrobenzene Reduction by Fe(II) in Goethite–Kaolinite Heterogeneous Suspensions. *Environ. Sci. Nano* **2017**, *4*, 325–334.
(174) Batley, G. E.; Gardner, D. Sampling and Storage of Natural Waters for Trace Metal Analysis. *Water Res.* **1977**, *11* (9), 745–756.
(175) Zhou, S.; Lewis, L. M.; Singh, S. K. Metal Leachables in Therapeutic Biologic Products: Origin, Impact and Detection. *Am. Pharm. Rev.* **2010**, *13* (4), 76–80.
(176) Waterman, K. C.; Adami, R. C.; Alsante, K. M.; Hong, J.; Landis, M. S.; Lombardo, F.; Roberts, C. J. Stabilization of Pharmaceuticals to Oxidative Degradation. *Pharm. Dev. Technol.* **2002**, *7* (1), 1–32.
(177) Benes, P.; Steinnes, S. Migration Forms of Trace Elements in Natural Fresh Waters and the Effect of the Water Storage. *Water Res.* **1975**, *9*, 741–749.
(178) Fischer, A. C.; Kroon, J. J.; Verburg, T. G.; Teunissen, T.; Wolterbeek, H. T. On the Relevance of Iron Adsorption to Container Materials in Small-Volume Experiments on Iron Marine Chemistry: ^{55}Fe-Aided Assessment of Capacity, Affinity and Kinetics. *Mar. Chem.* **2007**, *107* (4), 533–546.

References for Chapter 2

(1) Faivre, D. Introduction. In *Iron Oxides: From Nature to Applications*; Faivre, D., Ed.; Wiley - VCH: Weinheim, Germany, 2016.
(2) Cornell, R. M.; Schwertmann, U. *The Iron Oxides*; 1996.
(3) Lagroix, F.; Banerjee, S. K.; Jackson, M. J. Geological Occurrences and Relevance of Iron Oxides. In *Iron Oxides: From Nature to Applications*; Faivre, D., Ed.; Wiley - VCH: Weinheim, Germany, 2016.
(4) Schwertmann, U.; Murad, E. Effect of pH on the Formation of Goethite and Hematite from Ferrihydrite. *Clays Clay Miner.* **1983**, *31* (4), 277–284.
(5) Chopard, A.; Benzaazoua, M.; Bouzahzah, H.; Plante, B.; Marion, P. A Contribution to Improve the Calculation of the Acid Generating Potential of Mining Wastes. *Chemosphere* **2017**, *175*, 97–107.
(6) Valencia-Avellan, M.; Slack, R.; Stockdale, A.; Mortimer, R. J. G. Understanding the Mobilisation of Metal Pollution Associated with Historical Mining in a Carboniferous Upland Catchment. *Environ. Sci. Process. Impacts* **2017**, *19* (8), 1061–1074.
(7) Maqueda, C.; Undabeytia, T.; Villaverde, J.; Morillo, E. Behaviour of Glyphosate in a Reservoir and the Surrounding Agricultural Soils. *Sci. Total Environ.* **2017**, *593–594*, 787–795.
(8) Elsner, M.; Haderlein, S. B.; Kellerhals, T.; Luzi, S.; Zwank, L.; Angst, W.; Schwarzenbach, R. P. Mechanisms and Products of Surface-Mediated Reductive Dehalogenation of Carbon Tetrachloride by Fe(II) on Goethite. *Environ. Sci. Technol.* **2004**, *38* (7), 2058–2066.
(9) Howard, P. H.; Muir, D. C. G. Identifying New Persistent and Bioaccumulative Organics Among Chemicals in Commerce. III: Byproducts, Impurities, and Transformation Products. *Environ. Sci. Technol.* **2013**, *47* (10), 5259–5266.
(10) Strehlau, J. H.; Stemig, M. S.; Penn, R. L.; Arnold, W. A. Facet-Dependent Oxidative Goethite Growth as a Function of Aqueous Solution Conditions. *Environ. Sci. Technol.* **2016**, *50* (19), 10406–10412.
(11) Chun, C. L.; Penn, R. L.; Arnold, W. A. Kinetic and Microscopic Studies of Reductive Transformations of Organic Contaminants on Goethite. *Environ. Sci. Technol.* **2006**, *40* (10), 3299–3304.
(12) Pecher, K.; Haderlein, S. B.; Schwarzenbach, R. P. Reduction of Polyhalogenated Methanes by Surface-Bound Fe(II) in Aqueous Suspensions of Iron Oxides. *Environ. Sci. Technol.* **2002**, *36* (8), 1734–1741.
(13) Elsner, M.; Schwarzenbach, R. P.; Haderlein, S. B. Reactivity of Fe(II)-Bearing Minerals toward Reductive Transformation of Organic Contaminants. *Environ. Sci. Technol.* **2004**, *38* (3), 799–807.
(14) Scherer, M. M.; Richter, S.; Valentine, R. L.; Alvarez, P. J. J. Chemistry and Microbiology of Permeable Reactive Barriers for In Situ Groundwater Clean Up. *Crit. Rev. Environ. Sci. Technol.* **2000**, *30* (3), 363–411.

(15) Boparai, H. K.; Comfort, S. D.; Shea, P. J.; Szecsody, J. E. Remediating Explosive-Contaminated Groundwater by in Situ Redox Manipulation (ISRM) of Aquifer Sediments. *Chemosphere* **2008**, *71* (5), 933–941.
(16) Wehrli, B.; Sulzberger, B.; Stumm, W. Redox Processes Catalyzed by Hydrous Oxide Surfaces. *Chem. Geol.* **1989**, *78* (3–4), 167–179.
(17) Barron, V.; Torrent, J. Surface Hydroxyl Configuration of Various Crystal Faces of Hematite and Goethite. *J. Colloid Interface Sci.* **1996**, *177* (2), 407–410.
(18) Catalano, J. G.; Fenter, P.; Park, C.; Zhang, Z.; Rosso, K. M. Structure and Oxidation State of Hematite Surfaces Reacted with Aqueous Fe(II) at Acidic and Neutral pH. *Geochim. Cosmochim. Acta* **2010**, *74* (5), 1498–1512.
(19) Tanwar, K. S.; Petitto, S. C.; Ghose, S. K.; Eng, P. J.; Trainor, T. P. Structural Study of Fe(II) Adsorption on Hematite(1-102). *Geochim. Cosmochim. Acta* **2008**, *72* (14), 3311–3325.
(20) Williams, A. G. B.; Scherer, M. M. Spectroscopic Evidence for Fe(II)-Fe(III) Electron Fransfer at the Iron Oxide-Water Interface. *Environ. Sci. Technol.* **2004**, *38* (18), 4782–4790.
(21) Rosso, K. M.; Yanina, S. V.; Gorski, C. A.; Larese-Casanova, P.; Scherer, M. M. Connecting Observations of Hematite (a-Fe2O3) Growth Catalyzed by Fe(II). *Environ. Sci. Technol.* **2010**, *44* (1), 61–67.
(22) Larese-Casanova, P.; Scherer, M. M. Fe(II) Sorption on Hematite: New Insights Based on Spectroscopic Measurements. *Environ. Sci. Technol.* **2007**, *41* (2), 471–477.
(23) Rosso, K. M.; Smith, D. M. A.; Dupuis, M. An Ab Initio Model of Electron Transport in Hematite (α-Fe2O3) Basal Planes. *J. Chem. Phys.* **2003**, *118* (14), 6455–6466.
(24) Hofstetter, T. B.; Heijman, C. G.; Haderlein, S. B.; Holliger, C.; Schwarzenbach, R. P. Complete Reduction of TNT and Other (Poly)Nitroaromatic Compounds under Iron-Reducing Subsurface Conditions. *Environ. Sci. Technol.* **1999**, *33* (9), 1479–1487.
(25) Dunnivant, F. M.; Schwarzenbach, R. P.; Macalady, D. L. Reduction of Substituted Nitrobenzenes in Aqueous Solutions Containing Natural Organic Matter. *Environ. Sci. Technol.* **1992**, *26*, 2133–2141.
(26) Klausen, J.; Troeber, S. P.; Haderlein, S. B.; Schwarzenback, R. P. Reduction of Substituted Nitrobenzenes by Fe(II) in Aqueous Mineral Suspensions. *Environ. Sci. Technol.* **1995**, *29* (9), 2396–2404.
(27) Ju, K.-S.; Parales, R. E. Nitroaromatic Compounds, from Synthesis to Biodegradation. *Microbiol. Mol. Biol. Rev.* **2010**, *74* (2), 250–272.
(28) Vindedahl, A. M.; Arnold, W. A.; Penn, R. L. Impact of Pahokee Peat Humic Acid and Buffer Identity on Goethite Aggregation and Reactivity. *Environ. Sci. Nano* **2015**, *2*, 509–517.
(29) Jeon, B. H.; Dempsey, B. A.; Burgos, W. D.; Royer, R. A. Reactions of Ferrous Iron with Hematite. *Colloids Surfaces A Physicochem. Eng. Asp.* **2001**, *191* (1–2), 41–55.

(30) Jeon, B. H.; Dempsey, B. A.; Burgos, W. D. Kinetics and Mechanisms for Reactions of Fe(II) with Iron(III) Oxides. *Environ. Sci. Technol.* **2003**, *37* (15), 3309–3315.
(31) Pedersen, H. D.; Postma, D.; Jakobsen, R.; Larsen, O. Fast Transformation of Iron Oxyhydroxides by the Catalytic Action of Aqueous Fe(II). *Geochim. Cosmochim. Acta* **2005**, *69* (16), 3967–3977.
(32) Yang, H.; Lu, R.; Downs, R. T.; Costin, G. Goethite, Alpha-FeO(OH), from Single-Crystal Data. *Acta Crystallogr. Sect. E Struct. Reports Online* **2006**, *62* (12).
(33) Strehlau, J. H.; Schultz, J. D.; Vindedahl, A. M.; Arnold, W. A.; Penn, R. L. Effect of Nonreactive Kaolinite on 4-Chloronitrobenzene Reduction by Fe(II) in Goethite–Kaolinite Heterogeneous Suspensions. *Environ. Sci. Nano* **2017**, *4*, 325–334.
(34) Larese-Casanova, P.; Kappler, A.; Haderlein, S. B. Heterogeneous Oxidation of Fe(II) on Iron Oxides in Aqueous Systems: Identification and Controls of Fe(III) Product Formation. *Geochim. Cosmochim. Acta* **2012**, *91*, 171–186.
(35) Stemig, A. M.; Do, T. A.; Yuwono, V. M.; Arnold, W. A.; Penn, R. L. Goethite Nanoparticle Aggregation: Effects of Buffers, Metal Ions, and 4-Chloronitrobenzene Reduction. *Environ. Sci. Nano* **2014**, *1*, 478–487.
(36) Guo, H.; Barnard, A. S. Thermodynamic Modelling of Nanomorphologies of Hematite and Goethite. *J. Mater. Chem.* **2011**, *21* (31), 11566.
(37) Navrotsky, A.; Mazeina, L.; Majzlan, J. Size-Driven Structural and Thermodynamic Complexity in Iron Oxides. *Science* **2008**, *319*, 1635–1638.

References for Chapter 3

(1) Vindedahl, A. M.; Strehlau, J. H.; Arnold, W. A.; Penn, R. L. Organic Matter and Iron Oxide Nanoparticles: Aggregation, Interactions, and Reactivity. *Environ. Sci. Nano* **2016**, *3*, 494–505.
(2) Strehlau, J. H.; Toner, B. M.; Arnold, W. A.; Penn, R. L. Accessible Reactive Surface Area and Abiotic Redox Reactivity of Iron Oxyhydroxides in Acidic Brines. *Geochim. Cosmochim. Acta* **2017**, *197*, 345–355.
(3) Strehlau, J. H.; Stemig, M. S.; Penn, R. L.; Arnold, W. A. Facet-Dependent Oxidative Goethite Growth As a Function of Aqueous Solution Conditions. *Environ. Sci. Technol.* **2016**, *50* (19), 10406–10412.
(4) Voelz, J. L.; Arnold, W. A.; Penn, R. L. Redox-Induced Nucleation and Growth of Goethite on Synthetic Hematite Nanoparticles. *Am. Mineral.* **2018**, *103* (7), 1021–1029.
(5) Elsner, M.; Schwarzenbach, R. P.; Haderlein, S. B. Reactivity of Fe(II)-Bearing Minerals toward Reductive Transformation of Organic Contaminants. *Environ. Sci. Technol.* **2004**, *38* (3), 799–807.
(6) Luan, F.; Xie, L.; Li, J.; Zhou, Q. Abiotic Reduction of Nitroaromatic Compounds by Fe(II) Associated with Iron Oxides and Humic Acid. *Chemosphere* **2013**, *91* (7), 1035–1041.

(7) Vindedahl, A. M.; Stemig, M. S.; Arnold, W. A.; Penn, R. L. Character of Humic Substances as a Predictor for Goethite Nanoparticle Reactivity and Aggregation. *Environ. Sci. Technol.* **2016**, *50* (3), 1200–1208.
(8) Vindedahl, A. M.; Arnold, W. A.; Penn, R. L. Impact of Pahokee Peat Humic Acid and Buffer Identity on Goethite Aggregation and Reactivity. *Environ. Sci. Nano* **2015**, *2*, 509–517.
(9) Colón, D.; Weber, E. J.; Anderson, J. L. Effect of Natural Organic Matter on the Reduction of Nitroaromatics by Fe(II) Species. *Environ. Sci. Technol.* **2008**, *42* (17), 6538–6543.
(10) Gu, B.; Schmitt, J.; Chen, Z.; Liang, L.; McCarthy, J. F. Adsorption and Desorption of Different Organic Matter Fractions on Iron Oxide. *Geochim. Cosmochim. Acta* **1995**, *59* (2), 219–229.
(11) Feitosa-Felizzola, J.; Hanna, K.; Chiron, S. Adsorption and Transformation of Selected Human-Used Macrolide Antibacterial Agents with Iron(III) and Manganese(IV) Oxides. *Environ. Pollut.* **2009**, *157* (4), 1317–1322.
(12) Ritchie, J. D.; Perdue, M. Proton-Binding Study of Standard and Reference Fulvic Acids, Humic Acids, and Natural Organic Matter. *Geochim. Cosmochim. Acta* **2003**, *67* (1), 85–96.
(13) LaKind, J. S.; Stone, A. T. Reductive Dissolution of Goethite by Phenolic Reductants. *Geochim. Cosmochim. Acta* **1989**, *53* (5), 961–971.
(14) Korpany, K. V.; Majewski, D. D.; Chiu, C. T.; Cross, S. N.; Blum, A. S. Iron Oxide Surface Chemistry: Effect of Chemical Structure on Binding in Benzoic Acid and Catechol Derivatives. *Langmuir* **2017**, *33* (12), 3000–3013.
(15) Saikia, N.; Sarma, J.; Borah, J. M.; Mahiuddin, S. Adsorption of 3,4-Dihydroxybenzoic Acid onto Hematite Surface in Aqueous Medium: Importance of Position of Phenolic -OH Groups and Understanding of the Same Using Catechol as an Auxiliary Model. *J. Colloid Interface Sci.* **2013**, *398*, 227–233.
(16) Yuen, A. K. L.; Hutton, G. A.; Masters, A. F.; Maschmeyer, T. The Interplay of Catechol Ligands with Nanoparticulate Iron Oxides. *Dalt. Trans.* **2012**, *41* (9), 2545–2559.
(17) Yang, Y.; Yan, W.; Jing, C. Dynamic Adsorption of Catechol at the Goethite/Aqueous Solution Interface: A Molecular-Scale Study. *Langmuir* **2012**, *28* (41), 14588–14597.
(18) Bish, D. L.; Post, J. E. *Volume 20: Modern Powder Diffraction*; Ribbe, P. H., Ed.; Mineralogical Society of America: Chantilly, Virginia, 1989.
(19) McElfresh, M. *Fundamentals of Magnetism and Magnetic Measurements*; Purdue University: West Lafayette, Indiana, 1994.
(20) Maxbauer, D. P.; Feinberg, J. M.; Fox, D. L. Magnetic Mineral Assemblages in Soils and Paleosols as the Basis for Paleoprecipitation Proxies: A Review of Magnetic Methods and Challenges. *Earth-Science Rev.* **2016**, *155*, 28–48.

References for Chapter 4

(1) Morrice, E.; Colagiuri, R. Coal Mining, Social Injustice and Health: A Universal Conflict of Power and Priorities. *Heal. Place* **2013**, *19* (1), 74–79.

(2) Mudd, G. M.; Diesendorf, M. Sustainability of Uranium Mining and Milling: Toward Quantifying Resources and Eco-Efficiency. *Environ. Sci. Technol.* **2008**, *42* (7), 2624–2630.

(3) Prieto, B.; Silva, B.; Aira, N. Methodological Aspects of the Induction of Biofilms for Remediation of the Visual Impact Generated by Quartz Mining. *Sci. Total Environ.* **2006**, *370* (1), 254–261.

(4) Lu, X.; Wang, H. Microbial Oxidation of Sulfide Tailings and the Environmental Consequences. *Elements* **2012**, *8* (2), 119–124.

(5) Edraki, M.; Baumgartl, T.; Manlapig, E.; Bradshaw, D.; Franks, D. M.; Moran, C. J. Designing Mine Tailings for Better Environmental, Social and Economic Outcomes: A Review of Alternative Approaches. *J. Clean. Prod.* **2014**, *84* (1), 411–420.

(6) Massari, S.; Ruberti, M. Rare Earth Elements as Critical Raw Materials: Focus on International Markets and Future Strategies. *Resour. Policy* **2012**, *38* (1), 36–43.

(7) Müezzinoğlu, A. A Review of Environmental Considerations on Gold Mining and Production. *Crit. Rev. Environ. Sci. Technol.* **2003**, *33* (1), 45–71.

(8) Yelpaala, K.; Ali, S. H. Multiple Scales of Diamond Mining in Akwatia, Ghana: Addressing Environmental and Human Development Impact. *Resour. Policy* **2005**, *30* (3), 145–155.

(9) Chopard, A.; Benzaazoua, M.; Bouzahzah, H.; Plante, B.; Marion, P. A Contribution to Improve the Calculation of the Acid Generating Potential of Mining Wastes. *Chemosphere* **2017**, *175*, 97–107.

(10) Cornwell, J. C.; Morse, J. W. The Characterization of Iron Sulfide Minerals in Anoxic Marine Sediments. *Mar. Chem.* **1987**, *22* (2–4), 193–206.

(11) Johnson, D. B.; Hallberg, K. B. Acid Mine Drainage Remediation Options: A Review. *Sci. Total Environ.* **2005**, *338*, 3–14.

(12) Utgikar, V. P.; Harmon, S. M.; Chaudhary, N.; Tabak, H. H.; Govind, R.; Haines, J. R. Inhibition of Sulfate-Reducing Bacteria by Metal Sulfide Formation in Bioremediation of Acid Mine Drainage. *Environ. Toxicol.* **2002**, *17* (1), 40–48.

(13) Pastor, J.; Dewey, B.; Johnson, N. W.; Swain, E. B.; Monson, P.; Peters, E. B.; Myrbo, A. Effects of Sulfate and Sulfide on the Life Cycle of Zizania Palustris in Hydroponic and Mesocosm Experiments. *Ecol. Appl.* **2017**, *27* (1), 321–336.

(14) LaFond-Hudson, S.; Johnson, N. W.; Pastor, J.; Dewey, B. Iron Sulfide Formation on Root Surfaces Controlled by the Life Cycle of Wild Rice (Zizania Palustris). *Biogeochemistry* **2018**, *141* (1), 95–106.

(15) Poulton, S. W.; Krom, M. D.; Van Rijn, J.; Raiswell, R. The Use of Hydrous Iron (III) Oxides for the Removal of Hydrogen Sulphide in Aqueous Systems. *Water Res.* **2002**, *36* (4), 825–834.

(16) Poulton, S. W.; Krom, M. D.; Raiswell, R. A Revised Scheme for the Reactivity of Iron (Oxyhydr)Oxide Minerals towards Dissolved Sulfide. *Geochim. Cosmochim. Acta* **2004**, *68* (18), 3703–3715.

(17) Canfield, D. E.; Raiswell, R.; Bottrell, S. The Reactivity of Sedimentary Iron Minerals towards Sulfide. *Am. J. Sci.* **1992**, *292*, 659–683.

(18) Anastas, P.; Eghbali, N. Green Chemistry: Principles and Practice. *Chem. Soc. Rev.* **2010**, *39* (1), 301–312.
(19) Seager, T.; Selinger, E.; Wiek, A. Sustainable Engineering Science for Resolving Wicked Problems. *J. Agric. Environ. Ethics* **2012**, *25* (4), 467–484.
(20) Anschutz, A. J.; Penn, R. L. Reduction of Crystalline Iron(III) Oxyhydroxides Using Hydroquinone: Influence of Phase and Particle Size. *Geochem. Trans.* **2005**, *6* (3), 60–66.
(21) Voelz, J. L.; Arnold, W. A.; Penn, R. L. Redox-Induced Nucleation and Growth of Goethite on Synthetic Hematite Nanoparticles. *Am. Mineral.* **2018**, *103* (7), 1021–1029.
(22) Voelz, J. L.; Johnson, N. W.; Chun, C. L.; Arnold, W. A.; Penn, R. L. Quantitative Dissolution of Environmentally-Accessible Iron Residing in Iron-Rich Minerals: A Review. *Submitted*.
(23) McGuire, M. M.; Hamers, R. J. Extraction and Quantitative Analysis of Elemental Sulfur from Sulfide Mineral Surfaces by High-Performance Liquid Chromatography. *Environ. Sci. Technol.* **2000**, *34* (21), 4651–4655.
(24) Whitney, D. L.; Evans, B. W. Abbreviations for Names of Rock-Forming Minerals. *Am. Mineral.* **2010**, *95* (1), 185–187.
(25) Bish, D. L.; Post, J. E. *Volume 20: Modern Powder Diffraction*; Ribbe, P. H., Ed.; Mineralogical Society of America: Chantilly, Virginia, 1989.
(26) Rennert, T. Wet-Chemical Extractions to Characterise Pedogenic Al and Fe Species-a Critical Review. *Soil Res.* **2019**, *57* (1), 1–16.
(27) Poulton, S. W.; Canfield, D. E. Development of a Sequential Extraction Procedure for Iron: Implications for Iron Partitioning in Continentally Derived Particulates. *Chem. Geol.* **2005**, *214*, 209–221.
(28) Heron, G.; Crouzet, C.; Bourg, A. C. M.; Christensen, T. H. Speciation of Fe(II) and Fe(III) in Contaminated Aquifer Sediments Using Chemical Extraction Techniques. *Environ. Sci. Technol.* **1994**, *28* (9), 1698–1705.
(29) Zuo, Y.; Holgné, J. Formation of Hydrogen Peroxide and Depletion of Oxalic Acid in Atmospheric Water by Photolysis of Iron(III)-Oxalato Complexes. *Environ. Sci. Technol.* **1992**, *26*, 1014–1022.
(30) Cornell, R.; Schindler, P. Photochemical Dissolution of Goethite in Acid/Oxalate Solution. *Clays Clay Miner.* **1987**, *35* (5), 347–352.
(31) Finneran, K. T.; Johnsen, C. V.; Lovley, D. R. Rhodoferax Ferrireducens Sp. Nov., a Psychrotolerant, Facultatively Anaerobic Bacterium That Oxidizes Acetate with the Reduction of Fe(III). *Int. J. Syst. Evol. Microbiol.* **2003**, *53* (3), 669–673.
(32) Brezonik, P. L.; Arnold, W. A. *Water Chemistry: An Introduction to the Chemistry of Natural and Engineered Aquatic Systems*; Oxford University Press: New York, 2011.
(33) Pyzik, A. J.; Sommer, S. E. Sedimentary Iron Monosulfides: Kinetics and Mechanism of Formation. *Geochim. Cosmochim. Acta* **1981**, *45* (5), 687–698.
(34) West, P. W.; Gaeke, G. C. Fixation of Sulfur Dioxide as Disuifitomercurate(II) and Subsequent Colorimetric Estimation. *Anal. Chem.* **1956**, *28* (12), 1816–1819.

Appendix A. Supplemental Information for Chapter 1 – Quantitative Dissolution of Environmentally-Accessible Iron Residing in Iron-Rich Minerals

Section 1. Supporting Figures and Tables

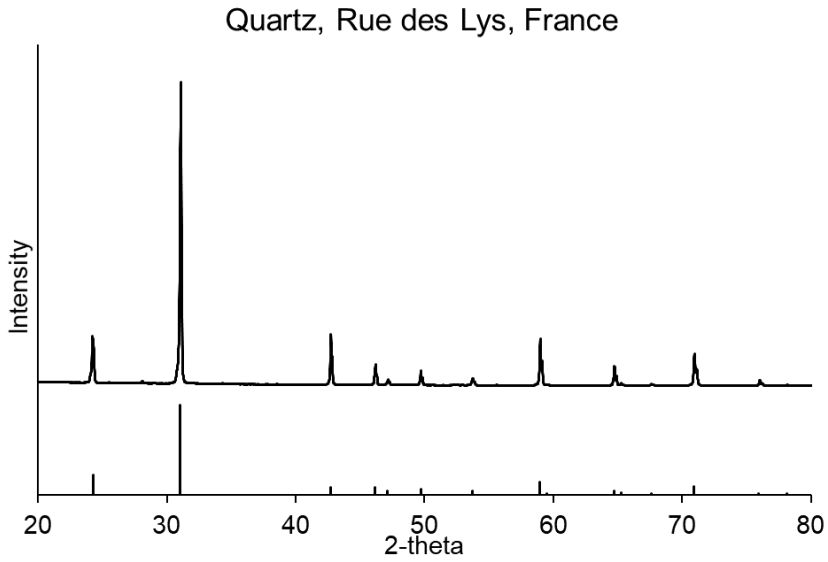

Figure A1. X-ray diffraction pattern of quartz reference mineral.

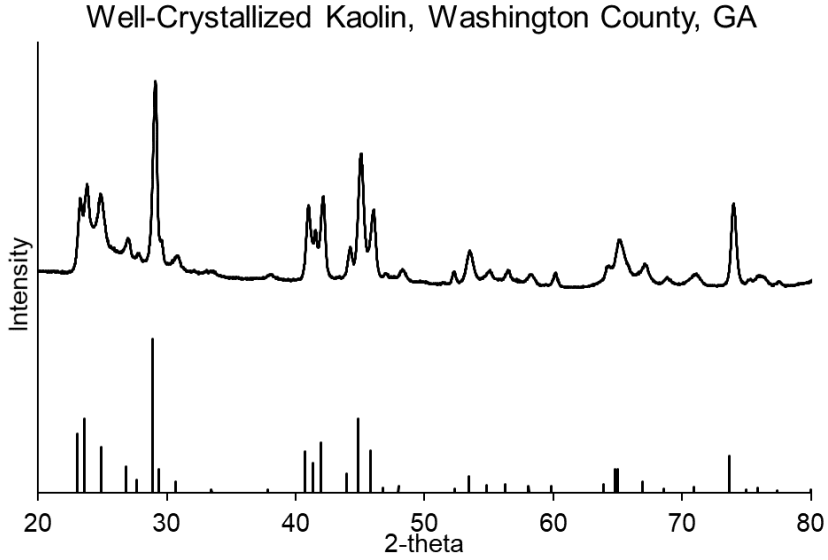

Figure A2. X-ray diffraction pattern of kaolinite reference mineral.

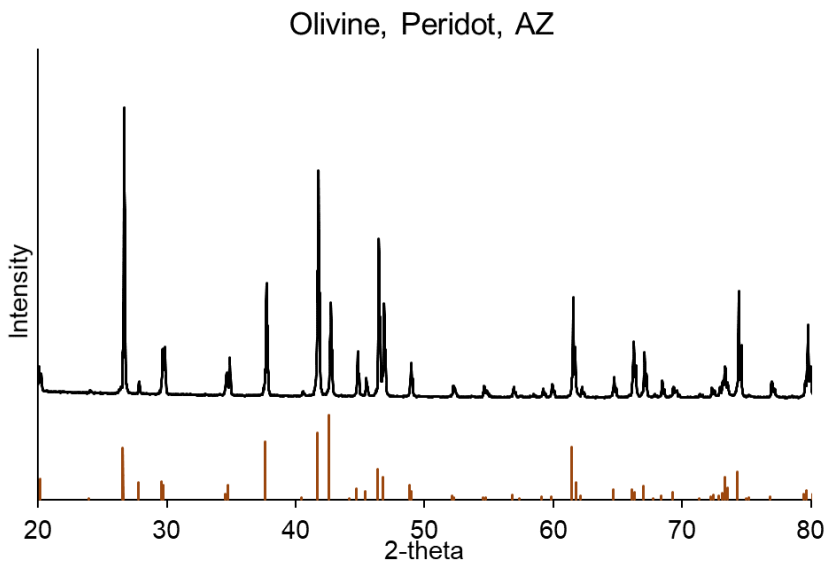

Figure A3. X-ray diffraction pattern of olivine reference mineral.

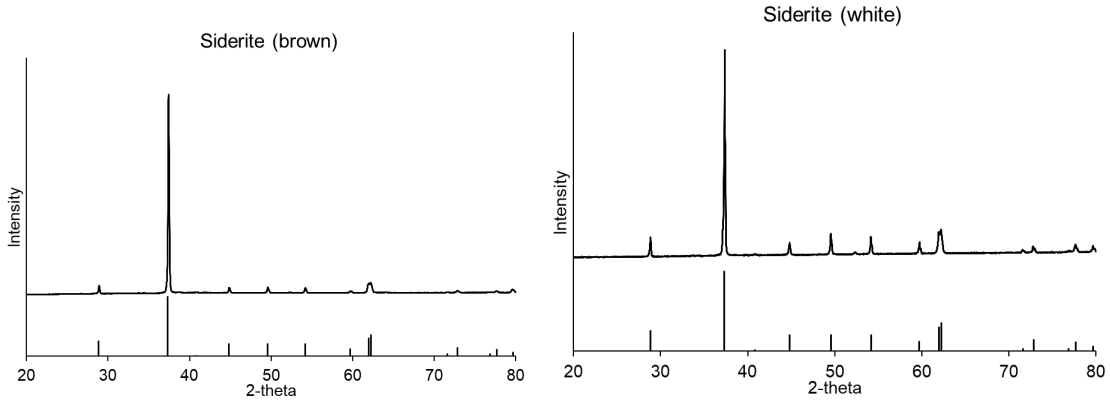

Figure A4. X-ray diffraction pattern of brown (left) and white (right) siderite reference minerals.

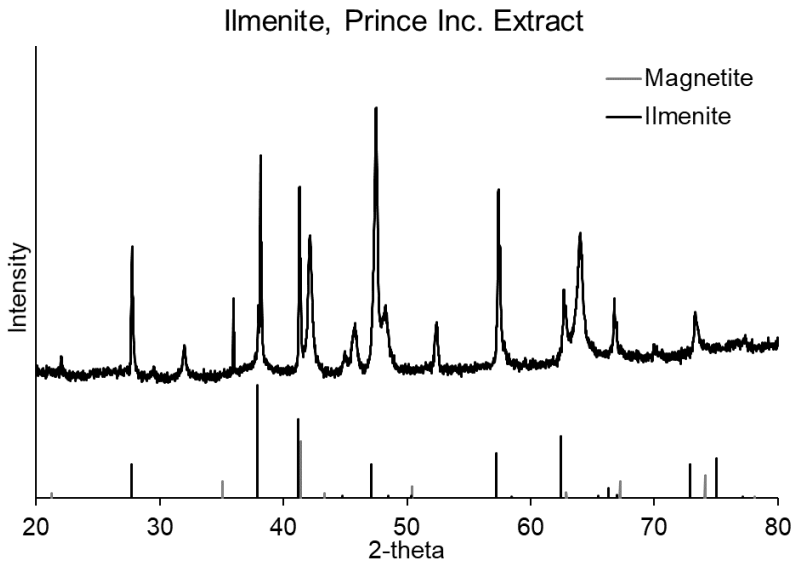

Figure A5. X-ray diffraction pattern of ilmenite reference mineral. Black peaks correspond to ilmenite and grey correspond to magnetite. Unassigned peaks correspond with titania (TiO_2) and silica (SiO_2).

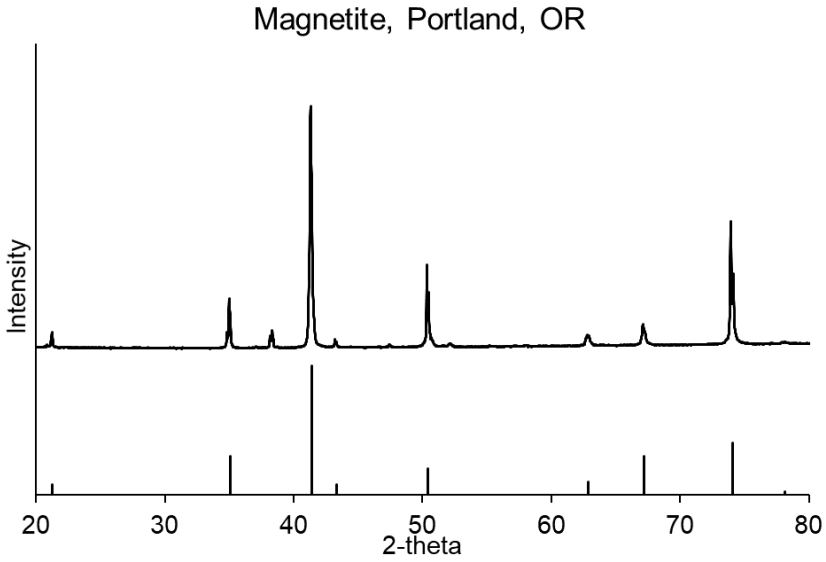

Figure A6. X-ray diffraction pattern of magnetite reference mineral.

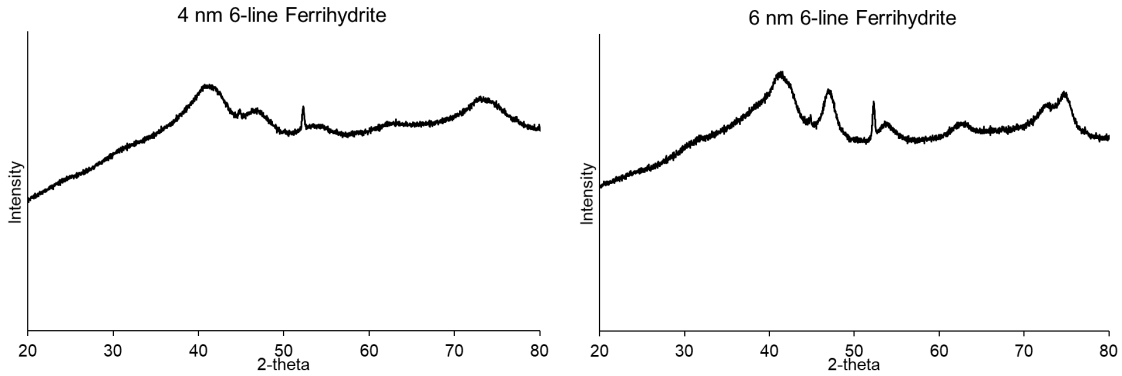

Figure A7. X-ray diffraction pattern of 4 nm (left) and 6 nm (right) ferrihydrite reference minerals. Sharp peak at circa 52 degrees is the sample holder.

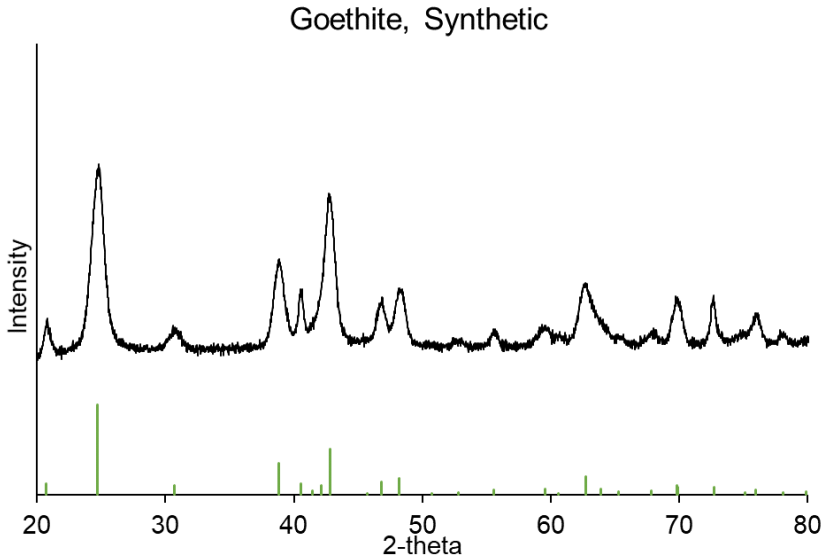

Figure A8. X-ray diffraction pattern of synthetic goethite reference mineral.

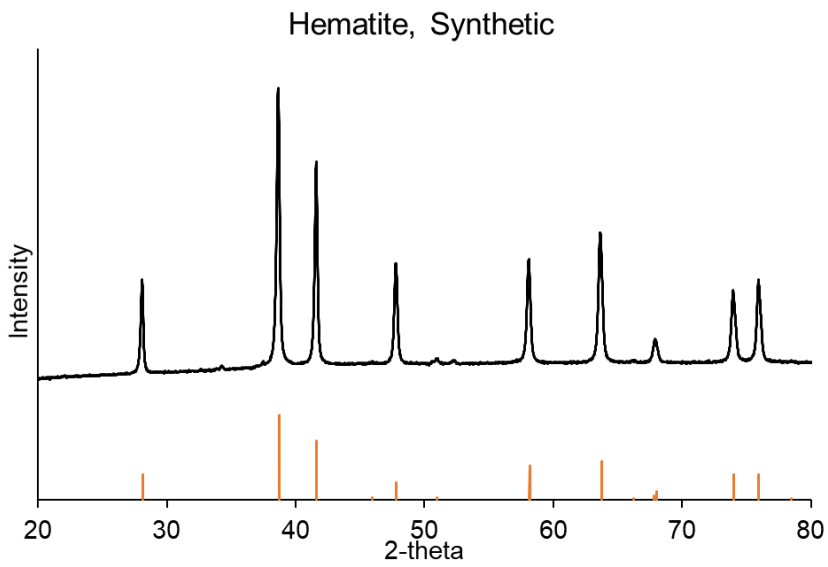

Figure A9. X-ray diffraction pattern of synthetic hematite reference mineral.

Table A1. Preparation details for calibration curve standards described in Figure 1.2, Table 1.5, and Figure A10. Oxalate buffer is the same solution used for the dissolution by oxalate, provided in the experimental.

Conc. (mM)	MQ (mL)	0.34 M Oxalate (mL)	0.15 mM Fe(II) (mL)	0.15 mM Fe(III) (mL)	5 mg/mL Ferrozine (mL)	1.4 M $HONH_2 \cdot HCl$ (mL)	10 M NH_4Ac (mL)	Vol. (mL)
0.005	2.700		0.100		0.200	0.300	0.100	3.400
0.010	2.600		0.200		0.200	0.300	0.100	3.400
0.020	2.400		0.400		0.200	0.300	0.100	3.400
0.010	2.600		0.100	0.100	0.200	0.300	0.100	3.400
0.020	2.400		0.200	0.200	0.200	0.300	0.100	3.400
0.040	2.000		0.400	0.400	0.200	0.300	0.100	3.400
0.005	2.700			0.100	0.200	0.300	0.100	3.400
0.010	2.600			0.200	0.200	0.300	0.100	3.400
0.020	2.400			0.400	0.200	0.300	0.100	3.400
0.005	2.600	0.100	0.100		0.200	0.300	0.100	3.400
0.010	2.500	0.100	0.200		0.200	0.300	0.100	3.400
0.020	2.300	0.100	0.400		0.200	0.300	0.100	3.400
0.010	2.500	0.100	0.100	0.100	0.200	0.300	0.100	3.400
0.020	2.300	0.100	0.200	0.200	0.200	0.300	0.100	3.400
0.040	1.900	0.100	0.400	0.400	0.200	0.300	0.100	3.400
0.005	2.600	0.100		0.100	0.200	0.300	0.100	3.400
0.010	2.500	0.100		0.200	0.200	0.300	0.100	3.400
0.020	2.300	0.100		0.400	0.200	0.300	0.100	3.400

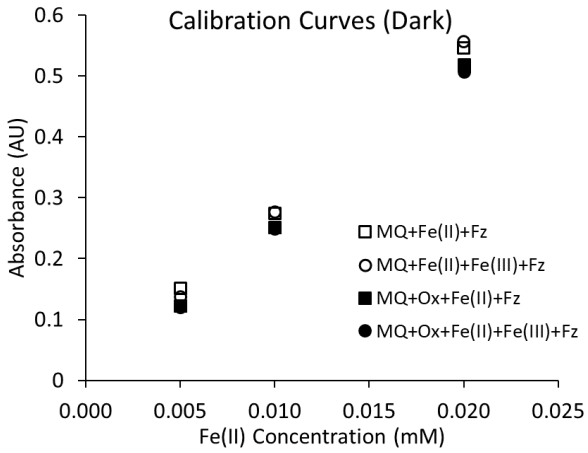

Figure A10. Calibration curves of standards containing Fe(II) or Fe(III) and Fe(II) with and without oxalate after 3 days of equilibration in darkness. Oxalate buffer slightly inhibits ferrozine complexation but using an equivalent concentration of oxalate in standards and in samples will counteract effect.

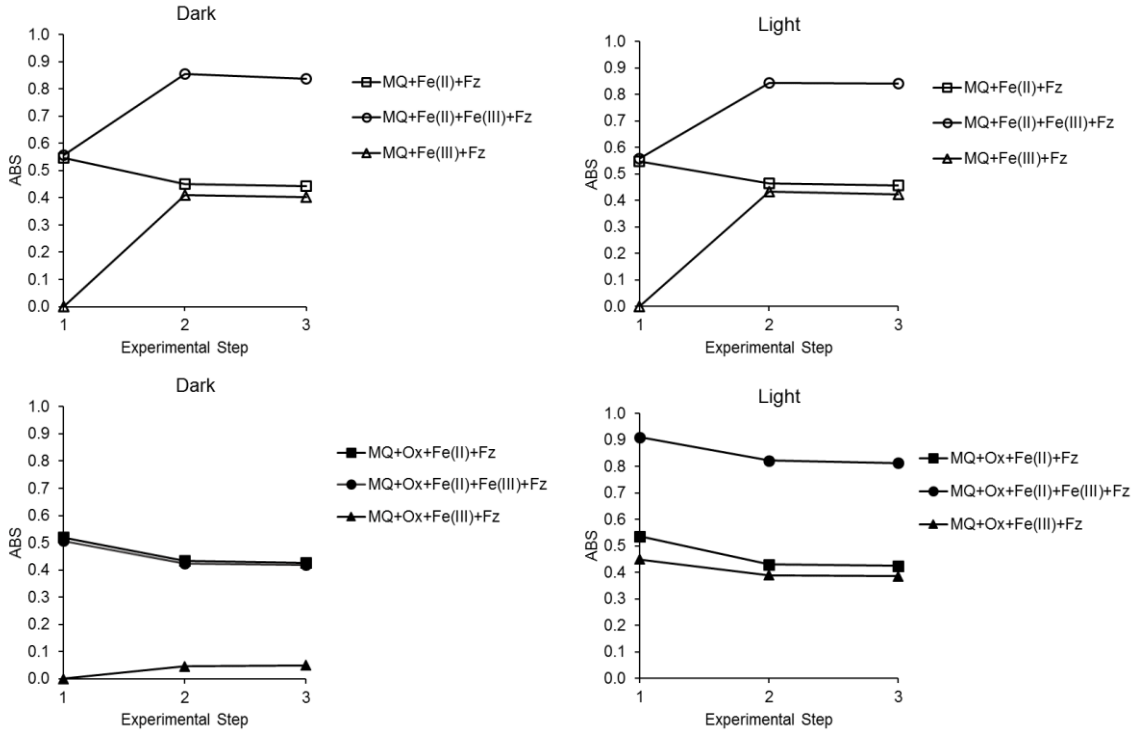

Figure A11. Absorbance of the Fe(II)-ferrozine complex after various steps performed in an anaerobic glove bag under darkness or in ambient light. Experimental steps were: (1) preparation using ultra-filtered water, oxalate buffer (if present), Fe(II) and/or equal parts Fe(III), and ferrozine, then equilibrated for 3 days; (2) chemical reduction by $HONH_2$-HCl, two-hour equilibration, pH adjustment with NH_4-acetate, and then 15-minute equilibration; and (3) five hours later. See Table A2 for cuvette preparation volumes and concentrations. Values are presented as Fe(II) concentration in Figure 1.2.

Table A2. Absorbance values for calibration curve standards after three days of anaerobic equilibration under darkness (D) or in ambient light (L). BDL indicates the absorbance was below detection limit.

Cuvette Contents	ABS 0.005 mM Fe(II)	ABS 0.01 mM Fe(II)	ABS 0.02 mM Fe(II)	y=mx+b	R^2
(D) MQ+Fe(II)+Fz	0.1307	0.2745	0.5458	26.437x + 0.015	0.9995
(D) MQ+Fe(II)+Fe(III)+Fz	0.1373	0.2765	0.5564	27.942x – 0.003	0.9999
% difference	5	0.7	2		
(L) MQ+Fe(II)+Fz	0.1372	0.2738	0.5482	27.404x + 0.0002	0.9999
(L) MQ+Fe(II)+Fe(III)+Fz	0.1399	0.2785	0.5576	27.853x + 0.0004	0.9999
% difference	2	2	2		

Section 2. Experimental

All solutions were prepared using ultra-filtered water (MilliPore Advantage A10, 18.2 MΩ•cm) and all experiments were performed in an anaerobic glove bag (Coy Laboratory Products 95 % N_2, 5% H_2 atmosphere). Solutions used in anaerobic conditions were deoxygenated by bubbling N_2 (Matheson, 99.998 %). Rotational agitation was performed in the anaerobic glove bag using a shaker table (Cole-Parmer, model 51700-13).

Reagents

Many of the same reagents were used for multiple experiments and their sources and purities are listed here: acetic acid (Aristar, glacial), ammonium acetate (Sigma-Aldrich, >97 %), ammonium hydroxide (Sigma-Aldrich, 30 %), ammonium oxalate (Sigma Aldrich 99%), oxalic acid (Fisher), ferrozine (5,6-diphenyl-3-(2-pyridyl)-1,2,4-triazine-4,4'-disulfonic acid disodium salt hydrate, Alfa Aesar, 98%), hydrochloric acid (1 and 2 M solutions made from glacial, Aristar), hydroxylamine-hydrochloride ($HOHN_2$-HCl; Sigma Aldrich, 99 %), and sodium hydroxide (0.5 M solution made from 50 %w/w, Fisher).

Ferrozine Assay

Three reagents were prepared for iron quantification by UV-vis spectroscopy: (A) 10 mM ferrozine in ultra-filtered water, (B) 1.4 M $HONH_2$-HCl in 2 M HCl, and (C) 10 M NH_4-acetate buffered to pH 9.5 with NH_4OH. Sample were prepared in polystyrene cuvettes under the same conditions used during dissolution experiments and contained (3 – *x*) mL ultra-filtered water, 0.2 mL Reagent A, and *x* mL filtered sample. The cuvettes were capped, inverted 3 times, and the absorbance was measured immediately. Then the Fe(III) was reduced by adding 0.3 mL of Reagent B to each cuvette and mixed well. After 2 hours, 0.1 mL of Reagent C was added to each cuvette and mixed well. The absorbance was monitored until it reached a maximum, generally after 10 – 60 minutes.

Mineral Specimens

Eleven reference minerals were collected, purchased, or synthesized: quartz (Rue des Lys, France), kaolinite (Washington County, Georgia), olivine (Kohlstedt Research Group, University of Minnesota; approx. Fo_{90}; Peridot, Arizona), white siderite (Ward's Science; Mt. St. Hilaire, Quebec), brown siderite (Institute for Rock Magnetism, University of Minnesota), ilmenite (Laguna Clay Company), magnetite (Gold Beach, Oregon), rhombohedral hematite (synthetic[1]), goethite (synthetic[2]), and 4 nm and 6 nm ferrihydrite (synthetic[2]). Both siderite specimens were received as bulk minerals, then were ground into powder using mortar and pestle. Ilmenite and magnetite were further purified upon receipt using neodymium magnets to separate the magnetic minerals from the sand and then ground into powder using mortar and pestle.

Solid-State Characterization

The mineral identity and composition of all specimens were assessed using X-ray diffraction (PANalytical, X'Pert PRO, Co K_α 1.7909 Å, X'Celerator detector). Scans were performed from 10 – 90 °2θ with a step size of 0.0167 °2θ and with an effective dwell time of 100 s per step. Patterns were compared with reference powder diffraction files available in the Crystallography Open Database.

Dissolution using Acetate/Acetic Acid

Each of the eleven reference minerals were massed in triplicate into 20 mL borosilicate scintillation vials and transferred to an anaerobic chamber for overnight equilibration. Specimens with low expected iron content (quartz and kaolinite) or solubility (olivine and ilmenite) contained 0.2 g and 0.08 g, respectively. All other samples contained 0.02 – 0.04 g of material. 1 M sodium acetate solution was prepared in a volumetric flask then transferred to a Nalgene bottle. Glacial acetic acid was added until the pH reached 4.5, resulting in a circa 2 M acetic acid/acetate solution. The buffer solution was deoxygenated under bubbling N_2 for 1 hour, transferred to an anaerobic chamber, and equilibrated for 24 hours. After equilibration, 15 mL of buffer solution was added to each scintillation vial. The vial threads were lined with Teflon tape, capped, sealed in air-tight glass jars (Mason), removed from the anaerobic chamber, and set on a rotational agitator (100 rpm, 2 cm diameter) inside a 55 °C oven for 48 hours. The glass jars were then returned to the anaerobic chamber for filtering and UV-vis ferrozine assay.

Dissolution using Hydroxylamine-HCl

Each of the eleven reference minerals were massed in triplicate into 20 mL borosilicate scintillation vials and transferred to an anaerobic chamber for overnight equilibration. Specimens with low expected iron content (quartz and kaolinite) or solubility (olivine) contained 0.2 g and 0.08 g, respectively. All other samples contained 0.02 – 0.04 g of material. A 3.6 M solution of $HONH_2$-HCl was prepared in a volumetric flask. To a 1 L volumetric flask was added 150 mL of the $HONH_2$-HCl solution and 350 mL of glacial acetic acid, then diluted to the mark with ultra-filtered water to yield a 1 M $HONH_2$-HCl solution in 35 %(v/v) acetic acid (pH 1.5). The buffer solution was deoxygenated under bubbling N_2 for 1 hour, transferred to an anaerobic chamber, and equilibrated for 24 hours. After equilibration, 10 mL of the 1 M $HONH_2$-HCl solution was added to each sample vial. The vials were capped, shaken well, and covered in Al foil. The vials were shaken by hand once a day for 4 days, then sampled by ferrozine analysis.

Dissolution using Oxalate/Oxalic Acid

The surface-accessible iron content of eleven reference minerals was assessed using mineral dissolution by oxalate. Three replicates of each specimen were prepared in borosilicate scintillation vials, containing 0.1 g of the mixed mineral specimens, 0.05 g of the high-iron reference minerals, or 0.2 g of low-iron reference minerals, then were transferred to an anaerobic chamber and equilibrated for 24 hours. Oxalate solution (0.2 M NH_4-oxalate, and 0.17 M oxalic acid) was deoxygenated for 1.5 hours, transferred to the anaerobic chamber, equilibrated for 1 hour, and then added to each mineral vial (10

mL each) under near total darkness. The vials were capped, covered in aluminum foil, and agitated at 150 rpm for 2 days. Under near total darkness, 1 mL of each solution was filtered (Agilent 0.2 μm, 13 mm, Nylon) and used to prepare triplicate cuvettes for ferrozine assay (sample volume x = 50 or 100 μM). The Fe(II) concentration was determined using calibration curve standards containing equivalent oxalate concentration. Sample absorbance was measured once by UV-visible spectroscopy at 562 nm, then returned to the anaerobic glove bag and exposed to laboratory light for 24 hours. The cuvettes were then removed from the glove bag and the absorbance measured again to yield total dissolved iron.

Dissolution using Hydrochloric Acid

The total iron content of eight reference minerals was assessed using mineral dissolution by HCl. Each mineral was massed (30 – 200 mg) in triplicate into borosilicate scintillation vials, transferred to an anaerobic glove bag, and uncapped for overnight equilibration. Concentrated HCl was deoxygenated for 30 minutes and transferred to the glove bag, and 5 mL was added to each vial. The vial threads were wrapped with Teflon tape, tightly capped, and transferred to a fume hood outside the glove bag. After 24 hours, approximately 1 mL of each solution was filtered (Agilent, 0.2 μm, nylon) and 0.5 mL were pipetted into 50 mL volumetric flasks then diluted to the mark with ultra-filtered water. Iron(II) was measured by UV-visible ferrozine assay and Fe(III) was determined by difference using reduction by hydroxylamine-HCl.

Testing Oxalate Interference in UV-Visible Spectroscopy

Calibration curve standards were prepared using ultra-filtered water, oxalate buffer reagent (0.2 M NH_4-oxalate + 0.17 M oxalic acid), ferrozine, and Fe(II) and/or Fe(III), added in that order. Typical UV-visible sample preparation for oxalate digests uses 50 – 100 μL of filtered digest solution, so standards were prepared by substituting 100 μL of the ultra-filtered water component with oxalate buffer. Samples were grouped into several sets: under darkness without oxalate, in light without oxalate, under darkness with oxalate, and in light with oxalate. The samples equilibrated for three days in an anaerobic glove bag, then the absorbance was measured by UV-visible spectroscopy. The samples were then chemically reduced with $HONH_2$-HCl, equilibrated for 2 hours, pH adjusted with NH_4-acetate, and then equilibrated for 15 minutes before measuring the absorbance again. The absorbance was also measured five hours later. Concentrations and volumes for each cuvette are given in Table A2.

References

(1) Voelz, J. L.; Arnold, W. A.; Penn, R. L. Redox-Induced Nucleation and Growth of Goethite on Synthetic Hematite Nanoparticles. *Am. Mineral.* **2018**, *103* (7), 1021–1029.

(2) Anschutz, A. J.; Penn, R. L. Reduction of Crystalline Iron(III) Oxyhydroxides Using Hydroquinone: Influence of Phase and Particle Size. *Geochem. Trans.* **2005**, *6* (3), 60–66.

Appendix B. Supplemental Information for Chapter 2 – Redox-Induced Nucleation and Growth of Goethite on Synthetic Hematite Nanoparticles

Section 1. Supplemental Figures and Tables

Mass Loading

The mass loading of particle stock suspensions was calculated using the dried masses of 0.250 – 4.000 mL of suspension. The mass of each weigh boat was recorded prior to the volumetric addition of the stock suspension and after the suspension dried at room temperature. Sample mass was determined by difference. Dried masses were plotted versus added volumes, where the slope defined the particle mass loading (Fig. B1).

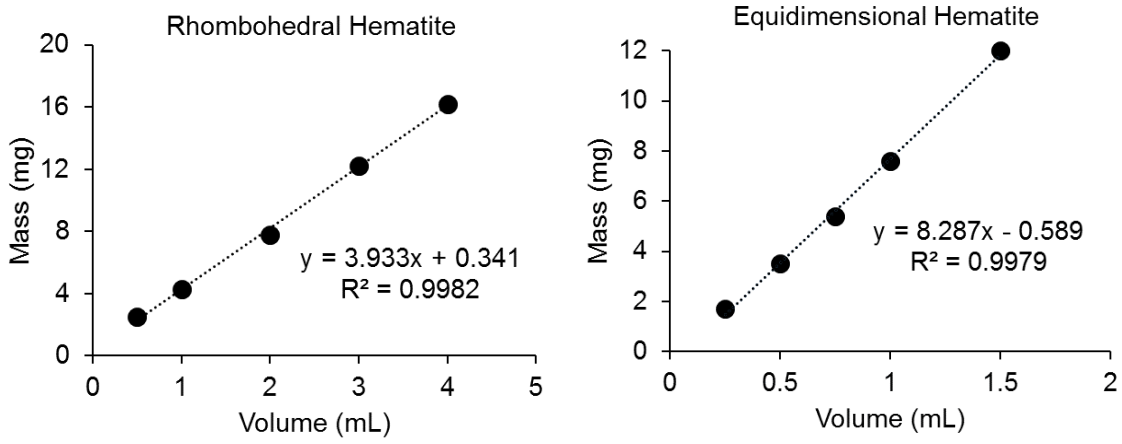

Figure B1. Mass loading plots for the stock suspensions of rhombohedral (left) and equidimensional (right) hematite. Slope of the fitted line describes mass loading in mg/mL of the suspension.

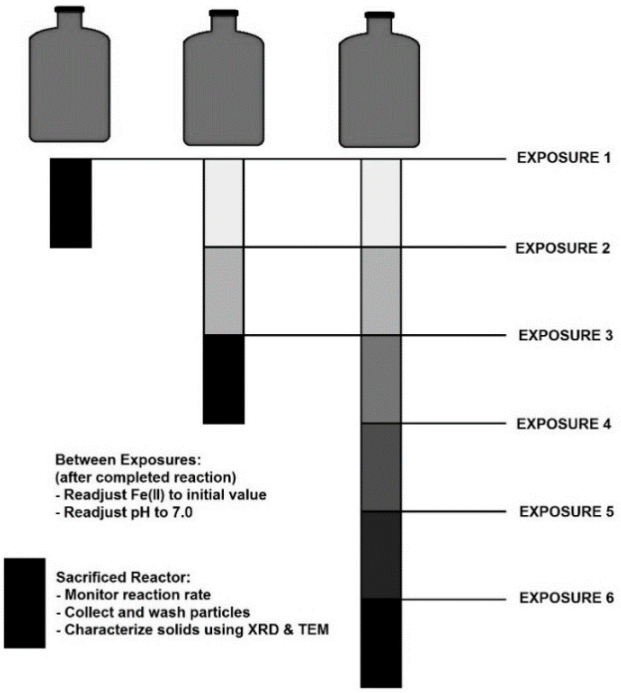

Figure B2. Reactor scheme for recurrent-exposure reactions, which are sacrificed after one, two, three, or six exposures of 4-ClNB. Between exposures, after the reaction is complete, the Fe(II) concentration is readjusted to its initial value (Fig. B6) and the pH is readjusted to 7.0. For a sacrificed reactor: reaction rate is determined by HPLC sampling, the particles are collected and washed, and the solids are characterized by XRD and TEM to determine mineral composition and morphology.

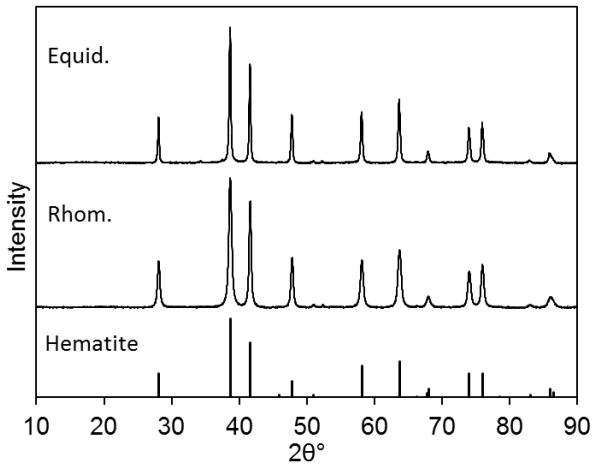

Figure B3. X-ray diffraction patterns of synthetic rhombohedral (R) and equidimensional (E) hematite. Both are consistent with pure hematite, as compared to reference PDF 33-0664.

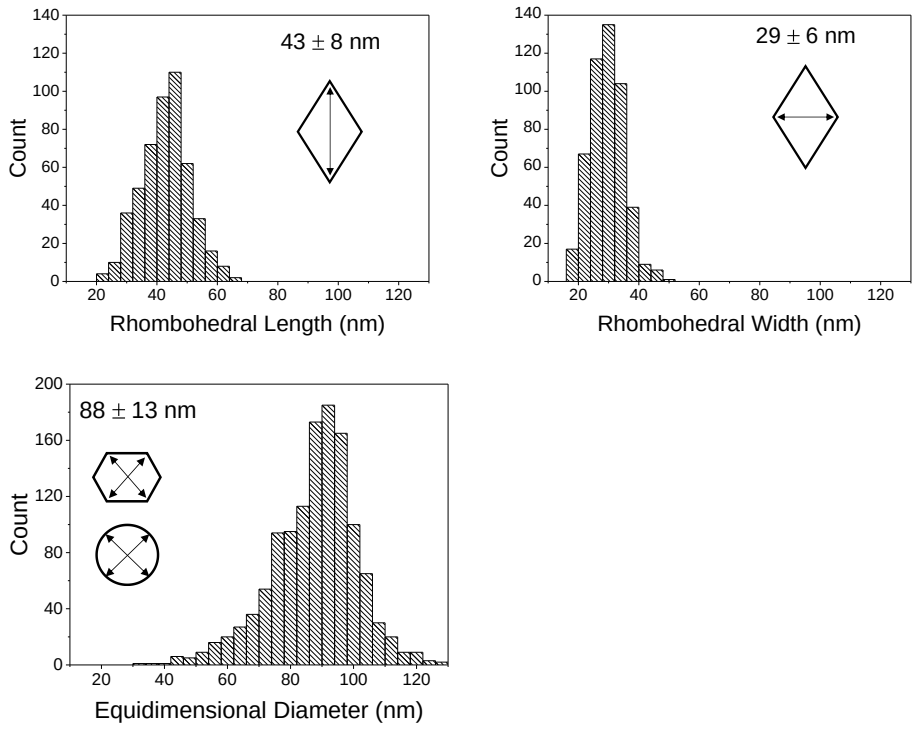

Figure B4. Measurement geometry for rhombohedral particles and equidimensional particles. Rhombohedral dimensions were calculated using 500 particles having clear boundaries in direction of measurement. Equidimensional measurements consisted of 500 particles, each having two perpendicular measurements. As some equidimensional particles exhibited an elongated hexagonal morphology, the measurements were made such that both perpendicular measurements represented the average size of the particle.

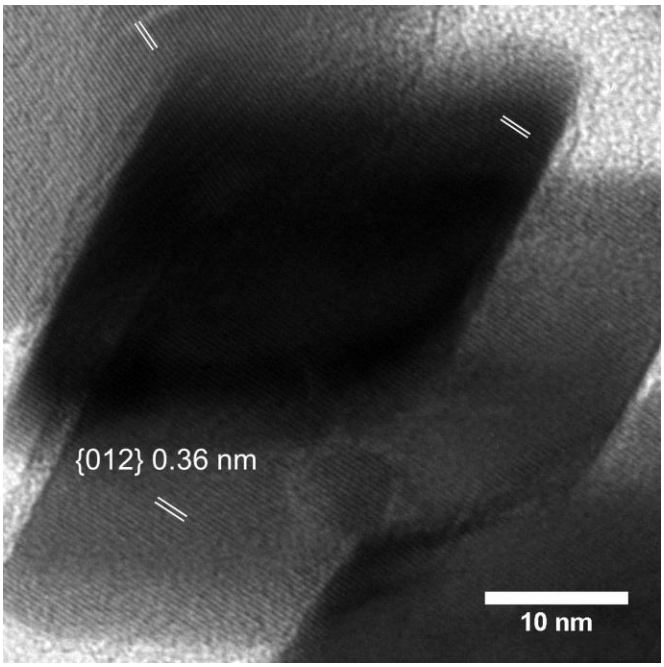

Figure B5. TEM image showing lattice fringes in pre-reaction rhombohedral (R) hematite. All white lattice indicators measure 0.36 nm, which corresponds to hematite {012}.

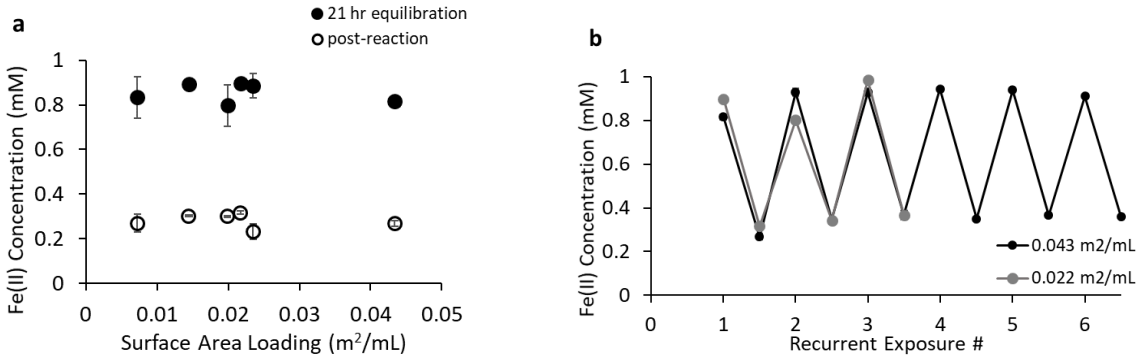

Figure B6. Iron(II) concentrations in (a) single-exposure reactors and (b) recurrent-exposure reactors after 21-hour equilibration and post-reaction. Error bars in both plots represent standard deviations. Data points are connected in recurrent-exposure reactors to guide the eye through changes in Fe(II) due to reaction and readjustment.

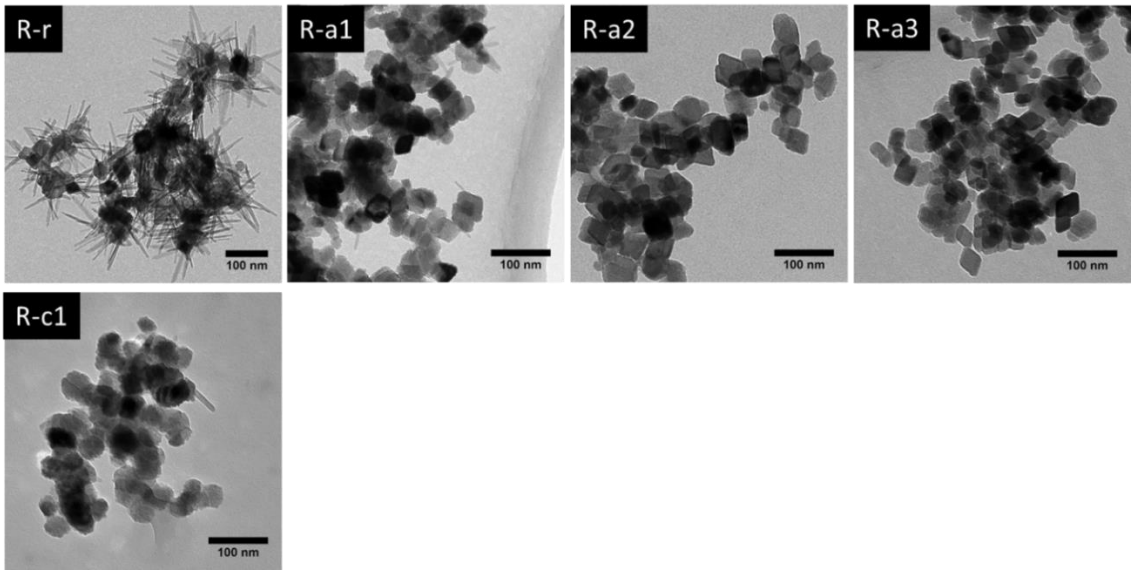

Figure B7. TEM images showing rhombohedral hematite particles after reaction with 100 uM 4-ClNB in the presence of 1 mM Fe(II) with increasing surface area loading (Table 2.1, Set a) and at pH 6.5 (Table 2.1, Set c) as compared to reference R-r. See Table 2.1 for sample identifiers.

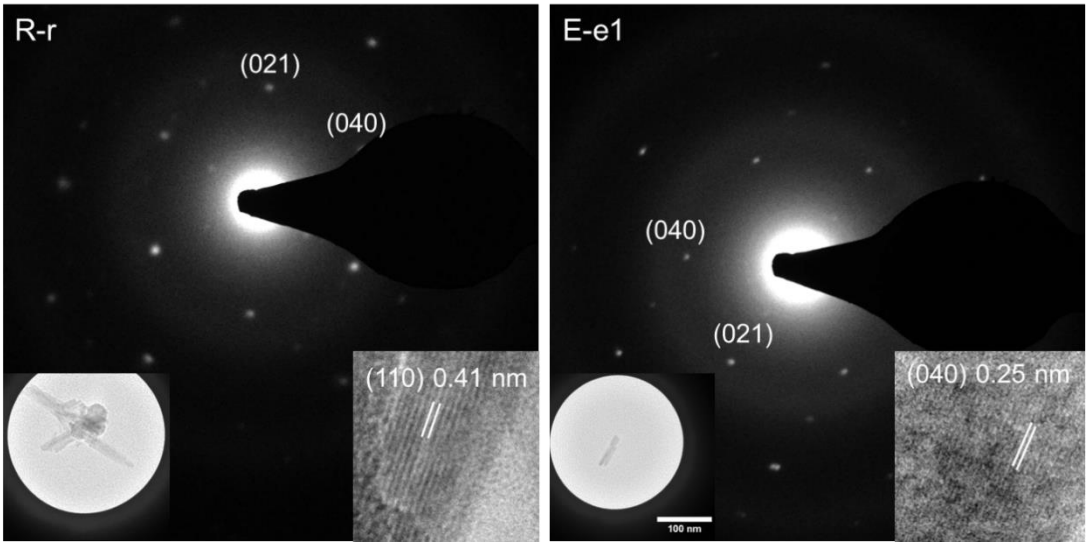

Figure B8. Additional TEM diffraction and lattice images showing the presence of goethite. Electron diffraction patterns are viewed down the [100] zone axis. See Table 2.1 for sample identifiers.

Table B1. Literature values for goethite reactivity.

Reference	Buffer	[4-ClNB] (μM)	[Fe(II)] (mM)	Volume (mL)	Mass Loading (mg/mL)	BET S.A. (m^2/g)	S.A. Loading (m^2/mL)	Reaction Rate (hr^{-1})
Vindedahl 2015	10 mM $NaHCO_3$	100	1.00	120	0.325	117	0.038	0.75
Stemig 2014	10 mM MOPS	100	1.00	50	0.325	117	0.038	0.90
Chun 2006	50 mM MOPS	100	1.00	123	0.650	137	0.089	3.42

Section 2. X-ray Diffraction Calibration Curve Calculations and Figures

Calibration standards prepared with minerals of identical morphology, or nominally similar in the case of goethite, to ensure that the peak widths were comparable. Standards prepared in this way have been shown to be accurate to 1 mass% (Barron et al. 1997). While most of the calibration standards were prepared using rhombohedral hematite, two standards of 15 mass% and 30 mass% goethite were also made using equidimensional particles. With the size and morphology differences between the two hematite morphologies, the XRD patterns of pure particles showed a slight difference, namely that the particle size affected the peak width as seen in Fig. B3. The equidimensional calibration standards, however, did not show a significant deviation from the linearity of the rhombohedral standards and thus the calibration curve was taken to be representative of both hematite morphologies.

To obtain reliable peak areas, one diffraction index from each mineral must be fully resolved from any nearby reflections and the selected diffraction index must be intensely scattering to maximize the signal to noise ratio. The goethite {110} and hematite {012} reflections are used here, shown in Fig. B9.

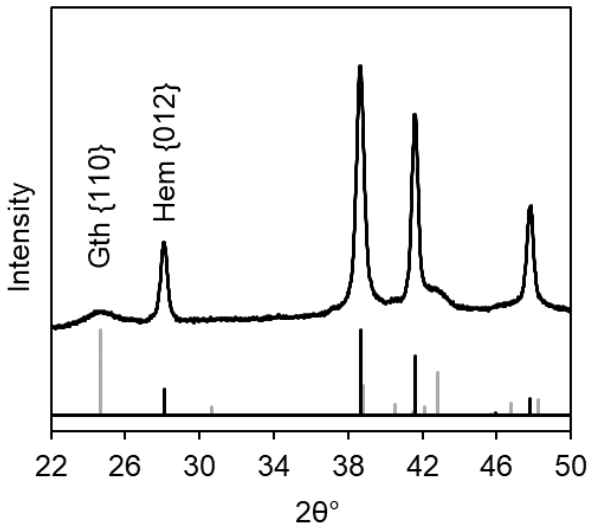

Figure B9. An unmodified x-ray diffraction pattern of reactor R-r showing the goethite {110} and hematite {012} reflections. The grey and black reference patterns are goethite and hematite, respectively.

As the goethite content increases, the {110} peak area is expected to increase. When graphing the goethite area fraction versus the goethite mass fraction, however, the trend is not linear because the scattering intensities of goethite and hematite differ. The area fractions were therefore adjusted for the scattering intensities to account for these differences. Generic calculations for this process are described in West (2014), and the detailed calculations for goethite {110} and hematite {012} are described below.

The atomic scattering amplitudes (f) for Fe and O were graphed versus $(\sin\theta)/\lambda$ (Fig. B10), as tabulated in the International Tables for Crystallography, Volume C (Prince 2006), where θ is half the 2θ peak position of the goethite {110} and hematite {012}, and λ is the Co K_α wavelength of the XRD X-ray source. Using known values of θ for goethite {110} and hematite {012} and λ based on the XRD analyses performed here, the atomic scattering amplitudes were found and are presented in Table B2.

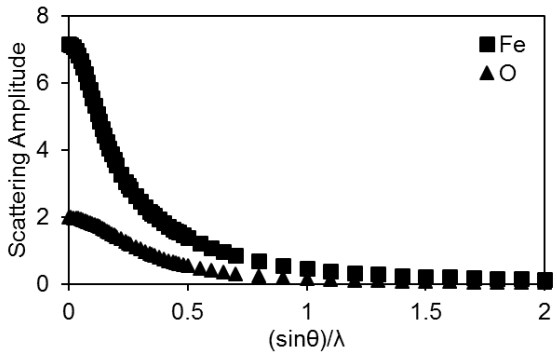

Figure B10. Atomic scattering amplitudes (f) for electrons of neutral atoms. Values for Fe and O are listed in International Tables for Crystallography, Volume C (Prince 2006).

Table B2. Constants and parameters involved in the calculation of scattering intensities of goethite and hematite.

	Constants	Hematite	Goethite
(hkl)		{012}	{110}
d-spacing (Å)		3.682	4.182
Co-K_α (Å)	1.7909		
θ °		14.075	12.364
(sin θ)/λ ($Å^{-1}$)		0.136	0.120
f_{Fe} (Å)		4.644	5.087
f_O (Å)		1.664	1.739
I_{hkl}		102.88	31.93

Scattering intensity is proportional to the square of the diffracted sine waves, which can be transformed from complex notation and written as Equation B1. The phase difference (δ) (Equation B2) was calculated from the Miller indices and atomic positions of Fe and O, which are reported in Pauling and Hendricks (1925) for hematite and Szytula et al. (1968) for goethite (Table B3). For hematite, the hexagonal atomic positions were adjusted to Cartesian coordinates. For goethite, the (110) facet was reverted to the original labeling system (101) rather than adjusting the Fe and O atomic

positions to correspond to the new labeling system. The current unit cell (abc) corresponds to (bca) when described by the original goethite space group Pbnm.

$$I_{hkl} \propto |F_{hkl}|^2 = \sum_j \left(f_j \cos \delta_j\right)^2 + \sum_j \left(f_j \sin \delta_j\right)^2 \quad \text{(B1)}$$

$$\delta = 2\pi(hx + ky + lz) \quad \text{(B2)}$$

Table B3. Atomic positions of iron and oxygen in hematite and goethite reported in the literature (Pauling and Hendricks 1925; Szytula et al. 1968) adjusted to correspond to Cartesian coordinates in the case of hematite.

Hematite	x	y	z	Goethite[a]	x	y	z
Fe	0.105	0.105	0.105	Fe	0.145	0.250	-0.045
	-0.105	-0.105	-0.105				
	0.395	0.395	0.395				
	0.605	0.605	0.605				
O	0.292	-0.292	0.000	O	-0.199	0.250	0.288
	-0.292	0.000	0.292		-0.053	0.250	-0.198
	0.000	0.292	-0.292				
	0.208	0.792	0.500				
	0.792	0.500	0.208				
	0.500	0.208	0.792				

[a] The reported values are given according to the original goethite labeling system. For calculation purposes, the goethite (110) plane was translated into the original system (i.e. (101)) rather than translating the atomic coordinates to the current space group Pbma.

By factoring in the scattering intensities using Equation B3 as the y-axis, the resulting linear calibration curve becomes a reliable tool for determining goethite mass percent (Fig. B11).

$$\frac{{F_{Gt(110)}}^2 Area_{Gt(110)}}{{F_{Gt(110)}}^2 Area_{Gt(110)} + {F_{Ht(012)}}^2 Area_{Ht(012)}} \quad \text{(B3)}$$

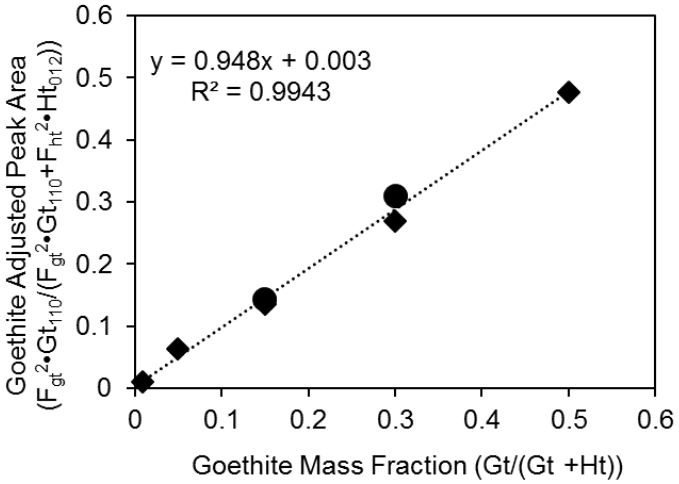

Figure B11. X-ray diffraction calibration curve showing goethite adjusted peak area versus goethite mass fraction for five rhombohedral hematite standards (diamonds) and two equidimensional standards (circle).

Appendix C. Supplemental Information for Chapter 3 – The Effects of Organic Matter and a Phenolic Surrogate on the Reactivity and Oxidative Growth of Hematite Nanoparticles

Table C1. List of abbreviations for each organic matter standard available through the International Humic Substances Society.

Abbreviation	Organic Matter Standard Material
ESFAI	Elliot Soil Fulvic Acid I
ESHA	Elliot Soil Humic Acid
LHA	Leonardite Humic Acid
PPFAI	Pahokee Peat Fulvic Acid I
PPHA	Pahokee Peat Humic Acid
SRFAI	Suwanee River Fulvic Acid I
SRFAII	Suwanee River Fulvic Acid II
SRHAI	Suwanee River Humic Acid I
SRHAII	Suwanee River Humic Acid II
SRNOM	Suwanee River Aquatic Natural Organic Matter
UMNOM	Upper Mississippi Aquatic Natural Organic Matter

Table C2. Calculation of catechol loading (uM) for various concentrations of organic carbon added to reactor vessels.

	Concentration of Organic Carbon (ppm)				
	1	5	10	20	50
	Catechol Equivalents (uM)				
SRHAI	2.1	11	21	42	106
SRNOM	2.0	9.9	20	39	99
SRHAII	1.9	9.3	19	37	93
SRFAI	1.5	7.3	15	29	73
SRFAII	1.4	7.1	14	28	71
PPFAI	1.2	5.8	12	23	58
LHA	1.2	5.8	12	23	58
ESFAII	1.1	5.7	11	23	57
PPHA	1.0	4.8	9.6	19	48
ESHA	0.9	4.7	9.4	19	47
UMNOM	0.4	2.1	4.2	8	21

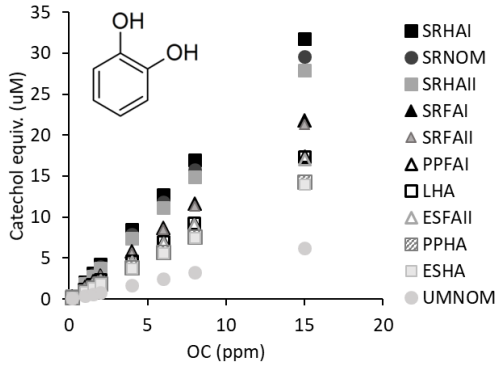

Figure C1. Plot of the calculated catechol equivalents (uM) versus organic carbon concentration (ppm) as tabulated in Table C2.

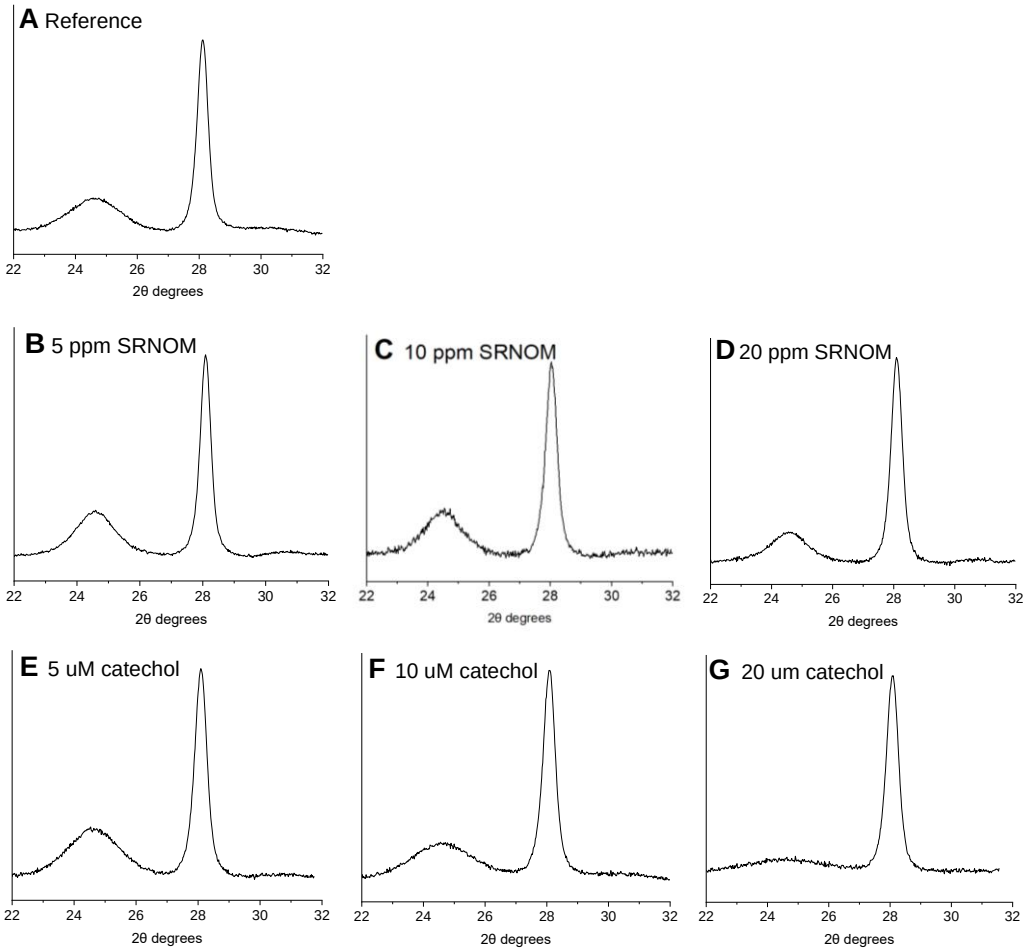

Figure C2. XRD patterns of post-reaction solids from reactors (A) without added organic carbon (as reference); with added OC as SRNOM at concentrations of (B) 5 ppm OC, (C) 10 ppm OC, and (D) 20 ppm OC; and with catechol at concentrations of (E) 5 µM, (F) 10 µM, and (G) 20 µM.

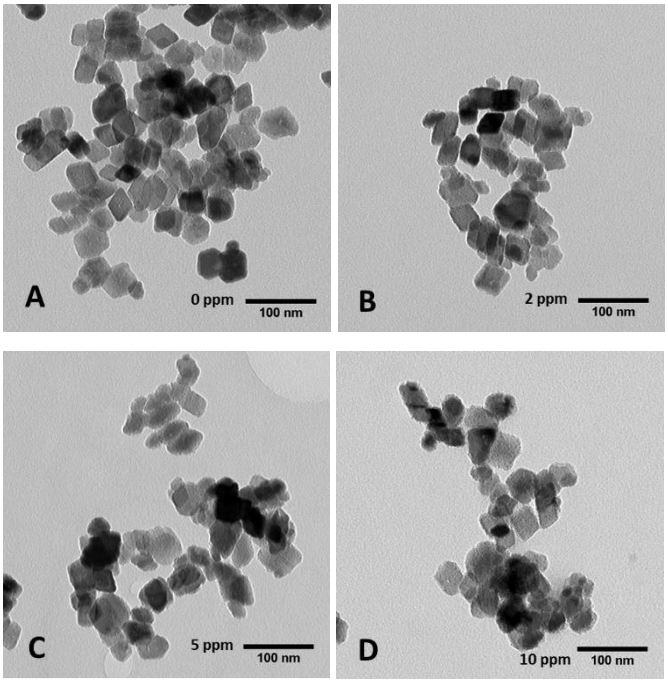

Figure C3. TEM images showing hematite morphology of post-reaction solids from reactors containing 0.023 m^2/mL hematite SAL. The reference reactor (A) did not contain added OC. Other reactors contained added OC as SRNOM in concentrations of (B) 2 ppm OC, (C) 5 ppm OC, and (D) 10 ppm OC.

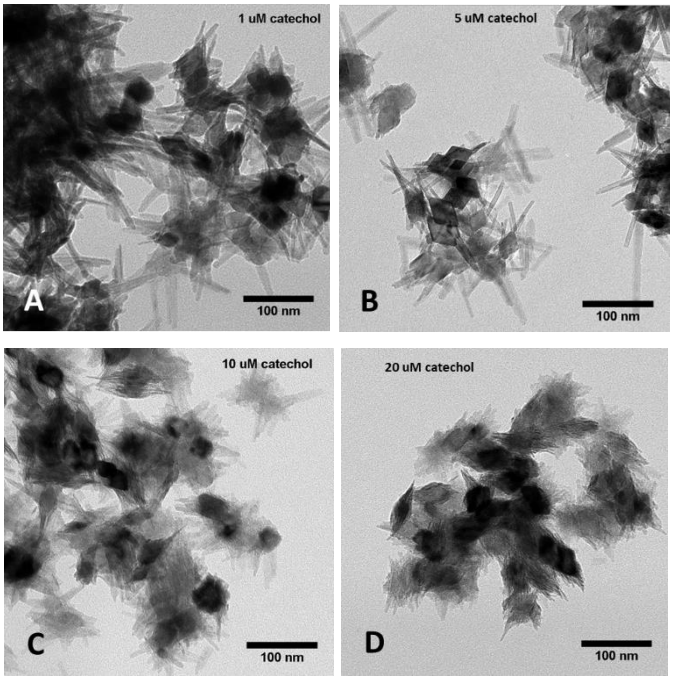

Figure C4. TEM images showing particle morphology of post-reaction solids from reactors containing 0.007 m^2/mL hematite SAL. The reactors contained catechol at concentrations of (A) 1 μM , (B) 5 μM, (C) 10 μM, and (D) 20 μM.

Appendix D. Supplemental Information for Chapter 4 – Iron-Bearing Minerals for Sulfide Removal from Industrial Aqueous Waste: Characterizing Low-Value Solid Wastes for Use as Feedstocks

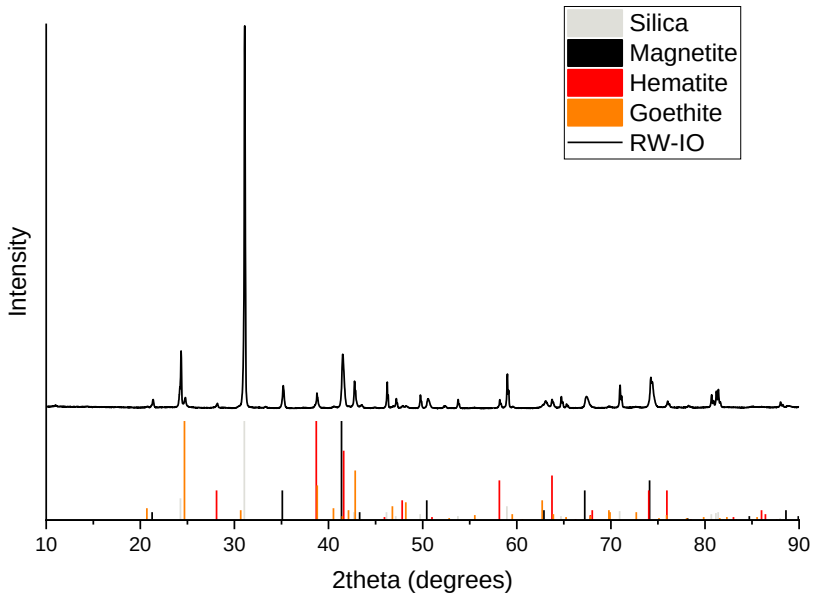

Figure D1. X-ray diffraction pattern of the dialyzed RW-IO material showing the presence of quartz, magnetite, goethite, and hematite.

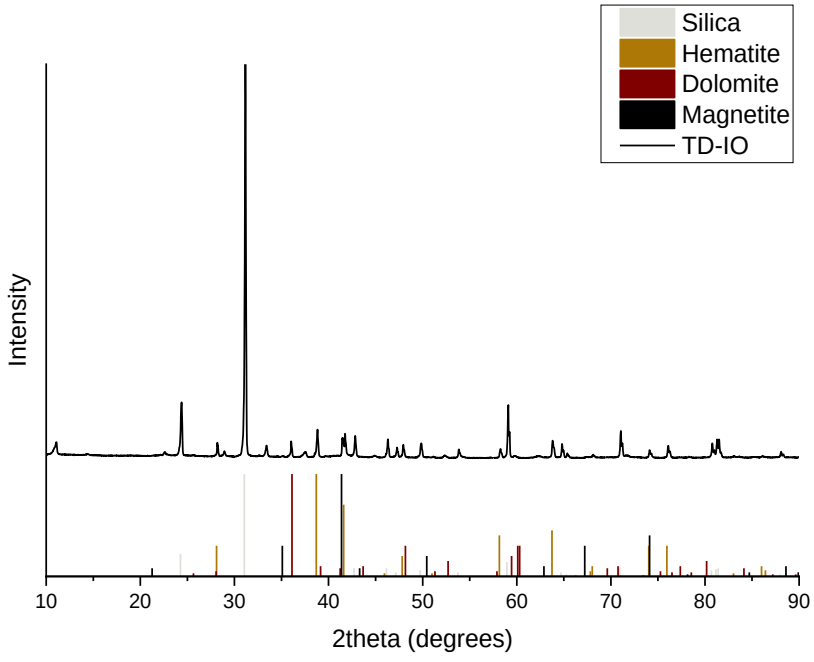

Figure D2. X-ray diffraction pattern of the dialyzed TD-IO material showing the presence of quartz, magnetite, hematite, and dolomite.

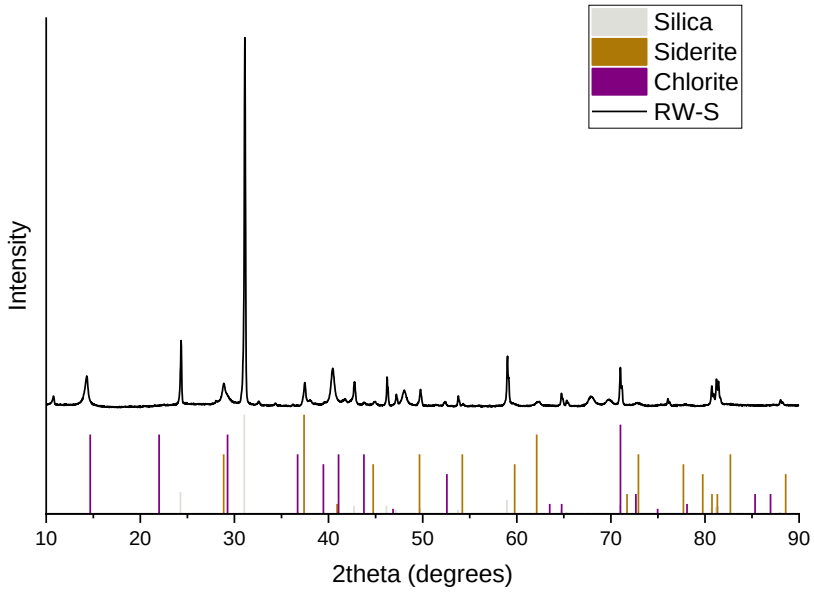

Figure D3. X-ray diffraction pattern of the dialyzed RW-S material showing the presence of quartz, siderite, and chlorite.

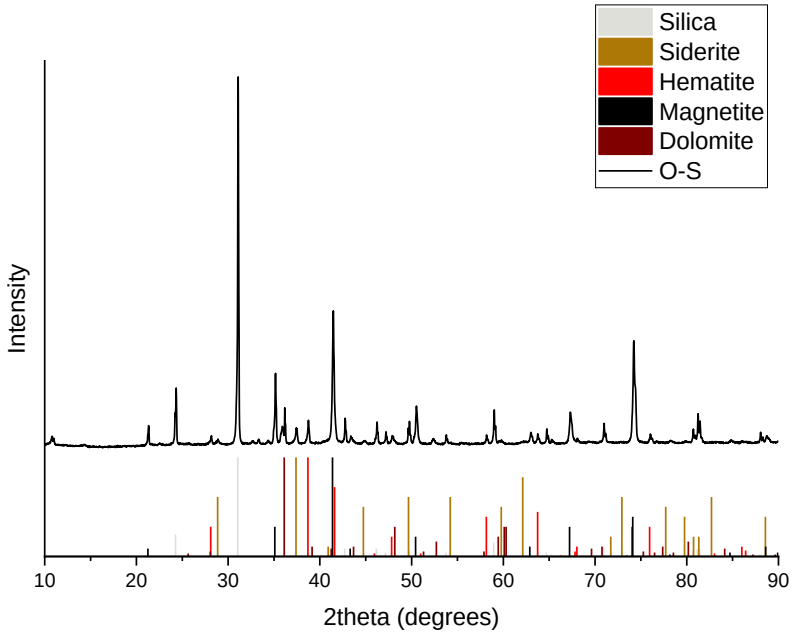

Figure D4. X-ray diffraction pattern of the dialyzed O-S material showing the presence of quartz, siderite, hematite, magnetite, and dolomite.

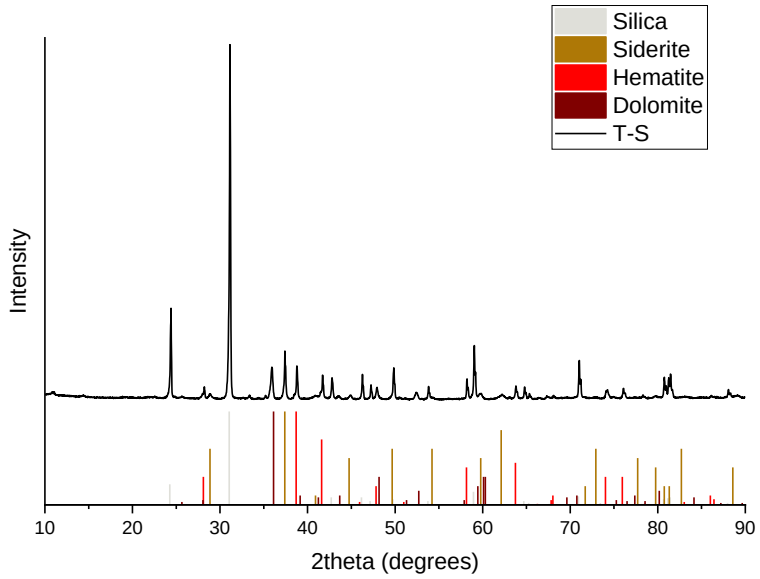

Figure D5. X-ray diffraction pattern of the dialyzed T-S material showing the presence of quartz, siderite, hematite, and dolomite.

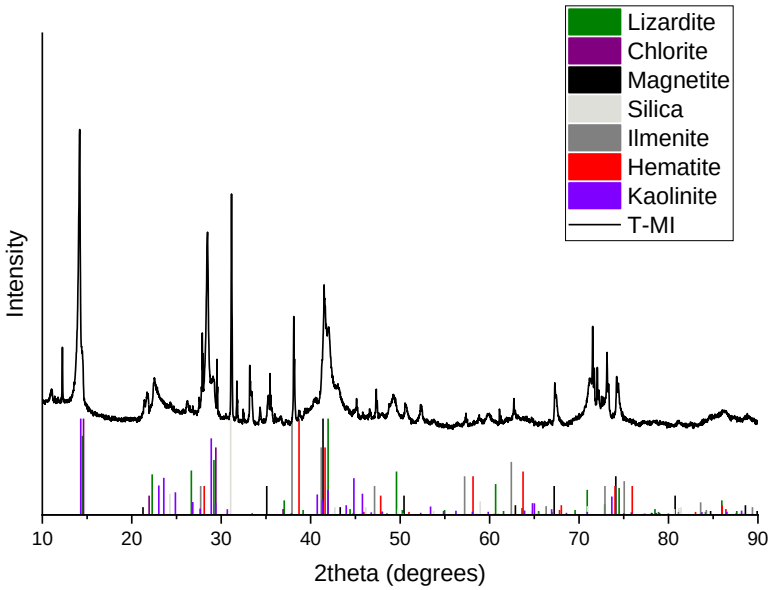

Figure D6. X-ray diffraction pattern of the dialyzed T-MI material showing the presence of lizardite, chlorite, magnetite, quartz, ilmenite, hematite, and kaolinite.

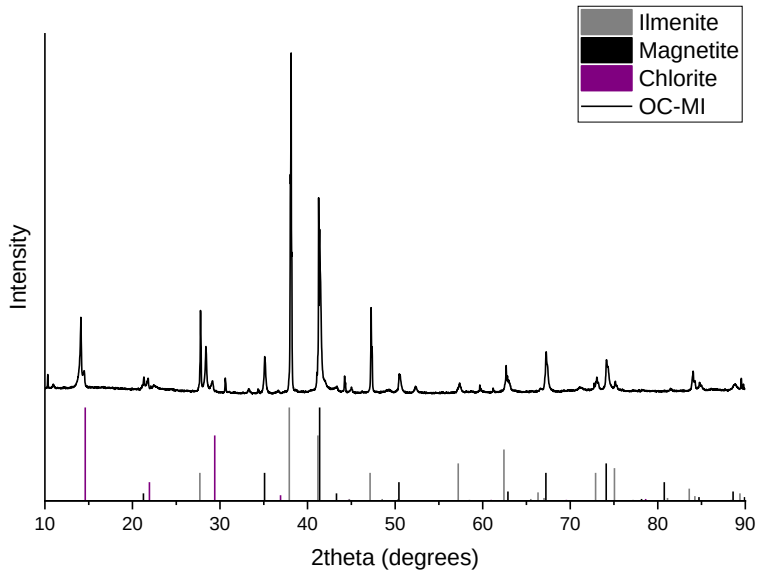

Figure D7. X-ray diffraction pattern of the dialyzed OC-MI material showing the presence of ilmenite, magnetite, and chlorite.

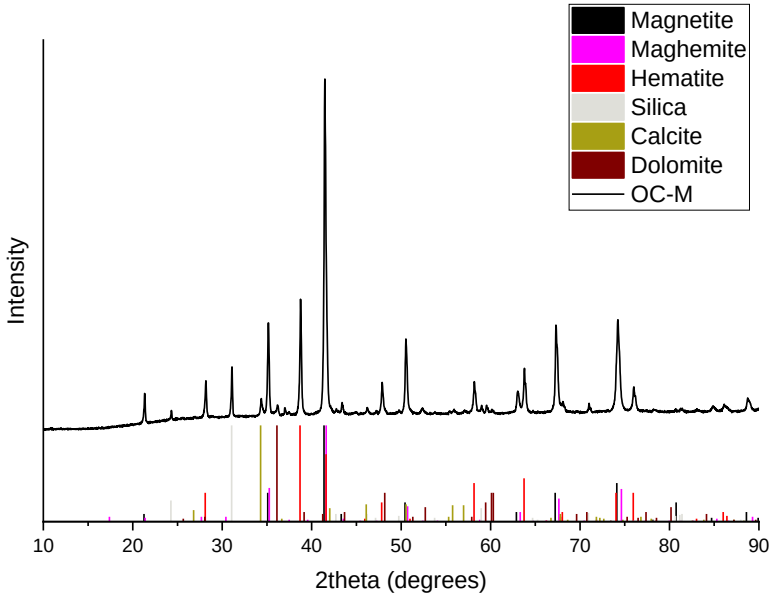

Figure D8. X-ray diffraction pattern of the dialyzed OC-M material showing the presence of magnetite, hematite, quartz, calcite, and dolomite.

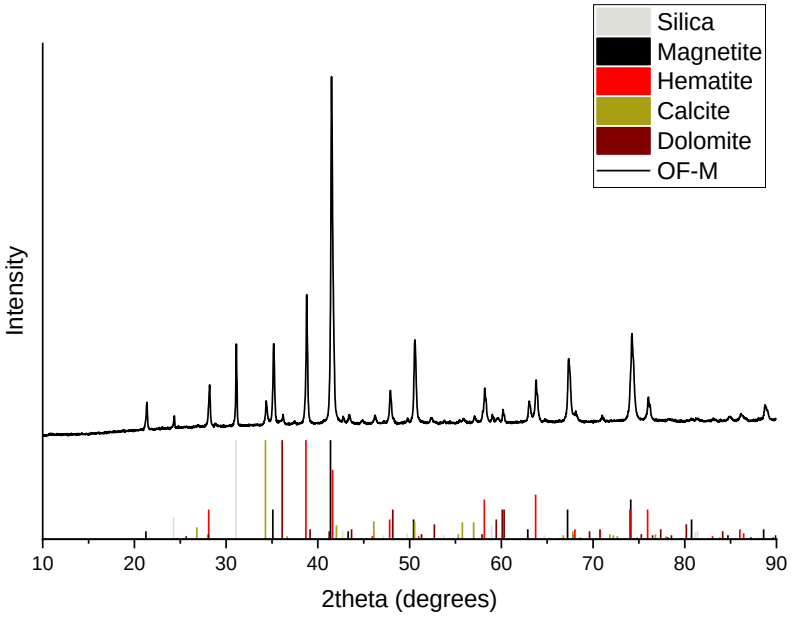

Figure D9. X-ray diffraction patterns of the dialyzed OF-M material showing the presence of magnetite, hematite, quartz, calcite, and dolomite.

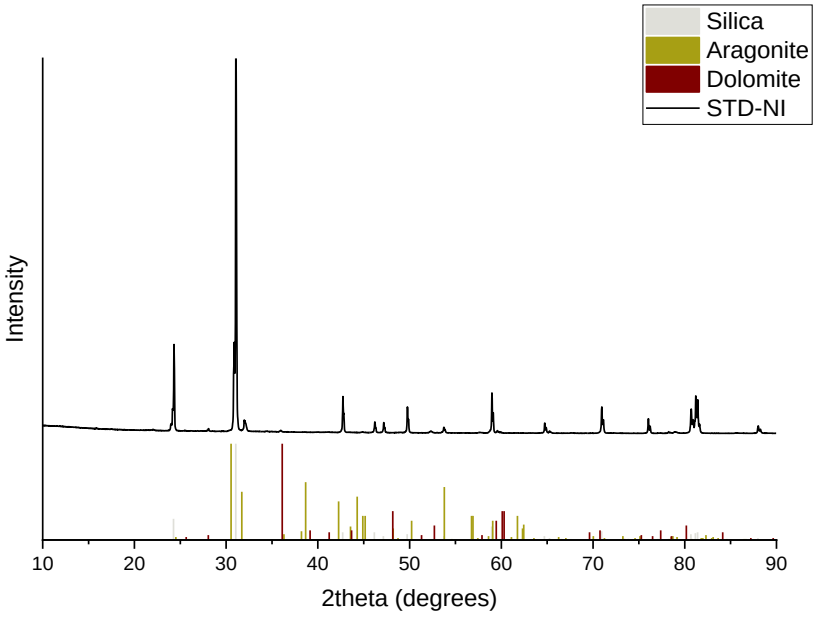

Figure D10. X-ray diffraction patterns of the dialyzed STD-NI material showing the presence of quartz, aragonite, and dolomite.

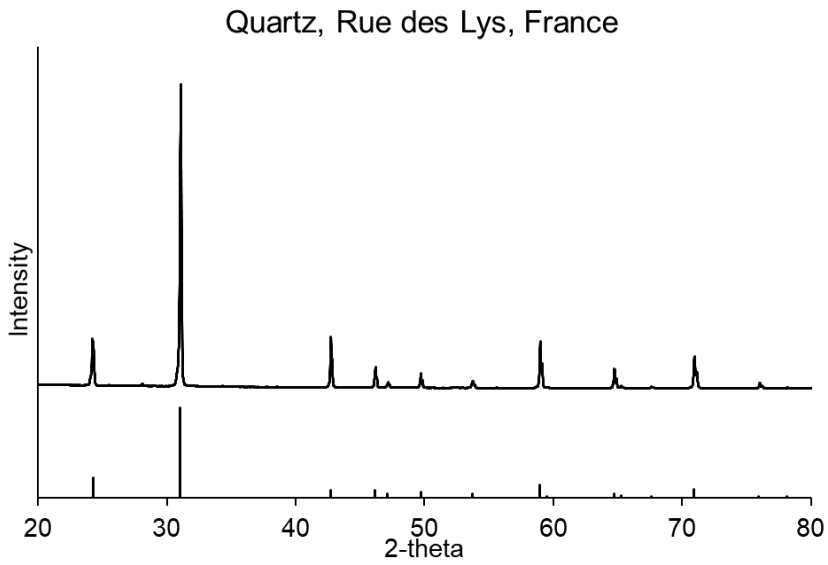

Figure D11. X-ray diffraction pattern of quartz reference mineral.

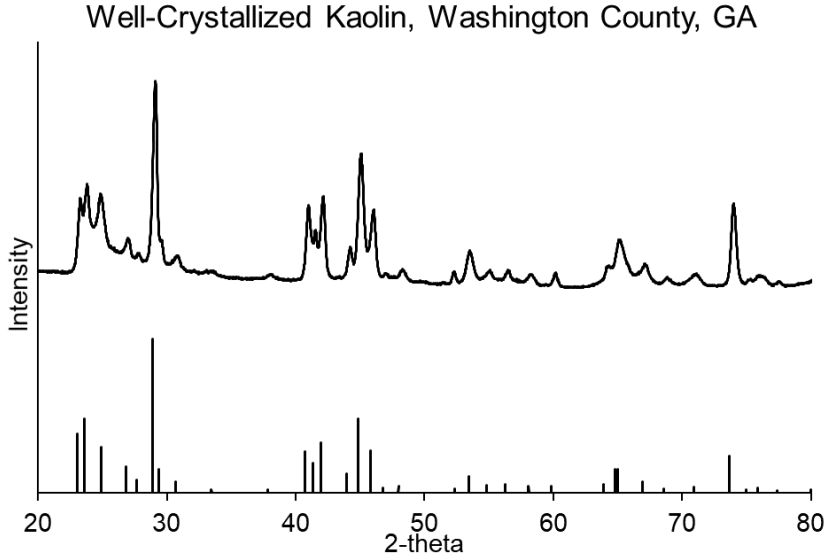

Figure D12. X-ray diffraction pattern of kaolinite reference mineral.

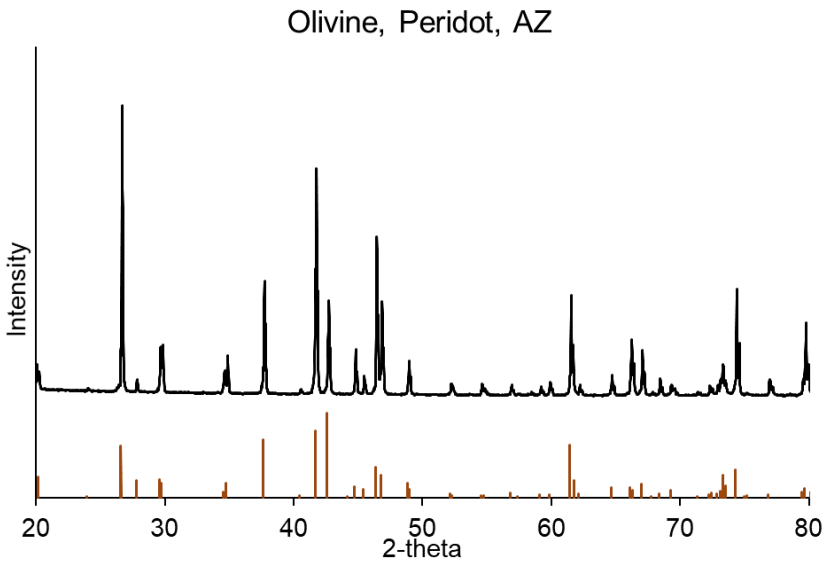

Figure D13. X-ray diffraction pattern of olivine reference mineral.

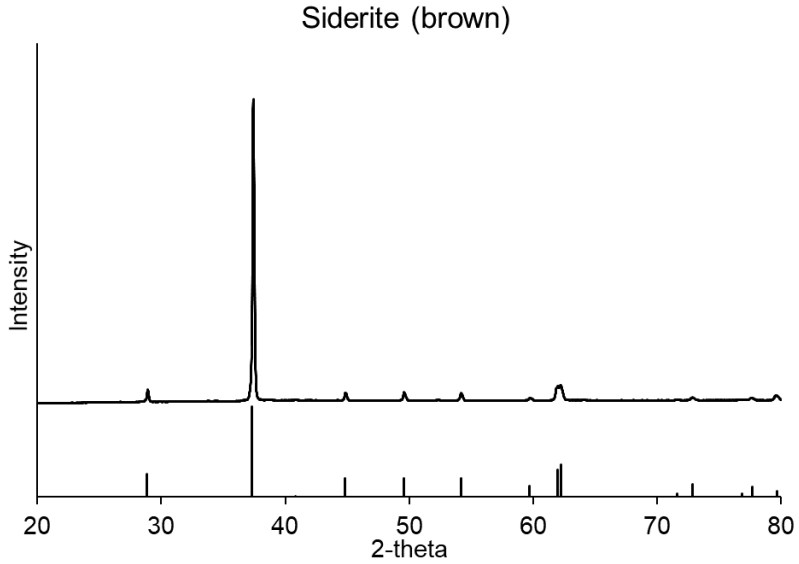

Figure D14. X-ray diffraction pattern of brown siderite reference mineral.

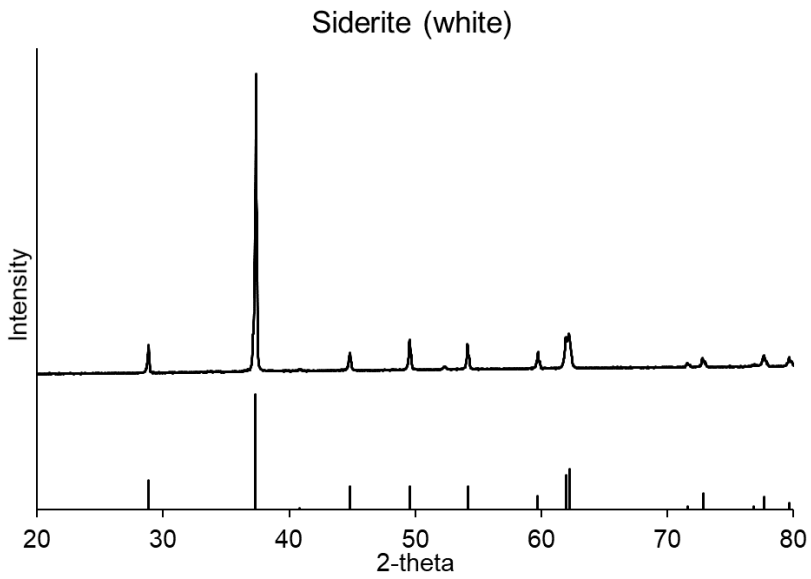

Figure D15. X-ray diffraction pattern of white siderite reference mineral.

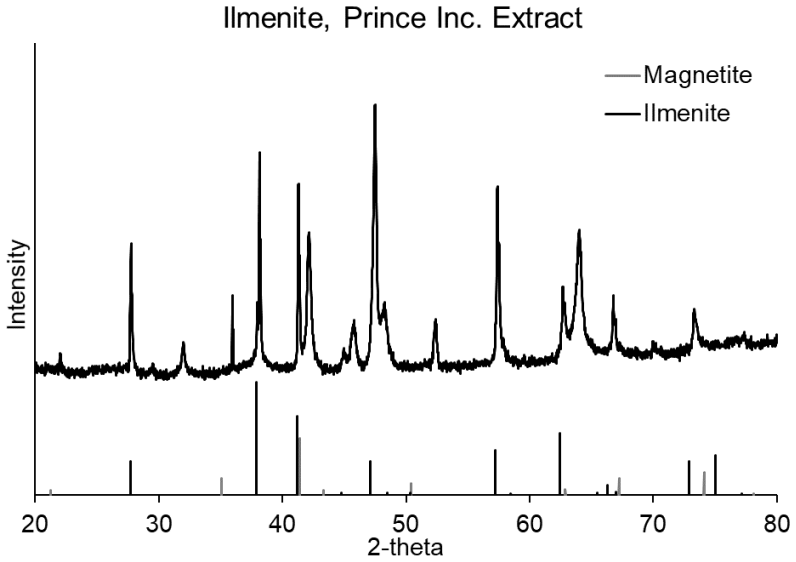

Figure D16. X-ray diffraction pattern of ilmenite reference mineral. Black peaks correspond to ilmenite and grey correspond to magnetite. Unassigned peaks correspond with titania (TiO_2) and silica (SiO_2).

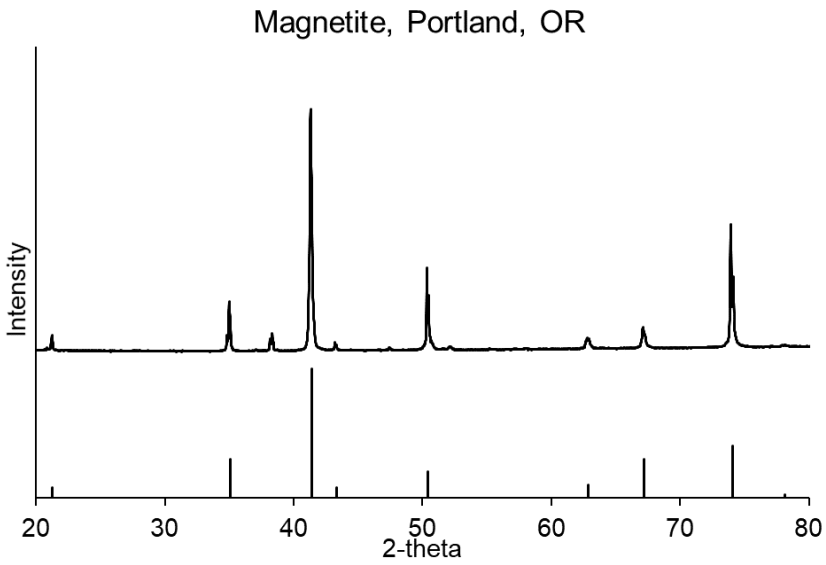

Figure D17. X-ray diffraction pattern of magnetite reference mineral.

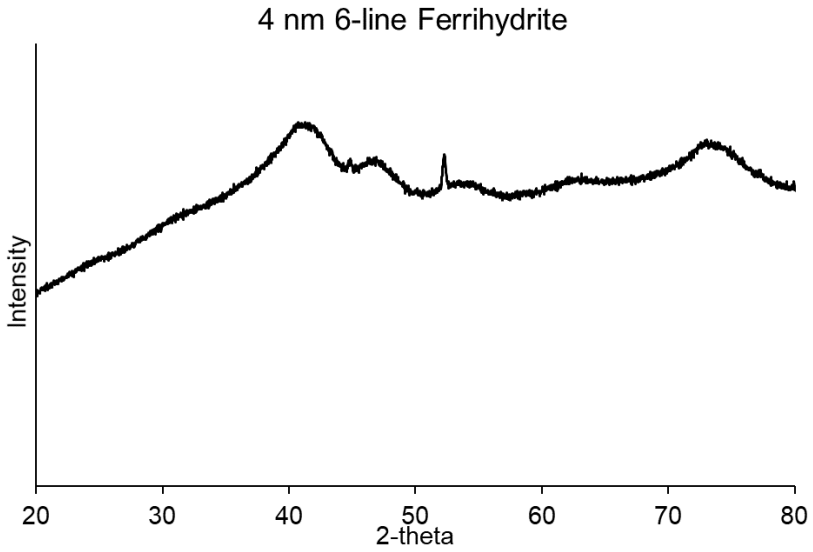

Figure D18. X-ray diffraction pattern of 4 nm ferrihydrite reference mineral. Sharp peak at circa 52 degrees is the sample holder.

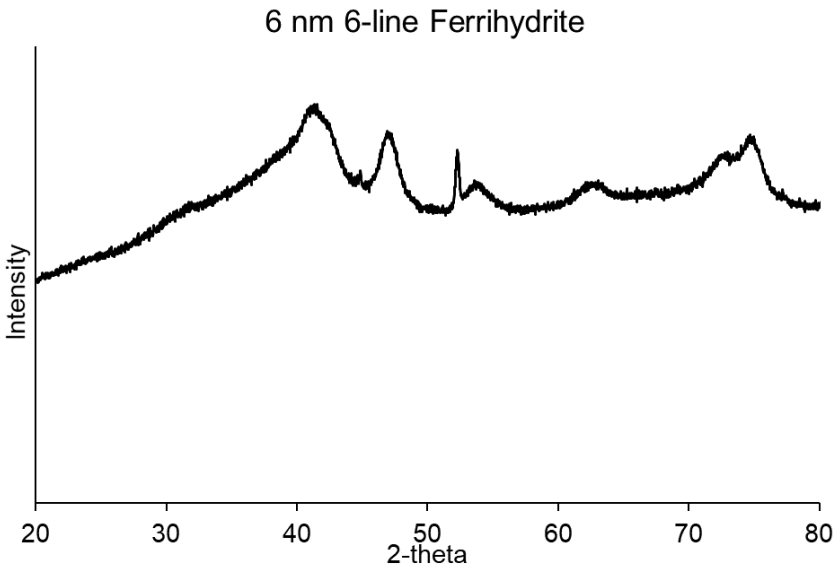

Figure D19. X-ray diffraction pattern of 6 nm ferrihydrite reference minerals. Sharp peak at circa 52 degrees is the sample holder.

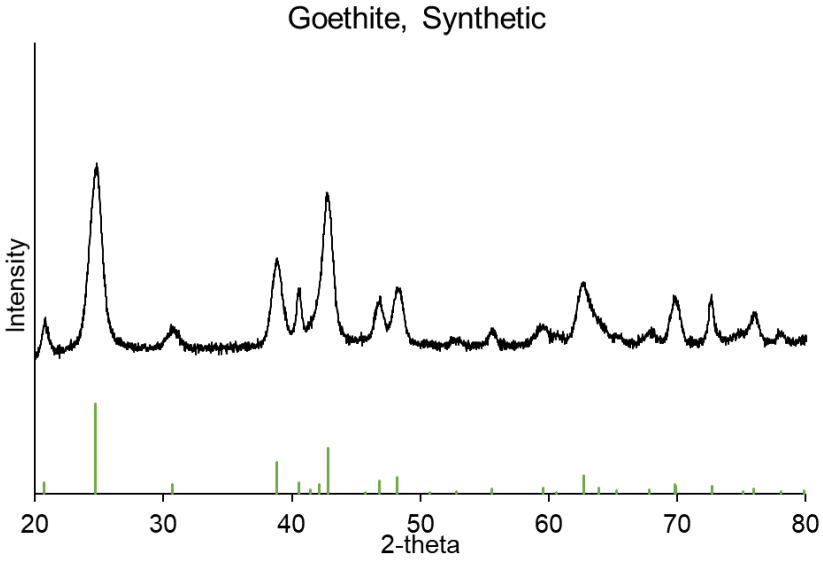

Figure D20. X-ray diffraction pattern of synthetic goethite reference mineral.

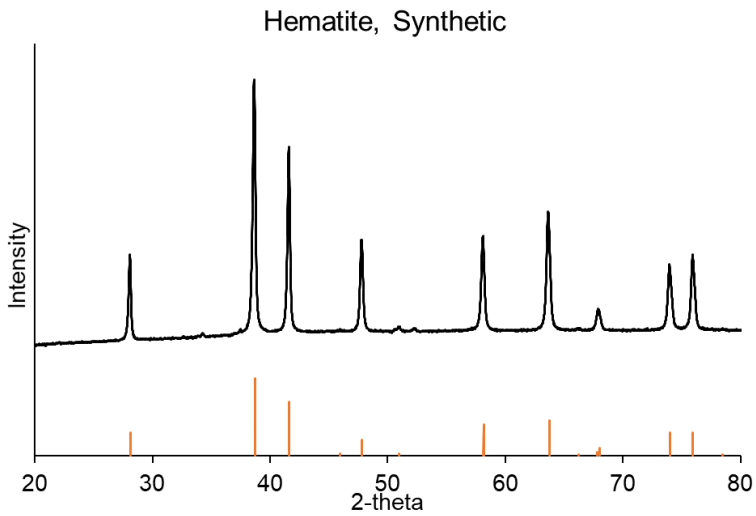

Figure D21. X-ray diffraction pattern of synthetic hematite reference mineral.

Table D1. Dissolution results from Figure 4.2A and 4.2B reporting the extracted mg Fe/g sample for reference minerals and mixed mineral specimens using concentrated HCl and aqua regia, respectively.

		Fe(II)		Fe(III)		Fe(tot)	
		Avg.	St.Dev.	Avg.	St.Dev.	Avg.	St.Dev.
HCl	Qtz	0	0	0	0	0	0
	Kao	0	0	0	0	0	0
	Ol	27	2	12	1	38	1
	B-Sd	317	17	104	4	418	16
	W-Sd	254	18	137	18	390	8
	Ilm	17	3	70	4	87	1
	Mag	135	17	450	19	585	10
	4nm 6LF	0	0	575	1	575	1
	6nm 6LF	0	0	618	17	618	17
	Gth	0	0	587	9	587	9
	Hem	0	0	695	10	695	10
Aqua regia	RW-IO					405	11
	TD-IO					109	6
	RW-S					217	8
	T-S					147	16
	O-S					425	70
	T-MI					141	5
	OC-MI					270	6
	OC-M					610	9
	OF-M					602	26
	STD-NI					0.6	0.0

Table D2. Dissolution results from Figure 4.2C and 4.2D reporting the extracted mg Fe/g sample for reference minerals and mixed mineral specimens using acetate.

		Fe(II)		Fe(III)		Fe(tot)	
		Avg.	**St.Dev.**	**Avg.**	**St.Dev.**	**Avg.**	**St.Dev.**
Acetate	Qtz	0	0	0	0	0	0
	Kao	0	0	0	0	0	0
	Ol	7	1	1.9	0.4	9.2	0.7
	B-Sd	207	9	0.3	0.1	205	7
	W-Sd	150	12	6	5	153	7
	Ilm	0	0	0	0	0	0
	Mag	0	0	0	0	0	0
	4nm 6LF	0	0	3	1	3	1
	6nm 6LF	0	0	0	0	0	0
	Gth	0	0	0	0	0	0
	Hem	0	0	0	0	0	0
Acetate	RW-IO	0	0	0.6	0.1	0.6	0.1
	TD-IO	16.5	0.2	0.9	0.3	17.4	0.1
	RW-S	11.2	0.5	4.6	0.4	15.9	0.3
	T-S	26.4	0.9	1.3	0.3	27.6	0.8
	O-S	12	3	4	3	16	1
	T-MI	1.8	0.5	1.0	0.3	2.8	0.2
	OC-MI	0.8	0.2	0.7	0.1	1.5	0.1
	OC-M	3.3	0.5	1.5	0.4	4.8	0.1
	OF-M	4.5	0.9	1.9	0.6	6	4
	STD-NI	0	0	0	0	0	0

Table D3. Dissolution results from Figure 4.2E and 4.2F reporting the extracted mg Fe/g sample for reference minerals and mixed mineral specimens using hydroxylamine-HCl.

		Fe(II)		Fe(III)		Fe(tot)	
		Avg.	St.Dev.	Avg.	St.Dev.	Avg.	St.Dev.
HONH2	Qtz					0	0
	Kao					0	0
	Ol					19.1	0.3
	B-Sd					327	7
	W-Sd					211	2
	Ilm					1.5	0.2
	Mag					8	2
	4nm 6LF					653	22
	6nm 6LF					690	11
	Gth					22.3	0.1
	Hem					6	1
HONH2	RW-IO					8.4	0.2
	TD-IO					29.2	0.5
	RW-S					129	3
	T-S					50	1
	O-S					40	2
	T-MI					31	1
	OC-MI					27	1
	OC-M					21.3	0.8
	OF-M					22.0	0.3
	STD-NI					0	0

Table D4. Dissolution results from Figure 4.2G and 4.2H reporting the extracted mg Fe/g sample for reference minerals and mixed mineral specimens using acetate.

		Fe(II)		Fe(III)		Fe(tot)	
		Avg.	St.Dev.	Avg.	St.Dev.	Avg.	St.Dev.
Oxalate	Qtz	0	0	0	0	0	0
	Kao	0	0	0	0	0	0
	Ol	6.3	0.1	0.14	0.01	6.4	0.1
	B-Sd	86	11	0	0	86	11
	W-Sd	77	5	2	3	78	4
	Ilm	0	0	1.8	0.2	1.8	0.2
	Mag	60	6	172	11	232	9
	4nm 6LF	0	0	350	10	350	10
	6nm 6LF	0	0	360	23	360	23
	Gth	0	0	103	8	103	8
	Hem	0	0	92	15	92	15
Oxalate	RW-IO	16	3	108	4	124	5
	TD-IO	14.6	0.1	39	1	53	1
	RW-S	24	1	12	1	36	2
	T-S	37	2	12.6	0.2	50	2
	O-S	44	3	36	1	80	3
	T-MI	9.4	0.2	35	2	44	2
	OC-MI	19	1	71	7	90	9
	OC-M	49	4	66	4	116	8
	OF-M	49	5	69	4	118	9
	STD-NI	0	0	0	0	0	0

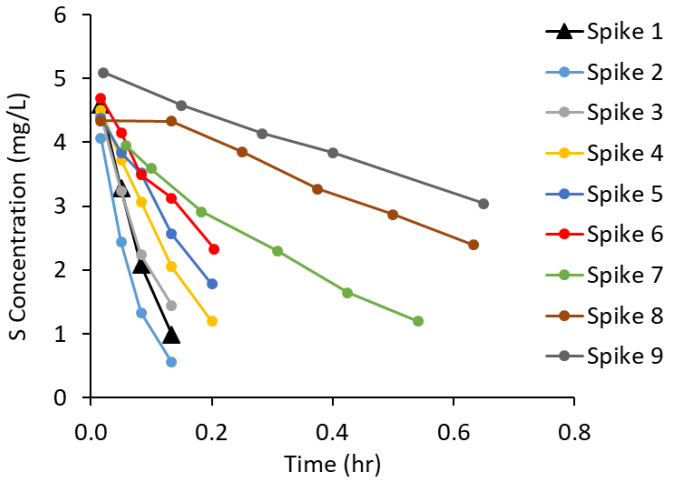

Figure D22. Sample plot of sulfide concentration as detected by the methylene blue method for UV-visible spectroscopy showing zero-order reaction kinetics. This reactor

contained goethite in 10 mM acetate buffer at pH 4.7 and received nine addition so sulfide until it was determined that it had reached its reaction capacity.

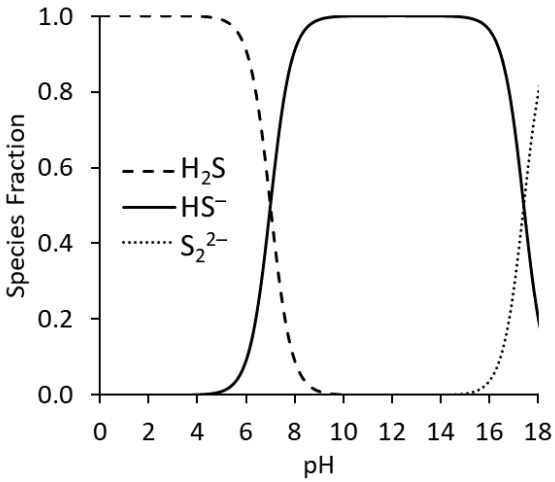

Figure D23. The speciation of sulfide species according to pH. Note that H_2S is the dominant species in the pH range 4 – 7 and HS^- is dominant in the range 7 – 10. The two species occur in equivalent concentrations at pH 7.

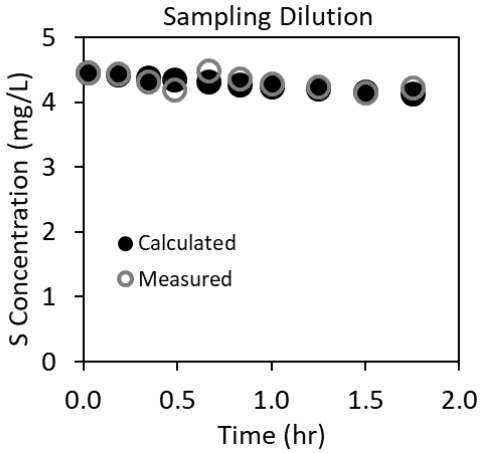

Figure D24. The concentration of sulfide in 10 mM sodium bicarbonate at pH 9.0 measured using the methylene blue method by UV-visible spectroscopy as compared to the calculated concentration expected by dilution through sampling. Sampling involved simultaneous injection and withdrawal to maintain a constant volume within a crimp-capped serum bottle, thereby preventing the formation of headspace into which $H_2S_{(g)}$ may evolve.

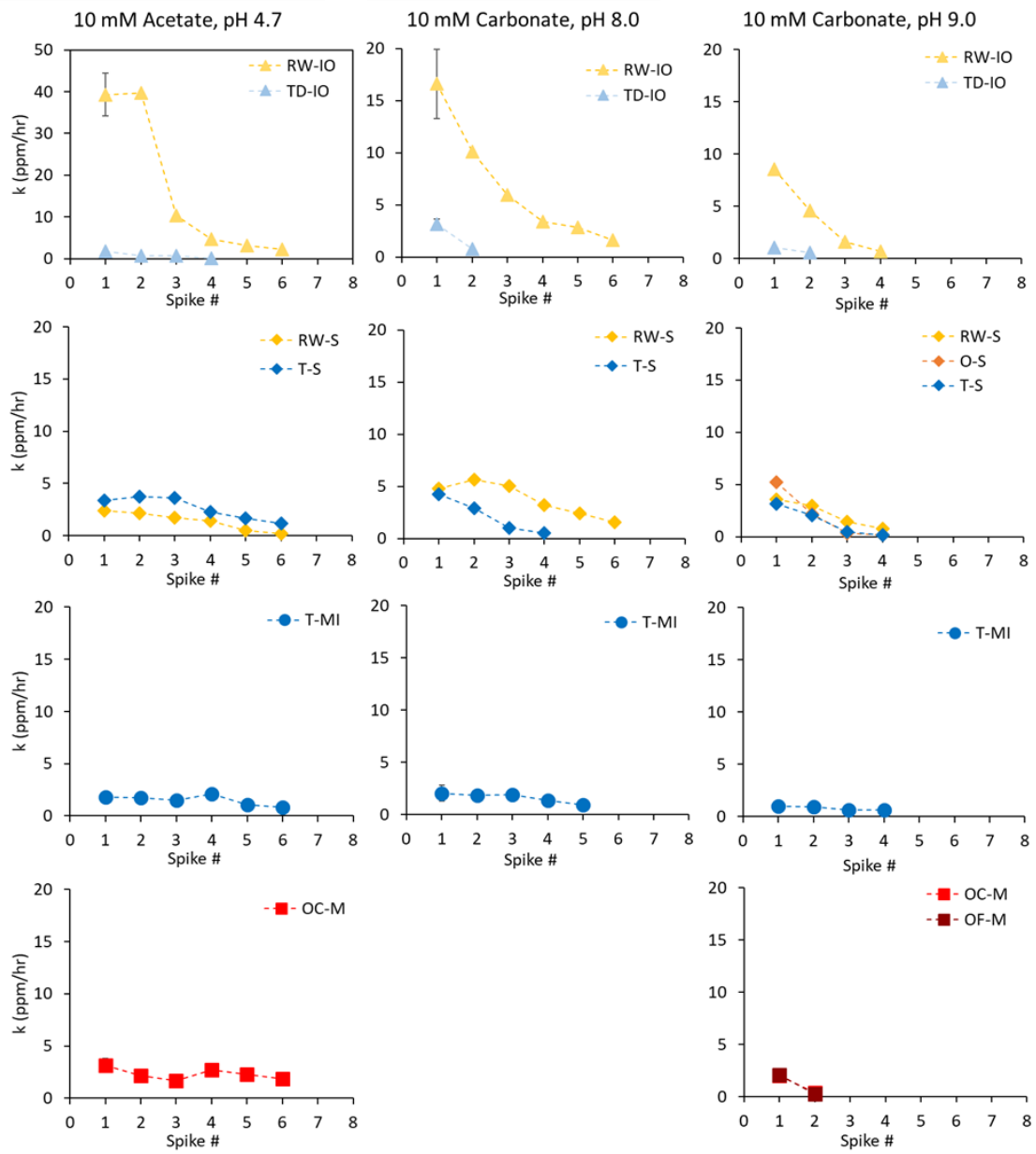

Figure D25. Zero-order rate constants for mining minerals reacting with multiple additions (spikes) of 150 µM (5 mg/L S) HS^- in 10 mM acetate at pH 4.7 (left column), 10 mM carbonate at pH 8.0 (center column), and 10 mM carbonate at pH 9.0 (right column). Divide k by 0.5 g to convert to the mass-normalized rate constant (ppm/g•hr). In descending order, mining specimens are separated into rows by class for clarity: iron oxides, siderites, mixed iron, and magnetites. Single spike reactors were run in replicate. Error bars not visible on single spike data points are smaller than the size of the data point symbol. Remaining spikes were not run in replicate. Note the scale on the y-axis for iron oxides in acetate is larger than the remaining plots.

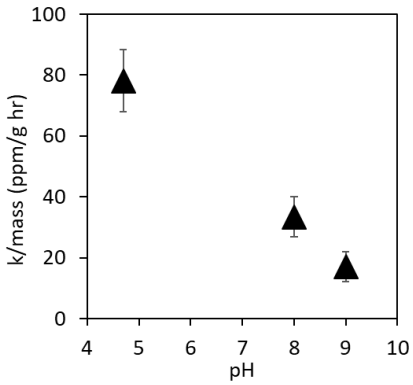

Figure D26. Mass-normalized initial rate constant (ppm/g•hr) vs pH for specimen RW-IO.

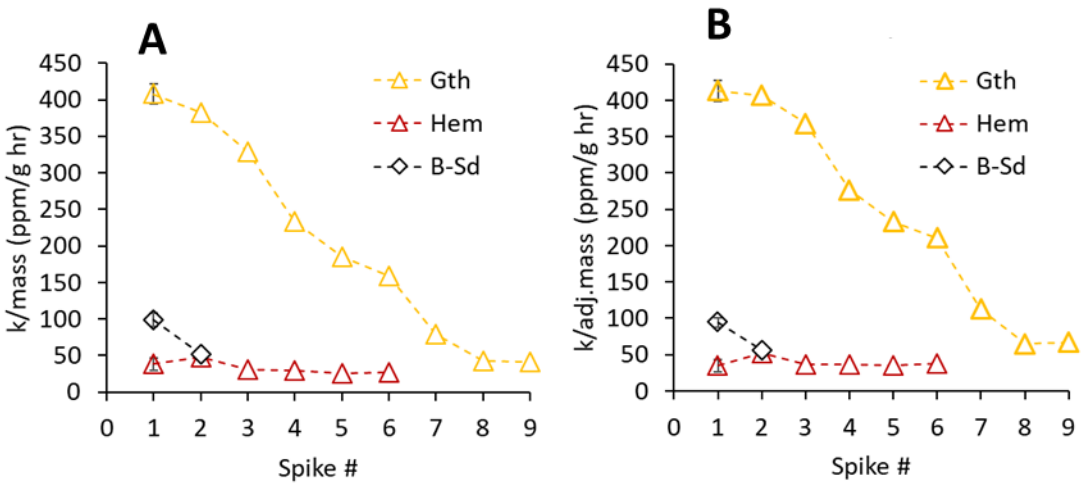

Figure D27. Comparison of mass-normalized initial rate constants without adjusting for mass loss during sampling (left) and with adjusting for mass loss (right) for the multispike reactions of 150 µM (5 mg/L S) HS^- in 10 mM acetate at pH 4.7. Adjusted specimen mass is defined as the average mineral mass present during a spike, accounting for mass lost during each sampling event. Each sampling event removes 0.8 % of mineral mass. Specimen S-Gth had 60.5 % of the mass remaining at the end of the nine spikes. The decrease in reaction rate over multiple spikes of HS^- is not attributed to mass loss during sampling.

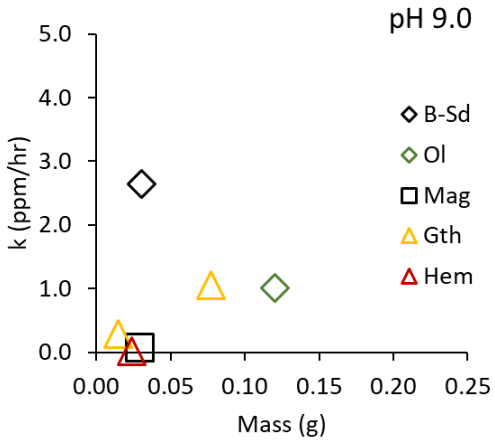

Figure D28. Comparison of normalized zero-order rate constants using adjusted specimen mass (left) and initial specimen mass (right) for each spike of 150 μM (5 mg/L S) HS^- in 10 mM acetate at pH 4.7. Adjusted specimen mass is defined as the average mineral mass present during the sampling event.

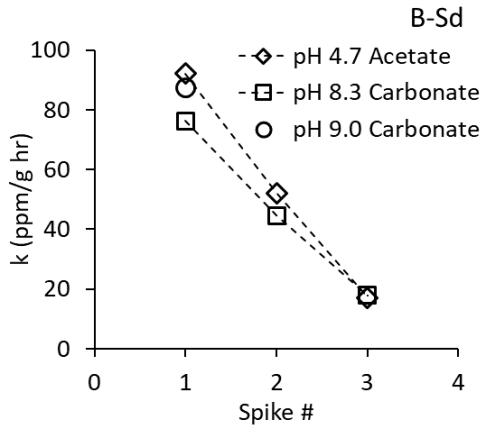

Figure D29. Initial mass-normalized rate constants for B-Sd at pH 4.7 in acetate (diamonds), pH 8.3 in carbonate (squares), and at pH 9.0 in carbonate (circle). At ca. 30 mg mass loading, only the first two spikes in the acetate system and the first spikes in the carbonate systems were within the limits defined by the reaction capacity.

Table D5. Tabulation of mass (g), reacted sulfur (umol), and initial rate constant (ppm/hr) for each mixed mineral specimen at three different pH along with the calculated parameters of reacted sulfur per mass (umol/g) and initial rate constant per mass (ppm/g•hr). These parameters are later mapped versus iron dissolution results.

		Mass (g)	Reacted S (umol)	Initial Rate (ppm/hr)	Reacted S per Mass (umol/g)	Initial Rate per Mass (ppm/hr*g)
pH 4.7	B-Sd	0.0805	19.3	7.4	239.8	91.9
	Gth	0.0774	74.9	30.8	967.9	397.9
	Hem	0.0767	62.6	2.6	816.2	33.9
pH 8.3	B-Sd	0.0303	3.7	2.3	122.1	75.9

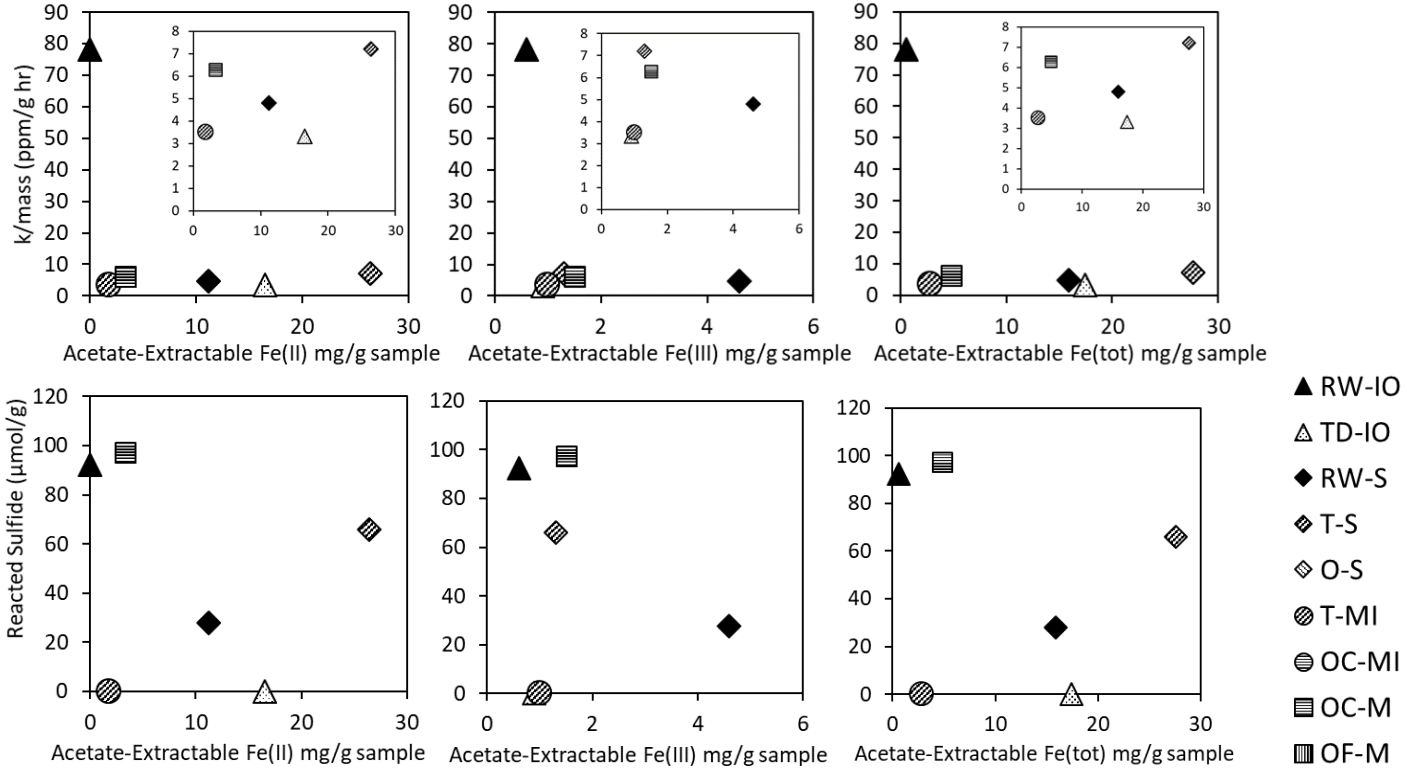

Figure D30. Plots mapping reaction parameters from reactions performed at pH 4.7 in acetate buffer versus acetate-extractable iron determined by chemical dissolution. (Top row) Rate constant normalized to sample mass versus acetate-extractable Fe(II), Fe(III), and total Fe in mg/g of sample, from left to right. (Bottom row) Reacted sulfide is normalized to sample mass versus acetate-extractable Fe(II), Fe(III), and total Fe in mg/g of sample, from left to right.

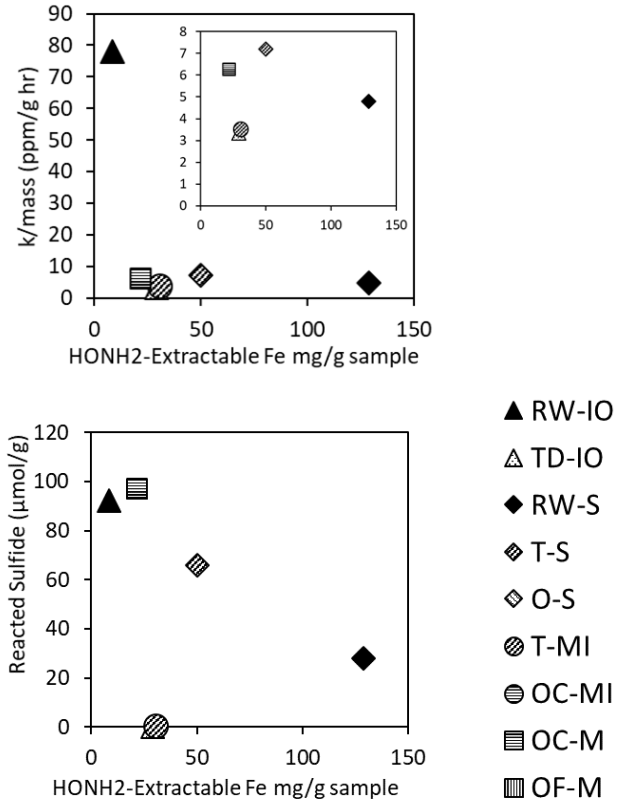

Figure D31. Plots mapping reaction parameters from reactions performed at pH 4.7 in acetate buffer versus $HONH_2$-extractable iron determined by chemical dissolution. (Top) Rate constant normalized to sample mass versus $HONH_2$-extractable Fe in mg/g of sample. (Bottom) Reacted sulfide is normalized to sample mass versus $HONH_2$-extractable Fe in mg/g of sample.

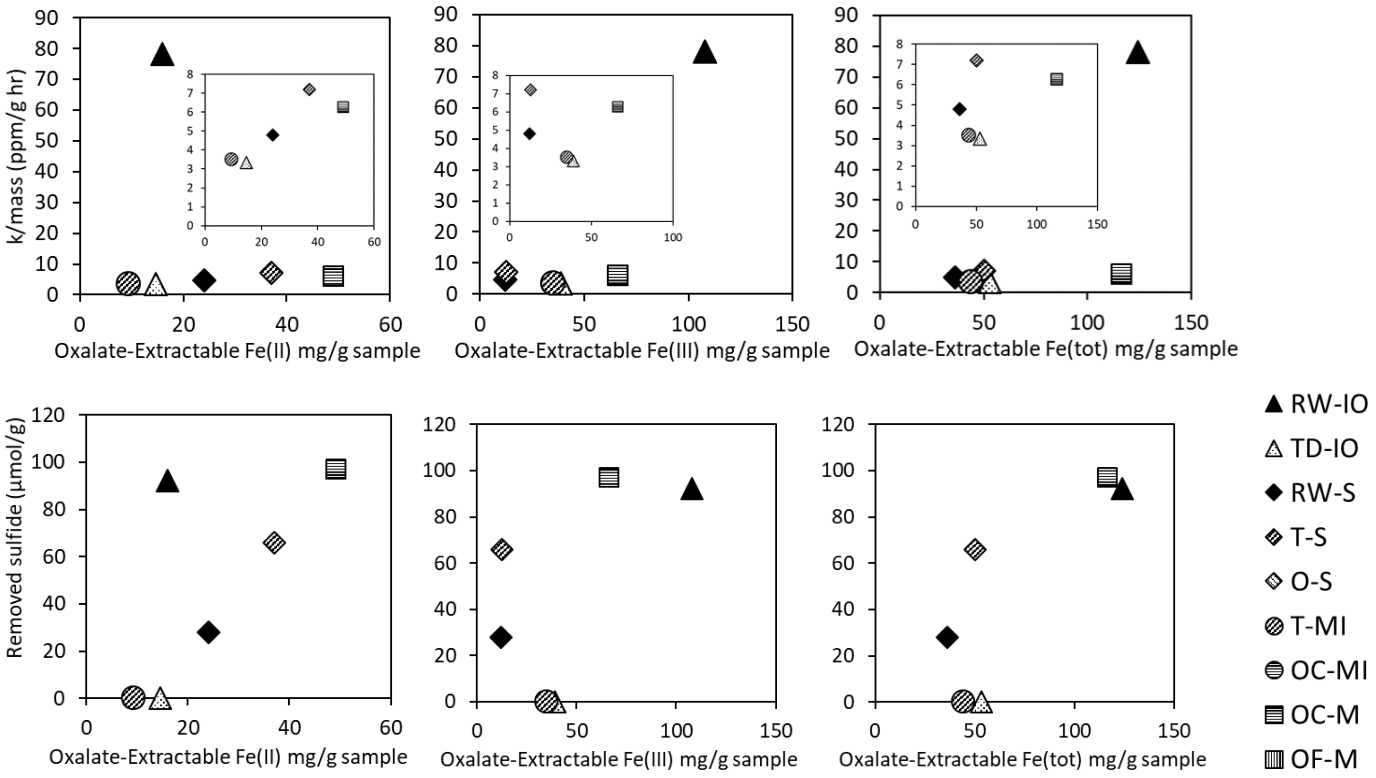

Figure D32. Plots mapping reaction parameters from reactions performed at pH 4.7 in acetate buffer versus oxalate-extractable iron determined by chemical dissolution. (Top row) Rate constant normalized to sample mass versus oxalate-extractable Fe(II), Fe(III), and

total Fe in mg/g of sample, from left to right. (Bottom row) Reacted sulfide is normalized to sample mass versus oxalate-extractable Fe(II), Fe(III), and total Fe in mg/g of sample, from left to right.

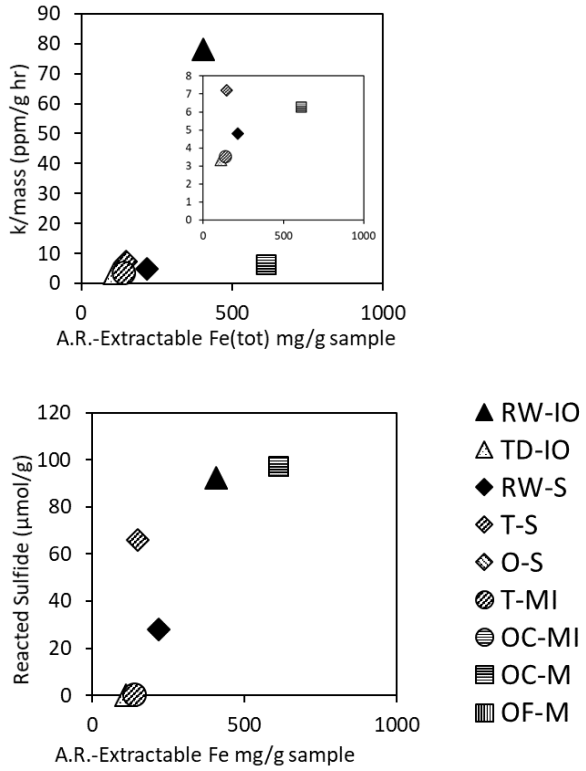

Figure D33. Plots mapping reaction parameters from reactions performed at pH 4.7 in acetate buffer versus aqua regia (A.R.)-extractable iron determined by chemical dissolution. (Top) Rate constant normalized to sample mass versus A.R.-extractable Fe in mg/g of sample. (Bottom) Reacted sulfide is normalized to sample mass versus A.R.-extractable Fe in mg/g of sample.

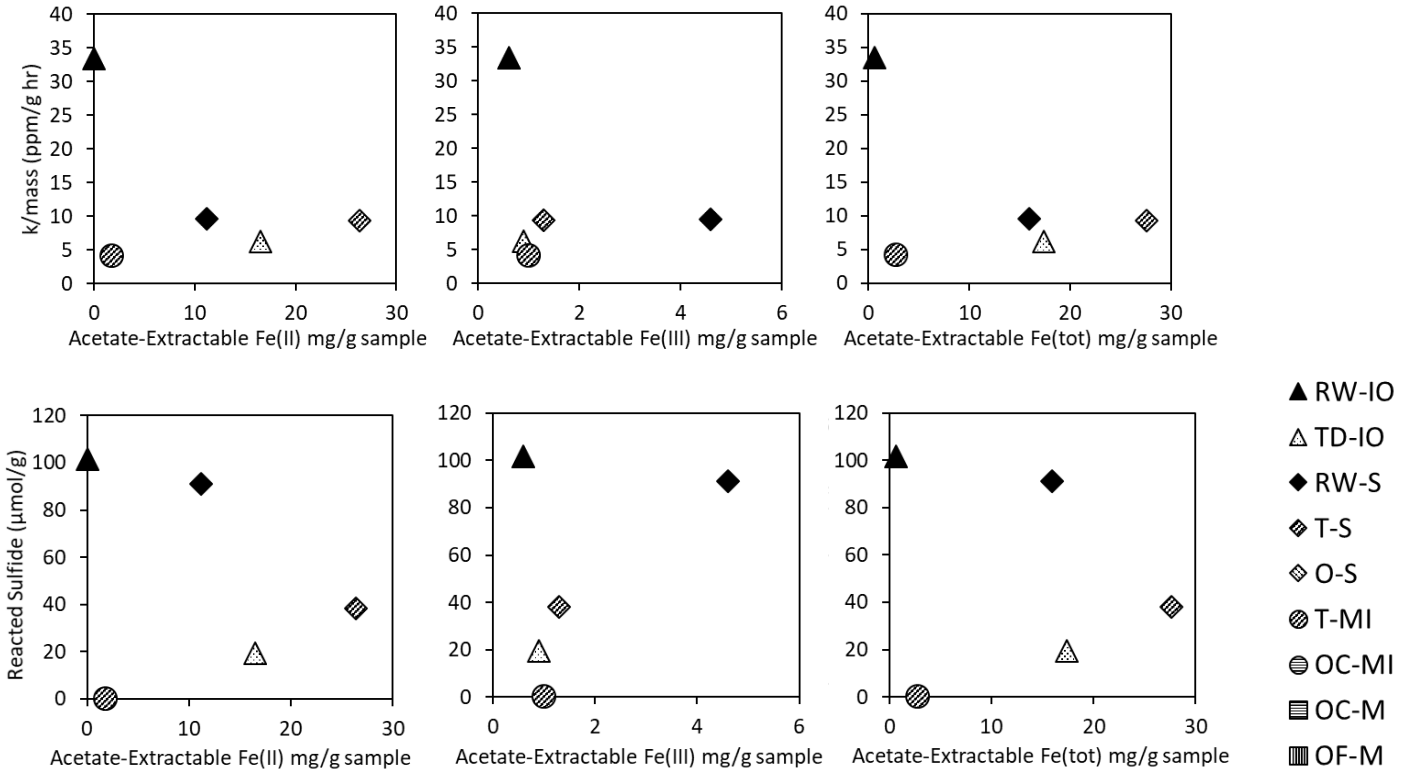

Figure D34. Plots mapping reaction parameters from reactions performed at pH 8.0 in acetate buffer versus acetate-extractable iron determined by chemical dissolution. (Top row) Rate constant normalized to sample mass versus acetate-extractable Fe(II), Fe(III), and total Fe in mg/g of sample, from left to right. (Bottom row) Reacted sulfide is normalized to sample mass versus acetate-extractable Fe(II), Fe(III), and total Fe in mg/g of sample, from left to right.

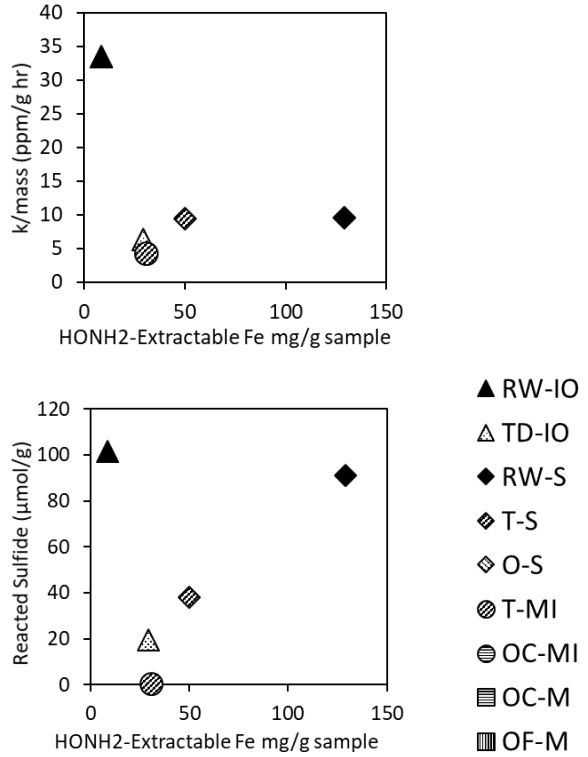

Figure D35. Plots mapping reaction parameters from reactions performed at pH 8.0 in acetate buffer versus $HONH_2$-extractable iron determined by chemical dissolution. (Top) Rate constant normalized to sample mass versus $HONH_2$-extractable Fe in mg/g of sample. (Bottom) Reacted sulfide is normalized to sample mass versus $HONH_2$-extractable Fe in mg/g of sample.

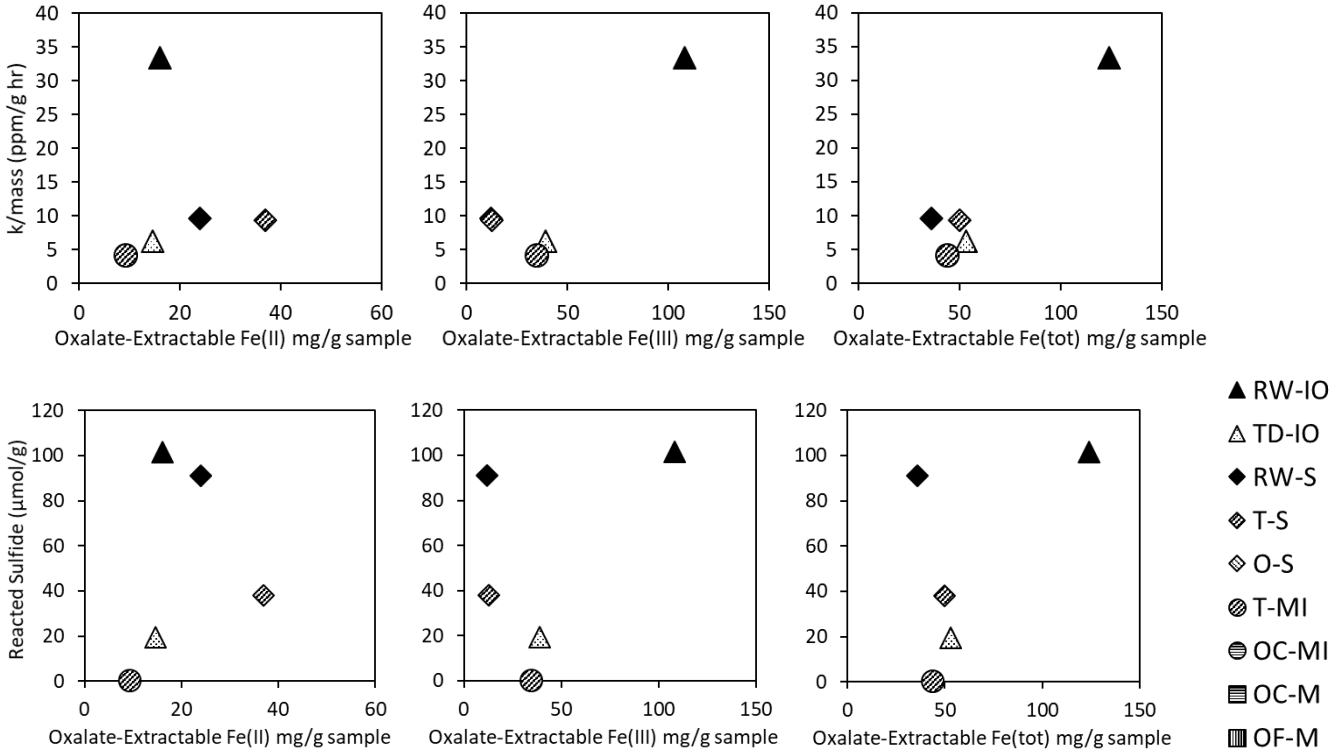

Figure D36. Plots mapping reaction parameters from reactions performed at pH 8.0 in acetate buffer versus oxalate-extractable iron determined by chemical dissolution. (Top row) Rate constant normalized to sample mass versus oxalate-extractable Fe(II), Fe(III), and total Fe in mg/g of sample, from left to right. (Bottom row) Reacted sulfide is normalized to sample mass versus oxalate-extractable Fe(II), Fe(III), and total Fe in mg/g of sample, from left to right.

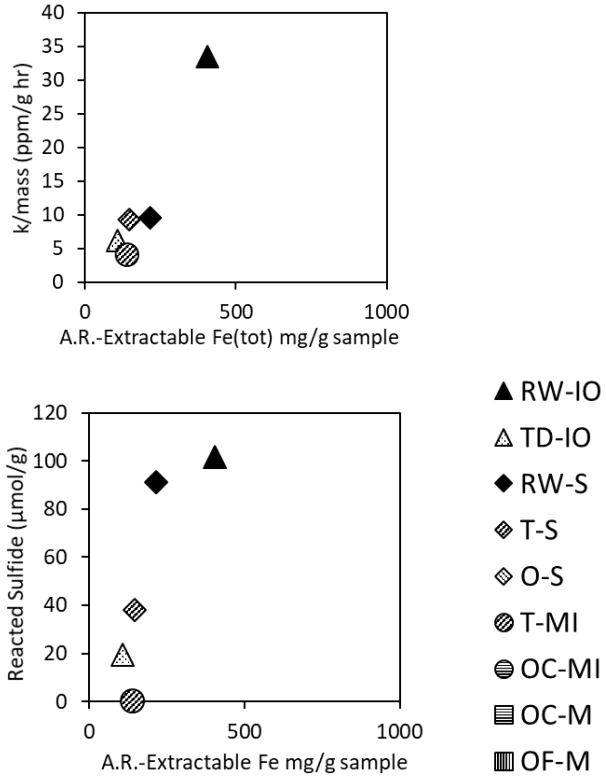

Figure D37. Plots mapping reaction parameters from reactions performed at pH 8.0 in acetate buffer versus aqua regia (A.R.)-extractable iron determined by chemical dissolution. (Top) Rate constant normalized to sample mass versus A.R.-extractable Fe in mg/g of sample. (Bottom) Reacted sulfide is normalized to sample mass versus A.R.-extractable Fe in mg/g of sample.

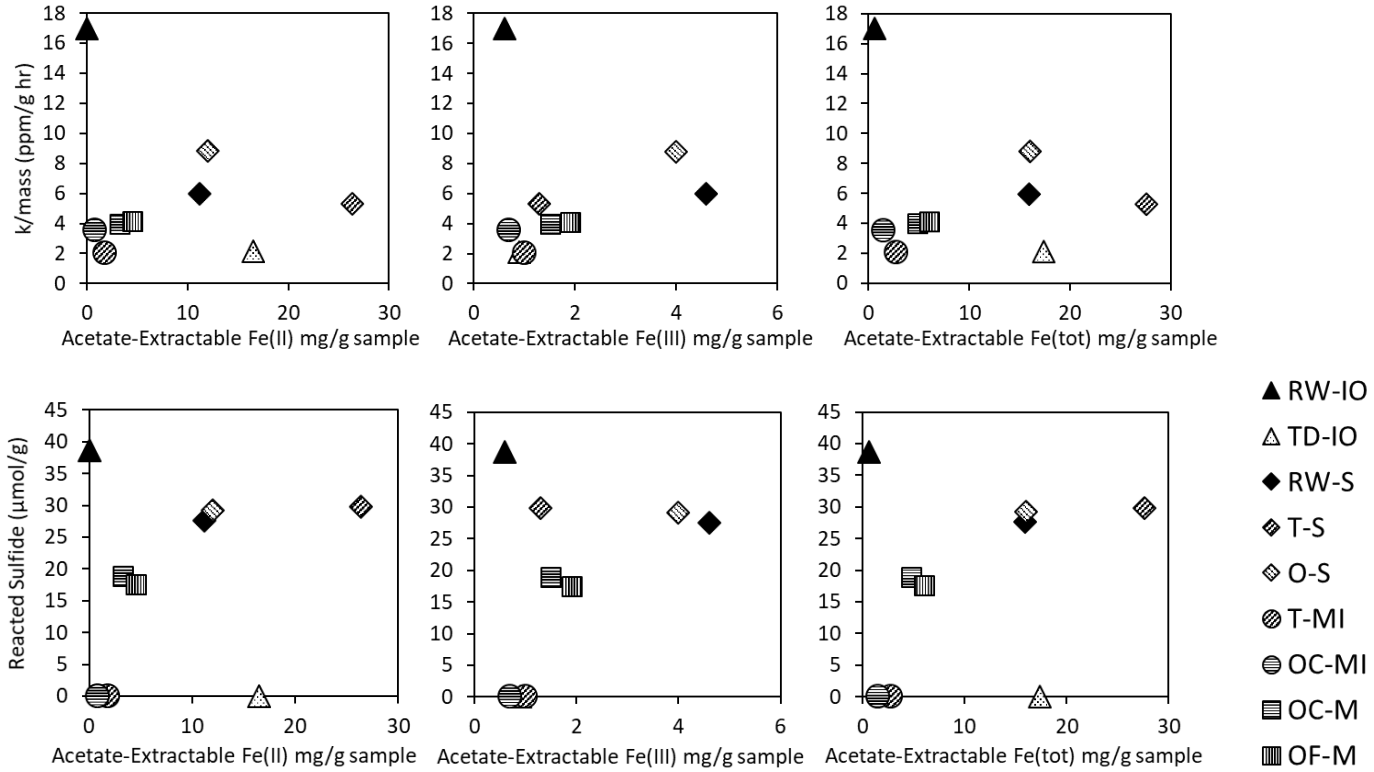

Figure D38. Plots mapping reaction parameters from reactions performed at pH 9.0 in acetate buffer versus acetate-extractable iron determined by chemical dissolution. (Top row) Rate constant normalized to sample mass versus acetate-extractable Fe(II), Fe(III), and total Fe in mg/g of sample, from left to right. (Bottom row) Reacted sulfide is normalized to sample mass versus acetate-extractable Fe(II), Fe(III), and total Fe in mg/g of sample, from left to right.

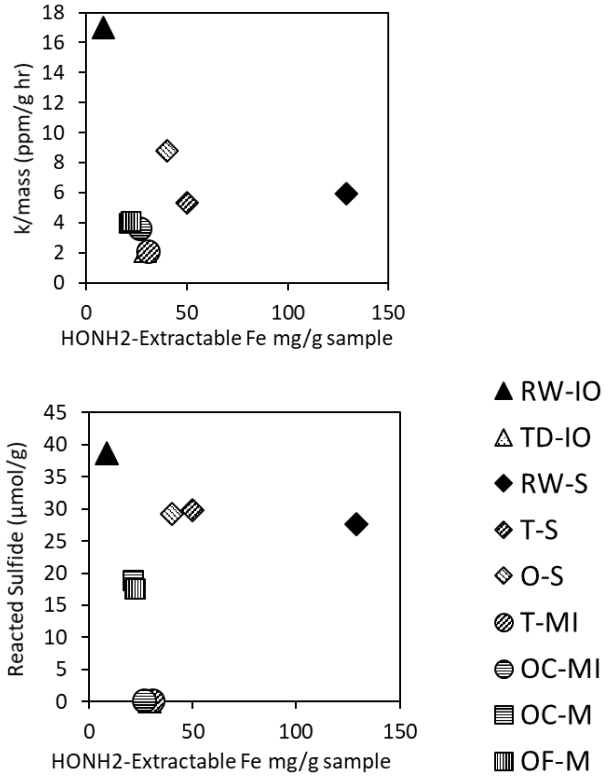

Figure D39. Plots mapping reaction parameters from reactions performed at pH 9.0 in acetate buffer versus $HONH_2$-extractable iron determined by chemical dissolution. (Top) Rate constant normalized to sample mass versus $HONH_2$-extractable Fe in mg/g of sample. (Bottom) Reacted sulfide is normalized to sample mass versus $HONH_2$-extractable Fe in mg/g of sample.

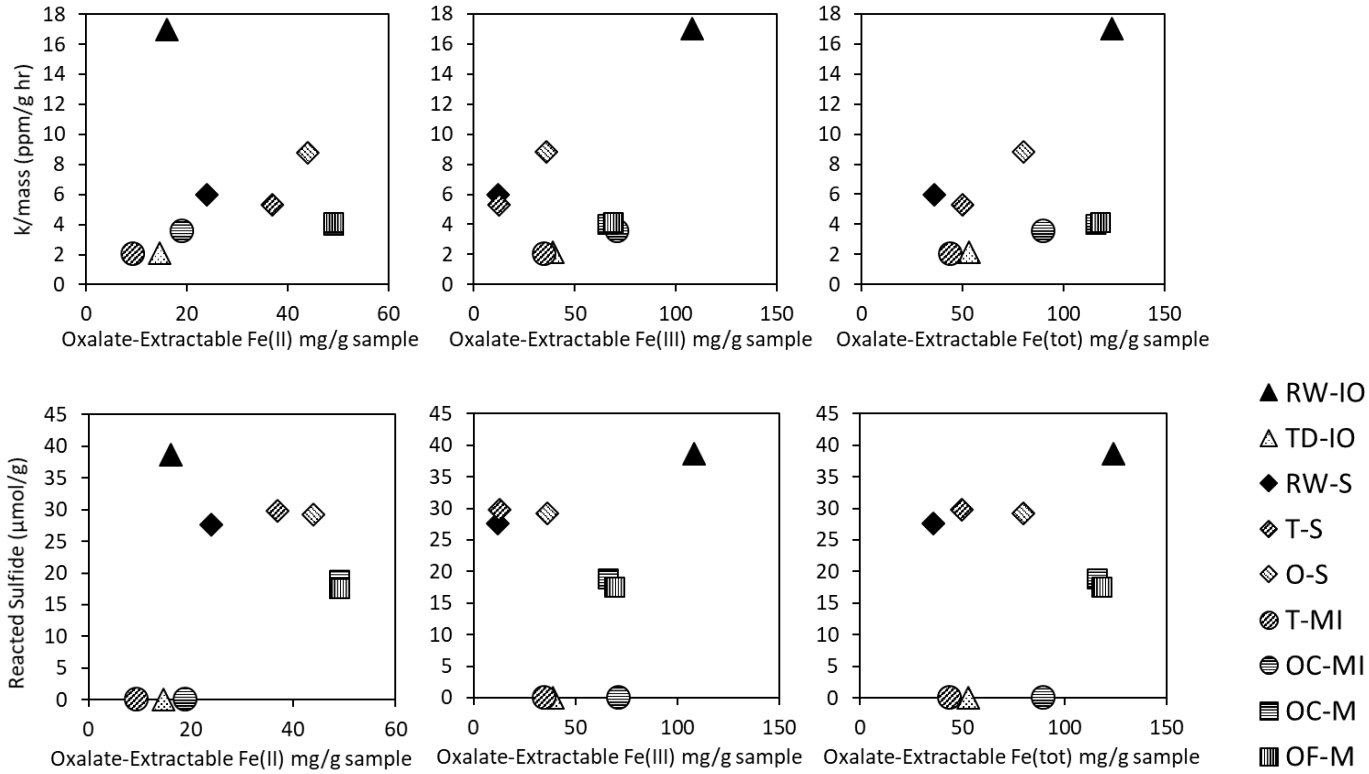

Figure D40. Plots mapping reaction parameters from reactions performed at pH 9.0 in acetate buffer versus oxalate-extractable iron determined by chemical dissolution. (Top row) Rate constant normalized to sample mass versus oxalate-extractable Fe(II), Fe(III), and total Fe in mg/g of sample, from left to right. (Bottom row) Reacted sulfide is normalized to sample mass versus oxalate-extractable Fe(II), Fe(III), and total Fe in mg/g of sample, from left to right.

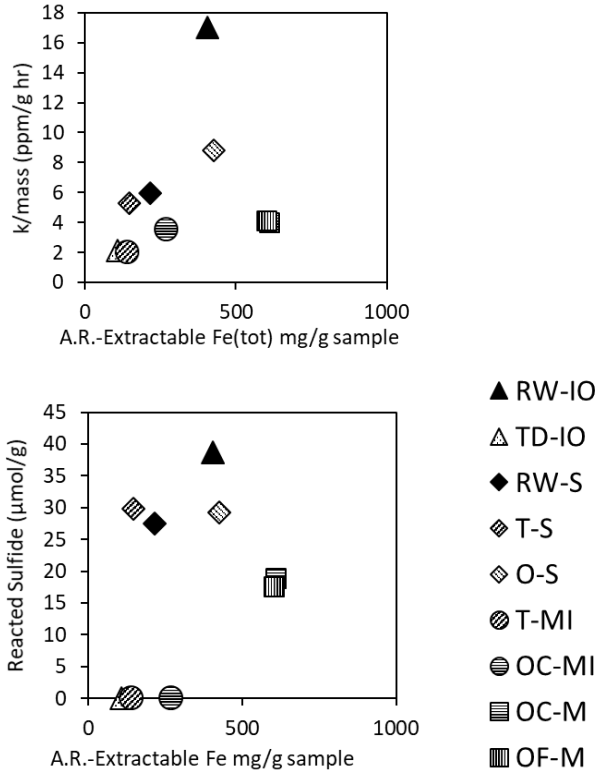

Figure D41. Plots mapping reaction parameters from reactions performed at pH 9.0 in acetate buffer versus aqua regia (A.R.)-extractable iron determined by chemical dissolution. (Top) Rate constant normalized to sample mass versus A.R.-extractable Fe in mg/g of sample. (Bottom) Reacted sulfide is normalized to sample mass versus A.R.-extractable Fe in mg/g of sample.

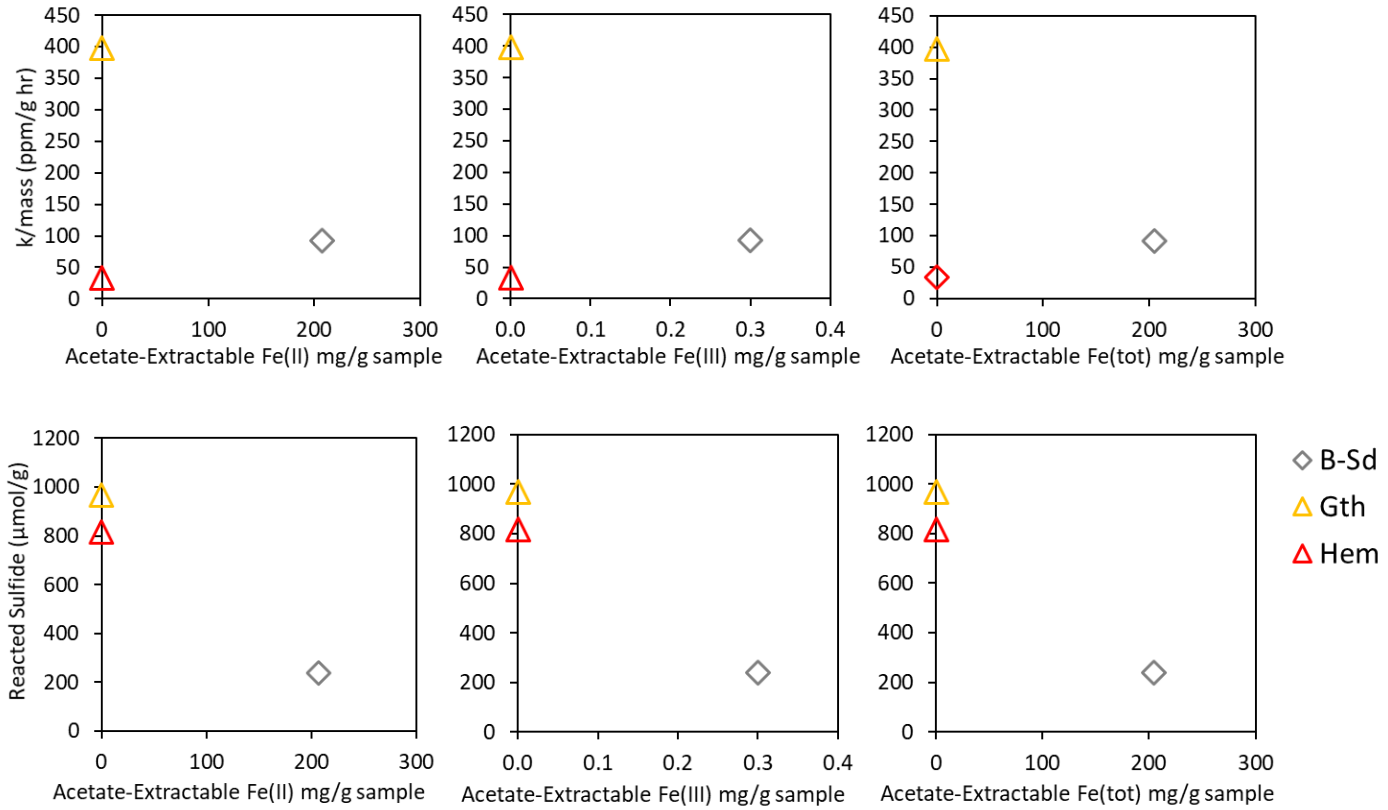

Figure D42. Plots mapping reaction parameters from reactions performed at pH 4.7 in acetate buffer versus acetate-extractable iron determined by chemical dissolution. (Top row) Rate constant normalized to sample mass versus acetate-extractable Fe(II), Fe(III), and total Fe in mg/g of sample, from left to right. (Bottom row) Reacted sulfide is normalized to sample mass versus acetate-extractable Fe(II), Fe(III), and total Fe in mg/g of sample, from left to right.

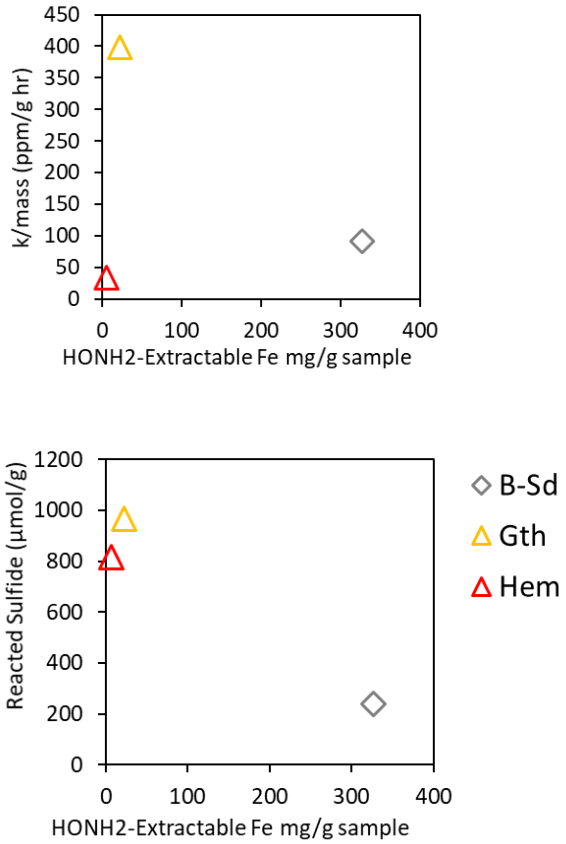

Figure D43. Plots mapping reaction parameters from reactions performed at pH 4.7 in acetate buffer versus $HONH_2$-extractable iron determined by chemical dissolution. (Top) Rate constant normalized to sample mass versus $HONH_2$-extractable Fe in mg/g of sample. (Bottom) Reacted sulfide is normalized to sample mass versus $HONH_2$-extractable Fe in mg/g of sample.

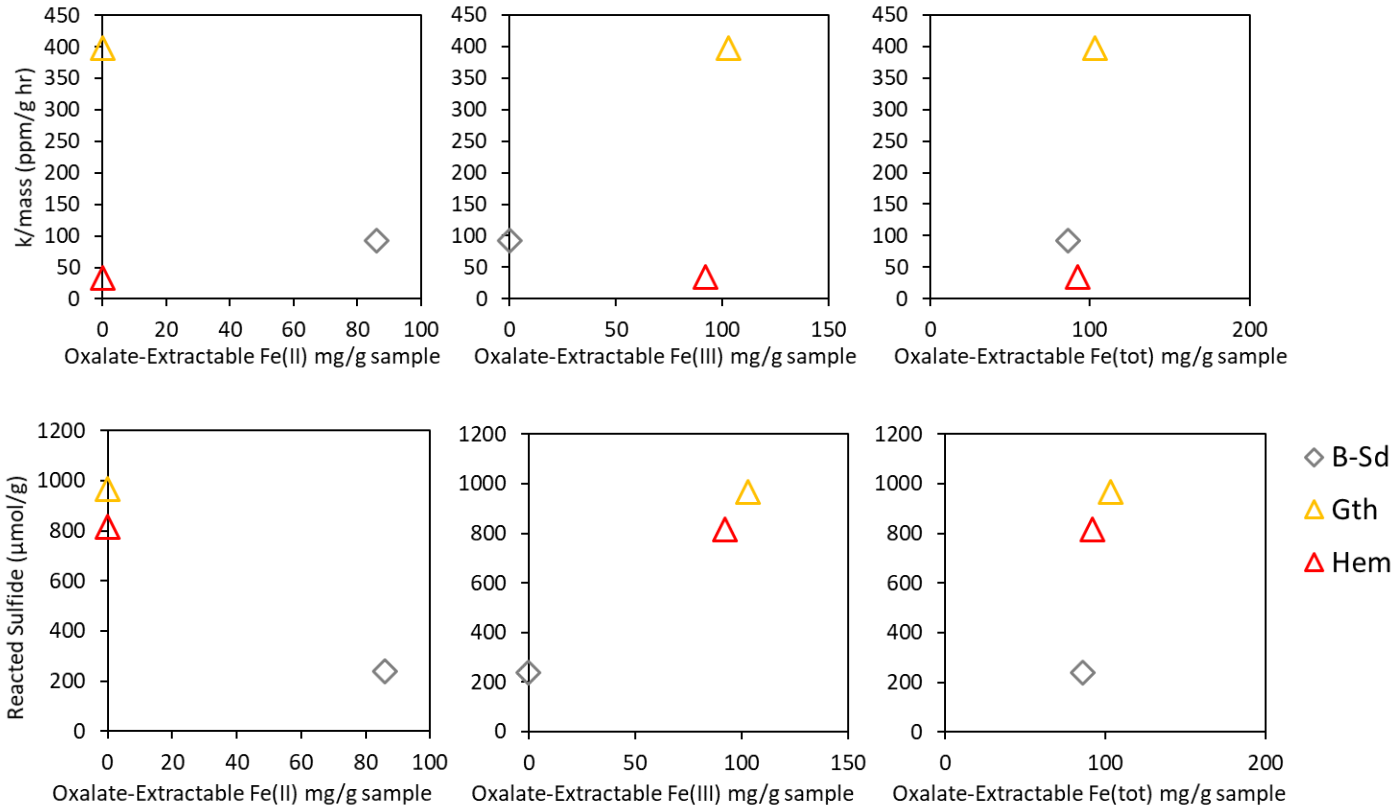

Figure D44. Plots mapping reaction parameters from reactions performed at pH 4.7 in acetate buffer versus oxalate-extractable iron determined by chemical dissolution. (Top row) Rate constant normalized to sample mass versus oxalate-extractable Fe(II), Fe(III), and total Fe in mg/g of sample, from left to right. (Bottom row) Reacted sulfide is normalized to sample mass versus oxalate-extractable Fe(II), Fe(III), and total Fe in mg/g of sample, from left to right.

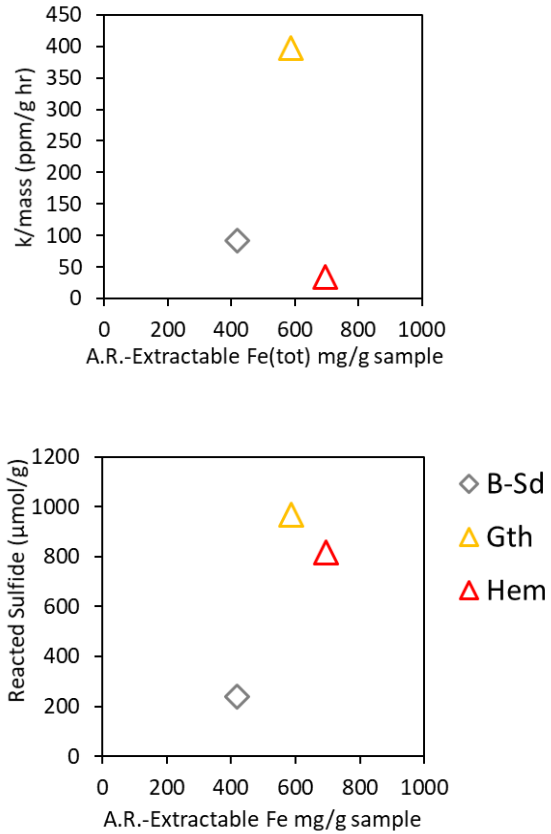

Figure D45. Plots mapping reaction parameters from reactions performed at pH 4.7 in acetate buffer versus aqua regia (A.R.)-extractable iron determined by chemical dissolution. (Top) Rate constant normalized to sample mass versus A.R.-extractable Fe in mg/g of sample. (Bottom) Reacted sulfide is normalized to sample mass versus A.R.-extractable Fe in mg/g of sample.

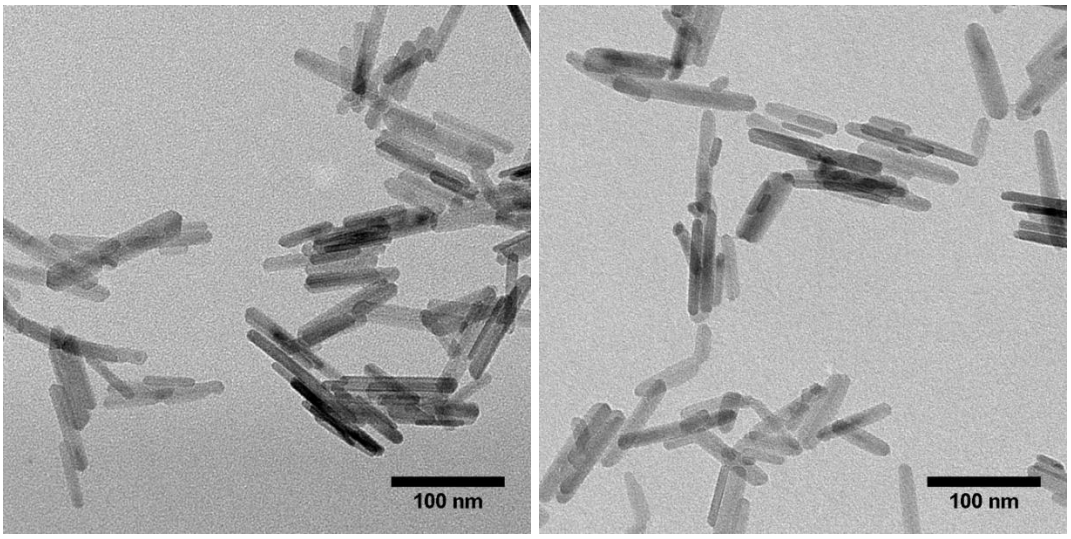

Figure D46. Unreacted particles (left) and post-reaction particles (right) for goethite, which received nine additions of sulfide at pH 4.7 to total 968 μmol S captured per gram of material.

Table D6. Sulfur content of the mixed mineral specimens as determined by ICP-MS, compared to the quantity of total sulfur added to reactors at pH 4.7, and adjusted by sample mass.

Sample ID	Average Initial Specimen S (μmol/g)	Sulfur Added (μmol)	Sample Mass (g)	Sulfur Added (Mass Norm.) (μmol/g)
RW-IO	10 ± 5	46.4	0.5028	92.3
TD-IO	27 ± 1			
RW-S	36 ± 2	47.6	0.5025	94.7
T-S	290 ± 27			
O-S	34 ±7			
T-MI	20 ± 3			
OC-MI	24 ± 2			
OC-M	9 ± 1	49.4	0.5045	97.9
OF-M	9 ± 1			
STD-NI	2 ± 2			

Appendix E. Water Legacy Board Game: A Cooperative Strategy Board Game for Teaching Concepts of Environmental Pollution and Remediation

(Reading level grade 9+, accommodates 3 – 40 students in up to 8 groups)

Students from Janesville-Waldorf-Pemberton High School test the crude oil set.

This appendix contains a description of a high school-level active-learning module that teaches students about environmental contamination. This project was led by Jeanette L. Voelz and R. Lee Penn. Others who contributed to this project (listed alphabetically) include Jennifer Magdal, Jacob Montgomery, Lukas Olson, Huitzilin Ortiz, Elizabeth Schoeller, and Sarah Schoeller.

Motivation

This game was developed in response to personal experience as a student in science classrooms. Concepts of environmental contamination were not well represented, disciplines within the sciences were often taught as compartmentalized areas, and science topics were often presented without real-world applications. In practice, there often is cross-over between disciplines and connections to non-science disciplines such as policy and economics, and real-world examples make concepts more concrete and relevant. Out of passion for environmental health and protection, this game was developed in an effort to make science topics more fun and relatable for students. The broader impact is to generate more interest in environmental protection so that students have a more positive impact as they become independent members of society.

Approach

The board game format stemmed from four main design points for an effective learning (and teaching) module. The first point considers an interactive learning environment where students take the lead role in searching for answers, discussing content with peers, and using several avenues to synthesize, absorb, and relay content knowledge. A hands-on activity that involves searching for and reading online content, watching informative videos, playing a game, discussing topics with peers, and writing responses to the related content helps to activate all types of learners. The variety in learning format and the inquiry-based approach may improve concept retention.

The second design point aimed for a format that allows for more interaction between students (versus a lecture or single-player game) to help develop interpersonal skills. Learning often evolves from asking questions, thinking through problems, explaining lines of thought, and debating courses of action. When more minds are involved, more perspectives are available to enrich the discussion and consider other avenues. Working together is also a valuable skill for students as they enter society.

Accessibility was also considered in this game development. Teachers in classrooms across the country too often struggle with access to the same technologies, equipment, and money that other schools have in abundance. For example, some classrooms have tablets for all students and 3D printers, while other classrooms have limited access to computers and sometimes do not have color printers. Some schools grant teachers funds for classroom activities, while others rely on teachers to find their own funding. With these access issues in mind, this game is developed in hard-copy format rather than as a digital interactive program, and will be available for free online in several file formats. It will also be accessible by mail through the Institute on the Environment, University of Minnesota.

The final aspect in game design was ease and flexibility of use. The game pieces were developed for easy printing on standard printers. No game pieces require special ordering and many components can be easily substituted with commonly-available materials. The format also allows for continual improvements to gameplay, language, and design so that it can evolve over time to become a more powerful learning activity.

Basic Description and Gameplay

Overview

Water Legacy is a cooperative strategy game where players must clean up a toxic spill before it overruns districts in the watershed and ruins the economy. Rolling the dice causes the pollution to spread, but players fight it back using **experts** and **treatment methods**. But it all comes with a cost. Collect **tokens** from the resources in your district, then hire experts, install treatment systems, share your tokens, and share your strategies. Work together and your group can beat this!

Components

- 1 rulebook
- 8 contaminant sets for 4 players each including:
    - 1 contaminant card
    - 4 district cards
    - 2 treatment cards
    - 36 wild cards
    - 18 expert cards
    - 2 dice
    - 4 contamination blocks
- 8 extra district cards
- 8 extra contamination blocks

Setup

This game is designed for 1 – 8 groups, with 3 – 5 players per group. Any one of the four district cards is removed for groups of 3 players, and one of the extra district cards is added for groups of 5 players. Each group is a separate, unrelated watershed within the same country. The pollutant card is placed at the center of the group (Figure E1). This pollutant represents a spill that occurs near the source water of the watershed. Each player manages a district downstream from the spill. One player should be selected to manage the tokens into two piles. One pile represents the bank and the other pile should be only for collecting tokens for installed treatments. The wild cards and the experts cards are placed in the center for everyone to access.

Figure E1. The game setup involves three to five players surrounding the central contaminant spill. Each player controls their own district. Wild cards and expert cards are placed in the center.

District Cards

Each district has a unique industry, such as housing, manufacturing, or farmland. These industries generate tax income for the player to hire experts and install treatment methods for their contamination issues. The district cards describe special characteristics of that district, list the order of play, and state how the game is won or lost. A grid separates the district into blocks that mark the level of contamination during the game. The water supply at the bottom of the district is the source of the district's drinking water.

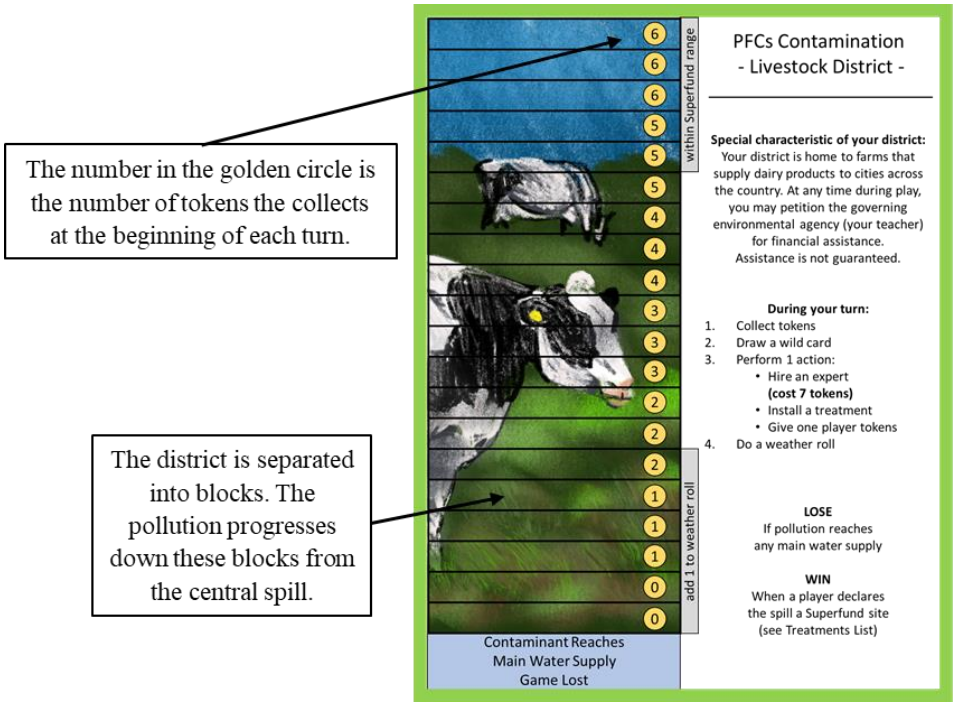

Figure E2. A sample district card identifying the value of monies generated by the district and describing aspects of gameplay.

Dice

Two dice are included in a contaminant set and each die has two sides for each value of 0, 1, and 2. The dice are used to start the game, to perform some actions during a turn, and to finish a turn in a "weather roll". The weather roll determines how much farther the pollutant progresses through the player's district. A spinner is an optional substitution for dice.

Wild Cards

Wild cards initiate events that are beneficial or detrimental to the drawer and/or the group. Drawing a wild card is the second step of a player's turn, after collecting tokens. Cards are used immediately, on the next turn, or at the player's discretion, as indicated on the card. The cards are then discarded into a pile, which is reshuffled into a draw pile if the cards runout during gameplay.

Experts Deck

Experts are needed to unlock different contaminant treatment methods. Each district card lists the cost of hiring an expert in that district. The tokens used to hire experts are returned to the bank and do not count towards the final token score. Players cannot give, sell, or trade experts to other players, unless allowed by a wild card.

Treatments

Two treatment cards are provided per group so that only two players are sharing each card. Each treatment has unlimited uses but players can only use a single treatment per turn. Treatments cost tokens, which are dropped into a collection pot in the center of the board and scored at the end of the game. Players must hire experts to use treatments, as indicated on the treatment list. Players do not lose experts when using treatments.

Gameplay

Players first take turns rolling two dice. The player with the highest number begins the game. For the starting round, each player does a weather roll to determine how far the spill has progressed through *their* district before the spill was detected. After the starting round, each turn has four steps:

1. Draw a wild card and use it as directed.
2. Collect the number of tokens from the district as determined by the pollutant spread. For example, if the pollutant has spread five blocks through this housing district, the player collects e tokens, as shown in Figure E3.
3. Perform 1 action
    - Hire and expert
    - Install a treatment method
    - Give tokens to another player
4. Perform a weather roll at the end of your turn.

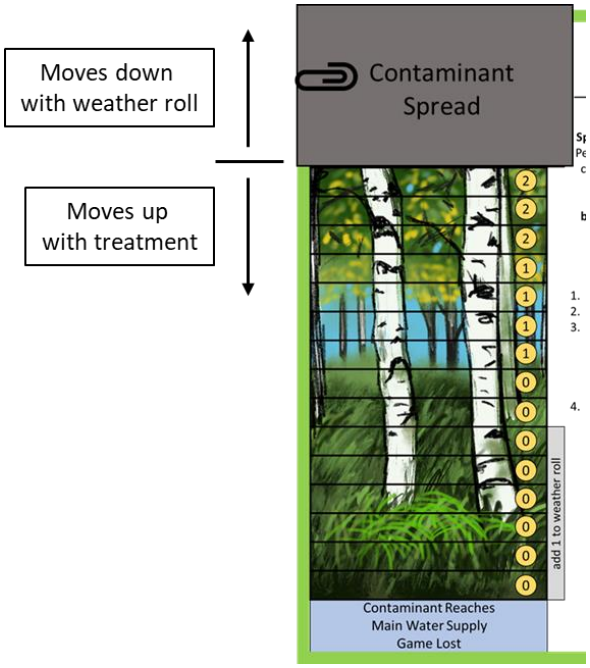

Figure E3. The weather roll makes the contaminant spread farther down a district according to the number of blocks shown on the dice. Treatment methods push the contaminant back according to the number of blocks designated by the treatment card.

Winning and Scoring

The game is over when a player can declare the spill a Superfund Site as outlined by the treatment card. This causes the pollution to be removed from every district in the watershed. If this is achieved, the group (or player) who spent the fewest tokens wins. If time runs out before it is declared a Superfund Site, the winning group (or player) is determined by the following formula:

Calculate final score:
Number of experts hired____×10 =____
Total A____

Tokens spent on treatments____
Blocks occupied by pollution____×2=____
Total B____

Score: A – B = ____ – ____ = ____
Highest score wins

Special Moves

March on the Capitol

During any player's turn, the player can initiate a March on the Capitol that requires participation from every player. Each player "sends" at least 1 expert to March on the Capitol by turning the expert card over. A player gets 8 tokens for each expert they send. Experts "return home" (card turned face up) on the player's subsequent turn and returns to employment. This does not count as an action. Maximum of 1 expert returns home during a turn.

Federal Government Directive

The instructor can direct the transfer of tokens from one group to the next. This allows for a group of players (perhaps a state) with overall higher tax income to subsidize a group with much lower tax income. The instructor asks the disadvantaged group how many tokens they need, decides if that is too much or too little, and then directs the advantaged group to pay those tokens. It is up to each group to decide who among them pays the tokens and how the tokens are distributed.

Case Studies

The case studies for each contaminant were selected based on known EPA superfund sites or brownfield sites, as well as from news reports of spills. Providing a real-world scenario in which this event has occurred gives students a concrete example of the impact that pollution has on society and the environment. The areas in which these spills have occurred is limited to the United States but spans the continent. The case studies were assigned as follows:

- Crude Oil: Deepwater Horizon, Gulf Coast
- Heavy Metals: Lead contamination, Los Angeles, CA
- Perfluorinated Chemicals: 3M, Woodbury, MN
- Acid Mine Drainage: Berkeley Pit, Butte, MT
- Nitrates: High Plains Aquifer, NE
- Uranium: Church Rock Mill, NM
- Chlorinated Compounds: Allied Paper, Kalamazoo, MI
- Nitroaromatic Compounds: Point Pleasant, WV

Classroom Implementation

To foster accessibility, these game materials will be provided for free in electronic format or at low cost in print format through the Institute on the Environment at the University of Minnesota. Worksheets and discussion points are currently being developed in a collaboration with high school science teachers at White Bear Lake High School and St. Louis Park High School. The following in a general outline of classroom implementation as it is currently envisioned.

This game would ideally be implemented over the course of several class periods to maximize student-led investigation, interactive learning, and discussions. The activities on Day 1 would include introducing vocabulary, separating students into the contaminant groups, and assigning work and/or homework based on class content and relating to the case studies provided for each district.

The activities for Day 2 include watching an instructional video (still to be developed) that covers the game rules and gameplay, playing the game and completing an accompanying worksheet, then assigning homework to follow up on the concepts covered in the game as they relate to the class content.

The final activities on Day 3 should mostly include discussions. Students can teach each other what they learned and discuss the complexities of environmental issues as it relates to economics and policy. The science topic discussion would focus on how the material fits into the class.

Day 1 Sample Worksheet

Use the following sources to investigate your contaminant and case study. You may also search other reputable sources.

- EPA Toxics Release Inventory (TRI) Program
- EPA Superfund & Brownfields
- State environmental protection agencies
- Encyclopedia Britannica

Contaminant:_____Case Study:_____

What specific molecules are found in this kind of contamination? Draw an example molecule.

Use the sources provided to investigate your assigned case study and describe your findings. Describe the scenario surrounding the contamination issue. What caused the contamination?

What is the extent of contamination?

What is the impact on the community and ecosystem in the watershed?

What treatment methods have been used to clean up the contamination?

How does this type of contamination affect human health? How does it impact environmental health?

How do scientists determine toxic levels of a compound?

Day 2 Sample Worksheet

Contaminant:_____

Describe two experts that were hired during play:

Use this area to answer the Wild Card questions that were drawn during play. Remember to write the question along with your answer.

Calculate your game score

Number of experts you have in play_____ × 10 = _____
Remaining tokens in your district = _____
Total A = _____

Tokens spent on treatments = _____
Blocks occupied by pollution_____ × 2 = _____
Total B = _____

Score = A - B = _____
Highest score wins

Day 3 Sample Discussion Questions

Chemicals are often put into products before external research groups like the EPA conduct detailed studies of toxicity and environmental impact. Why is this? What effects does this have?

What do you think constitutes ‘due diligence’ with regard to toxicity studies of new chemicals, or chemicals used in manufactured products? How much of the contamination issue up to the company to solve?

What are some complications affecting the cleanup of your chemical that occur in the real world?

As globalization leads to the manufacturing, transport, and use of chemicals in large volumes, what should be done to prevent environmental contamination?

Content & Learning Outcomes

The science concepts presented within the game and in the supplemental materials should represent the interdisciplinary nature of environmental projects in the real world. This involves overlap of topics from chemistry, biology, ecology, toxicology, geology, hydrology, climatology, and engineering, among others. Additional topics that also arise in environmental issues include economics, policy, and legal implications.

The topics covered and the depth of discussion should be tied to specific national science standards for various grade levels. Those standards that are addressed by aspects of this game should be highlighted in a teachers booklet to help teachers determine how best to implement this game as a learning module in their classroom. An example of where national science standards are incorporated in this game, for example, is the in the expert cards where STEM careers are presented with a description of the career and the required degree level.

Besides content knowledge, learning outcomes include reasoning skills, problem solving, planning, and budgeting. Additional outcomes include character building through sharing resources for the greater good, developing a sense of responsibility for the watershed, and feeling responsible to protect the community.

Next Steps

The version of this game presented herein is a first version that results from many hours of playtesting with graduate students, non-expert adults, and some high school students. More playtesting is needed to further refine gameplay and language. Students will be asked for feedback regarding what was difficult to understand, what they enjoyed, and what they learned. Teachers who allow this game to be tested in their class will be asked about ease of implementation, appropriateness of discussion points, and depth of learning. This game will be tested in many classrooms at multiple grade levels. Additional insight regarding the effectiveness of this game will be gained through assessing the retention of concepts months after the game was played. Continued collaboration with science teachers will be crucial for refining gameplay, game content, and accompanying materials

Acknowledgements

This project was funded by the Institute on the Environment at the University of Minnesota – grant #MS-0006-18. Thank you to the numerous play-testers who generously gave their time and suggestions and were an essential part of developing this game (listed alphabetically): Louis Corcoran, Eric Kehoe, Anna Luke, Joann Taijala, Taavi Taijala, and Yiran Tong.

Attachments

8 contaminant cards

32 contaminant-specific district cards

1 general district card

1 treatment card

18 expert cards

36 wild cards

Wild Cards

Draw a wild card at the start of your turn. After using wild cards, place in a discard pile. Shuffle discard pile when all the cards have been used and return the deck to play.

Experts Deck

Red cards are engineers, blue cards are other scientists. Hire these experts to unlock treatment methods and beat the spill.

Wild Cards

Draw a wild card at the start of your turn. After using wild cards, place in a discard pile. Shuffle discard pile when all the cards have been used and return the deck to play.

Experts Deck

Red cards are engineers, blue cards are other scientists. Hire these experts to unlock treatment methods and beat the spill.

Wild Cards

Draw a wild card at the start of your turn. After using wild cards, place in a discard pile. Shuffle discard pile when all the cards have been used and return the deck to play.

Experts Deck

Red cards are engineers, blue cards are other scientists. Hire these experts to unlock treatment methods and beat the spill.

Wild Cards

Draw a wild card at the start of your turn. After using wild cards, place in a discard pile. Shuffle discard pile when all the cards have been used and return the deck to play.

Experts Deck

Red cards are engineers, blue cards are other scientists. Hire these experts to unlock treatment methods and beat the spill.

Wild Cards

Draw a wild card at the start of your turn. After using wild cards, place in a discard pile. Shuffle discard pile when all the cards have been used and return the deck to play.

Experts Deck

Red cards are engineers, blue cards are other scientists. Hire these experts to unlock treatment methods and beat the spill.

Wild Cards

Draw a wild card at the start of your turn. After using wild cards, place in a discard pile. Shuffle discard pile when all the cards have been used and return the deck to play.

Experts Deck

Red cards are engineers, blue cards are other scientists. Hire these experts to unlock treatment methods and beat the spill.

Experts Deck

Red cards are engineers, blue cards are other scientists. Hire these experts to unlock treatment methods and beat the spill.

Wild Cards

Draw a wild card at the start of your turn. After using wild cards, place in a discard pile. Shuffle discard pile when all the cards have been used and return the deck to play.

Experts Deck

Red cards are engineers, blue cards are other scientists. Hire these experts to unlock treatment methods and beat the spill.

Wild Cards

Draw a wild card at the start of your turn. After using wild cards, place in a discard pile. Shuffle discard pile when all the cards have been used and return the deck to play.

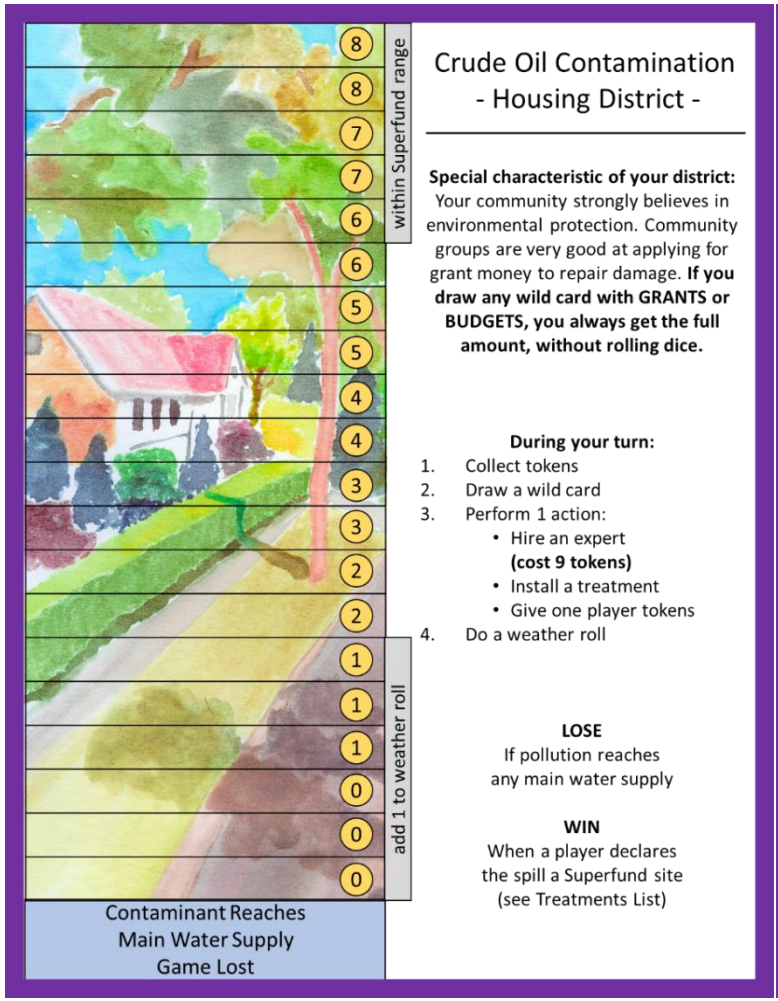

Crude Oil Contamination - Housing District -

Special characteristic of your district: Your community strongly believes in environmental protection. Community groups are very good at applying for grant money to repair damage. **If you draw any wild card with GRANTS or BUDGETS, you always get the full amount, without rolling dice.**

During your turn:

1. Collect tokens
2. Draw a wild card
3. Perform 1 action:
   - Hire an expert **(cost 9 tokens)**
   - Install a treatment
   - Give one player tokens
4. Do a weather roll

LOSE
If pollution reaches any main water supply

WIN
When a player declares the spill a Superfund site (see Treatments List)

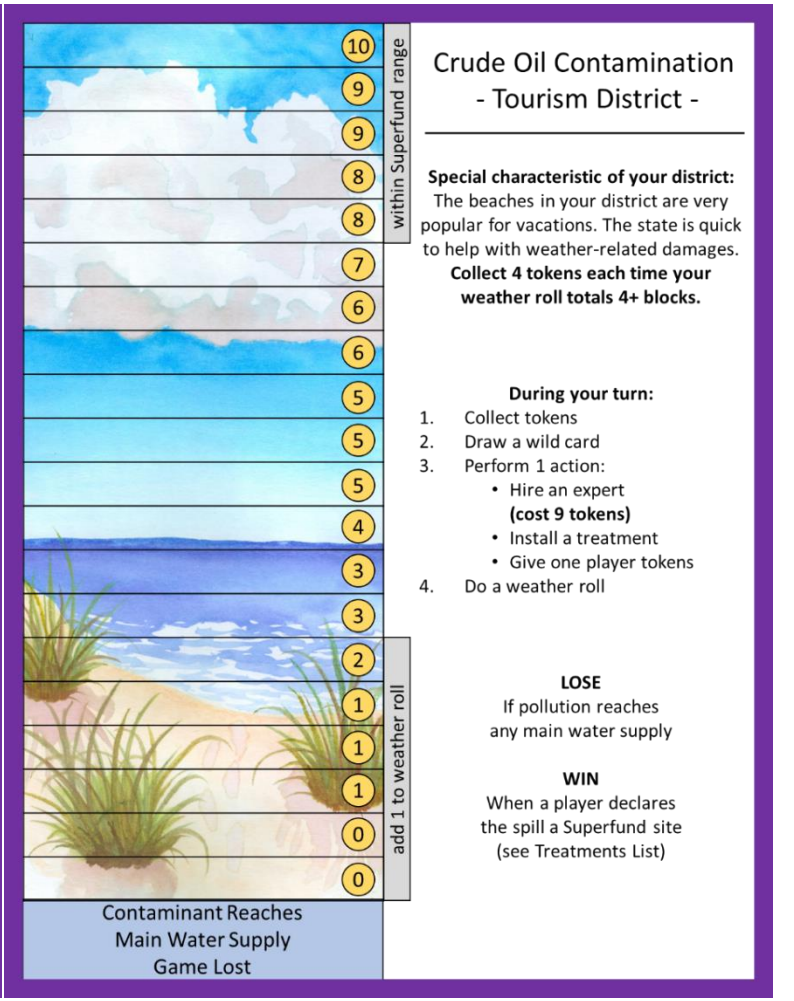

Crude Oil Contamination - Tourism District -

Special characteristic of your district: The beaches in your district are very popular for vacations. The state is quick to help with weather-related damages. **Collect 4 tokens each time your weather roll totals 4+ blocks.**

During your turn:

1. Collect tokens
2. Draw a wild card
3. Perform 1 action:
   - Hire an expert **(cost 9 tokens)**
   - Install a treatment
   - Give one player tokens
4. Do a weather roll

LOSE
If pollution reaches any main water supply

WIN
When a player declares the spill a Superfund site (see Treatments List)

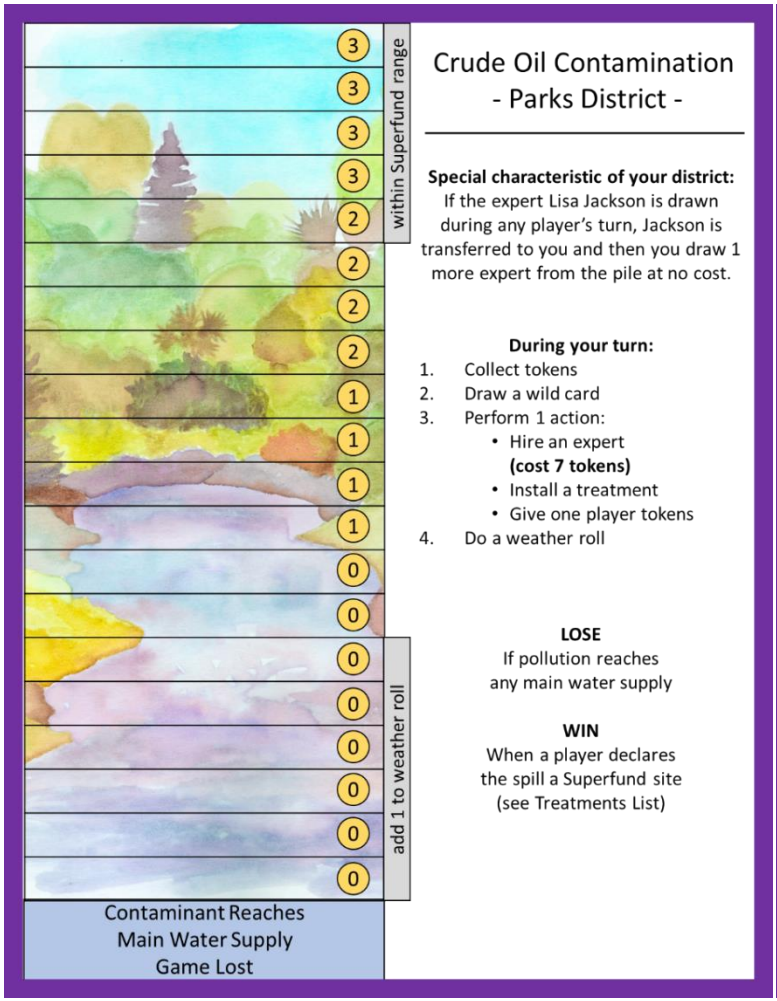
3
3
3
3
2
2
2
2
1
1
1
1
0
0
0
0
0
0
0
0
within Superfund range
add 1 to weather roll
Contaminant Reaches
Main Water Supply
Game Lost
Crude Oil Contamination
- Parks District -
Special characteristic of your district:
If the expert Lisa Jackson is drawn during any player's turn, Jackson is transferred to you and then you draw 1 more expert from the pile at no cost.
During your turn:
1. Collect tokens
2. Draw a wild card
3. Perform 1 action:
• Hire an expert
(cost 7 tokens)
• Install a treatment
• Give one player tokens
4. Do a weather roll
LOSE
If pollution reaches any main water supply
WIN
When a player declares the spill a Superfund site (see Treatments List)

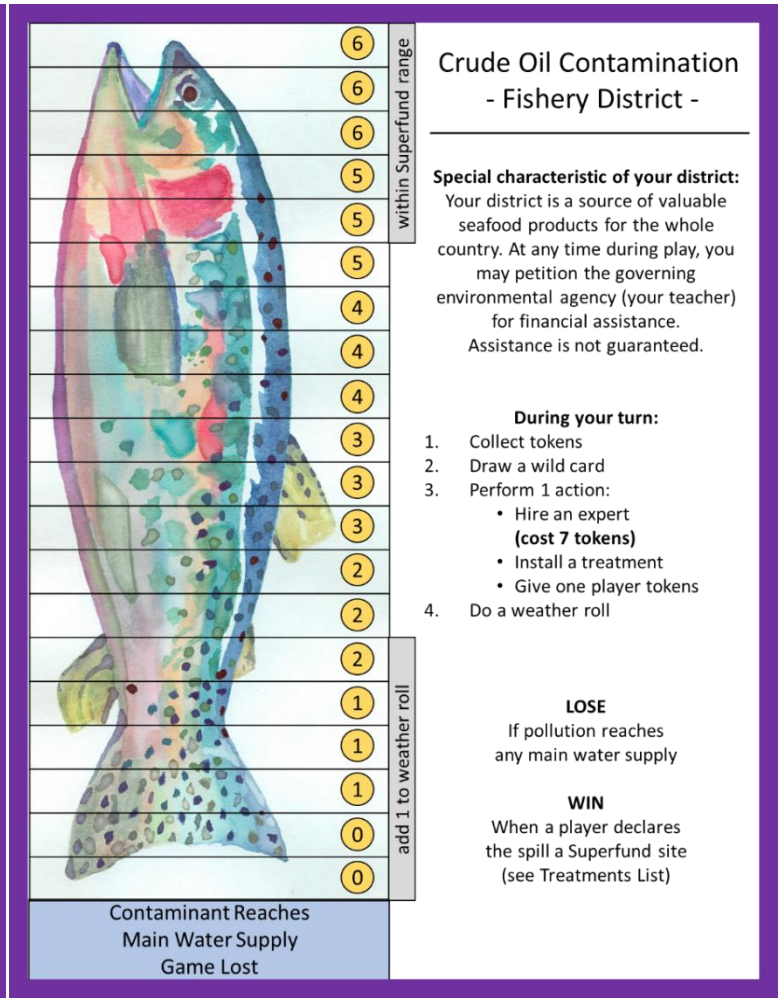
6
6
6
5
5
5
4
4
4
3
3
3
2
2
2
1
1
1
0
0
within Superfund range
add 1 to weather roll
Contaminant Reaches
Main Water Supply
Game Lost
Crude Oil Contamination
- Fishery District -
Special characteristic of your district:
Your district is a source of valuable seafood products for the whole country. At any time during play, you may petition the governing environmental agency (your teacher) for financial assistance.
Assistance is not guaranteed.
During your turn:
1. Collect tokens
2. Draw a wild card
3. Perform 1 action:
• Hire an expert
(cost 7 tokens)
• Install a treatment
• Give one player tokens
4. Do a weather roll
LOSE
If pollution reaches any main water supply
WIN
When a player declares the spill a Superfund site (see Treatments List)

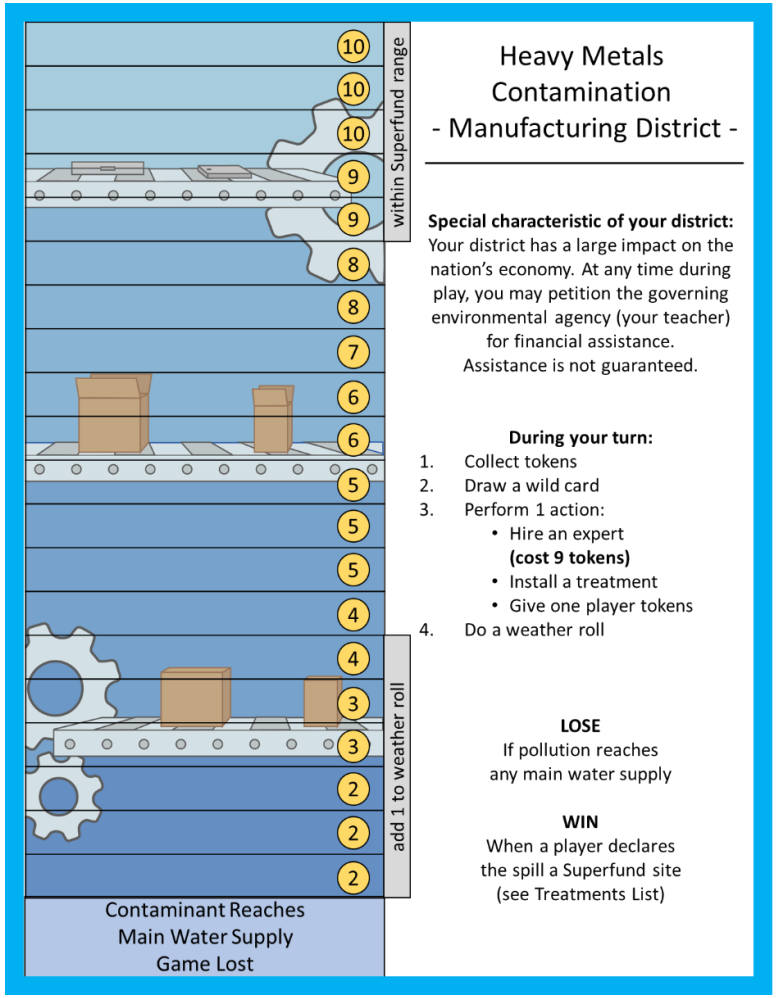

Heavy Metals Contamination - Manufacturing District -

Special characteristic of your district:
Your district has a large impact on the nation's economy. At any time during play, you may petition the governing environmental agency (your teacher) for financial assistance.
Assistance is not guaranteed.

During your turn:

1. Collect tokens
2. Draw a wild card
3. Perform 1 action:
   - Hire an expert **(cost 9 tokens)**
   - Install a treatment
   - Give one player tokens
4. Do a weather roll

LOSE
If pollution reaches any main water supply

WIN
When a player declares the spill a Superfund site (see Treatments List)

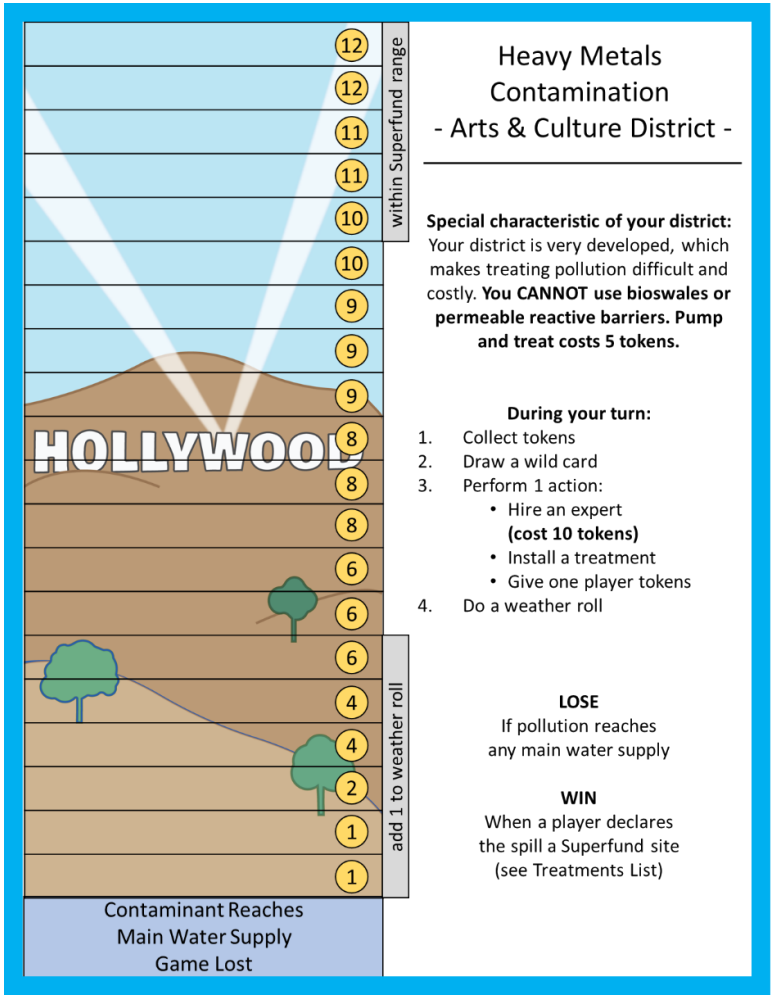

Heavy Metals Contamination - Arts & Culture District -

Special characteristic of your district:
Your district is very developed, which makes treating pollution difficult and costly. **You CANNOT use bioswales or permeable reactive barriers. Pump and treat costs 5 tokens.**

During your turn:

1. Collect tokens
2. Draw a wild card
3. Perform 1 action:
   - Hire an expert **(cost 10 tokens)**
   - Install a treatment
   - Give one player tokens
4. Do a weather roll

LOSE
If pollution reaches any main water supply

WIN
When a player declares the spill a Superfund site (see Treatments List)

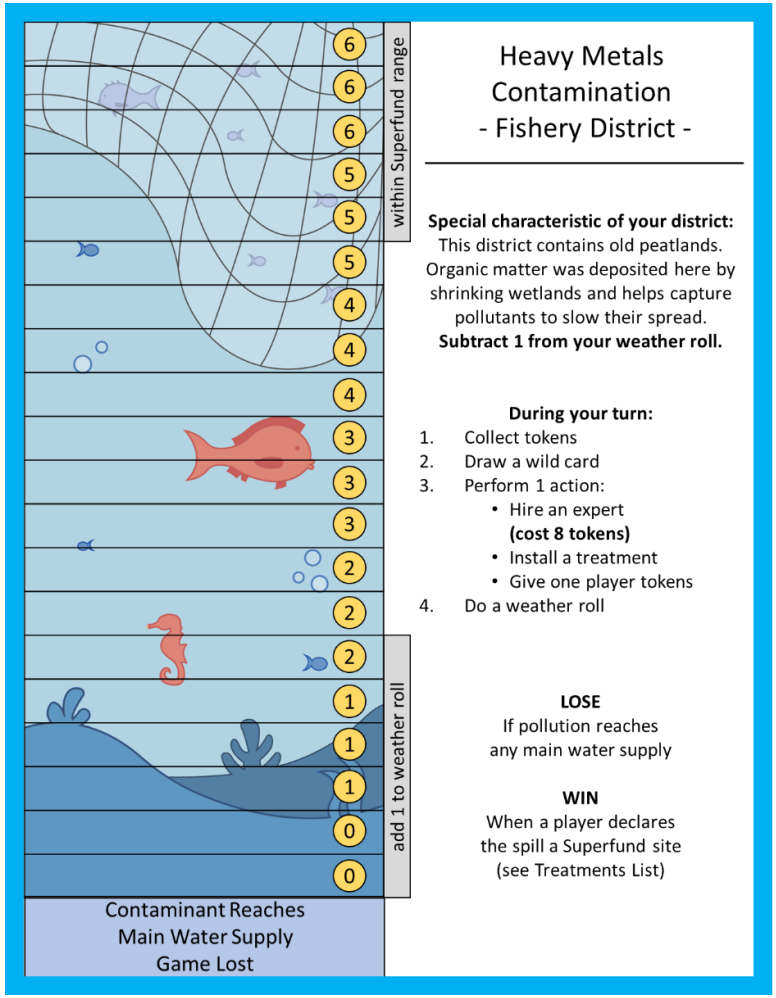

Heavy Metals Contamination - Fishery District -

Special characteristic of your district:
This district contains old peatlands. Organic matter was deposited here by shrinking wetlands and helps capture pollutants to slow their spread.
Subtract 1 from your weather roll.

During your turn:

1. Collect tokens
2. Draw a wild card
3. Perform 1 action:
   - Hire an expert **(cost 8 tokens)**
   - Install a treatment
   - Give one player tokens
4. Do a weather roll

LOSE
If pollution reaches any main water supply

WIN
When a player declares the spill a Superfund site (see Treatments List)

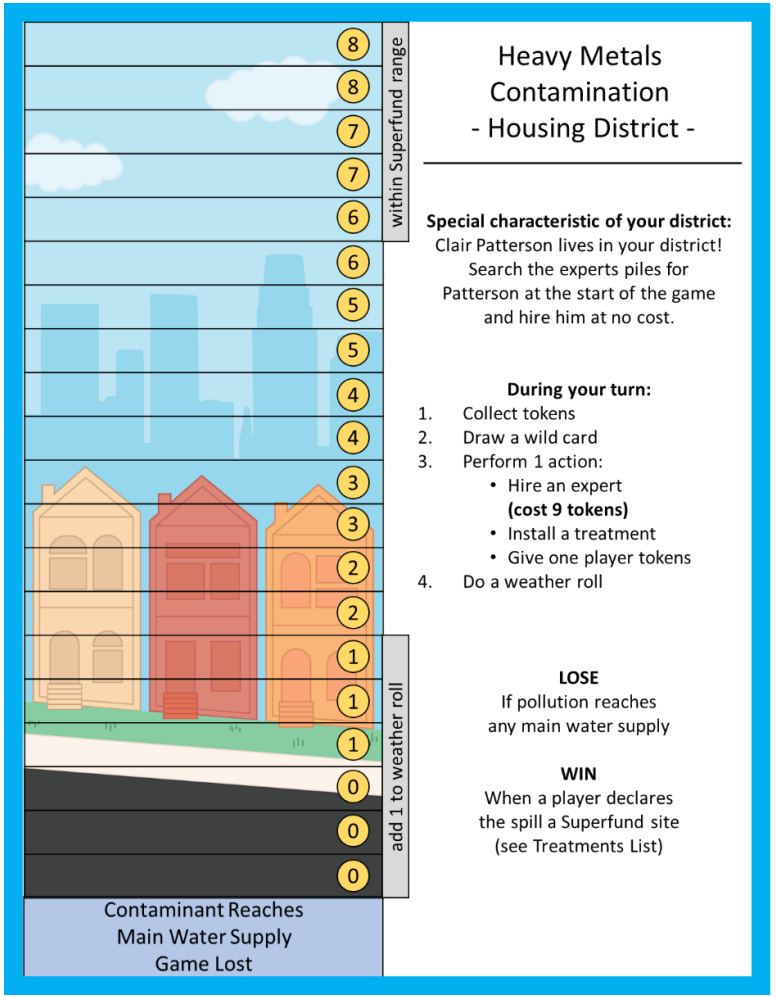

Heavy Metals Contamination - Housing District -

Special characteristic of your district:
Clair Patterson lives in your district! Search the experts piles for Patterson at the start of the game and hire him at no cost.

During your turn:

1. Collect tokens
2. Draw a wild card
3. Perform 1 action:
   - Hire an expert **(cost 9 tokens)**
   - Install a treatment
   - Give one player tokens
4. Do a weather roll

LOSE
If pollution reaches any main water supply

WIN
When a player declares the spill a Superfund site (see Treatments List)

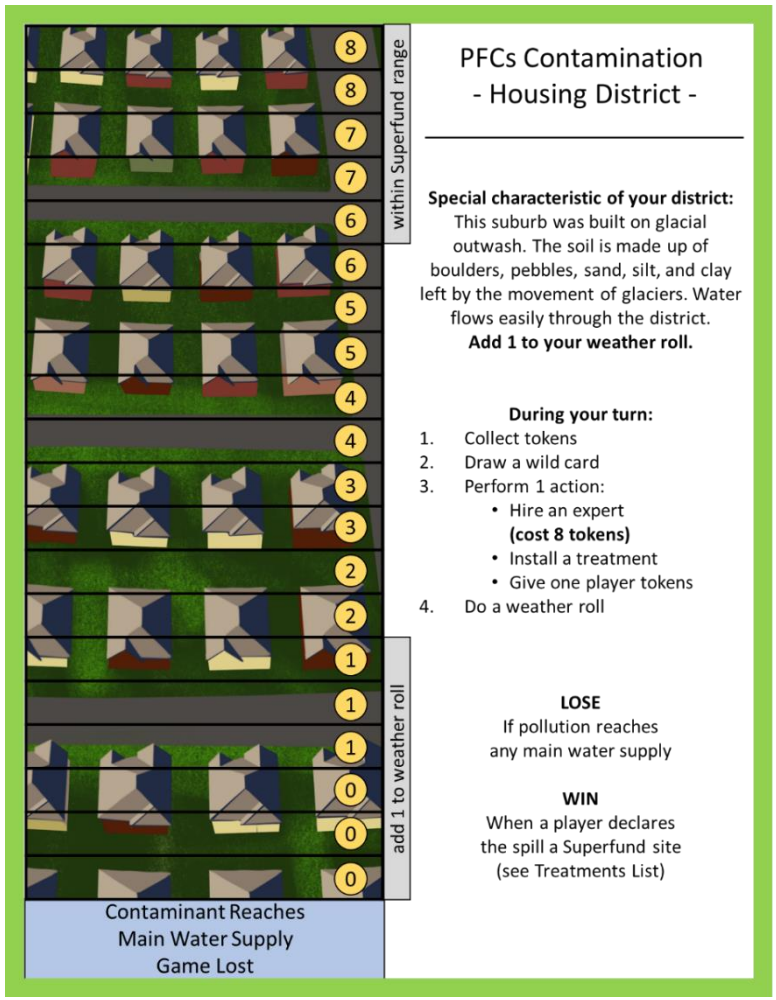

PFCs Contamination
- Housing District -

Special characteristic of your district:
This suburb was built on glacial outwash. The soil is made up of boulders, pebbles, sand, silt, and clay left by the movement of glaciers. Water flows easily through the district.
Add 1 to your weather roll.

During your turn:

1. Collect tokens
2. Draw a wild card
3. Perform 1 action:
   - Hire an expert **(cost 8 tokens)**
   - Install a treatment
   - Give one player tokens
4. Do a weather roll

LOSE
If pollution reaches any main water supply

WIN
When a player declares the spill a Superfund site (see Treatments List)

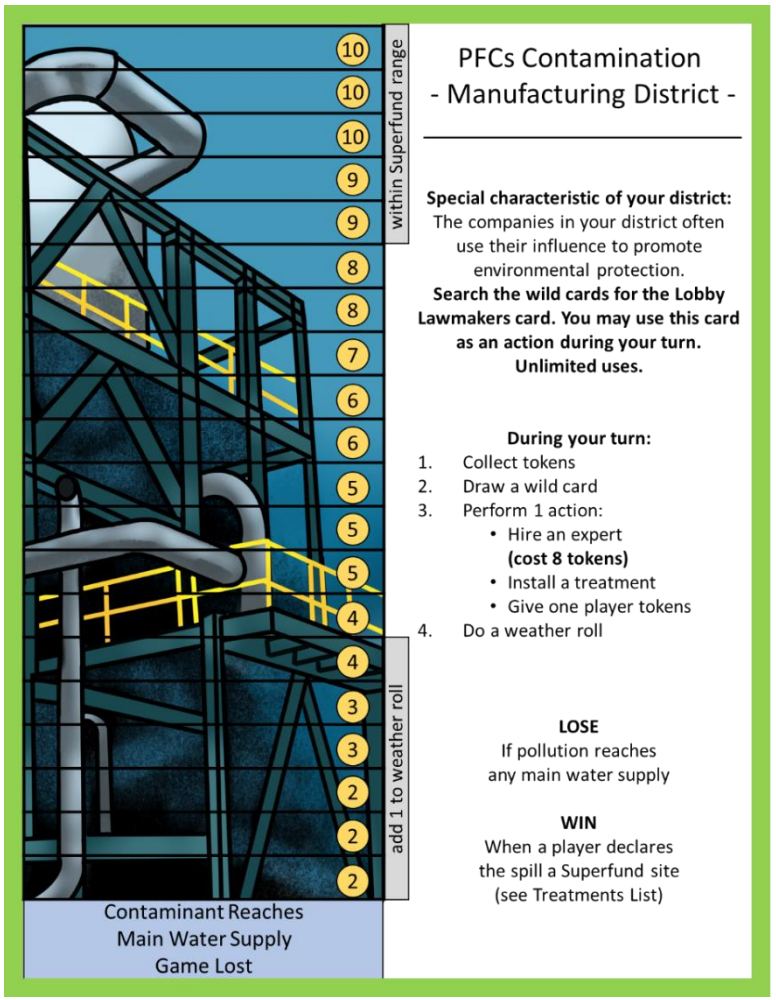

PFCs Contamination
- Manufacturing District -

Special characteristic of your district:
The companies in your district often use their influence to promote environmental protection.
Search the wild cards for the Lobby Lawmakers card. You may use this card as an action during your turn. Unlimited uses.

During your turn:

1. Collect tokens
2. Draw a wild card
3. Perform 1 action:
   - Hire an expert **(cost 8 tokens)**
   - Install a treatment
   - Give one player tokens
4. Do a weather roll

LOSE
If pollution reaches any main water supply

WIN
When a player declares the spill a Superfund site (see Treatments List)

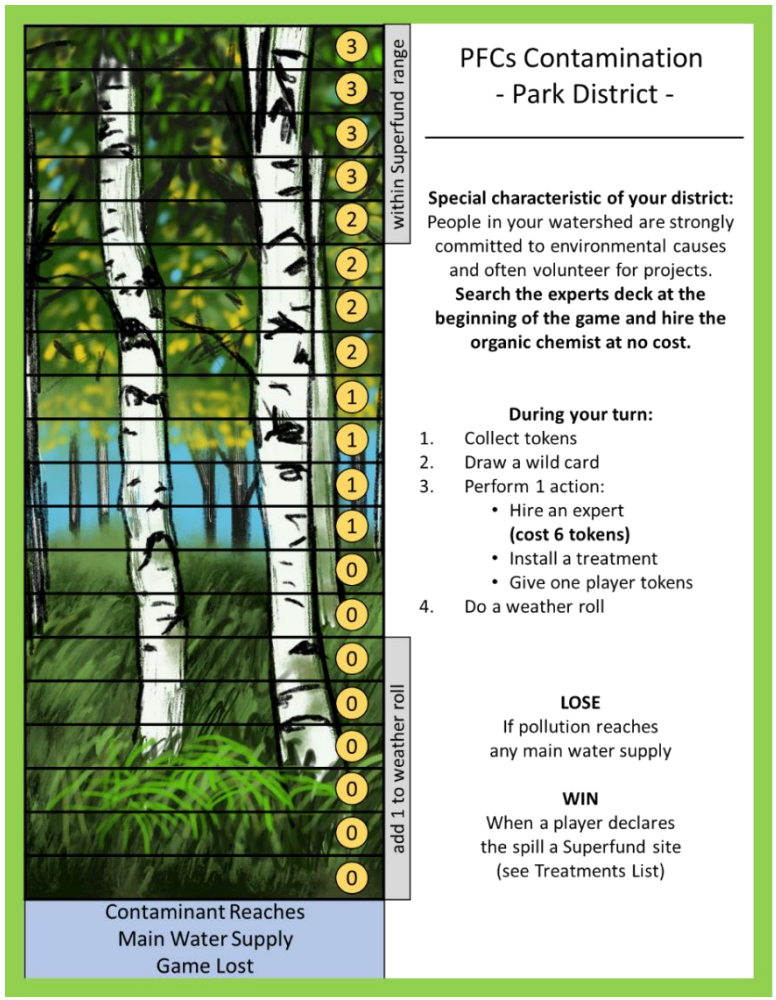

PFCs Contamination
- Park District -

Special characteristic of your district:
People in your watershed are strongly committed to environmental causes and often volunteer for projects.
Search the experts deck at the beginning of the game and hire the organic chemist at no cost.

During your turn:

1. Collect tokens
2. Draw a wild card
3. Perform 1 action:
   - Hire an expert **(cost 6 tokens)**
   - Install a treatment
   - Give one player tokens
4. Do a weather roll

LOSE
If pollution reaches any main water supply

WIN
When a player declares the spill a Superfund site (see Treatments List)

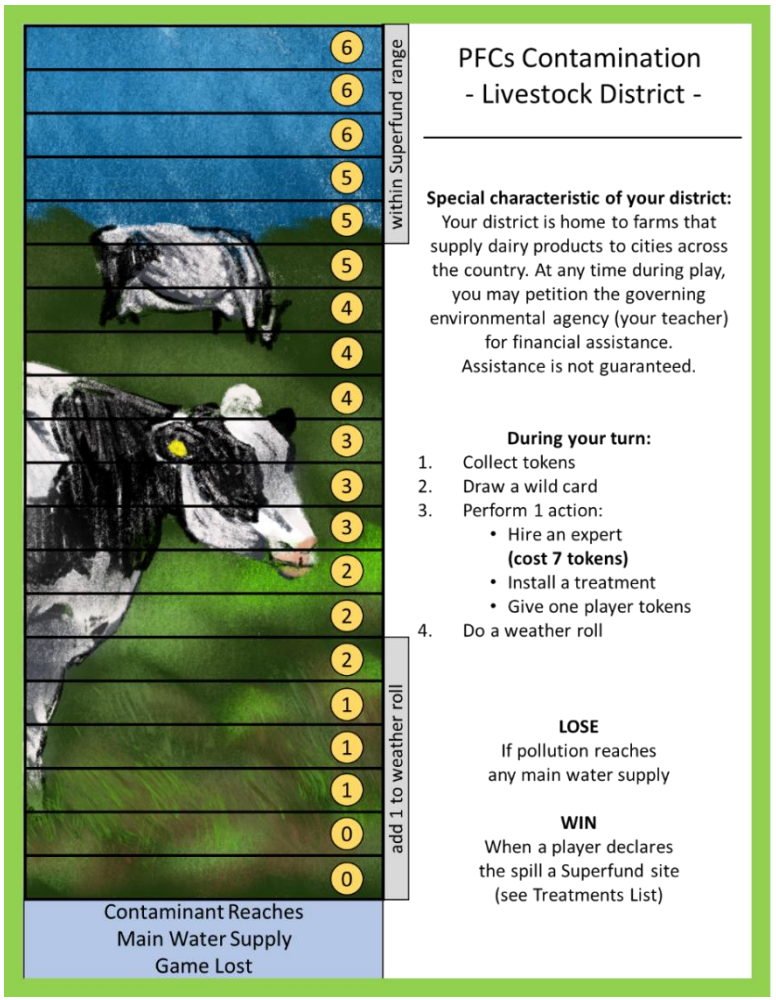

PFCs Contamination
- Livestock District -

Special characteristic of your district:
Your district is home to farms that supply dairy products to cities across the country. At any time during play, you may petition the governing environmental agency (your teacher) for financial assistance.
Assistance is not guaranteed.

During your turn:

1. Collect tokens
2. Draw a wild card
3. Perform 1 action:
   - Hire an expert **(cost 7 tokens)**
   - Install a treatment
   - Give one player tokens
4. Do a weather roll

LOSE
If pollution reaches any main water supply

WIN
When a player declares the spill a Superfund site (see Treatments List)

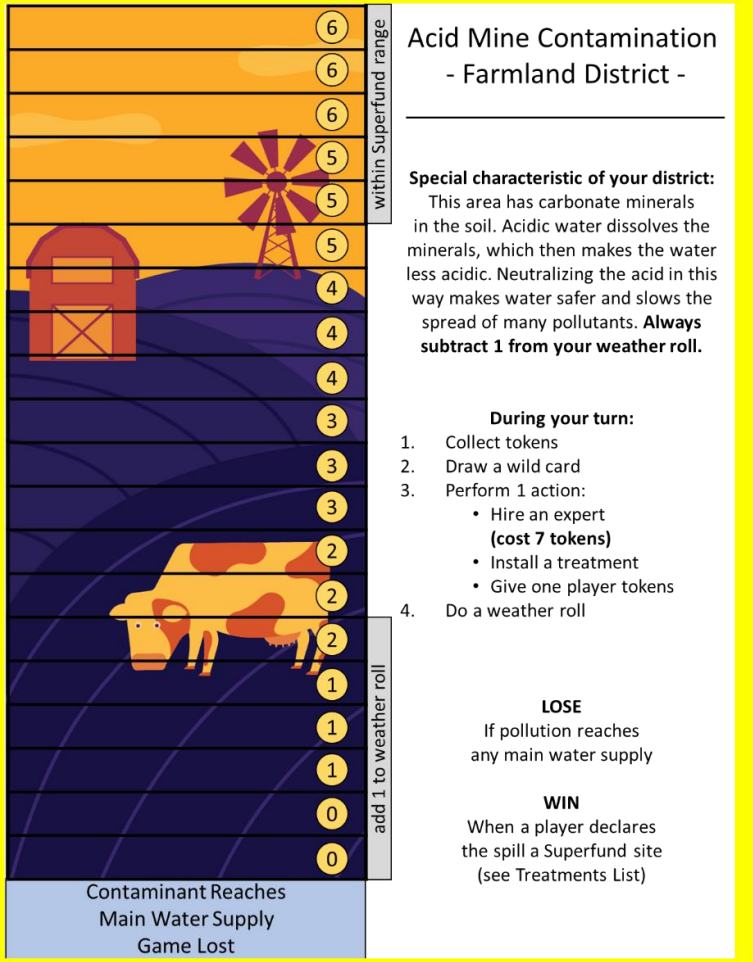

Acid Mine Contamination - Farmland District -

Special characteristic of your district:
This area has carbonate minerals in the soil. Acidic water dissolves the minerals, which then makes the water less acidic. Neutralizing the acid in this way makes water safer and slows the spread of many pollutants. **Always subtract 1 from your weather roll.**

During your turn:

1. Collect tokens
2. Draw a wild card
3. Perform 1 action:
   - Hire an expert **(cost 7 tokens)**
   - Install a treatment
   - Give one player tokens
4. Do a weather roll

LOSE
If pollution reaches any main water supply

WIN
When a player declares the spill a Superfund site (see Treatments List)

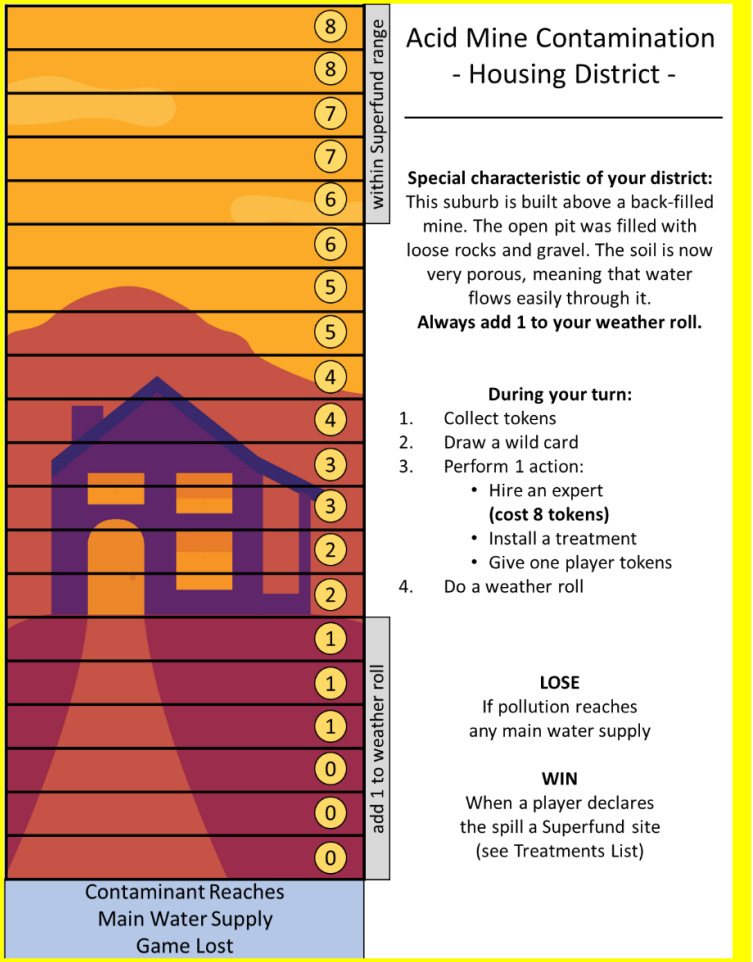

Acid Mine Contamination - Housing District -

Special characteristic of your district:
This suburb is built above a back-filled mine. The open pit was filled with loose rocks and gravel. The soil is now very porous, meaning that water flows easily through it.
Always add 1 to your weather roll.

During your turn:

1. Collect tokens
2. Draw a wild card
3. Perform 1 action:
   - Hire an expert **(cost 8 tokens)**
   - Install a treatment
   - Give one player tokens
4. Do a weather roll

LOSE
If pollution reaches any main water supply

WIN
When a player declares the spill a Superfund site (see Treatments List)

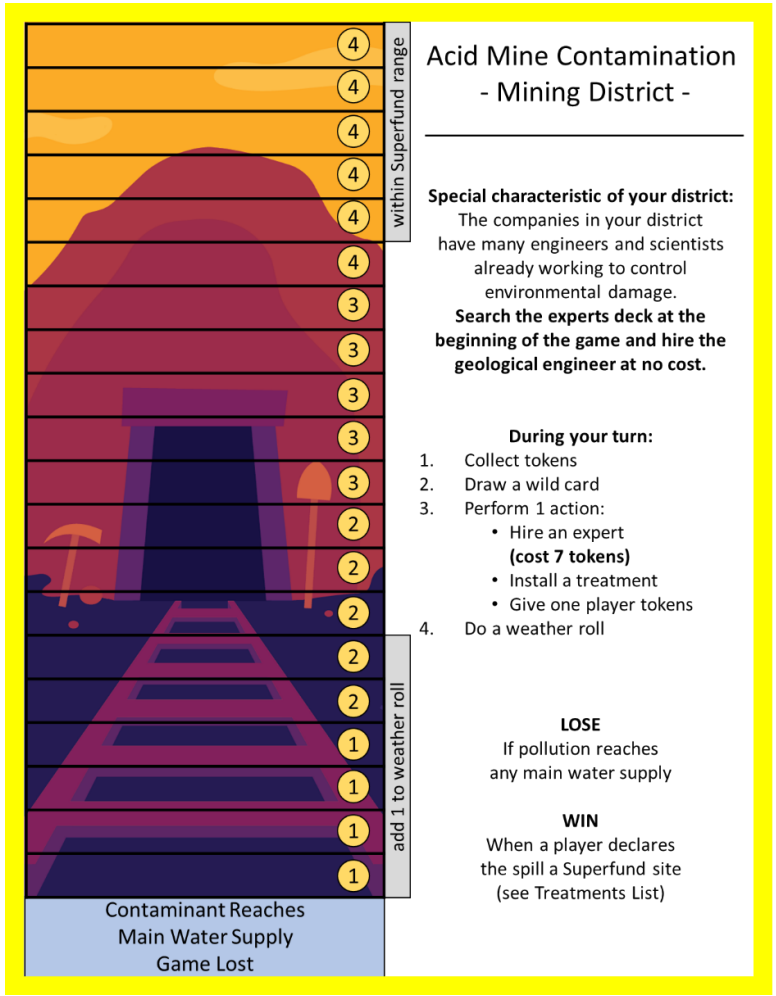

Acid Mine Contamination
- Mining District -

Special characteristic of your district:
The companies in your district have many engineers and scientists already working to control environmental damage.
Search the experts deck at the beginning of the game and hire the geological engineer at no cost.

During your turn:

1. Collect tokens
2. Draw a wild card
3. Perform 1 action:
   - Hire an expert **(cost 7 tokens)**
   - Install a treatment
   - Give one player tokens
4. Do a weather roll

LOSE
If pollution reaches any main water supply

WIN
When a player declares the spill a Superfund site (see Treatments List)

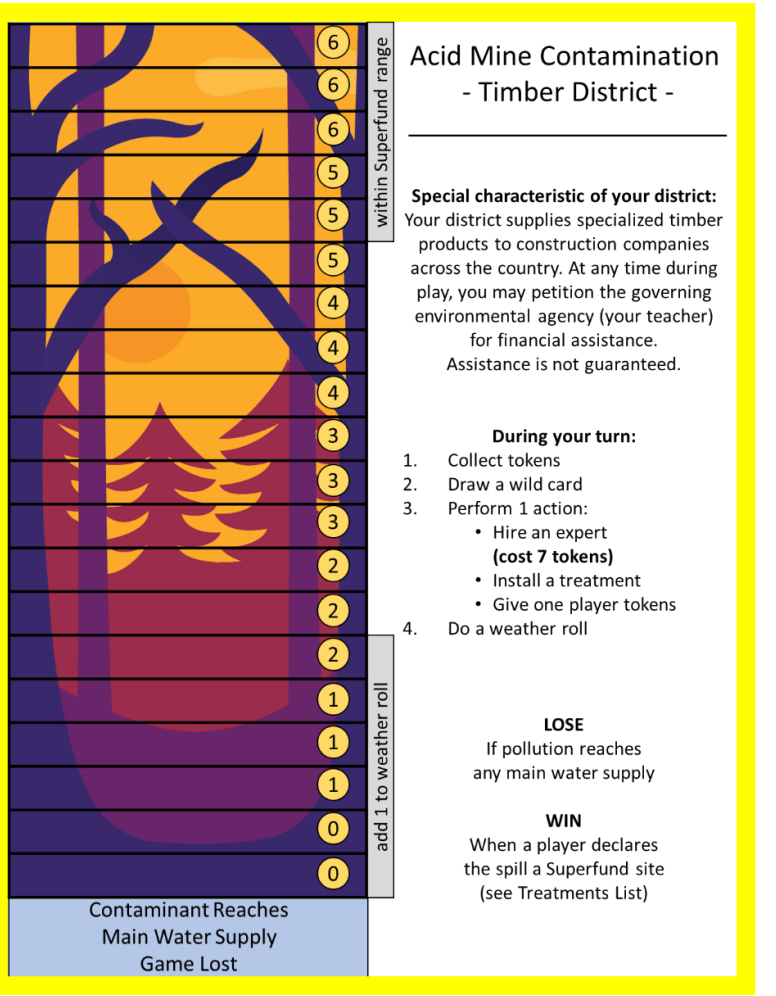

Acid Mine Contamination
- Timber District -

Special characteristic of your district:
Your district supplies specialized timber products to construction companies across the country. At any time during play, you may petition the governing environmental agency (your teacher) for financial assistance.
Assistance is not guaranteed.

During your turn:

1. Collect tokens
2. Draw a wild card
3. Perform 1 action:
   - Hire an expert **(cost 7 tokens)**
   - Install a treatment
   - Give one player tokens
4. Do a weather roll

LOSE
If pollution reaches any main water supply

WIN
When a player declares the spill a Superfund site (see Treatments List)

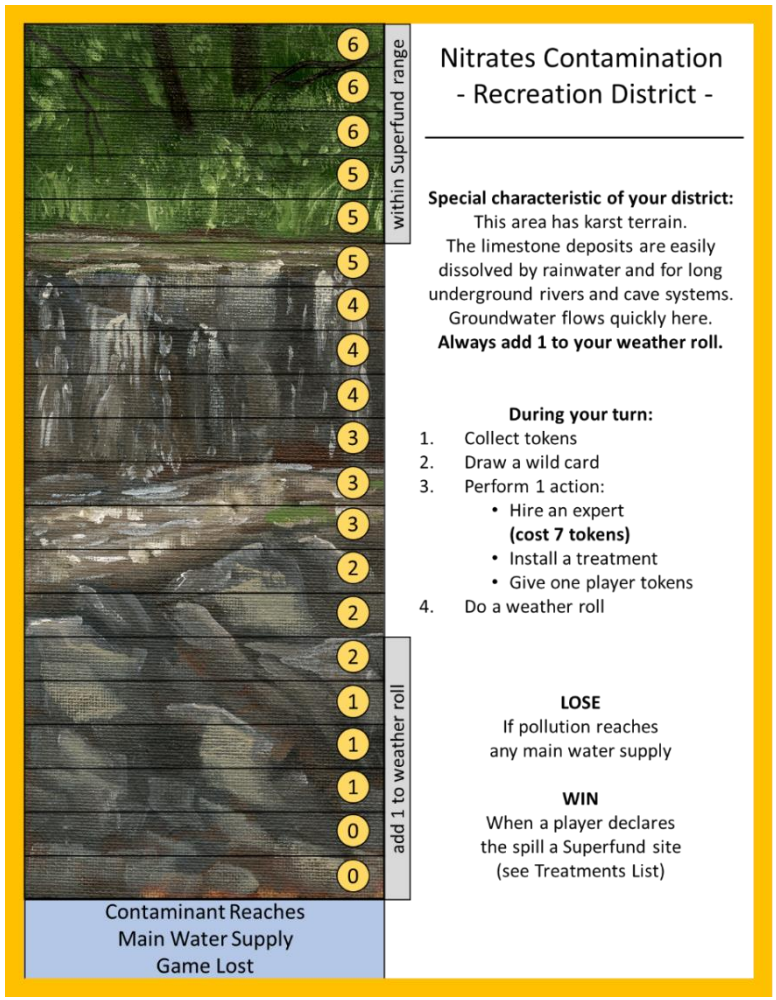

Nitrates Contamination - Recreation District -

Special characteristic of your district:
This area has karst terrain. The limestone deposits are easily dissolved by rainwater and for long underground rivers and cave systems. Groundwater flows quickly here.
Always add 1 to your weather roll.

During your turn:

1. Collect tokens
2. Draw a wild card
3. Perform 1 action:
   - Hire an expert **(cost 7 tokens)**
   - Install a treatment
   - Give one player tokens
4. Do a weather roll

LOSE
If pollution reaches any main water supply

WIN
When a player declares the spill a Superfund site (see Treatments List)

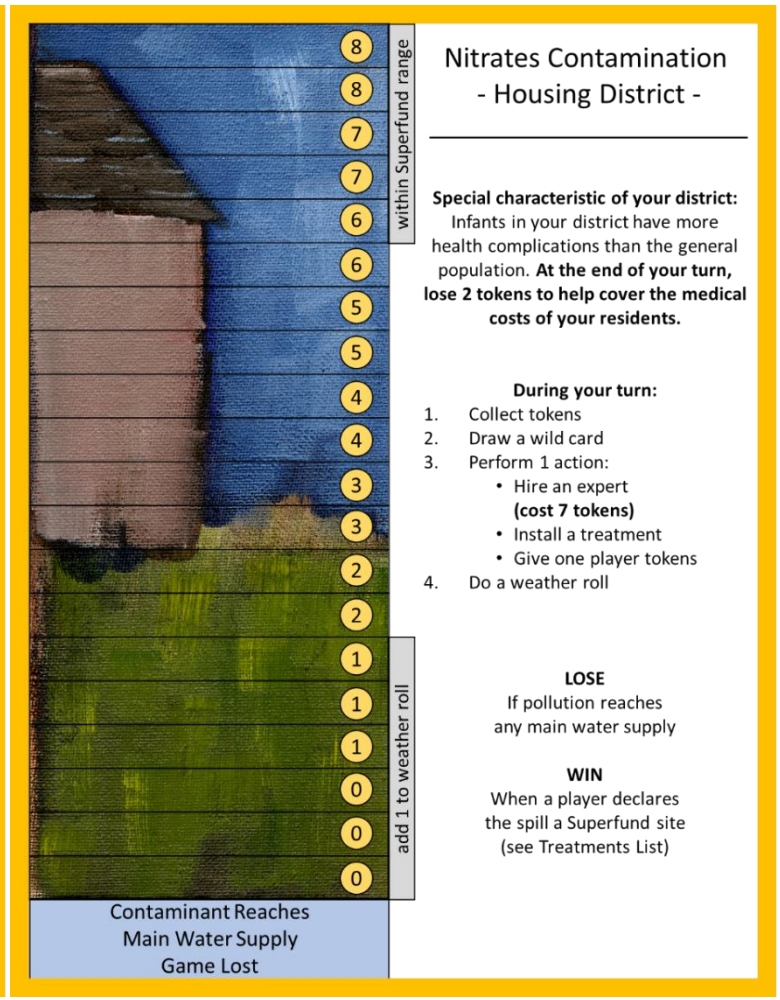

Nitrates Contamination - Housing District -

Special characteristic of your district:
Infants in your district have more health complications than the general population. **At the end of your turn, lose 2 tokens to help cover the medical costs of your residents.**

During your turn:

1. Collect tokens
2. Draw a wild card
3. Perform 1 action:
   - Hire an expert **(cost 7 tokens)**
   - Install a treatment
   - Give one player tokens
4. Do a weather roll

LOSE
If pollution reaches any main water supply

WIN
When a player declares the spill a Superfund site (see Treatments List)

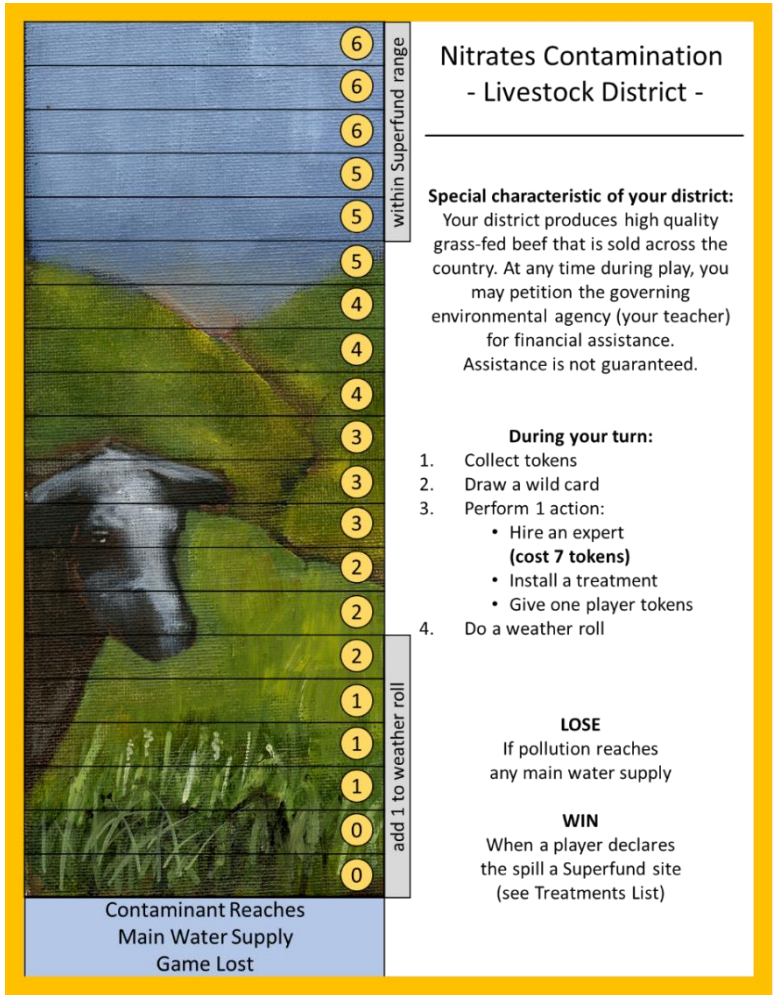

Nitrates Contamination
- Livestock District -

Special characteristic of your district:
Your district produces high quality grass-fed beef that is sold across the country. At any time during play, you may petition the governing environmental agency (your teacher) for financial assistance.
Assistance is not guaranteed.

During your turn:

1. Collect tokens
2. Draw a wild card
3. Perform 1 action:
   - Hire an expert **(cost 7 tokens)**
   - Install a treatment
   - Give one player tokens
4. Do a weather roll

LOSE
If pollution reaches any main water supply

WIN
When a player declares the spill a Superfund site (see Treatments List)

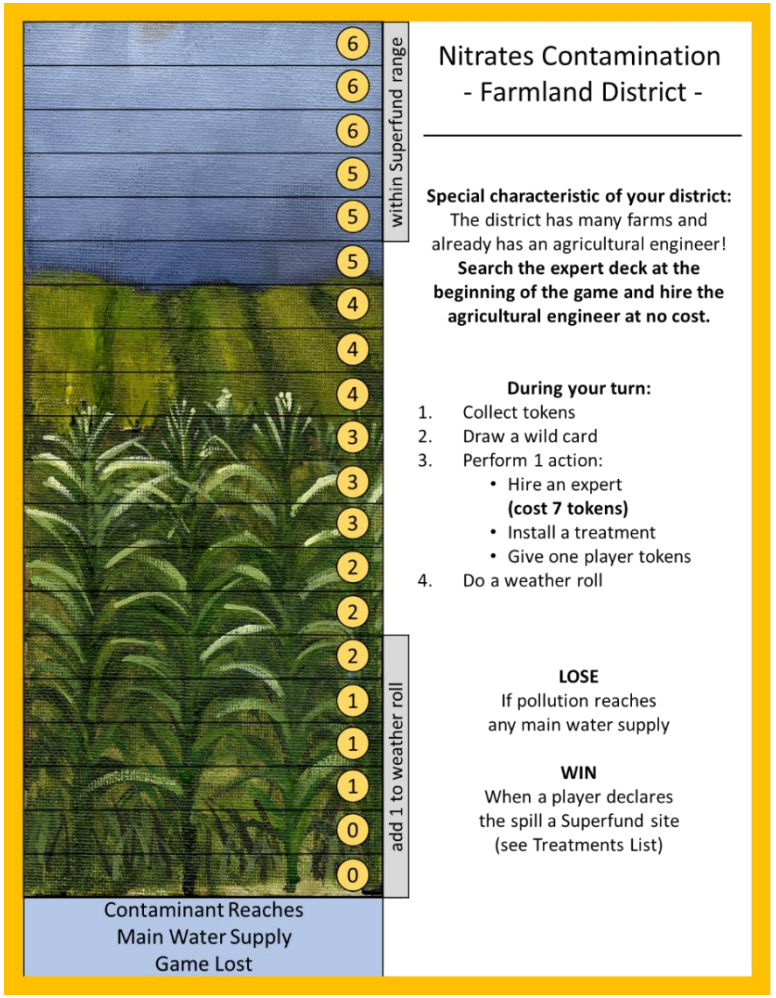

Nitrates Contamination
- Farmland District -

Special characteristic of your district:
The district has many farms and already has an agricultural engineer!
Search the expert deck at the beginning of the game and hire the agricultural engineer at no cost.

During your turn:

1. Collect tokens
2. Draw a wild card
3. Perform 1 action:
   - Hire an expert **(cost 7 tokens)**
   - Install a treatment
   - Give one player tokens
4. Do a weather roll

LOSE
If pollution reaches any main water supply

WIN
When a player declares the spill a Superfund site (see Treatments List)

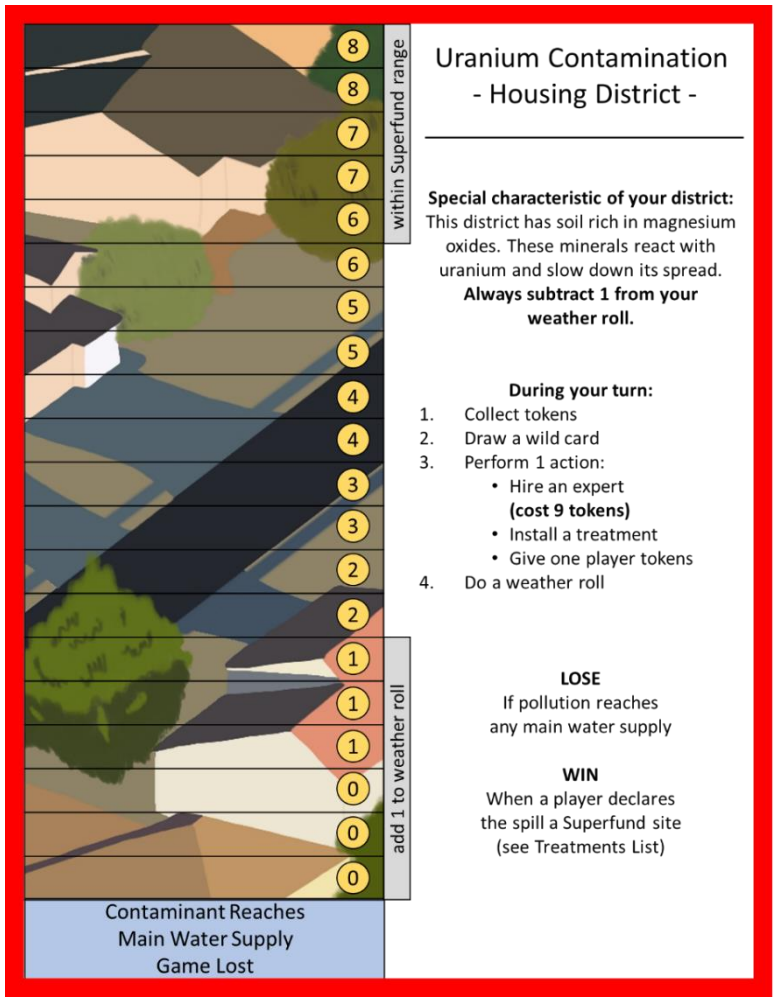

Uranium Contamination - Housing District -

Special characteristic of your district:
This district has soil rich in magnesium oxides. These minerals react with uranium and slow down its spread. **Always subtract 1 from your weather roll.**

During your turn:

1. Collect tokens
2. Draw a wild card
3. Perform 1 action:
   - Hire an expert **(cost 9 tokens)**
   - Install a treatment
   - Give one player tokens
4. Do a weather roll

LOSE
If pollution reaches any main water supply

WIN
When a player declares the spill a Superfund site (see Treatments List)

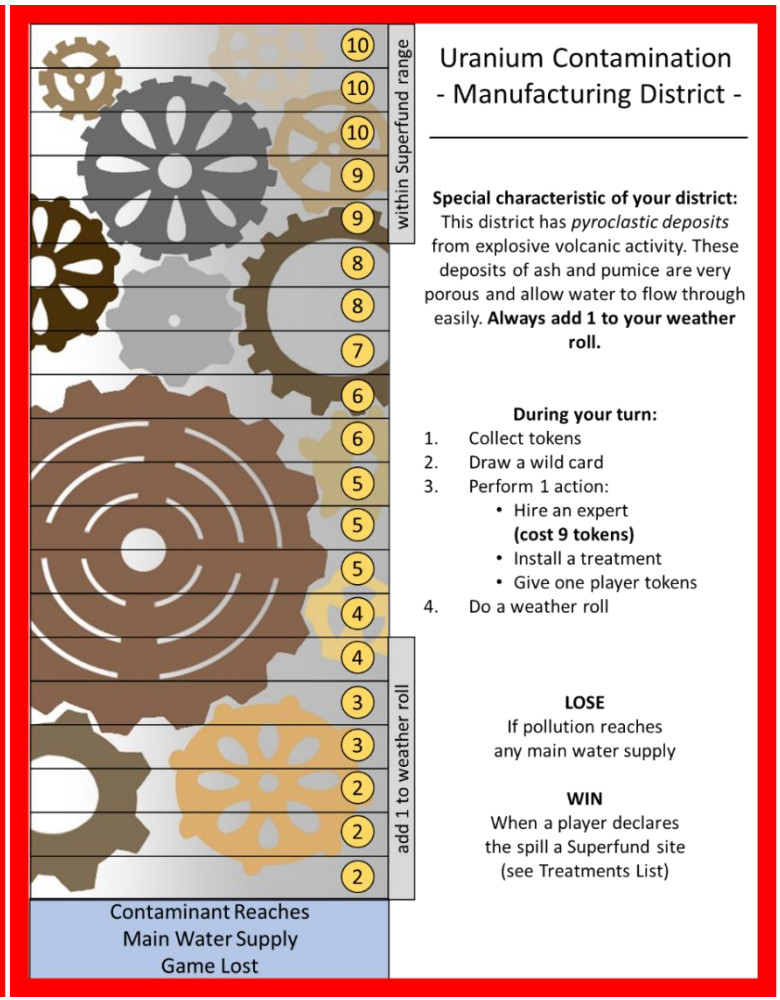

Uranium Contamination - Manufacturing District -

Special characteristic of your district:
This district has *pyroclastic deposits* from explosive volcanic activity. These deposits of ash and pumice are very porous and allow water to flow through easily. **Always add 1 to your weather roll.**

During your turn:

1. Collect tokens
2. Draw a wild card
3. Perform 1 action:
   - Hire an expert **(cost 9 tokens)**
   - Install a treatment
   - Give one player tokens
4. Do a weather roll

LOSE
If pollution reaches any main water supply

WIN
When a player declares the spill a Superfund site (see Treatments List)

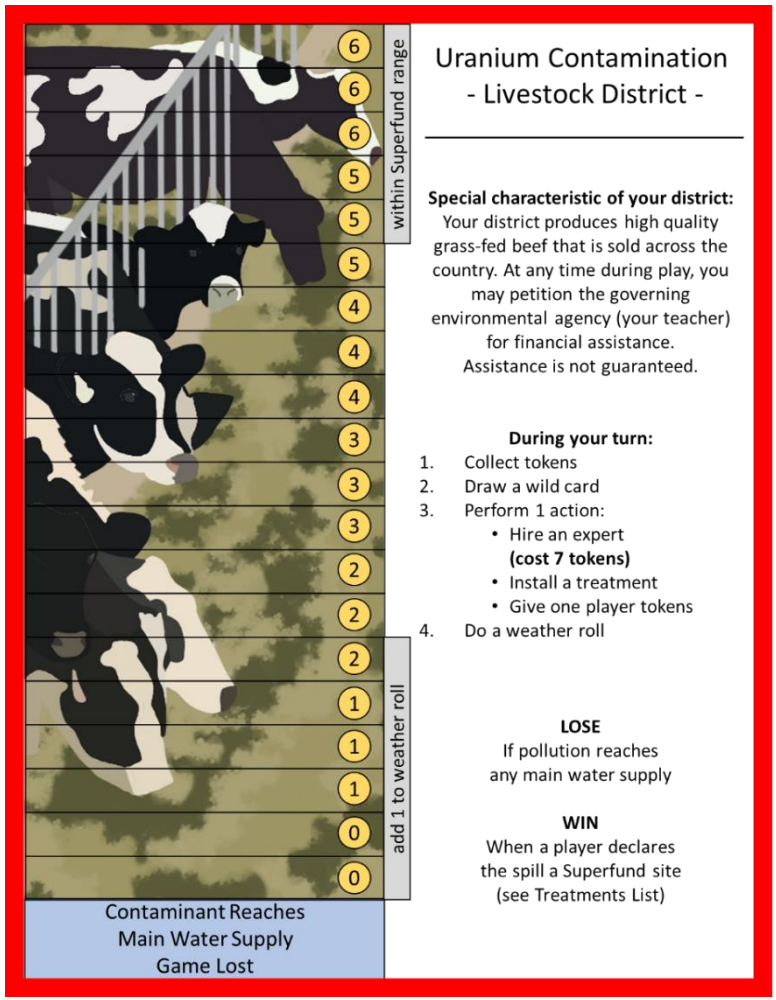

Uranium Contamination - Livestock District -

Special characteristic of your district:
Your district produces high quality grass-fed beef that is sold across the country. At any time during play, you may petition the governing environmental agency (your teacher) for financial assistance. Assistance is not guaranteed.

During your turn:

1. Collect tokens
2. Draw a wild card
3. Perform 1 action:
   - Hire an expert **(cost 7 tokens)**
   - Install a treatment
   - Give one player tokens
4. Do a weather roll

LOSE
If pollution reaches any main water supply

WIN
When a player declares the spill a Superfund site (see Treatments List)

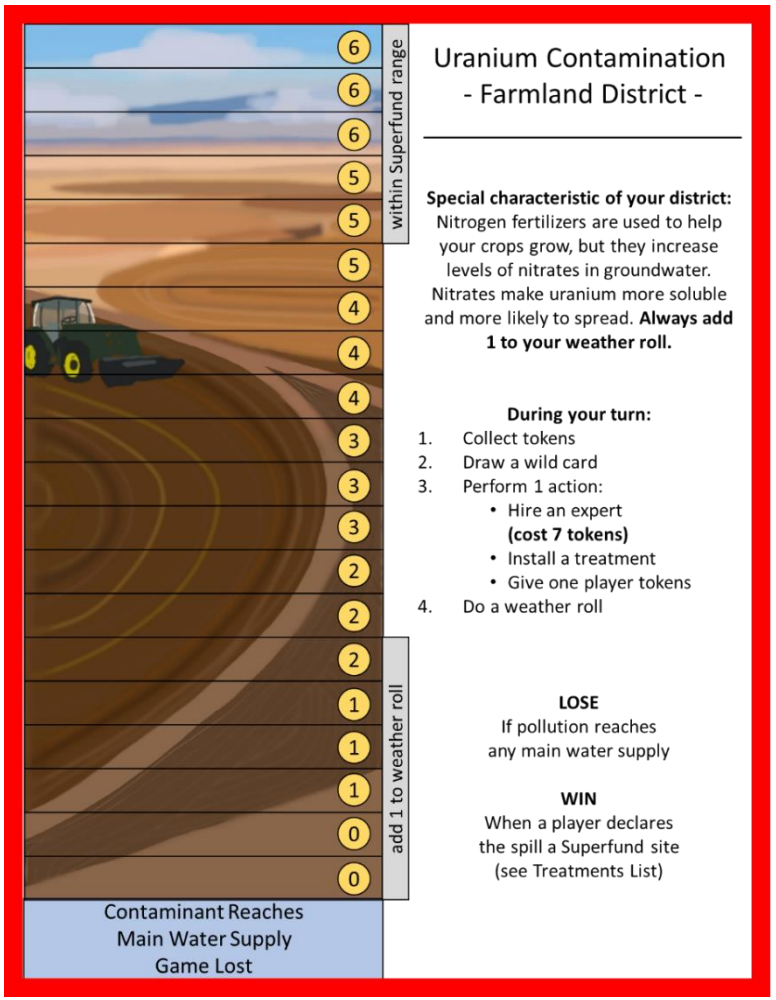

Uranium Contamination - Farmland District -

Special characteristic of your district:
Nitrogen fertilizers are used to help your crops grow, but they increase levels of nitrates in groundwater. Nitrates make uranium more soluble and more likely to spread. **Always add 1 to your weather roll.**

During your turn:

1. Collect tokens
2. Draw a wild card
3. Perform 1 action:
   - Hire an expert **(cost 7 tokens)**
   - Install a treatment
   - Give one player tokens
4. Do a weather roll

LOSE
If pollution reaches any main water supply

WIN
When a player declares the spill a Superfund site (see Treatments List)

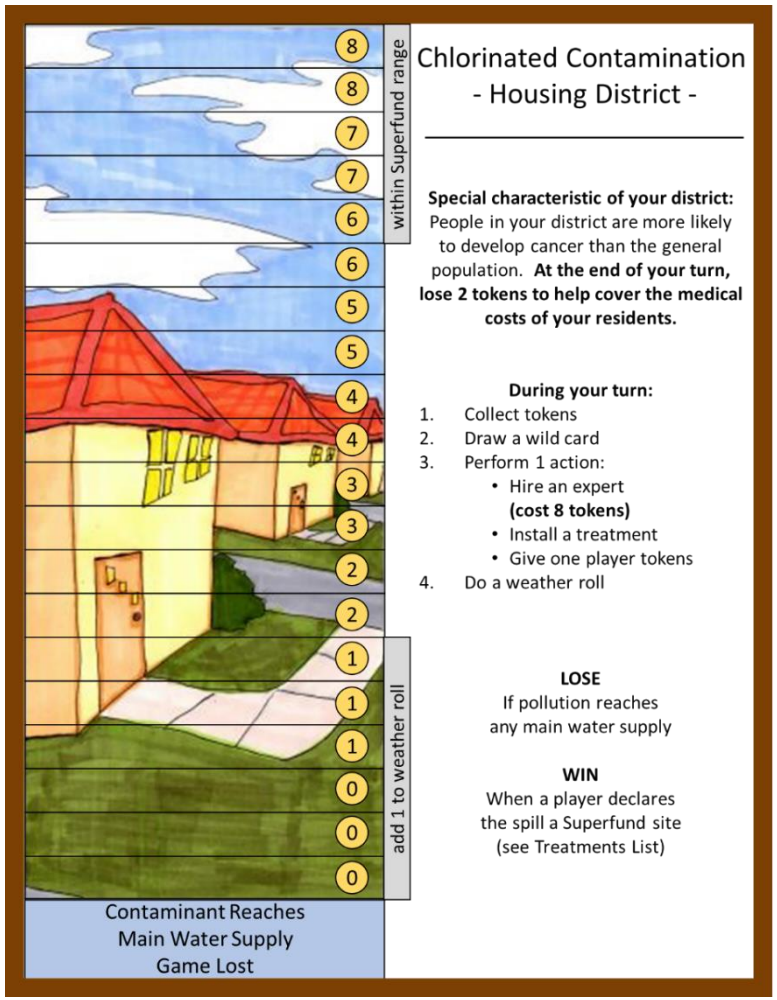

Chlorinated Contamination - Housing District -

Special characteristic of your district: People in your district are more likely to develop cancer than the general population. **At the end of your turn, lose 2 tokens to help cover the medical costs of your residents.**

During your turn:

1. Collect tokens
2. Draw a wild card
3. Perform 1 action:
   - Hire an expert **(cost 8 tokens)**
   - Install a treatment
   - Give one player tokens
4. Do a weather roll

LOSE
If pollution reaches any main water supply

WIN
When a player declares the spill a Superfund site (see Treatments List)

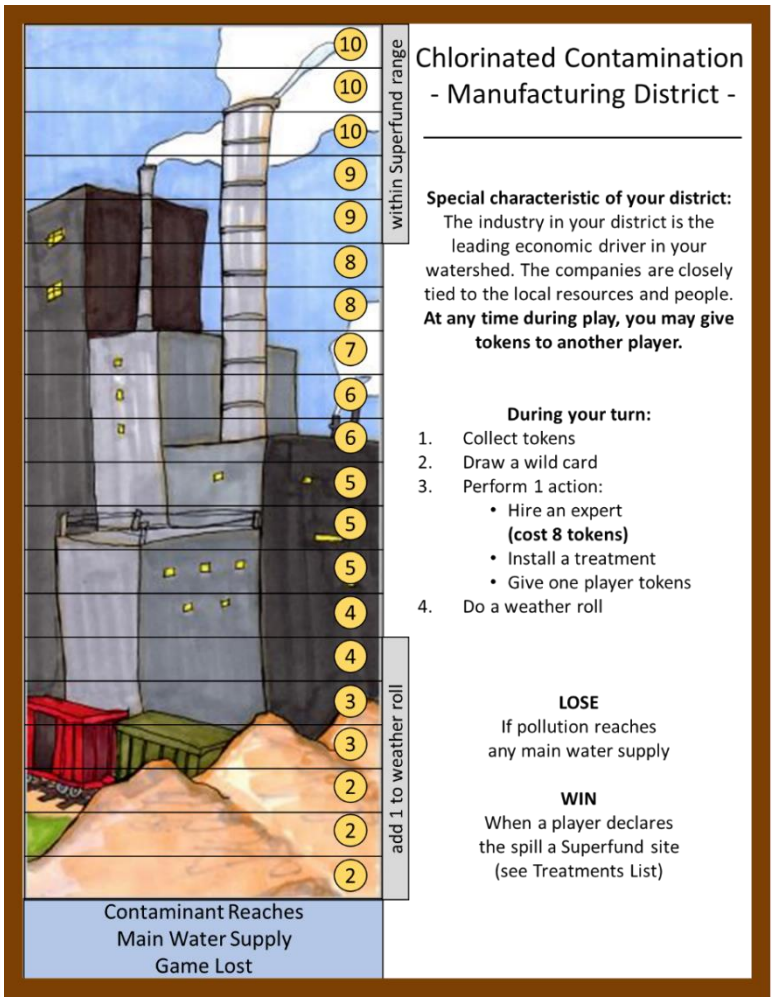

Chlorinated Contamination - Manufacturing District -

Special characteristic of your district: The industry in your district is the leading economic driver in your watershed. The companies are closely tied to the local resources and people. **At any time during play, you may give tokens to another player.**

During your turn:

1. Collect tokens
2. Draw a wild card
3. Perform 1 action:
   - Hire an expert **(cost 8 tokens)**
   - Install a treatment
   - Give one player tokens
4. Do a weather roll

LOSE
If pollution reaches any main water supply

WIN
When a player declares the spill a Superfund site (see Treatments List)

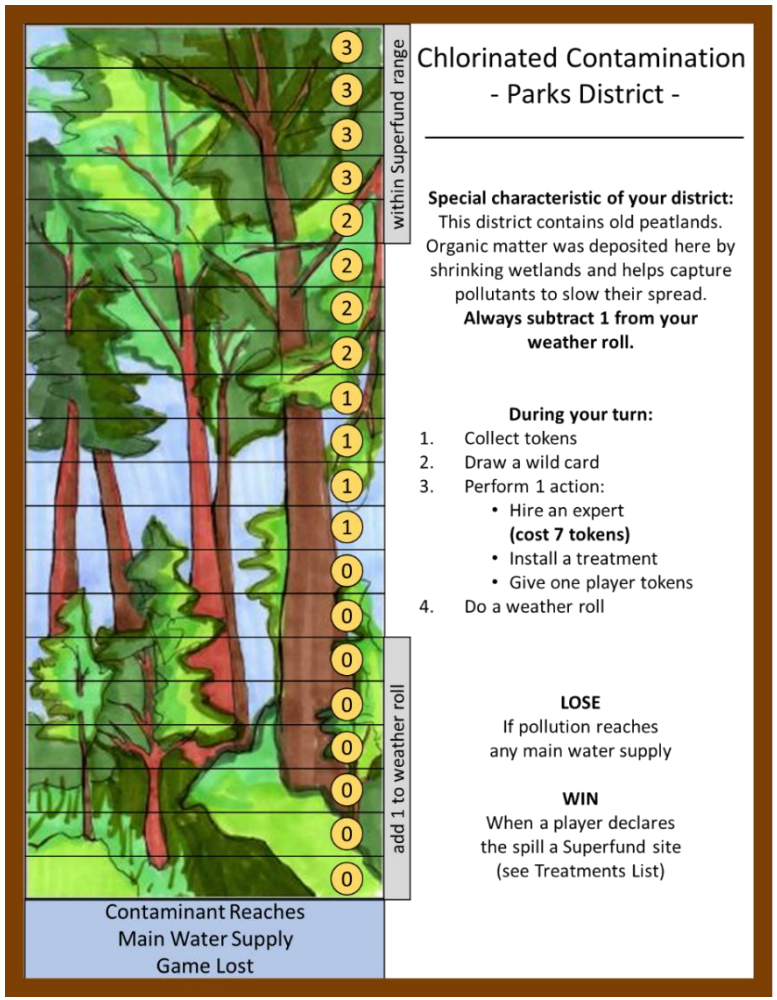
3
3
3
3
2
2
2
2
1
1
1
1
0
0
0
0
0
0
0
within Superfund range
add 1 to weather roll
Contaminant Reaches
Main Water Supply
Game Lost
Chlorinated Contamination
- Parks District -
Special characteristic of your district:
This district contains old peatlands. Organic matter was deposited here by shrinking wetlands and helps capture pollutants to slow their spread.
Always subtract 1 from your weather roll.
During your turn:
1. Collect tokens
2. Draw a wild card
3. Perform 1 action:
• Hire an expert
(cost 7 tokens)
• Install a treatment
• Give one player tokens
4. Do a weather roll
LOSE
If pollution reaches any main water supply
WIN
When a player declares the spill a Superfund site (see Treatments List)

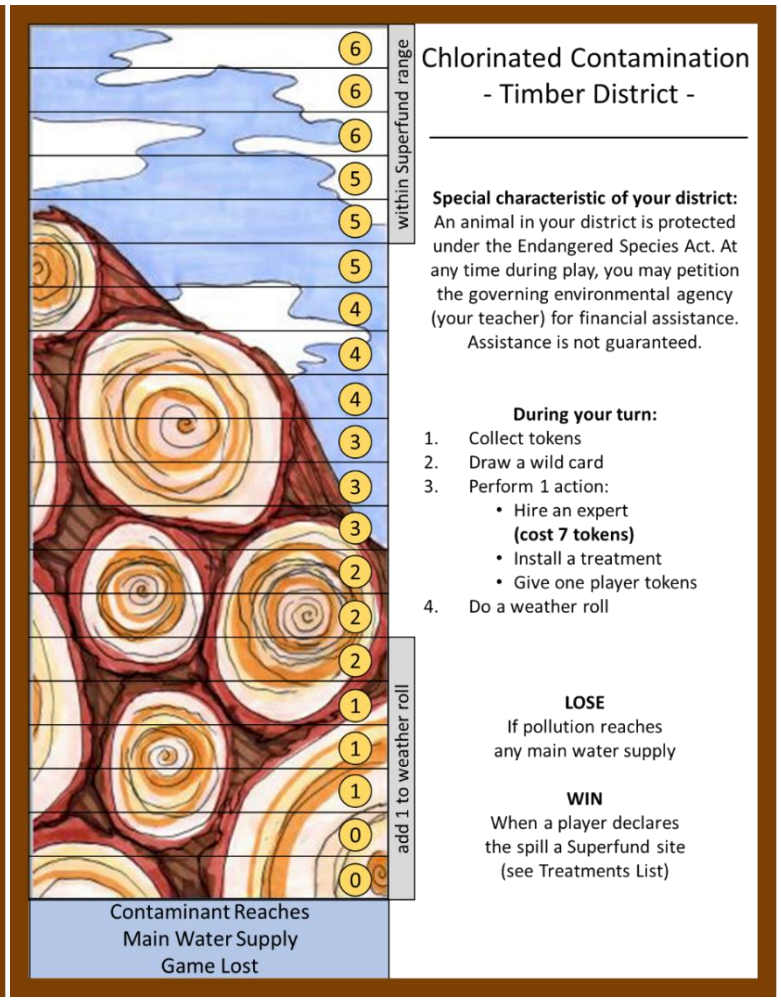
6
6
6
5
5
5
4
4
4
3
3
3
2
2
2
1
1
1
0
0
within Superfund range
add 1 to weather roll
Contaminant Reaches
Main Water Supply
Game Lost
Chlorinated Contamination
- Timber District -
Special characteristic of your district:
An animal in your district is protected under the Endangered Species Act. At any time during play, you may petition the governing environmental agency (your teacher) for financial assistance. Assistance is not guaranteed.
During your turn:
1. Collect tokens
2. Draw a wild card
3. Perform 1 action:
• Hire an expert
(cost 7 tokens)
• Install a treatment
• Give one player tokens
4. Do a weather roll
LOSE
If pollution reaches any main water supply
WIN
When a player declares the spill a Superfund site (see Treatments List)

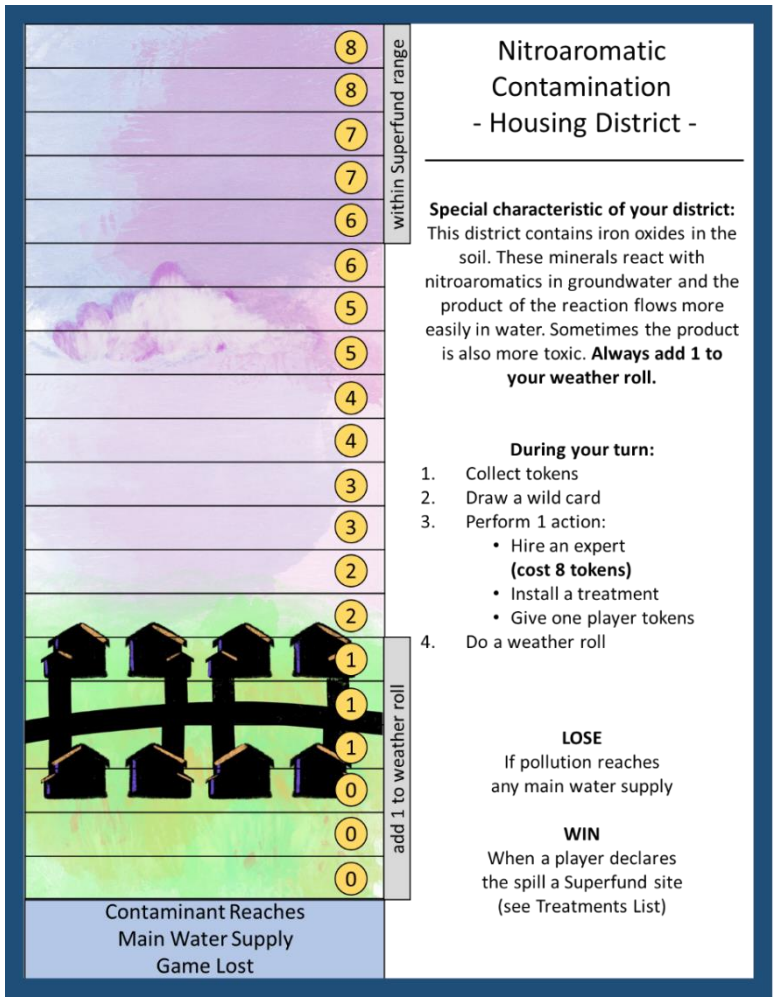

Nitroaromatic Contamination - Housing District -

Special characteristic of your district: This district contains iron oxides in the soil. These minerals react with nitroaromatics in groundwater and the product of the reaction flows more easily in water. Sometimes the product is also more toxic. **Always add 1 to your weather roll.**

During your turn:

1. Collect tokens
2. Draw a wild card
3. Perform 1 action:
   - Hire an expert **(cost 8 tokens)**
   - Install a treatment
   - Give one player tokens
4. Do a weather roll

LOSE
If pollution reaches any main water supply

WIN
When a player declares the spill a Superfund site (see Treatments List)

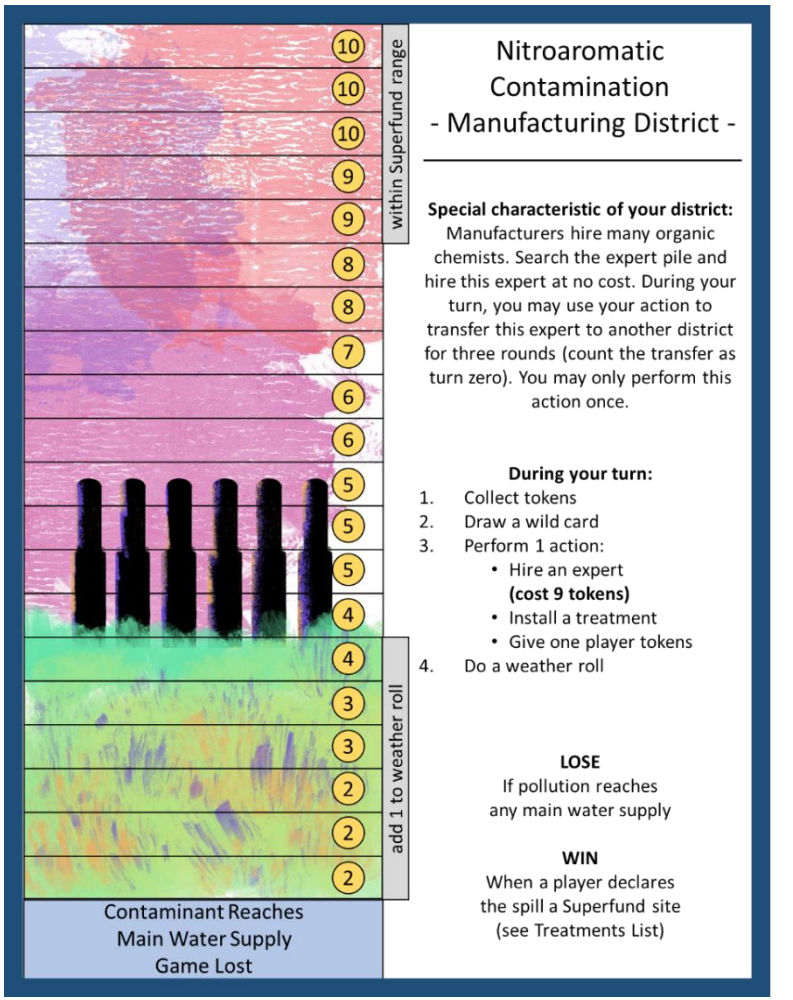

Nitroaromatic Contamination - Manufacturing District -

Special characteristic of your district: Manufacturers hire many organic chemists. Search the expert pile and hire this expert at no cost. During your turn, you may use your action to transfer this expert to another district for three rounds (count the transfer as turn zero). You may only perform this action once.

During your turn:

1. Collect tokens
2. Draw a wild card
3. Perform 1 action:
   - Hire an expert **(cost 9 tokens)**
   - Install a treatment
   - Give one player tokens
4. Do a weather roll

LOSE
If pollution reaches any main water supply

WIN
When a player declares the spill a Superfund site (see Treatments List)

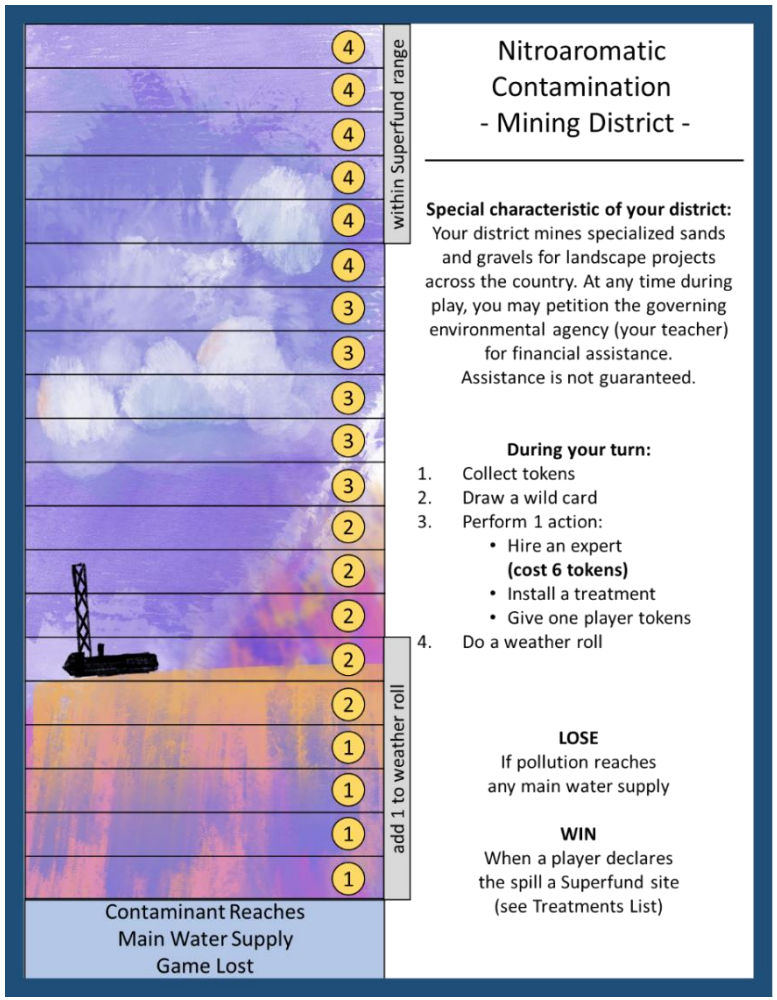

Nitroaromatic Contamination - Mining District -

Special characteristic of your district: Your district mines specialized sands and gravels for landscape projects across the country. At any time during play, you may petition the governing environmental agency (your teacher) for financial assistance. Assistance is not guaranteed.

During your turn:

1. Collect tokens
2. Draw a wild card
3. Perform 1 action:
   - Hire an expert **(cost 6 tokens)**
   - Install a treatment
   - Give one player tokens
4. Do a weather roll

LOSE
If pollution reaches any main water supply

WIN
When a player declares the spill a Superfund site (see Treatments List)

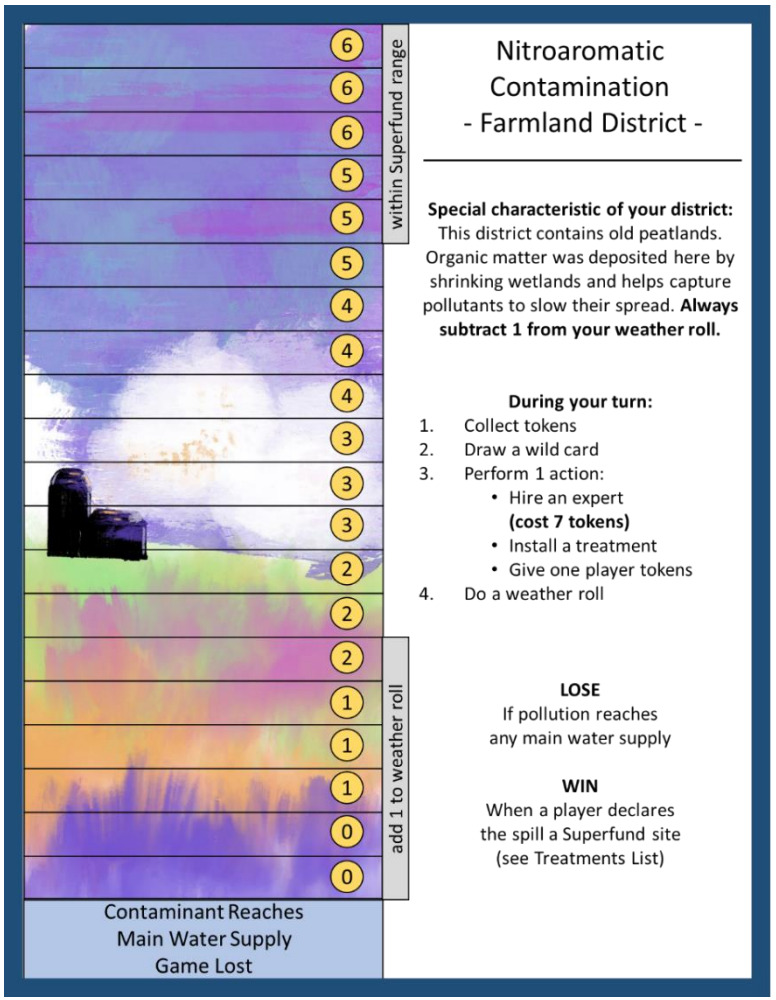

Nitroaromatic Contamination - Farmland District -

Special characteristic of your district: This district contains old peatlands. Organic matter was deposited here by shrinking wetlands and helps capture pollutants to slow their spread. **Always subtract 1 from your weather roll.**

During your turn:

1. Collect tokens
2. Draw a wild card
3. Perform 1 action:
   - Hire an expert **(cost 7 tokens)**
   - Install a treatment
   - Give one player tokens
4. Do a weather roll

LOSE
If pollution reaches any main water supply

WIN
When a player declares the spill a Superfund site (see Treatments List)

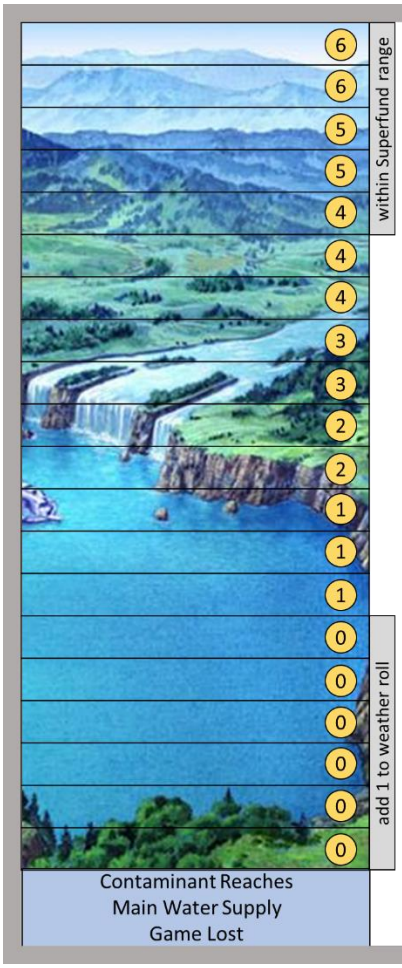

General Contamination
- Water Reservoir -

Special characteristic of your district:
You control an additional water supply for the districts around you. **At any point during play, you may charge service fees to any or all districts. You can only use the collected tokens during your turn.**

During your turn:

1. Collect tokens
2. Draw a wild card
3. Perform 1 action:
   - Hire an expert **(cost 7 tokens)**
   - Install a treatment
   - Give one player tokens
4. Do a weather roll

LOSE
If pollution reaches any main water supply

WIN
When a player declares the spill a Superfund site (see Treatments List)

Treatments List

Each treatment has unlimited uses. Maximum of 1 treatment per turn.
At the end of the game, count the tokens paid for treatments to calculate game score.
You do not lose experts when using treatments.

Hire these experts…	using this many tokens…	to regain this many blocks in your district.	Treatment Methods
	1 token	2 blocks	**Bioswale** Use basins to capture rainwater and filter contaminants to prevent further contamination from surface spills.
	3 tokens	4 blocks	**Treatment Systems Upgrade** Upgrade treatment systems to prevent further contaminant discharge and more effectively treat the current contamination.
	4 tokens	5 blocks	**Pump and Treat** Pump groundwater from wells, treat the contamination, and pump the cleaned water back into the aquifer.
	5 tokens	7 blocks	**Permeable Reactive Barrier** Dig trenches to install filters or reactive materials that capture the contaminant or transform it into a less hazardous product.
	4 tokens *from each player*	5 blocks *for each player*	**Declare Superfund Site** The site is transferred to the federal government to contain the contaminant and establish long-term treatments.

The top graphcs of the experts deck and wild cards.

Rachel Carson

Biologist, Author

Carson's influential book, *Silent Spring*, described the environmental destruction caused by using pesticides without regulation. The publication started the environmental movement.

Clair Patterson

Geochemist

Patterson used uranium-lead dating to determine the age of the Earth. His research uncovered wide-spread lead contamination and influenced the ban of leaded gasoline.

Health & Safety Technician

Conduct tests and identify hazards to prevent harm to workers, property, the environment, and the public.

Median Pay: $61,000
Entry Degree: Bachelor's

BONUS

This expert may be traded as needed between districts, but the trade counts as an ACTION.

Toxicologist

Research the effects of chemicals on plants and animals. Determine the concentration where the chemical becomes toxic. The information about toxicity levels influences many policy decisions.

Median Pay: $91,000
Entry Degree: Doctoral

Hydrologist

Study how water moves over, around, and through geological formations like hills and aquifers. The knowledge of water movement helps to solve issues of water quality and availability.

Median Pay: $81,000
Entry Degree: Bachelor's

Geomicrobiologist

Study bacteria, viruses, algae, fungi, and parasites. Determine how these organisms live, grow, and interact with their environments. Some microbes generate minerals that react with some pollutants.

Median Pay: $70,000
Entry Degree: Bachelor's

Environmental Scientist

Monitor environmental health. Use knowledge of natural interactions to clean up polluted areas, advise policy-makers, and work with industrial companies to reduce pollution.

Median Pay: $69,000
Entry Degree: Bachelor's

Soil Scientist

Study soil quality including nutrients, pollutants, and water content. These qualities affect the ways that chemicals interact with the soil and move through it.

Median Pay: $62,000
Entry Degree: Bachelor's

Organic Chemist

Specialize in the chemical reactions of molecules that contain carbon. Understanding these reactions is important for figuring out how molecules behave in the environment. Many reactions change in different conditions, like in water or in sunshine.

Median Pay: $81,000
Entry Degree: Bachelor's

Biochemist

Study how chemicals affect physical characteristics of living things. Many chemicals affect biological processes like cell development, growth, and disease. These processes are often impacted by environmental conditions, like the presence of pollutants.

Median Pay: $91,000
Entry Degree: Doctoral

Lisa Jackson

Chemical Engineer, Policy-Maker
From 2006–2013, Jackson initiated reform of the Toxic Substances Control Act of 1976, fought against expansion of oil pipelines, and improved National Ambient Air Quality Standards.

Materials Engineer

Design, develop, and test materials like metals, plastics, and composites. Materials that are stronger, lighter, more flexible, and more durable are important for high-tech applications.

Median Pay: $95,000
Entry Degree: Bachelor's

Geological Engineer

Specialize in structural properties of natural formations like the stability of bedrock. This knowledge is important for constructing safer mines, buildings, and bridges.

Median Pay: $94,000
Entry Degree: Bachelor's

Environmental Engineer

Identify environmental pollutants from industrial activities. Determine how fast the pollutants are spreading. Knowledge about the hazards is important for designing treatment systems for soil, water, and air.

Median Pay: $86,000
Entry Degree: Bachelor's

Civil Engineer

Design, construct, and maintain infrastructure like roads, bridges, and water treatment systems.

Median Pay: $85,000
Entry Degree: Bachelor's

Structural Engineer

Design, construct, operate, and maintain infrastructure like tunnels, dams, and water treatment systems.

Median Pay: $85,000
Entry Degree: Bachelor's

Agricultural Engineer

Solve problems of agricultural pollution. Design systems to protect the environment from agricultural contaminants. Improve methods for storage and use of agricultural products.

Median Pay: $75,000
Entry Degree: Bachelor's

Chemical Engineer

Design more efficient and safer industrial processes. Test hazardous waste treatment systems. Monitor safe operating practices. This work is important for reducing costs, minimizing hazards, and preventing pollution.

Median Pay: $105,000
Entry Degree: Bachelor's

Booming Economy

Your district is highly active in the trading of goods and services.

Collect 2 additional tokens on next turn.

Keep card until used.

Apply for Research Grant

Your community needs research funding.

Roll 1 dice:
0: Grant denied
1 or 2: Grant awarded
If awarded, roll 2 dice and collect tokens equal to the number shown.

Drought

What states in the USA are currently experiencing severe drought or worse? List them on your lab sheet.

Skip weather roll this turn.

Low Cost of Living

Your district attracts people looking for lower-cost housing.

Your next expert costs 2 tokens less.

Keep card until used.

Apply for Research Grant

Your community needs research funding.

Roll 1 dice:
0: Grant denied
1 or 2: Grant awarded
If awarded, roll 2 dice and collect tokens equal to the number shown.

Drought

What states in the USA are currently experiencing severe drought or worse? List them on your lab sheet.

Skip weather roll this turn.

Transfer Request

A professional wants to move to another district.

Choose 1 expert in play to move to your district.
Discard if no experts are in play.

Technological Advance

Scientific research found better ways to treat pollution!

Your next treatment costs 2 tokens less.

Keep card until used.

Grant Awarded

Your grant proposal was funded!

Roll 2 dice and collect tokens equal to the number shown.

Test New Treatment Method

Research suggests testing a modified treatment method to save money.

During your next treatment, roll 2 dice:

0 or 4: Major failure, ineffective treatment
1: Minor failure, removes 1 fewer block
2: Treatment works perfectly!
3: Treatment works and you get a subsidy for your efforts. Get a refund of your tokens.

Accountability

The State enters a court case against the company suspected of causing the pollution.

Roll 2 dice:

0: Deliberate pollution, all players gain 4 tokens
1: Negligence, Superfund now costs 3 tokens each
2: Accidental spill, all players gain 1 token
3: Not guilty, lose 1 token in legal fees
4: Prolonged case, lose 2 tokens in legal fees

Lobby Lawmakers

Ask lawmakers for help with environmental issues in your district.

Roll 2 dice:

0 or 4: Lobby failed, nothing happens
1 or 3: You gain 4 tokens
2: Everyone gains 3 tokens

Uncertain Economic Activity

The trading of goods and services through your district is changing rapidly.

Roll 2 dice:

0: Lose 4 tokens
1: Lose 2 tokens
2: Nothing happens
3: Gain 2 tokens
4: Gain 4 tokens

New Budget Proposal

The State proposes a new distribution of funds.

Roll 2 dice:

0: Lose 2 tokens
1: Lose 1 token
2: No funding changes
3: Gain 2 tokens
4: Gain 3 tokens

President's Budget Approved

The President asks Congress to increase the budget for environmental pollution projects. Congress agrees.

All players gain 4 tokens.

Uncertain Economic Activity

The trading of goods and services through your district is changing rapidly.

Roll 2 dice:

0: Lose 4 tokens
1: Lose 2 tokens
2: Nothing happens
3: Gain 2 tokens
4: Gain 4 tokens

New Budget Proposal

The State proposes a new distribution of funds.

Roll 2 dice:

0: Lose 2 tokens
1: Lose 1 token
2: No funding changes
3: Gain 2 tokens
4: Gain 3 tokens

Transfer Request

An expert from your district wishes to move elsewhere.

Send 1 of your experts to another district.

Competitive Wages

A neighboring district offers better salary.

Lose 1 expert to the district on your right.
Discard if you have no experts.

Incoming Storm

A major storm is heading to the watershed!

Roll 2 dice:
0: Pollution progresses 2 blocks for every player
1: Pollution progresses 1 block for every player
2: You and district to your right progress 2 blocks
3: Pollution in your district progresses 2 blocks
4: Storm track changes, no damage occurs

Aging Infrastructure

Dams, sewers, and water collection systems in your district are getting old.

Roll 2 dice:
0 or 4: Major failure, pollution progresses 4 blocks
1 or 3: Minor failure, pollution progresses 2 blocks
2: Detected before failure, pay 2 tokens to repair

Retirement

An expert in your district has reached the age of retirement.

Return 1 expert to the bottom of the draw deck.

Storm of the Century

What storm had the heaviest rainfall in US history? Write 3 facts about it on your lab sheet.

Pollution advances 2 blocks for every player.

Severe Storm

Search for a major storm to hit the USA. Write 3 facts about it on your lab sheet.

Add 1 to your next weather roll.

Government Shutdown

Permits are stalled, funds are frozen, consulting specialists are unavailable.

End your turn now and perform weather roll.

Competitive Wages

A neighboring district offers better salary.

Lose 1 expert to the district on your left.
Discard if you have no experts.

Severe Storm

Search for 3 ways to reduce storm water runoff and write a list on your lab sheet.

Add 1 to your next weather roll.

High Cost of Living

Your district attracts people seeking the lower cost of living expenses like housing.

Your next expert costs 2 extra tokens.

Keep card until used.

Lateral Contamination

Natural features direct groundwater to flow between neighboring districts.

Roll 2 dice:
0 or 4: Nothing happens
1: District on left progresses 2 blocks
2: Two adjacent districts progress 1 block
3: District to your right progresses 2 blocks

Bioaccumulation

Define bioaccumulation on your lab sheet and give an example.

Roll 2 dice and lose tokens equal to the number shown.

Poor Water Quality

People with weakened immune systems visiting your district got sick!

Roll 2 dice and lose tokens equal to the number shown.

Overworked

An expert in your district is exhausted and needs time off.

Roll 2 dice. The number shown is the number of rounds 1 expert is on vacation. Turn the card over until the expert returns. Re-roll if dice show 0. Discard if you have no experts.

Bioaccumulation

Define bioaccumulation on your lab sheet and give an example.

Roll 2 dice and lose tokens equal to the number shown.

Weakened Economy

The trading of goods and services through your district is severely affected by the spreading pollution.

At the start of your next turn, do not collect any tokens.

Keep card until used.

Repair Needed

Critical infrastructure in your district needs urgent repair.

Roll 2 dice and lose tokens equal to the number shown.

Lateral Contamination

Natural features direct groundwater to flow between neighboring districts.

Roll 2 dice:
0 or 4: Nothing happens
1: District on left progresses 2 blocks
2: Two adjacent districts progress 1 block
3: District to your right progresses 2 blocks

Appendix F. Ideological Foundations

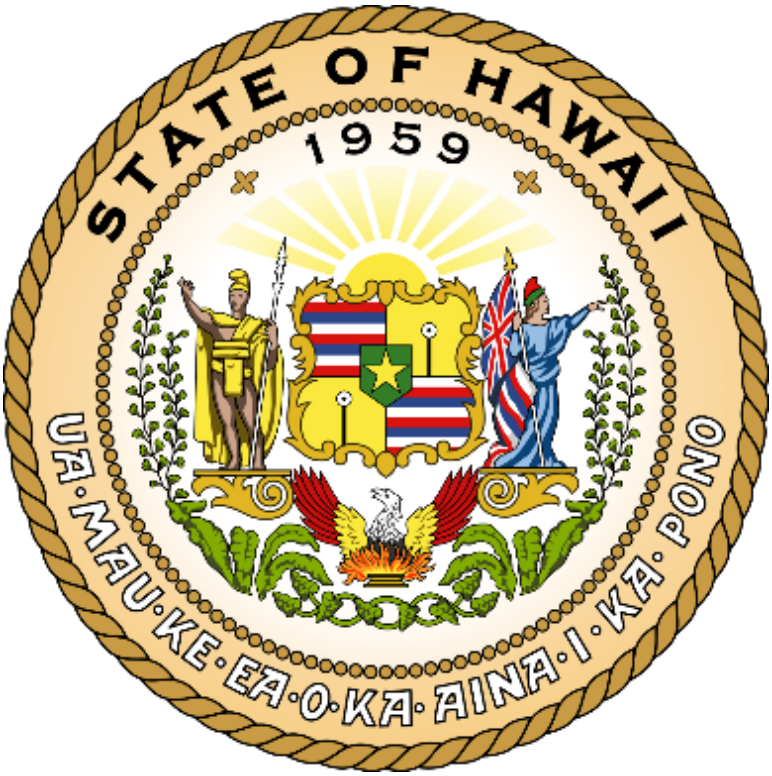

The official seal of Hawai'i with the state motto.

ua mau ke ea o ka ʻāina i ka pono.

(Pronunciation: *oo-ah maoo keh eh-ah oh kah aye-nah ee kah poh-no*)

I was raised in a community that has a strong cultural connection to the land, to water, and to the many creatures that share this planet with us. The close connection that the Hawaiian people have to the environment arises from living harmoniously within a small island ecosystem for centuries, where sustainability was the key to survival. It is more than a respect for places, things, and creatures; the feeling is a spiritual connection to everything in the natural world that comes from trading energy with, receiving influence from, and working in harmony with other things. Although I lack the ancestral link to Hawai'i, I was accepted into the community and they instilled these values in me, which now manifest in my personal ideologies, lifestyle choices, and career direction.

These Hawaiian values are even stronger in present-day life as Hawaiian communities revisit and revive the ancient practices of sustainability as a remedy to modern issues of climate change, food scarcity, high cost of living, and invasive species. Sustainability, stewardship, and service are so deeply engrained in the Hawaiian culture that many official state documents were written to declare these ideals 'law of the land'. Two such documents are presented here to formally express these cultural foundations and state their importance. Section 1 is an excerpt from the Hawai'i Statewide Forest Assessment and Strategies (2010) report that provides historical context and insight into the multi-faceted meaning of the Hawai'i state motto. Section 2 is an excerpt of Hawai'i state law written to define the cultural principle of Aloha and to declare the importance of adhering to these ideals to foster unity and prosperity. Both excerpts provide insight into the source and depth of my commitment to environmental protection and community service.

Section 1. The Hawai'i State Motto and Land Stewardship

This maxim was designated as the official State motto soon after Hawai'i became a state in 1959. The official English translation is "The life of the land is perpetuated in righteousness", but there is a much deeper meaning. These words were first spoken by King Kamehameha III on July 31, 1843 in a speech of gratitude on the day that sovereignty was restored to the Kingdom of Hawai'i by British Navy Admiral Richard Thomas. Months earlier, the Captain of another British warship had unilaterally seized control of Hawai'i and claimed it as a territory of Great Britain. Upon hearing this news Queen Victoria was outraged and directed Admiral Thomas to restore sovereignty of the Kingdom of Hawai'i. In his speech, the King proclaimed "Ua mau ke ea o ka 'aina i ka pono", meaning that the Kingdom's 'aina (land), was once again ea (independent) ua mau (steadfast, solid, forever), i ka pono (through righteousness, justice, or virtue).

The Hawaiian language is rich and poetic. Every chant and proverb has hidden within it double or triple entendre, or kauna (*kaoo-nah*). The King chose his words carefully; there are dozens of words for "land", but he chose the word 'aina for its special connotation. The root of the word 'aina is 'ai, (to feed), thus, the 'aina is a term of endearment for the land that feeds and sustains us. The word pono is also significant, for it carries a connotation of doing the right thing, doing what is fair or just. Today, many residents of Hawai'i, be they native Hawaiian or not, often use the words 'aina and pono in every day speech because there simply isn't a word in English that means just that. So a less formal, but more meaningful translation of the King's words might be: "Our independence will forever be sustained by our precious life-giving land if we do what is good and just."

Section 2. The Aloha Act - Hawai'i Revised Statutes § 5-7.5

§ 5-7.5 "Aloha Spirit".

(a) "Aloha Spirit" is the coordination of mind and heart within each person. It brings each person to the self. Each person must think and emote good feelings to others. In the contemplation and presence of the life force, "Aloha", the following unuhi laulā loa (*oo-noo-hee laoo-lah lo-ah*) may be used:

"Akahai", meaning kindness to be expressed with tenderness; (*ah-kah-haye*)

"Lōkahi", meaning unity, to be expressed with harmony; (*lo-kah-hee*)

"'Olu'olu" meaning agreeable, to be expressed with pleasantness; (*oh-loo-oh-loo*)

"Ha'aha'a", meaning humility, to be expressed with modesty; (*ha-ah-ha-ah*)

"Ahonui", meaning patience, to be expressed with perseverance. (*ah-ho-noo-ee*)

These are traits that express the charm, warmth and sincerity of Hawai'i's people.
It was the working philosophy of native Hawaiians and was presented as a gift to the people of Hawai'i. "Aloha" is more than a word of greeting or farewell or a salutation. "Aloha" means mutual regard and affection and extends warmth in caring with no obligation in return. "Aloha" is the essence of relationships in which each person is important to every other person for collective existence. "Aloha" means to hear what is not said, to see what cannot be seen, and to know the unknowable.

(b) In exercising their power on behalf of the people and in fulfillment of their responsibilities, obligations and service to the people, the legislature, governor, lieutenant governor, executive officers of each department, the chief justice, associate justices, and judges of the appellate, circuit, and district courts may contemplate and reside with the life force and give consideration to the "Aloha Spirit". [L 1986, c 202, § 1]